DEVELOPMENTS IN
CARDIOVASCULAR MEDICINE

Lancée CT, ed: Echocardiology. 1979. ISBN 90-247-2209-8.
Baan J, Arntzenius AC, Yellin EL, eds: Cardiac dynamics. 1980. ISBN 90-247-2212-8.
Thalen HJT, Meere CC, eds: Fundamentals of cardiac pacing. 1970. ISBN 90-247-2245-4.
Kulbertus HE, Wellens HJJ, eds: Sudden death. 1980. ISBN 90-247-2290-X.
Dreifus LS, Brest AN, eds: Clinical applications of cardiovascular drugs. 1980. ISBN 90-247-2295-0.
Spencer MP, Reid JM, eds: Cerebrovascular evaluation with Doppler ultrasound. 1981. ISBN 90-247-90-247-2348-1.
Zipes DP, Bailey JC, Elharrar V, eds: The slow inward current and cardiac arrhythmias. 1980. ISBN 90-247-2380-9.
Kesteloot H, Joossens JV, eds: Epidemiology of arteral blood pressure. 1980. ISBN 90-247-2386-8.
Wackers FJT, ed: Thallium – 201 and technetium-99m-pyrophosphate myocardial imaging in the coronary care unit. 198. ISBN 90-247-2396-5.
Maseri A, Marchesi C, Chierchia S, Trivella MG, eds: Coronary care units. 1981. ISBN 90-247-2456-2.
Morganroth J, Moore EN, Dreifus LS, Michelson EL, eds: The evaluation of new anti-arrhythmic drugs. 1981. ISBN 90-247-2474-0.
Alboni P: Intraventricular conduction disturbances. 1981. ISBN 90-247-2483-X.
Rijsterborgh H, ed: Echocardiology. 1981. ISBN 90-247-2491-0.
Wagner GS, ed: Myocardial infarction: Measurement and intervention. 1982. ISBN 90-247-2513-5.
Meltzer RS, Roelandt J, eds: Contrast echocardiography. 1982. ISBN 90-247-2531-3.
Amery A, Fagard R, Lijnen R, Staessen J, eds: Hypertensive cardiovascular disease; pathophysiology and treatment. 1982. ISBN 90-247-2534-8.
Bouman LN, Jongsma HJ, eds: Cardiac rate and rhythm. 1982. ISBN 90-247-2626-3.
Morganroth J, Moore EM, eds: The evaluation of beta blocker and calcium antagonist drugs. 1982. ISBN 90-247-2642-5.
Rosenbaum MB, ed: Frontiers of cardiac electrophysiology. 1982. ISBN 90-247-2663-8.
Roelandt J, Hugenholtz PG, eds: Long-term ambulatory electrocardiography. 1982. ISBN 90-247-2664-8.
Adgey AAJ, ed: Acute phase of ischemic heart disease and myocardial infarction. 1982. ISBN 90-247-2675-1.
Hanrath P, Bleifeld W, Souquet, eds: Cardiovascular diagnosis by ultrasound. Transesophageal, computerized, contrast, Doppler echocardiography. 1982. ISBN 90-247-2692-1.
Roelandt, J., ed: The practice of M-mode and two-dimensional echocardiography. 1983. ISBN 90-247-2745-6.

ADVANCES IN NONINVASIVE CARDIOLOGY

Ultrasound, computed tomography, radioisotopes, digital angiography

edited by

JÜRGEN MEYER, MD
PETER SCHWEIZER, MD
RAIMUND ERBEL, MD

Department of Internal Medicine I
Rheinisch-Westfälische Technische Hochschule
Aachen
Federal Republic of Germany

Copyright

CONTENTS

III. REGIONAL WALL MOTION IN MYOCARDIAL ISCHEMIA

IV. DETECTION AND QUANTIFICATION OF ACUTE
    MYOCARDIAL INFARCTION

V. TISSUE ANALYSIS

PREFACE

Many noninvasive examination methods of the heart have not held out against the invasive methods, which modern cardiac therapy, surgically or with catheterization, requires. They have disappeared completely or are only used by isolated groups of researchers. However, there is an obvious tendency to apply the invasive procedures as the last diagnostic possibility.

In the attempt to select clinically relevant methods, the expert authors of this book demonstrate that echocardiography, expanded with contrast and Doppler, has been developed into one of the most important noninvasive methods. The results with tissue characterization show that the possibilities of this method have not yet been fully explored.

Nuclear procedures are widely used, although they should only be applied in direct connection with clinical cardiology.

The new lead methods of the ecg, such as ecg-mapping, show that standard electrocardiography of electrical functions is not yet fully exploited.

The rapidly developing method of computer tomography is also being applied to cardiology. Since nuclear magnetic resonance requires extensive equipment construction, its future is as yet unsure.

Of course, a book like this does not intend to treat the subject of noninvasive cardiology in extensive detail. Established methods like standard electrocardiography, phonocardiography and sphygmography are not discussed. The aim of this book is rather to demonstrate the trend of present developments in the field.

LIST OF CONTRIBUTORS

Ameling, W., Rogowski-Institut für Elektronik, Rheinisch-Westfälische Technische Hochschule, Goethestrasse 27/29, D-5100 Aachen, FRG.

Bachmann, K., Medizinische Poliklinik, Universität Erlangen-Nürnberg, Östliche Stadtmauerstrasse 29, D-8520 Erlangen, FRG.

Baumer, A., Radiologische Universitätsklinik, Klinikum Grosshadern, Marchionistrasse 15, D-8000 München 70, FRG.

Bethge, H.D., Medizinische Poliklinik, Universität Erlangen-Nürnberg, Östliche Stadtmauerstrasse 29, D-8520 Erlangen, FRG.

Bleifeld, W., Universitätskrankenhaus Eppendorf, Medizinische Klinik, Kardiologische Abteilung, Martinistrasse 52, D-2000 Hamburg 20, FRG.

Bom, A.H.A., Interuniversity Cardiology Institute and Thorax Centre, Erasmus University Rotterdam, P.O. Box 1738, 3000 DR Rotterdam, The Netherlands.

Bookstein, F.L., Division of Radiologic Physics, Department of Radiology, University of Michigan, Ann Arbor, MI 48109, USA.

Brennecke, R., Abteilung für Kinderkardiologie und Biomedizinische Technik, Klinikum der Christian-Albrechts-Universität, Schwanenweg 20, D-2300 Kiel 1, FRG.

Brower, R.B., Interuniversity Cardiology Institute and Thorax Centre, Erasmus University Rotterdam, P.O. Box 1738, 3000 DR Rotterdam, The Netherlands.

Brundage, B., Department of Radiology and Medicine and Cardiovascular Research Institute, University of California, Medical Center, San Francisco, CA 94143, USA.

Brutsaert, P., Department of Physiology, University of Antwerp (RUCA), Groenenborgerlaan 171, B-2020 Antwerp, Belgium.

Buda, A.J., Division of Cardiology, University Hospital, 1405 East Ann Street, Ann Arbor, MI 48109, USA.

Bürsch, J.H., Abteilung für Kinderkardiologie und Biomedizinische Technik, Klinikum der Christian-Albrechts-Universität, Schwanenweg 20, D-2300 Kiel 1, FRG.

Cannon, S., Cardiology, Veterans Hospital University of Texas Health Science Center, San Antonio, TX 78284, USA.

Chivers, R.C., Physics Department, University of Surrey, Guildford, Surrey GU2 5XH, United Kingdom.

Claes, V.A., Department of Physiology, University of Antwerp (RUCA), Groenenborgerlaan 171, B-2020 Antwerp, Belgium.

Collins, S.M., Department of Electrical and Computer Engineering, University of Iowa, Iowa City, IO 52242, USA.

Daniel, W.G., Medizinische Hochschule Hannover, Abteilung für Kardiologie, Konstanty-Gutschow-Strasse 8, D-3000 Hannover 61, FRG.

Delp, E.J., Department of Electrical and Computer Engineering, University of Michigan, Ann Arbor, MI 48109, USA.

Distante, A., Istituto di Fisiologia Clinica, CNR e Università di Pisa, Via Savi 8, I-56100 Pisa, Italy.

Döhring, W., Medizinische Hochschule Hannover, Abteilung für Kardiologie, Konstanty-Gutschow-Strasse 8, D-3000 Hannover 61, FRG.

Effert, S., Abteilung Innere Medizin I, Medizinische Fakultät, Rheinisch-Westfälische Technische Hochschule, Goethestrasse 27-29, D-5100 Aachen, FRG.

Erbel, R., Abteilung Innere Medizin I, Rheinisch-Westfälische Technische Hochschule, Goethestrasse 27-29, D-5100 Aachen, BRD. Present address: II. Medizinische Klinik und Poliklinik, Johannes Gutenberg Universität, Langenbeckstrasse 1, D-6500 Mainz, FRG.

Essen von, R., Abteilung Innere Medizin I, Rheinisch-Westfälische Technische Hochschule, Goethestrasse 27-29, D-5100 Aachen, FRG.

Fischbach, T., Medizinische Einrichtungen der Universität Düsseldorf, I. Medizinische Klinik B, Moorenstrasse 5, D-4000 Düsseldorf 5, FRG.

Goldstein, J., Departments of Radiology and Medicine and the Cardiovascular Research Institute, University of California, Medical Center, San Francisco, CA 94143, USA.

Hanrath, P., Universitätskrankenhaus Eppendorf, Medizinische Klinik, Kardiologische Abteilung, Martinistrasse 52, D-2000 Hamburg 20, FRG.

Hauke, R., Toshiba Medical Systems, Grafenberger Allee 115-117, D-4000 Düsseldorf 1, FRG.

Heintzen, P.H., Abteilung Kinderkardiologie und Biomedizinische Technik, Klinikum der Christian-Albrechts-Universität, Schwanenweg 20, D-2300 Kiel 1, FRG.

Herfkens, R., Department of Radiology and Medicine and the Cardiovascular Research Institute, University of California, Medical Center, San Francisco, CA 94143, USA.

Hinsen, R., Helmholtz Institute for Biomedical Engineering, Rheinisch-Westfälische Technische Hochschule, Goethestrasse 27-29, D-5100 Aachen, FRG.

Huang, S.C., University of California, Laboratory of Nuclear Medicine, UCLA School of Medicine, Los Angeles, CA 90024, USA.

Jehle, J., Medizinische Einrichtungen der Universität Düsseldorf, I. Medizinische Klinik B, Moorenstrasse 5, D-4000 Düsseldorf 1, FRG.

Jenkins, J.M., Department of Electrical and Computer Engineering, University of Michigan, Ann Arbor, MI 48109, USA.

Jensch, P., Rogowski-Institut für Elektronik, Rheinisch-Westfälische Technische Hochschule, Goethestrasse 27-29, FRG.

Katen ten, H.J., Interuniversity Cardiology Institute and Thorax Centre, Erasmus University Rotterdam, P.O. Box 1738, 3000 DR Rotterdam, The Netherlands.

Kirsch, C.M., Radiologische Universitätsklinik, Klinikum Grosshadern, Marchionistrasse 15, D-8000 München 70, FRG.

Köster, O., Department of Radiology, University of Bonn, Sigmund-Freud-Strasse, D-5300 Bonn-Venusberg, FRG.

Kramer, P., Departments of Radiology and Medicine and the Cardiovascular Institute, University of California, Medical Center, San Francisco, CA 94143, USA.

Krebs, W., Abteilung Innere Medizin I, Rheinisch-Westfälische Technische Hochschule, Goethestrasse 27-29, D-5100 Aachen, FRG.

Kubalski, W., Rogowski-Institut für Elektronik, Rheinisch-Westfälische Technische Hochschule, Goethestrasse 27-29, D-5100 Aachen, FRG.

Lackner, K., Department of Radiology, University of Bonn, Sigmund-Freud-Strasse, D-5300 Bonn-Venusberg, FRG.

Langenstein, B.A., Universitätskrankenhaus Eppendorf, Medizinische Klinik, Kardiologische Abteilung, Martinistrasse 52, D-2000 Hamburg 20, FRG.

Lauber, A., Medizinische Einrichtungen der Universität Düsseldorf, I. Medizinische Klinik B, Moorenstrasse 5, D-4000 Düsseldorf 1, FRG.

Lichtlen, P.R., Medizinische Hochschule Hannover, Abteilung für Kardiologie, Konstanty-Gutschow-Strasse 8, D-3000 Hannover 61, FRG.

Lipton, M.J., Departments of Radiology and Medicine and Cardiovascular Research Institute, Uni-

versity of California, Medical Center, San Francisco, CA 94143, USA.

Marhoff, P., Abteilung Medizin-Technik, Siemens, Erlangen, FRG.

Melton, H.E., Department of Electricaland Computer Engineering, University of Iowa, Iowa City, IA 52242, USA.

Merx, W., Abteilung Innere Medizin I, Rheinisch-Westfälische Technische Hochschule, Goethestrasse 27-29, D-5100 Aachen, FRG.

Meyer, C.R., Division of Radiologic Physics, Department of Radiology, University of Michigan, Ann Arbor, MI 48109, USA.

Meyer, J., Abteilung Innere Medizin I, Rheinisch-Westfälische Technische Hochschule, Goethestrasse 27-29, D-5100 Aachen, BRD. Present address: II. Medizinische Klinik und Poliklinik, Johannes-Gutenberg Universität, Langenbeckstrasse 1, D-6500 Mainz, FRG.

Meyer-Ebrecht, D., Philips GmbH, Forschungslaboratorium Hamburg, Vogt-Köllnstrasse 30, D-2000 Hamburg, FRG.

Ocken van, E., Department of Physiology, University of Antwerp (RUCA) Groenenborgerlaan 171, B-2020 Antwerp, Belgium.

Ogris, E., Kardiologische Universitätsklinik, Allgemeines Krankenhaus der Stadt Wien, Garnisongasse 14, A-1097 Wien, Austria.

Pachinger, O., Kardiologische Universitätsklinik, Allgemeines Krankenhaus der Stadt Wien, Garnisongasse 14, A-1097 Wien, Austria.

Phelps, M.E., University of California, Laboratory of Nuclear Medicine, UCLA School of Medicine, Los Angeles, CA 90042, USA.

Pitt, B., Division of Cardiology, University Hospital, 1405, East Ann Street, Ann Arbor, MI 48109, USA.

Pölitz, B., Medizinische Einrichtungen der Universität Düsseldorf, I. Medizinische Klinik B, Moorenstrasse 5, D-4000 Düsseldorf, FRG.

Probst, P., Kardiologische Universitätsklinik, Allgemeines Krankenhaus der Stadt Wien, Garnisongasse 14, A-1097 Wien, Austria.

Rau, G., Helmholtz-Institut, Rheinisch-Westfälische Technische Hochschule, Goethestrasse 27-29, D-5100 Aachen, FRG.

Richards, K.L., Department of Cardiology, Veterans Hospital and University of Texas Health Science Center, San Antonio, TX 78284, USA.

Rienmüller, R., Radiologische Universitätsklinik, Klinikum Grosshadern, Marchioninistrasse 15, D-8000 München 70, FRG.

Roelandt, J., Thorax Centre, Erasmus University Rotterdam, P.O. Box 1738, 3000 DR Rotterdam, The Netherlands.

Schelbert, H.R., University of California, Laboratory of Nuclear Medicine, UCLA School of Medicine, Los Angeles, CA 90024, USA.

Schenkels, P., Department of Physiology, University of Antwerp (RUCA), Groenenborgerlaan 171, B-2000 Antwerp, Belgium.

Schicha, H., Division of Nuclear Medicine, University of Göttingen, Robert-Koch-Strasse 40, D-3400 Göttingen, FRG.

Schlüter, M., Universitätskrankenhaus Eppendorf, Medizinische Klinik, Kardiologische Abteilung, Martinistrasse 52, D-2000 Hamburg, FRG.

Schmiel, F.K., Medizinische Einrichtungen der Universität Düsseldorf, I. Medizinische Klinik B, Moorenstrasse 5, D-4000 Düsseldorf 1, FRG.

Schwaiger, M., University of California, Laboratory of Nuclear Medicine, UCLA School of Medicine, Los Angeles, CA 90024, USA.

Schweizer, P., Abteilung Innere Medzin I, Rheinisch-Westfälische Technische Hochschule, Goethestrasse 27-29, D-5100 Aachen, BRD. Present address: Evangelisches Krankenhaus, Ferrenbergstrasse 24, 5060 Bergisch-Gladbach 2, FRG.

Serruys, P., Interuniversity Cardiology Institute and Thorax Centre, Erasmus University Rotterdam,

XIV

P.O. Box 1738, 3000 DR Rotterdam, The Netherlands.

Shah, A., University of California, Laboratory of Nuclear Medicine, UCLA School of Medicine, Los Angeles, CA 90024, USA.

Silny, H., Helmholtz Institute for Biomedical Engineering, Rheinisch-Westfälische Technische Hochschule, Goethestrasse 27-29, D-5100 Aachen, FRG.

Skorton, D.J., Department of Internal Medicine, University of Iowa and Iowa City VA Medical Center, Iowa City, IA 52242, USA.

Smith, D.N., Department of Electrical and Computer Engineering, University of Michigan, Ann Arbor, MI 48109, USA.

Sochor, H., Kardiologische Universitätsklinik, Allgemeines Krankenhaus der Stadt Wien, Garnisongasse 14, A-1097 Wien, Austria.

Spiller, P., Medizinische Einrichtungen der Universität Düsseldorf, I. Medizinische Klinik B, Moorenstrasse 5, D-4000 Düsseldorf 1, FRG.

Stender, H.St., Medizinische Hochschule Hannover, Abteilung für Kardiologie, Konstanty-Gutschow-Strasse 8, D-3000 Hannover 61, FRG.

Strauer, B.E., Medizinische Klinik I, Klinikum Grosshadern, Marchionistrasse 15, D-8000 München 70, FRG.

Thier, W., Universitätskrankenhaus Eppendorf, Medizinische Klinik, Kardiologische Abteilung, Martinistrasse 52, D-2000 Hamburg, FRG.

Thuru, P., Department of Radiology, University of Bonn, Sigmund-Freud-Strasse, D-5300 Bonn-Venusberg, FRG.

I. ADVANCES IN METHODOLOGY

1. COMPUTER STRUCTURES FOR DIGITAL IMAGING

WALTER AMELING

1. INTRODUCTION

In the near future most areas of the medical field will be confronted with data-gathering and computer-systems. Therefore it is worthwhile looking at the main problems and criteria which are involved with such systems. Methods and models have to be discussed which will very soon lead to technical restrictions and limitations for the application, especially in the area of *online-computing*. Nowadays the speed of single- or multiprocessor-systems enables mathematical and statistical describing functions to be used, which were not thought about some years ago. The evolution in technology allows us today to realize computer-systems which are highly flexible, expandable, very efficient and easy to adapt to different problems. First we have to recognize that the only way to increase the speed and power of a computer-system in a given technology is by *parallel processing*; that means we are led to complex computer structures, e.g. multiprocessor-systems. In the medical field, especially for digital image processing, we need extremely powerful systems for online and real-time computation.

In this paper the different aspects of *static and dynamic image analysis* and the related computer systems are discussed. We will determine the limitations and different parameters which rule the system-design and the specifications. Images are usually analyzed for:

– image enhancement
  (noise filtering, contrast enhancement, color enhancement, restoration of de-focused and motion-blurred images)
– geometric manipulations
  (image rotation, zooming, scrolling, topographic operations, transformation)
– image classification
  (pattern recognition, feature extraction)
– image sequence processing
  (flow analysis).

Tasks for the analysis of image sequences, so called dynamic image processing, are transient recording, real-time-filtering and fast data processing. The necessary high
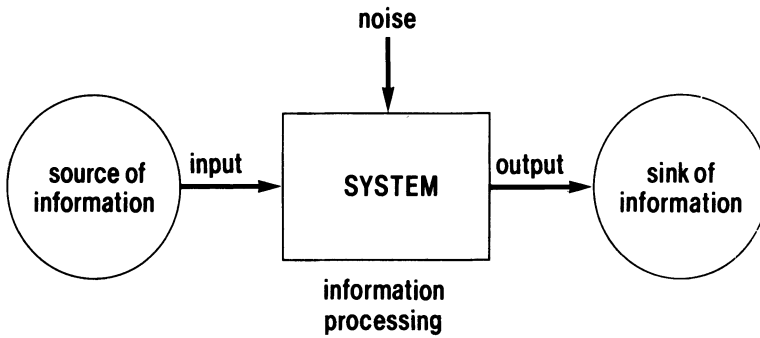
Figure 1. Information processing system.

performance can be achieved by independent data and/or instruction paths. These features lead to pipeline and/or parallel processing.

The optical nature of images originally requires optical manipulation. Since images have to be couverted, the optical information has to be couverted (film, video-tape). This simplifies image processing very much, because optical manipulations are much more difficult than analog or digital ones. The high processing speed and high accuracy of modern digital computers have restrained analog processing, so that nearly all image processing is done digitally today. As an example of a *digital image processing* system, the ISPS system developed at the Rogowski Institute, Aachen Technical University, is presented. The high performance in this case is achieved by parallel data handling and processing due to multi-port devices, use of a multiprocessor subsystem and independent data paths.

2. CHARACTERISTIC VARIABLES OF ONLINE-PROCESSING

The common operational principle of different information processing systems is shown in Figure 1. An arbitrary source inputs the information to the system which then processes and outputs it to the information sink. The processing system computes the output information according to a given function. In the area of measuring devices the main function is to provide maximum coincidence of input and output information (minimum distortions). In the area of data processing (e.g. automatic measuring and value processing) more complex functions are used to eliminate distortions caused by external noise and to compute characteristic properties of the input information. This provides support in diagnosis for medical applications, because carefully registered and well documented data are required.

Information processing in most cases requires *conversions* (e.g. analog-digital conversion) without loss of information (Figure 2). Unfortunately any conversion adds some noise, which may cause errors in processing later on. In order to provide an adequate conversion we have to consider all parameters of an information-
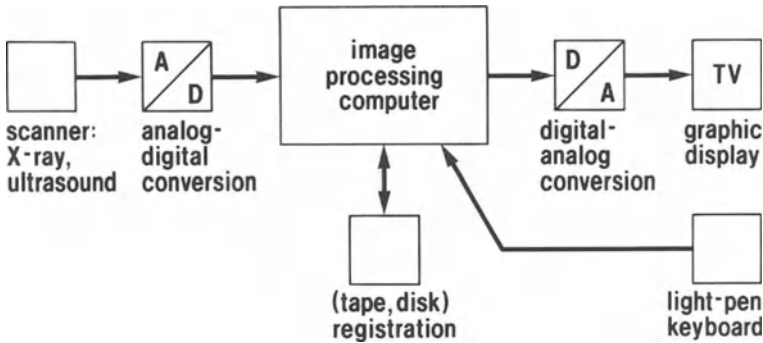
Figure 2. Image processing system.

carrying signal. Most signals carry information as intensity levels dependent on time. The simplest signal of this kind is a *sinusoidal wave* $x(t)$

$$x(t) = \hat{x} \cdot \sin(\omega t + \varphi)$$

where $\hat{x}$ is the peak intensity, φ is the phase shift and ω is the radian frequency.

However, most signals are not sinusoidal. Any periodic signal $f(t)$ can be approximated by a sum $g(t)$ of sinusoidal signals (harmonics) with different intensities and frequencies:

$$g(t) = \frac{a_0}{2} + \sum_{m=1}^{n} a_m \cdot \cos(m\omega t) + \sum_{m=1}^{n} b_m \cdot \sin(m\omega t)$$

with:

$$\frac{a_0}{2} = \frac{1}{T} \cdot \int_{t_0}^{t_0 + T} f(t)\mathrm{d}t$$

$$a_m = \frac{2}{T} \cdot \int_{t_0}^{t_0 + T} f(t) \cos(m\omega t)\mathrm{d}t \qquad m \neq 0$$

$$b_m = \frac{2}{T} \cdot \int_{t_0}^{t_0 + T} f(t) \sin(m\omega t)\mathrm{d}t.$$

The accuracy of the approximation is the better the larger the number n of harmonics. Non-periodic signals can be approximated in a similar way: the discrete frequency spectrum is replaced with a continuous one. In either case, a characteristic property of the signal is the frequency of the highest harmonic.

In order to digitize an analog signal, it has to be divided into discrete-time and discrete-intensity values. *Shannon's theorem* requests that the sampling rate f_a of an A/D-converter at minimum must be twice the frequency f_g of the highest harmonic:
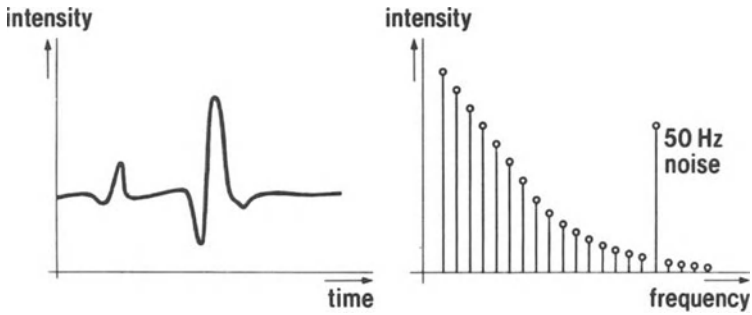
Figure 3. ECG-signal and its Fourier transform.

$$f_a \geq 2 \cdot f_g.$$

An ECG-A/D-converter therefore must provide a minimum sampling rate of 100 Hz since the highest harmonic is about 50 Hz. Sampling rates of 200 Hz to 250 Hz are common today (Figure 3).

The sampling rate f_a gives us the maximum time U_T for conversion:

$$U_T \leq \frac{1}{f_a}.$$

U_T is the step size for the discrete-time axis. For ECG-applications U_T is 4 to 5 ms.

3. REQUIREMENTS ON THE COMPUTER SYSTEM

In order to determine the *data-input-rates* to the computer, we look at different applications:
- online ECG-classification (for comparison reasons only)
- offline 2D and 3D image processing
- online 2D and 3D image processing.

These applications differ in the number of variables involved and the restrictions of processing time:

- *two variables*:
  (a) intensity over time or
  (b) intensity over 1D-position.
  ECG-classification is a typical example of medical applications. The sampling rate of the A/D-conversion is 200 Hz, the intensity resolution is 256 steps. This results in 8 bit every 5 ms, i.e. the data-transfer rate is 1600 bit/s.

- *three variables*:
  intensity (grey-level + color) over position (area). The horizontal and vertical resolution of a 2D-image should be 512, 1024 or 2048 steps in either direction. Each sample is characterized by an 8-bit grey level (256 intensity levels) and a 4 to 8 bit color information (16 to 256 colors). These resolutions have turned out to be sufficient for present image processing applications. Under these circumstances, the total data quantity of a 2D-image varies from 10^6 to 10^8 bit.

- *four variables*:
  (a) intensity over 2D-position and time
  (b) intensity over 3D-position.

  (a) Time constraints to 2D-image manipulations are given by the frame rate. The frame rate on the one hand depends on the resolution of time-dependent processes (e.g. flow processes), on the other hand on the human eye which expects to observe a continuous motion despite time-discrete displaying. This requires a frame rate greater than 20 per second. Typical frame rates are 33 Hz for ultrasound and 50 Hz for X-ray applications. The total processing time for one frame therefore varies from 20 ms to 30 ms. This gives a data-transfer-rate from 10^7 to 10^9 bit/s.
  (b) Similar to 2D-images, a single 3D-image offers a total data quantity of 10^9 to 10^{11} bit.

- *five variables*:
  intensity over 3D-position and time.
  Online 3D-image processing is the most expensive case of large data-transfer-rates. According to the above mentioned online 2D-image processing, te data-transfer-rates vary from 10^{10} to 10^{12} bit/s.

In order to summarize the above results we introduce the variable "instructions per second" (IPS) as a characteristic value for the computing power required to meet the requirements of offline and online image processing. All estimations base on a computing effort of 100 instructions per pixel (picture element $\hat{=}$ pixel) executed on a 8-bit computer. They should be interpreted as orders of magnitude not as exact values:

- ECG-filtering and -classification
  (200 Hz sampling rate, resolution 8 bit)
  $2 \cdot 10^4$ IPS
- 2D-image manipulation (offline: 10 s)
  ($1024 \times 1024 \times (8 + 8)$ bit)
  $2 \cdot 10^7$ IPS
- 2D-image manipulation (online 50 Hz)
  10^{10} IPS
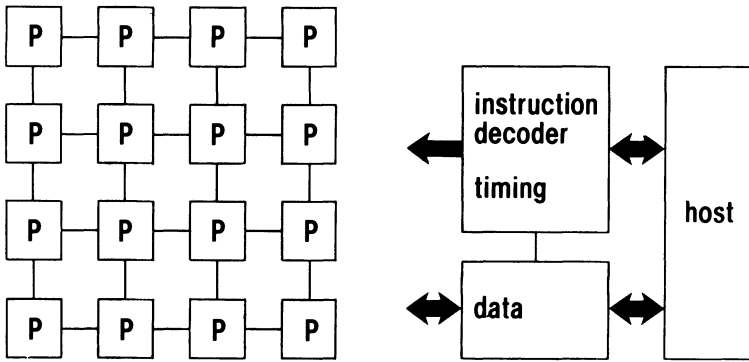
Figure 4. Array-computer.

- 3D-image manipulation (offline: 10 s)
  ($1024 \times 1024 \times 1024 \times (8 + 8)$ bit)
  $2 \cdot 10^{10}$ IPS
- 3D-image manipulation (online 50 Hz)
  10^{13} IPS.

If we look to the actual technological restrictions, we see that due to switching times from 10^{-9} to 10^{-6} s, the maximum *processing rates* vary from 10^6 IPS (micro-computers and minicomputers, inexpensive) to 10^9 IPS (super computers, very expensive). That means that only 2D-image processing with simple manipulations are feasible whereas complex 2D-manipulations and 3D-manipulations can be realized offline only. Future development in technology will not provide a *speed-up* in computing power more than 10^2 to 10^3 for single processors so that complex online manipulations are very restricted.

4. DESIGN OF COMPUTER ARCHITECTURES FOR IMAGING

All estimations have been made under the assumption that only a single processor is used. Improvements in processing speed can be achieved by:

- *hardware support* for important functions such as scrolling, zooming, histogram, addition and subtraction of frames, simple filtering. The gain in speed versus software realizations range from 10 to 100. The specialization along with hardware implementation produce high-technology special-purpose computers.
- *parallel computation* by multiple processing elements. Given, that the computation of an algorithm in image processing consists of several widely independent tasks, these tasks can be computed by specialized processors sequentially. The different stages of computation can be used simultaneously for different data. This parallel processing is called *pipelining*.
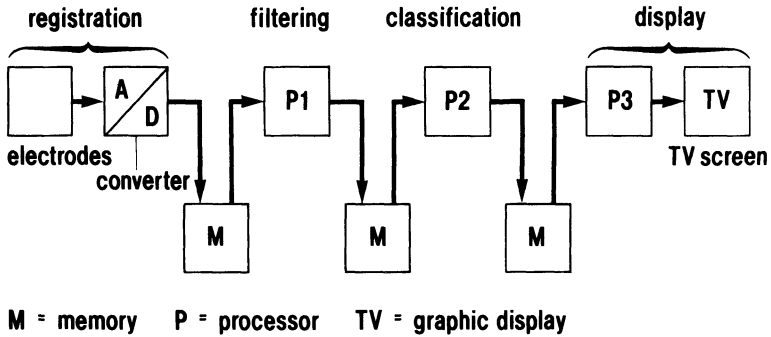
Figure 5. Pipeline-computer (e.g. ECG-classification).

Digital image representation involves a great quantity of data (pixels). For a lot of manipulations based on *matrix-operations* parallelism can be achieved at the data level. One single algorithm has to be executed on each of the pixels and the computation of a single pixel is not dependent on other pixels or depends only on a very restricted environment (kernel). That means, that data exchanges occur mainly to neighbor pixels, so that the appropriate computer architecture is the *array* (Figure 4).

These two types of computer architectures can be classified by a scheme proposed by Flynn according to the number of data and instruction streams. The four different classes are:

- single instruction single data stream   SISD
  (single processor system)
- single instruction multiple data stream   SIMD
  (array processor system)
- multiple instruction single data stream   MISD
  (pipeline processor system)
- multiple instruction multiple data stream   MIMD
  (multiprocessor system).

Let us consider two examples for pipeline and array computers:

(a) *Pipeline computer*
The above mentioned ECG-filtering and classification fits well into this class (see Figure 5). The analog signals of the electrodes are converted to digital information and stored into memory. Processor P1 is specialized (by software or hardware) for filtering 50 Hz noise and other distortions involved in ECG-registration. The filtered data are presented via memory (called mailbox) to processor P2 which classifies the ECG-signals and gives the results to processor P3 for output on

graphic-display. This procedure transmits data through a pipe. The slowest stage determines the *throughput-rate*. Parallelism is given by the fact that the number of data involved simultaneously is the number of stages in the pipe. Since this number is very restricted, the speed-up due to parallel computation is rather small but greater due to the specialized stages.

(b) *Array-computer*

All processing elements in an array usually provide restricted computing capacity compared to minicomputers, for example. The elements are specialized in very important functions for matrix-manipulation as add, subtract, multiply, divide and compare. Since only one or a few data are handled by one element at a time, the memory capacity is rather small. The large speed-up in total processing rate is achieved by the *synchronous* execution of instructions which are fetched from program memory and decoded only once for all processing elements. Input and output is performed by a *host computer*.

Parallel computation in an array can be demonstrated very well with 2D-image filtering. The filter algorithm requires that the grey-level of each pixel be replaced with the mean grey-level of its environment (e.g. 4×4 or 16×16 kernel). Since the computation of each pixel does not depend on the computation of any other, the filtering can be done simultaneously. Maximum speed is achieved if the dimension of the array corresponds directly to the image to be processed. That means, a 1024×1024-image can be computed by 1.048.576 processing elements at maximum. Latest developments in array processors involve $128 \times 128 = 16384$ elements at unknown costs. This proves that the maximum parallelism in image processing cannot be fully exploited because of difficult hardware implementation and too high costs.

For the above reasons, typical medium-cost image processing systems today are *special-purpose computers* with multiple pipelines and hardware support for elementary operations. Array processors are mainly used in high-cost high-technology systems. The features of such a typical medium-cost system are:

- input rate: 10^7 bit/s, 16 frames memory
- online: 30 frames per second
  addition, subtraction of frames, zooming transforms (1D-Fourier, Hadamard, exponential)
- nearly online: histogram, convolution, noise filtering
- some minutes: classifications, Gaussian filter, 2D-Fourier.

5. REGISTRATION OF DIGITAL IMAGES

Digital image registration is another important area in image processing, since it allows for fast and accurate access to stored information for offline computations. An estimation demonstrates the required storage capacities and data-transfer-rates for an *image sequence registration*:

- image sequence registration over 10 seconds (2D)
  ($1024 \times 1024 \times (8 + 8)$ bit, 50 frames per second)
  → data transfer rate: 10^8 bit/s
       required capacity: 10^9 bit $\approx 10^8$ byte
- image sequence registration over 10 seconds (3D)
  ($1024 \times 1024 \times 1024 \times (8 + 8)$ bit, 50 frames per second)
  → data transfer rate: 10^{11} bit/s
       required capacity: 10^{12} bit $\approx 10^{11}$ byte.

Unfortunately, actual *mass storages* as disks or tapes provide capacities from 10^8 to 10^9 byte and transfer rates up to 10^7 bit/s. That means, that online 2D-image registration is possible today only with sophisticated hardware. 3D-image registration with digital representation over periods of some seconds will be impossible in the near future.

6. IMAGE SEQUENCE PROCESSING SYSTEM ISPS

The above treatment shows, that main image processing problems are designing appropriate computer architectures and applying numerical algorithms in an inexpensive (memory space and computation time) way.

For application the Rogowski Institute has developed a system to handle the following subtasks:

- real-time data acquisition for scenes
- transient recording
- image enhancement by real-time filtering
- fast off-line data processing.

The overall system architecture of the Image-Sequence Processing System is shown in Figure 6. Opposed to conventional structures of data processing systems, this architecture contains multi-port devices. By this we allow implementation of data flow concepts and parallel processing and we avoid the "von Neumann bottleneck" due to a single link between memory and control/operation units of classical computing systems.

The most important component of the system is a 3-port paged memory which is used
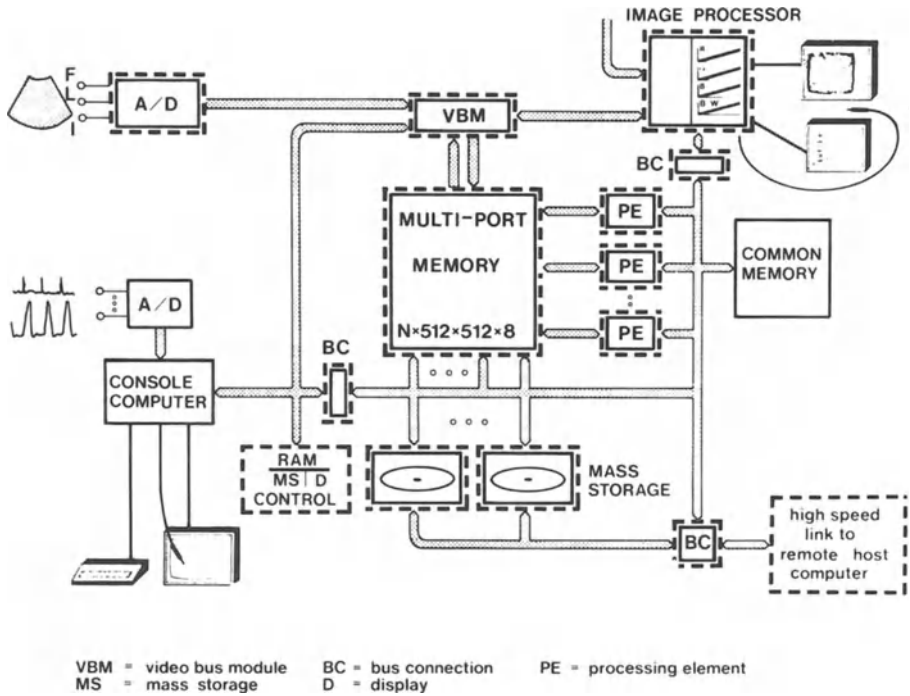
Figure 6. Image Sequence Processing System (ISPS).

- to input digitized analog data or output data for video display
- to transmit data to disk drives
- to allow the processing of image data by several processing elements in parallel.

The memory therefore is accessed by

- display processor (basic manipulations)
- A/D converter
- multiprocessor system
  (complex operations, SIMD-mode supported)
- console computer
  (registration, I/O)
- host computer

The results show, that this architecture fulfills all our specifications and guaranties an efficient software implementation. The high performance is achieved by parallel data handling and processing due to multiport devices and a multiprocessor system with independent data paths.

REFERENCES

1. Cannon TM, Hunt BR: Image processing by computer. Sci Am 245:214–225, 1981.
2. Driscoll T, Walker C: Evolution of image processing algorithms from software to hardware. International Imaging Systems, Milipitas, California, internal paper no 2.
3. Jensch P, Ameling W, Kubalski W, Heuck N, Meyer J, Effert S: A data aquisition and processing system for sequences of ultrasound echoes and video images. Comput Cardiol, Williamsburg 1980, IEEE 1980, CH 1606–3/80, 227–230.
4. Ameling W: Rechnereinsatz bei der Echtzeit-Datenverarbeitung in der Medizin – Probleme und technische Möglichkeiten. Biomed Techn 24:67–70, 1979.
5. Meyer J, Hagemann K, Jensch P, Platte G, Ruppert G, Ameling W, Effert S: Umfassende On-Line-Berechnung von Kontraktilitätsparametern mit einem Computersystem – Möglichkeiten und Probleme. Verh Dtsch Ges Kreislaufforschung 42:271–274, 1976.

2. DIGITAL OPTICAL RECORDING – THE KEY TO MASS PICTURE STORAGE

D. MEYER-EBRECHT

ABSTRACT

Digital imaging is being increasingly applied in diagnostic medicine. New digital image modalities are extending the range of diagnostic techniques, and it is anticipated that novel imaging technologies will gradually replace the traditional photographic X-ray process. They all produce digital data sets which are far beyond those data volumes handled by conventional computer systems. New technologies are, therefore, required to build distributed picture information systems which support the user during acquisition and evaluation of all the types of pictures. Key components of such systems are storage modalities. Storage systems to store millions of pictures which are needed for background storage, i.e. picture archives, will be feasible by the application of the Digital Optical Recording (DOR) technology. Digital optical disks of 30 cm in diameter will store $1.6 \cdot 10^{10}$ bit of data which is equivalent to some 10.000 digital pictures such as CT or some 1000 digitized large format X-rays. Digital Picture Archiving and Communication Systems based on this technology will probably have an essential impact on the way of operating with pictorial information in diagnostic medicine.

INTRODUCTION

Digital Optical Recording (DOR) has much popularity in the picture processing community because it outperforms any other established storage technology with respect to storage density and storage costs. Therefore, when considering the amount of bits per digitized picture and the number of pictures produced every year, DOR seems at present to be the only realistic solution for digital mass picture storage, which in turn is a highly desirable modality because it will extend the functions of computer systems to support the routine work with pictures. Moreover, besides simply replacing a hospital's picture archive and providing immediate access to pictorial information at any workplace, the digital Picture Archiving and Communication Systems (PACS) [1] will provide the necessary infrastructure to embed the growing number of digital imaging and image processing modalities. Because of its importance as a key component we will dedicate this lecture to an
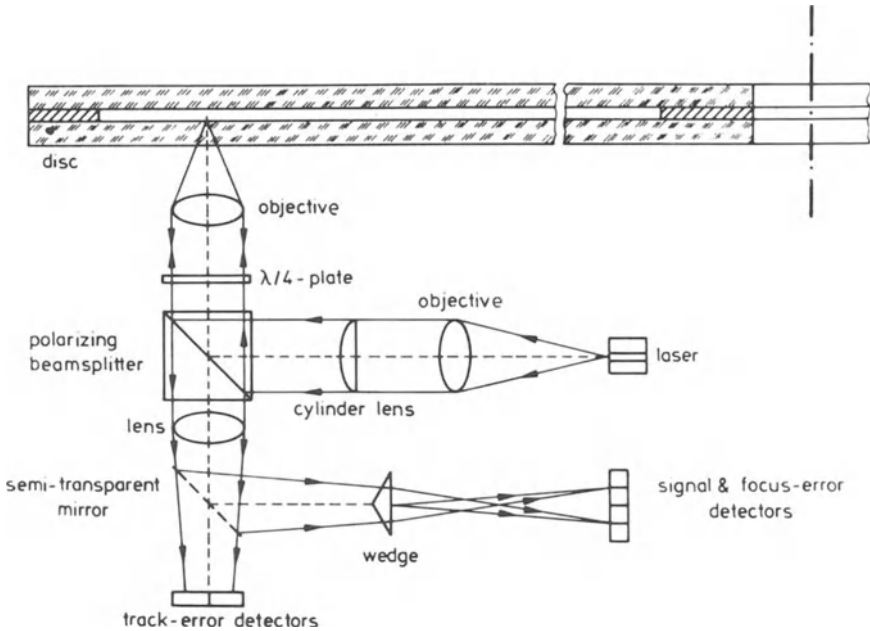
Figure 1. Functional scheme of the DOR mechanism: disk sandwich (top), laser and detector optics for write and read (bottom).

introduction into the DOR technology, and discuss how a DOR-based PACS could make an impact on the daily work with pictures in diagnostic medicine.

DIGITAL OPTICAL RECORDING: AN INTRODUCTION

The concept of optical information recording is based on the application of lasers and optics to produce, on the surface of a spinning disk, patterns at a resolution close to the wavelength of light, thus achieving a very high information storage density. This storage concept found its first applications in the consumer area, viz. the Video Long Play (VLP) disk and the Compact Disk (CD) for audio. Both approaches start with writing a spiral track with the analog resp. digital signal pattern onto the light sensitive surface of a master disk from which, in a fabrication process similar to that of conventional grammophone records, the final *pre*recorded VLP's or CD's are derived.

Many of the principles and production techniques applied for the consumer disks are also used for the professional Digital Optical Recording (DOR) approach which, in contrast to the prerecorded consumer disks, provide the user with the possibility of writing information, and reading this information immediately after recording at random access [2, 3, 4]. The DOR storage medium is again a disk of
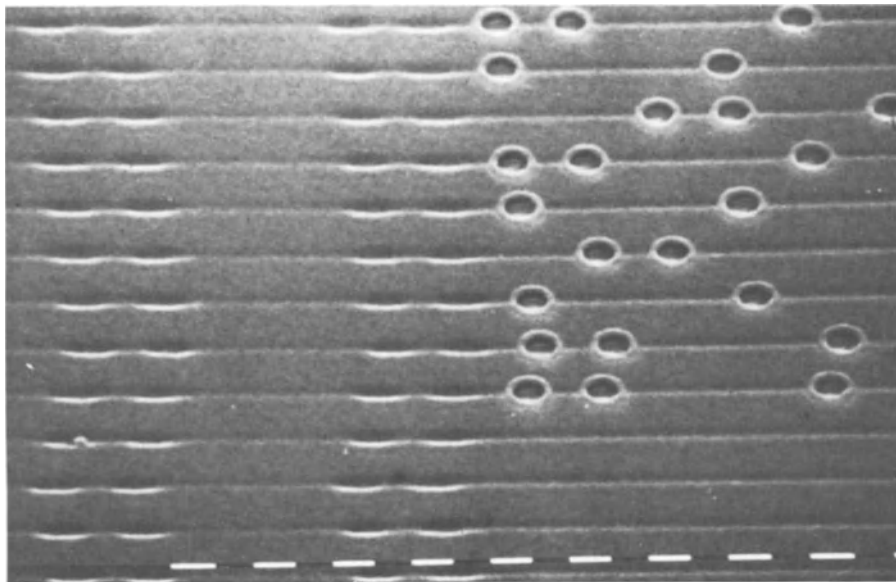
Figure 2. Electron microscope photograph of DOR disk surface: holes of less than one micron in diameter burned by the laser (top right), pre-recorded sector heading codes (left), three empty grooves and scale of micron units (bottom).

30–cm diameter. The disk is formed from two glass substrates placed back-to-back in a sealed air-tight construction ("sandwich") (Figure 1, top). Evaporated metal layers are fitted to the inner surfaces of the substrates on top of a spiral groove which is equivalent to 32,000 circular tracks. The groove is used to track the beam of a solid-state laser by means of an electro-mechanically deflected lens-and-mirror system (Figure 1, centre), and to focus it onto the middle of the groove. Switching the laser from low-power to full-power will result in melting holes of below one micron diameter into the metal coating (Figure 2). These holes represent the user-recorded bits.

In practice the DOR disk is not a completely empty disk. Rather, the prerecorded groove is structured into sectors, and track and sector addresses are prerecorded in so-called sector headers. Further, a complex data coding and decoding scheme is applied for the sake of error protection resulting in an error rate of 10^{-12}. In spite of these means the net data capacity is about $1.6 \cdot 10^{10}$ bits on both sides of a disk. Comparing the recorded bits per unit volume, this density is far beyond any conventional computer storage medium.

A further advantage of the DOR disk is its rugged and compact design. Handling for the purpose of exchanging disks on the recorder drive is as simple as handling, for example, floppy disks. Also, automatic disk exchange has already been practiced by a so-called "juke box", which will be the key to far larger data stores.

Finally the lifetime of the disk will be much longer than that of magnetically recorded data. Accelerated life tests give rise to anticipation of a guaranteed lifetime of far beyond ten years. Thus the persistency of recorded data due to negligible ageing effects as well as due to the inherent principle of non-erasable recording seems to be an ideal pre-condition to meet legal requirements for picture archive integrity.

AN ELECTRONIC HOSPITAL PICTURE ARCHIVE BASED ON DOR

A DOR is not yet an electronic picture archive, although it will obviously be the key component of it. When considering picture archives of several millions of pictures (e.g. a hospital's picture production during a period of ten years) an appropriate structuring into a hierarchy of storage levels becomes necessary.

The basic storage medium will be the digital optical disk with a storage capacity of $1.6 \cdot 10^{10}$ bits. This corresponds to between 10^3 and 10^4 pictures per disk depending on the type of picture (see Table 1). Accompanying α-numeric information will occupy only a negligible additional storage space if it is directly typed in. Otherwise written documents could be scanned with a facsimile scanner and processed like pictures.

A complete electronic picture archive will, therefore, contain several thousand disks. The question arises of how the access to that amount of disks can be made sufficiently fast. Fortunately, in general there is a strong decrease of the average retrieval frequency as a function of the age of the retrieved pictures. Pictures are most frequently retrieved during the stay of a patient (some weeks), less frequently during the first two or three years, when follow-up investigations may occur, and far less frequently during the following years. Although this situation may change to some degree as a result of the faster and more convenient access to electronic picture archives, it will still be an acceptable archive strategy to have access time increase as the duration of the storage also increases.

This feature results in a picture base structure (see chapter 4.3 in [5]) where one or more optical data disks containing only the most active pictures are mounted on DOR drives – the highest storage level within a storage hierarchy. At this level the

Table 1. Data volumes of digitized pictures

Large format X-ray film	2000^2 pel @	8 bit =	32 Mbit
High-resolution X-ray TV frame	1000^2 pel @	8 bit =	8 Mbit
CT scan	512^2 pel @	12 bit =	3 Mbit
Ultrasound scan	512^2 pel @	4 bit =	1 Mbit
Radionuclide scan	256^2 pel @	6 bit =	0.4 Mbit
A4 Page, typewritten, coded	2500 char. @	8 bit =	20 kbit
Facsimile scan of A4 page	$1700 \cdot 2300$ pel @	1 bit =	4 Mbit

latency time, i.e. the average time of physical arrival at the start address of the desired picture, will be a fraction of a second as determined by the limitations of the disk drive actuating mechanism. Optical data disks with older pictures will be stored in a "juke box" at the second storage level. Access to the desired disk and its transport to a disk drive could be performed in less than 10 sec, provided that a linear arrangement of disks limited to a capacity of about 100 disks is used. Instead of employing a large number of linear "juke boxes" it may be a cheaper solution to store, at the lowest storage level, those disks containing very old pictures in a two-dimensional disk exchange unit. Due to the more complicated disk transport mechanism a latency time beyond 10 sec will probably have to be tolerated at this level.

If non-erasable optical data disks are used throughout the picture base it would not be convenient to re-organize the archive. As a result, in some applications related pictures which are filed at different times will be located on different disks at different storage levels. The retrieval of sets of related pictures (e.g. when scanning the case history of a patient over a period of several years) may be speeded up by means of a management and control system which transfers pictures due for retrieval into a magnetic disk foreground memory at the highest storage level immediately after the first picture of a sequence has been accessed.

SOME CONSIDERATIONS ON THE IMPACT OF ELECTRONIC MASS PICTURE STORAGE

An electronic picture archive based on DOR storage devices can be regarded as a one-to-one replacement of the current hospital film archive if the storage system is equipped with appropriate picture input and picture output devices such as high resolution laser film scanners and grey-level hardcopy devices [6, 7]. To make full use, however, of the potential of electronic picture storage it will be required to implement three further logical steps:

- direct connection of all electronic image sources,
- introduction of terminal-type picture workstations with direct connections to the picture archiving system, and, finally,
- integration of the resulting Picture Archiving and Communication System (PACS) with existing Hospital Information Systems (HIS).

It is obvious that the growing number of electronic imaging modalities is strongly stimulating the development of PACS. Indeed it is an unsatisfying situation to operate a highly sophisticated digital imaging machine such as a CT while being constrained to archive the high-quality digital picture on film at a strongly limited performance. On the other hand the availability of a suitable digital background will certainly stimulate the introduction of novel image pick-up devices such as Large-Area Detectors (LAD) or high-resolution Image Intensifier TV cameras
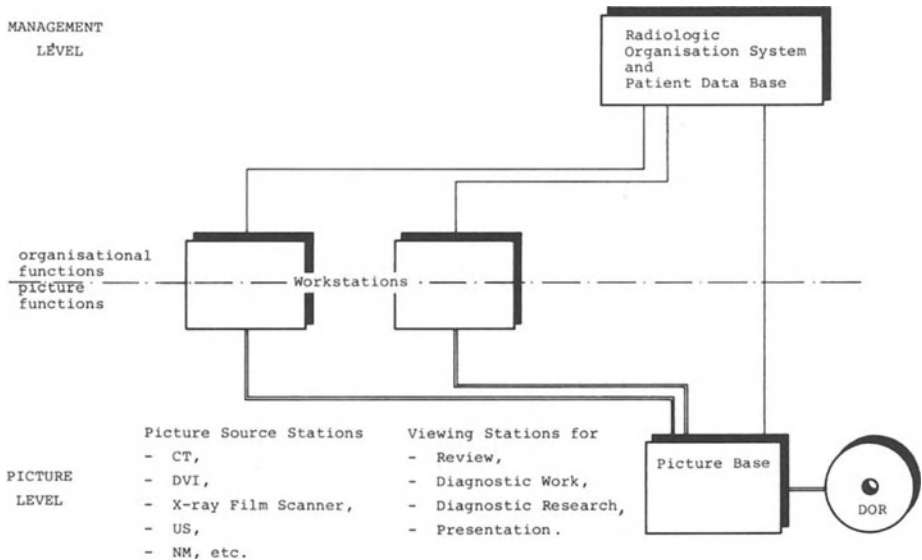
Figure 3. Hierarchical concept for a distributed picture information system.

which can potentially replace the photographic film in a number of diagnostic applications.

The concept of the Digital Diagnostic Workstation, though being the next logical extension, will certainly be a far more critical item, because it would possibly cause essential changes in the work of medical personnel. We are anticipating that display terminals will be available which will offer

- high-resolution display capabilities (at least 1000^2 pel display with "real time" zoom and scroll options etc.),
- response time (period elapsing between a user command and the completion of a retrieval or processing operation) of a few seconds at maximum, and
- extended processing capabilities (manipulation, enhancement, quantitative evaluation etc.).

A research prototype of such a workstation which employs a novel picture computer architecture is currently under investigation at our research laboratory.

It will be a point of major research interest to optimize the man–machine interface, and tailor it to the specific needs of the medical user. Provided that the technical, ergonomic, and psycho-visual problems will be solved, then we assume that the advantages of

- having immediate access to all filed pictures,
- applying picture manipulations and processing under visual control, and

Figure 4. Experimental PACS based on an early laboratory prototype of a DOR drive, and a laboratory model high-power picture processor for workstation application.

- being supported by convenient data base functions (delivery of related alpha-numeric information, and guidance to the desired pictures)

will balance well against the inconvenience of changing from the present light-wall viewing to a display-oriented work.

A final step towards a consistent diagnostic documentation system must be the integration of pictures and all other types of diagnostic data. From a systems architecture point of view it is recommended to maintain a strict separation of pictorial information and all other types of information – physically. Logically the picture storage system should be treated as an extension of the hospital or departemental patient data base, to which the user will have access from his diagnostic workstation in a well-established manner [8] (Figure 3). First experiments are being performed in a laboratory environment applying a prototype DOR system under the superior management of the Philips RADOS System (radiologic department data base and organisation system) [9] (Figure 4).

20

ACKNOWLEDGEMENT

REFERENCES

1. Duerinckx AJ (ed): Proceedings of the 1st International Conference and Workshop on Picture Archiving and Communication Systems (PACS) for Medical Applications, Vol 318, SPIE, Bellingham, Washington, 1982.
2. Bulthuis K. et al: Ten billion bits on a disk. IEEE Spectrum 16:26–33, 1979.
3. Kenney GC et al: An optical disk replaces 26 mag. tapes. IEEE Spectrum 16:33–38, 1979.
4. Digital Optical Recording: Introduction to DOR. Philips Data Systems Nederland BV, The Hague, The Netherlands.
5. Bell AE (ed): High Density Optical Recording, Van Nostrand Reinhold, New York, 1982.
6. Killat U: Modern optical methods for the storage of radiographs. In: Orton CG (ed), Progress in Medical Radiation Physics, Plenum Press, New York, pp 323–376, 1982.
7. Meyer-Ebrecht D et al: Medical picture base systems. In: Höhne K-H (ed), Digital Image Processing in Medicine, Lecture Notes in Medical Informatics 15, Springer, Berlin, pp 133–148, 1981.
8. Meyer-Ebrecht D: The management and processing of medical pictures: an architecture for systems and processing devices. In: Proc. IEEE Workshop on Picture Data Description and Management, Asilomar pp 202–206, 1980.
9. Meyer-Ebrecht D et al: A laboratory prototype system for the archiving of CT pictures on optical disks. SPIE Proc 318: 303–310, 1982.

3. ADVANCES AND PERSPECTIVES IN ULTRASOUND TECHNOLOGY

R. HAUKE

The pulse-echo method can be divided into three areas of technology with respect to the medical application.

These are compound-scan, B-scan and sector scan systems. The decision about which system is used for which examination is mainly given by the available acoustic window, resolution and scan speed required for medical diagnosis. It is known that compound systems have slow frame rates but a very good contour resolution (Figure 1). It is not possible to visualize structures which are almost parallel to the direction of propagation of the ultrasound pulse. To get the complete contour of the boundary, one has to project the structure by different angles in order to get the complete contour information. An example is given in Figure 2, where a foetal head is imaged with a sector scan system, demonstrating clearly the lack of contour resolution. In linear-array-systems the lack of complete contour information is often due to shadowing which occurs, for example, behind highly reflecting or absorbing tissue or stones (Figure 3). Again, using appropriate compound techniques (different projections of the same target) it is possible to get complete information (Figure 4). Moreover, the resolution can be improved [1]. In order to get faster imaging, Kossoff [2] has proposed an automated compound system (Octoson) using up to eight mechanical sector scanners simultaneously but real-time for cardiac application is still not obtained (Figure 5).

In achieving real-time, the first approach used mechanical B-systems of the Vidoson type. It turned out that the frame rates were still limited and that the handling of the mechanical transducer was not acceptable. Therefore the development led to linear arrays with microangulation where high speed switching of groups of transducer elements with electronic focussing is possible (Figure 6).

For applications where only small acoustical windows (especially cardiology) are available, there is a strong demand for sector scanners. In the past, mechanical systems were used (Figure 7). The development here replaced the mechanical systems by electronic beam steering and focussing devices using so-called phased array systems [3]. The advantage of electronic systems is the high flexibility of image formation. Due to this fact it is possible to get simultaneously not only the sector image (Figure 8a), but, by appropriate ECG gating, systolic and diastolic images (Figure 8b) or several TM displays (Figure 8c) with B-display, or even TM and Doppler information at the same time (Figure 8d).

22
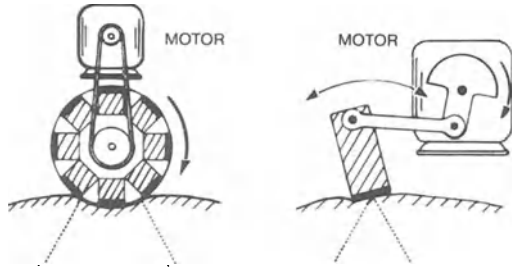
Figure 1.   SEVERAL ROTATING TRANSDUCERS   SINGLE OSCILLATED TRANSDUCER

Figure 2.

Figure 3.
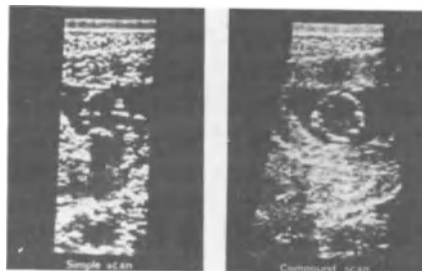
Figure 4.
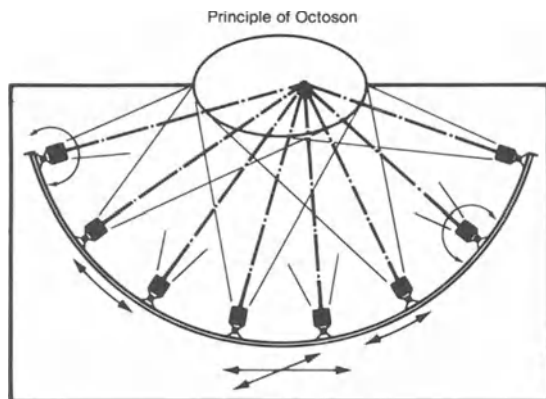
Figure 5.
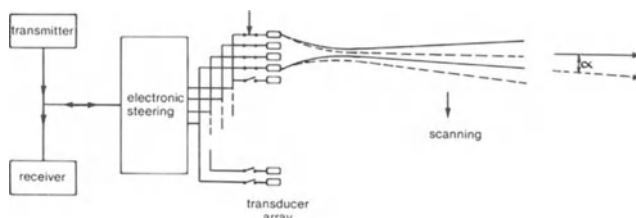
Figure 6.
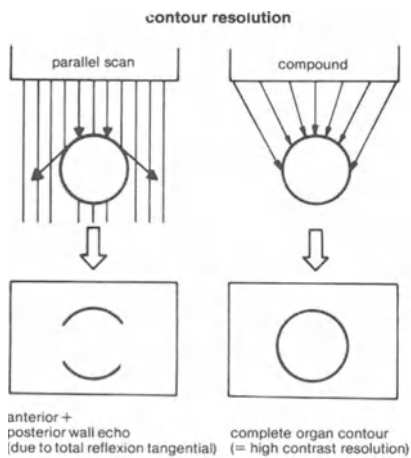
Figure 7.
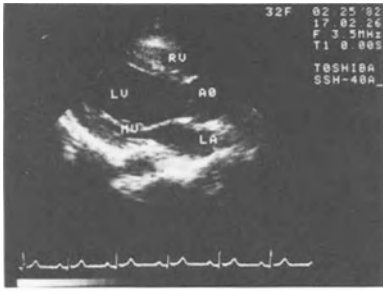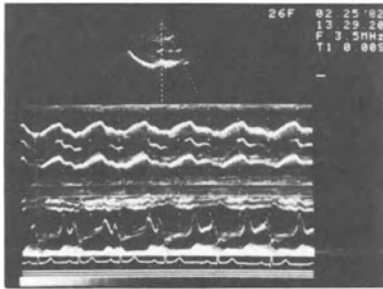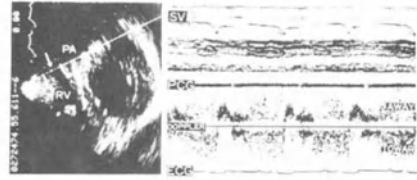
24

(a)

Figure 8.

(b)

(c)

(d)

Figure 9.

Summary

Compound ⟶ automated RTC
Mech. B-Scan ⟶ Linear Array } MULTI MODE
Mech. Sector ⟶ Phased Array } LINEAR ARRAY

only disadvantage: price?

parallel scan   angulated scan

sector scan   trapezium scan

compound scan
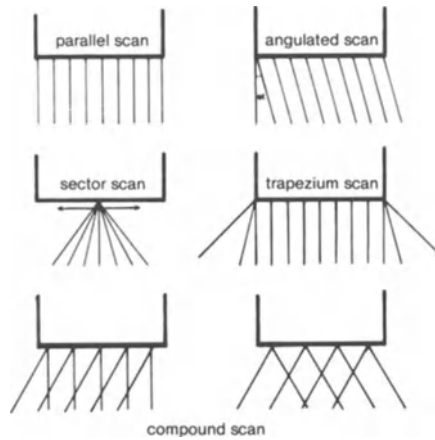
Figure 10.

Figure 11.

(a) (b) (c) (d)
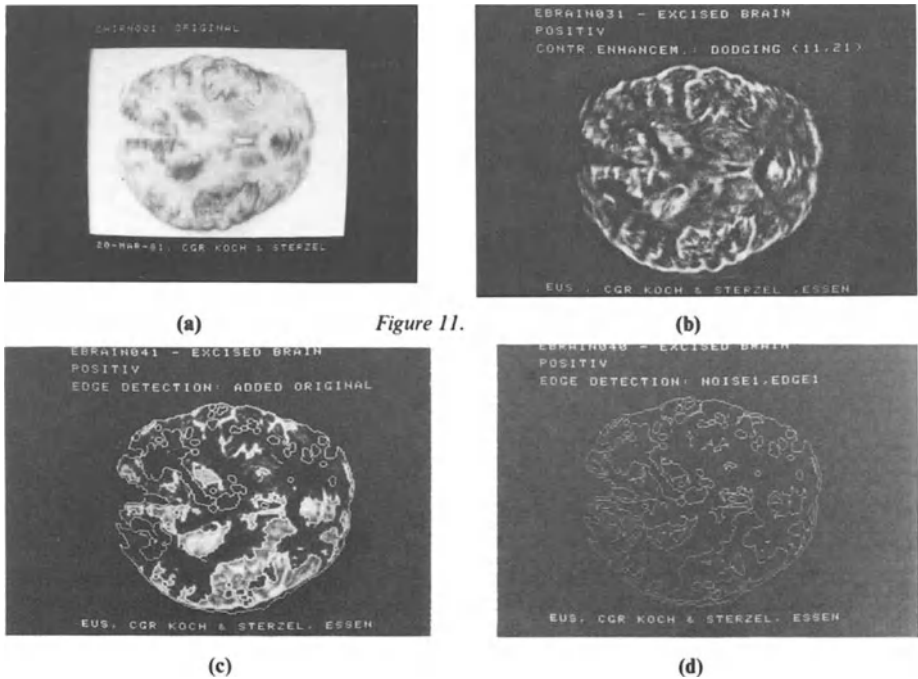
Above is a summary of the history of the replacement of mechanical systems by electronic scanners. As indicated in Figure 9 a future system which could combine all applications in one system would be a Multimode Linear Array. Figure 10 gives the different types of scan modes which could be produced using the same tranducer without any mechanical displacement.

Using this technology [4] the following results were obtained in neurology: Figure 11 a gives the ultrasonic image of an in-vivo-brain.

Figure 11b shows the same object after using a 11×21 filter mask for contrast enhancement. Figure 11c gives the result of automatic contour detection and Figure 11d is the superposition of 11a and 11c.

In cardiology similar results can be obtained using the same technology. Figure 12a and b demonstrate some resolution limits for cardiac applications in the use of an exised heart. Left ventricle (LV), right ventricle (RV), intra ventricular septum (IVS) and trabecular structures are clearly shown.

In cardiology high resolution real time images can be obtained by segmented real time compound (RTC), where only some projections are used for image formation. For higher image rates one could restrict the compound imaging to a small limited area or segment.

In conclusion the impact of using Multimode Linear Array (MMLA) in cardiology would be:
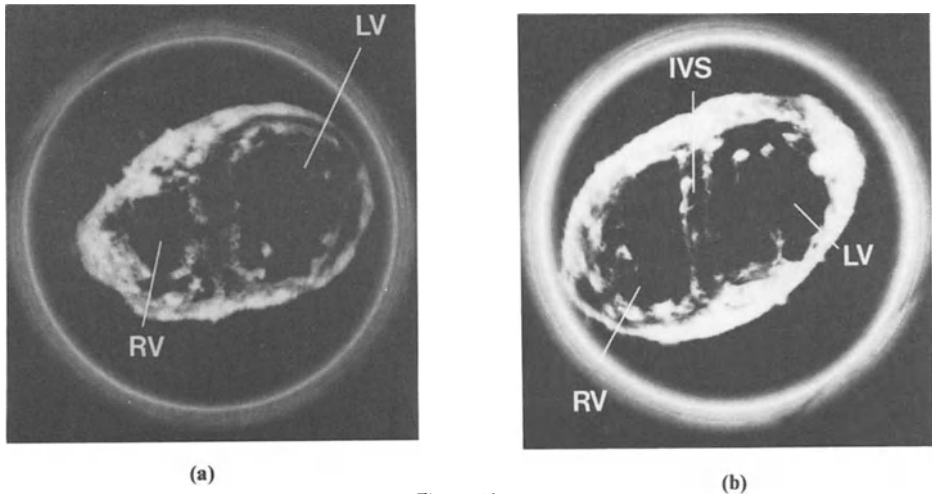
Figure 12.

1. high resolution imaging (segmented RTC)
   (a) precision of volume measurement improved
   (b) automated tracing of ventricular edges
   (c) differential diagnosis improved (infarcted areas ...)
2. greater field of view, even proximal
3. Doppler improved, giving better flow results
4. increased possibility of computer aided information extraction.

REFERENCES

1. Frank, Schneekloth, Albers, Hauke: Ultraschalltomographie abdomineller Organe und der Schild-drüse, Ferdinand Enke Verlag. To be published May 1983.
2. Kossoff G, Carpenter DA: Octoson – A new rapid general purpose echoscope. In: White D (ed), Proceedings of the 20th Annual Meeting of the American Institute of Ultrasound in Medicine. Ultrasound in Medicine, Vol. 2, p 333, Plenum Press, New York, London, 1976.
3. Somer JC: Electronic sector scanning for ultrasonic diagnosis. Ultrasonics 6:153, 1968.
4. Hauke R: Computerisiertes Ultraschall-Sector-Scan-System zur intracraniellen Diagnostik. BMFT Vorhaben 01VI097-ZK/NT/MT 224 A, p. 118, 1982.

4. AUTOMATIC EVALUATION OF LEFT VENTRICULAR CONTOUR FROM TWO-DIMENSIONAL ECHOCARDIOGRAPHY

E. van Ocken, P. Schenkels, V.A. Claes and D.L. Brutsaert

The present study describes a method to evaluate left ventricular function by on-line digital storage and automatic contour detection of ECG synchronized two-dimensional echocardiography. The electronic sector scanner starts synchronized with the ECG (within 2.4 ms) and is connected on-line with the computer in order to store on disc all the two dimensional ultrasound frames over a period of at least 10 consecutive heartbeats (50 frames/s). To improve image quality and to reduce the noise, the pixels in corresponding frames of the 10 cardiac cycles are time averaged to one single cycle. From the grey levels in the averaged heart cycle, the contour of the left ventricular cavity is automatically outlined by the computer. The same procedure is repeated for each frame of the averaged heart cycle. The computer program provides a plot of the full set of contours throughout the cardiac cycle. To study regional heart function the contours can also be displayed as an unrolled 3D-surface which represents wall displacement versus time. A few clinical cases are presented illustrating the possibilities of this method to study left ventricular function in a more quantitative way.

INTRODUCTION

Two-dimensional echocardiography is normally used for qualitative observation of the heart structures and movement, but it can now also be processed as a quantitative non-invasive method for evaluating global and regional ventricular function. The main problem in quantification of 2D-echocardiography is to reduce the enormous amount of data stored in the consecutive heart frames in order to obtain an overview of the movement of the ventricular wall in space and time.

DATA INPUT

To manage this large amount of pictorial data in the image of a heart cycle, we interfaced on-line a two-dimensional echosystem (Toshiba SSH-10A) with a computer (Hewlett-Packard 1000F). The electronic sector scanner is switched to ECG-synchronized mode in order to resynchronize the frames with the ECG-timebase at
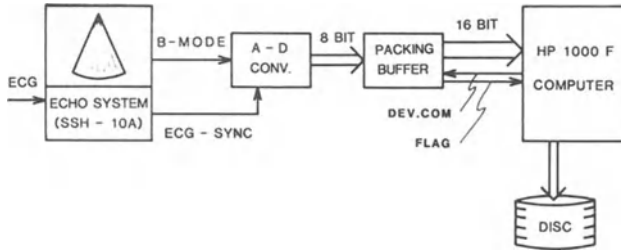
Figure 1.

each QRS-complex. The analog to digital converter converts the ultrasound B-mode information at a rate of 128 points (8 bit) per line. The data are sent in packed format to the computer. The input-procedure is elaborated to handle a continuous data flow coming from the echosystem interface and to store these data on a peripheral disk unit (HP7925-120Mbyte). The used data rate is 358400 points per second (128 points/line; 112 lines/frame; 25 frames/sec) and is far below the maximum possibilities of the input procedure (672000 points/sec). The total recording time is only limited by the available disk space. In our system a maximum of about 80 seconds of heart pictures can be stored, but for clinical use the recording period is mostly limited to 10 seconds. In this time, a sufficient number of heart cycles are available for averaging. Quantitative evaluation of the ventricular movement can be disturbed if the echo-quality is poor. In this case, a pre-treatment of the pictures is performed. The frames are stored in a consecutive way and at each QRS-complex the frames are resynchronized. Consequently the frames in each heart cycle are scanned at the same instant after the QRS-complex. If nothing has changed during the recording period, the corresponding pictures of the consecutive heart cycles should be equal and the pictures can be averaged linearly.

(Note: a hardware averaging interface is in preparation and will soon become commercially available from our laboratory.)

In the resulting averaged heartcycle the noise is remarkably reduced, resulting in improved delineation of the myocardium, and more particularly the endocardial contour can more easily be delined. This averaged heartcycle will be used as basic cycle for further automatic contour detection.

AUTOMATIC EVALUATION

In the analysis of the contraction of the heart, time dependence is very important. Therefore the resolution in time is improved by doubling the frame-rate. During the storage and the averaging of the data the pixels are treated as points of an individual echoline. The electronic sector scanner sweeps twice over the frame in interlaced mode. The frames composed of 112 echolines can be subdivided into two subframes of 56 echolines. The first subframe contains the odd, and the second one the even

ultrasound lines. In this manner we can increase the frame-rate from 25 frames a second to 50 frames a second. On the other hand, the line density is depressed by a factor of two, but this is due to the limited convergence of the echobeam. The spatial resolution is mainly limited by the lateral divergence of the echobeam, hence reducing the line density gives only a slight depression of the spatial resolution.

The contour detection proceeds as follows: the operator has to indicate by lightpen a point in the left ventricle on the end-systolic and on the end-diastolic frame, and a provisional systolic and diastolic contour will be filling up, calculated by the ventricular cavity. From the radius of the systolic boundary – decreased by one third – and that of the diastolic boundery – increased by one third – the inner and outer limits for the contour detection are fixed.

A problem for automatic outlining are the drop-outs in weakly echogenetic regions, e.g. where the ultrasound beam hits the wall tangentially. Therefore a coloured circle is traced as a safety belt around the ventricle (in order) to close the drop-outs and to avoid incorrectable artefacts in the calculation of inner and outer boundaries.

Between the smallest and the largest boundary contour the endocardium is outlined in each frame of the cardiac cycle.

DISPLAYING

Once all the contours are calculated, the computer provides a clear overview of ventricular performance in a clinical report where cross-sectional surface and volume are plotted versus time together with the ECG and the ejection fraction. Diastolic and systolic contours are also plotted. The continuous movement of the wall during the averaged heartcycle from systolic to diastolic contour is displayed in a three-dimensional graphial representation. The radius of the contour is plotted versus the different direction (angles form $0°$ to $360°$) and in the depth on a tilted axis the time is represented. This three-dimensional surface provides an aerial view of the systolic valley and of the diastolic hill. The plot can also been rotated horizontally over $90°$ for a better view-point of region wall motion.

CONCLUSION

By continous on-line computer storage, averaging and automatic computer detection of the endocardial contour of the left ventricle of each frame in the cardiac cycle, 2D-echocardiography has now been extended into a fast, fully non-invasive method for quantitative analysis of total as well as regional function of the heart.

5. CLINICAL IMPLICATIONS OF TRANSESOPHAGEAL ECHO-CARDIOGRAPHY PRESENT STATUS AND FUTURE ASPECTS

PETER HANRATH, MICHAEL SCHLÜTER, WOLFGANG THIER, BURKHART A. LANGEN-STEIN AND WALTER BLEIFELD

Imaging of the heart and its motion can provide valuable diagnostic information. However, cardiac imaging from standard transthoracic transducer locations can be compromised in a certain percentage of patients, mainly by the interposition of ribs and air-containing lung tissue between the ultrasound transducer and the target. In order to overcome these limitations, Frazin et al [1] introduced transesophageal imaging of the heart by M-mode echocardiography. He and others demonstrated the value of this technique as a diagnostic tool and as a unique approach to evaluate left ventricular performance during open-heart surgery or during exercise [2, 3, 4, 5, 6]. The feasibility of transesophageal cross-sectional imaging of the heart with a mechanical sector scanner or with a linear array scanner was reported in 1978 and 1980, respectively [7, 8]. In this paper we describe transesophageal cardiac imaging in humans with a specially designed phased array transducer system incorporated into the shaft of a commercially available gastroscope [9].

TRANSDUCER DESIGN

Two prototypes of endoscopic ultrasound systems were tested in our laboratory (Figure 1). One consists of a 3.5 MHz array of 32 elements attached to the flexible tip of a standard gastroscope (Figure 1, right hand side). It obtains cardiac cross-sections in a horizontal plane. The 3.5 MHz transducer head of the second system holds two adjacent arrays mounted at right angles to each other for horizontal as well as sagittal cross-sectional imaging of the heart (Figure 1, left hand side). The rigid parts of both systems are represented by the outer dimensions of the transducer heads which are $35 \times 15 \times 16 \, \text{mm}^3$ and $40 \times 17 \times 15 \, \text{mm}^3$, respectively. The shaft of the gastroscope-like probe has a diameter of 9 mm. Further technical information concerning transducer technology was given in detail by Souquet et al. [10].

TRANSESOPHAGEAL IMAGING TECHNIQUE

Investigations with the ultrasonic gastroscope are comparable to routine endo-
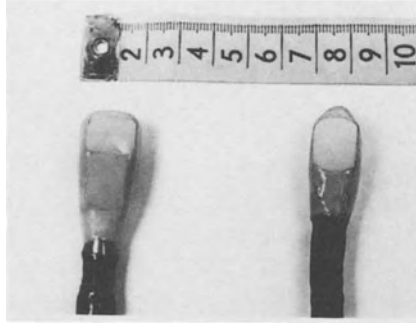
Figure 1. Transducer heads of two prototype ultrasonic gastroscope systems. Head on the right contains single array of 32 elements for horizontal cross-sectional imaging. Head on the left holds two adjacent arrays, one for horizontal and one for sagittal imaging.
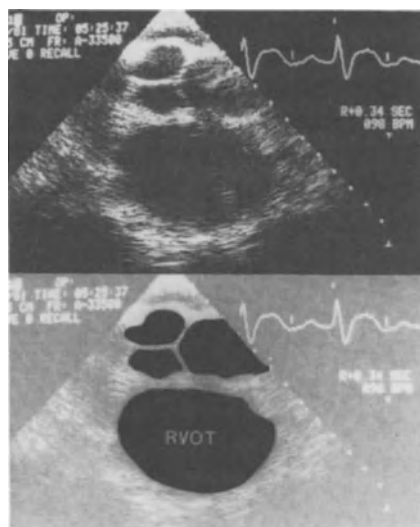
Figure 2. Aortic root with all three cusps in transesophageal short-axis view.
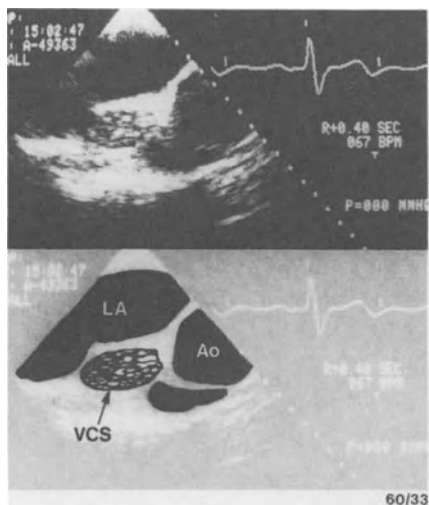
Figure 3. Transesophageal horizontal view with left atrium (LA), vena cava superior (VCS) and aorta (Ao). VCS is filled with echo contrast due to peripheral venous injection of saline.
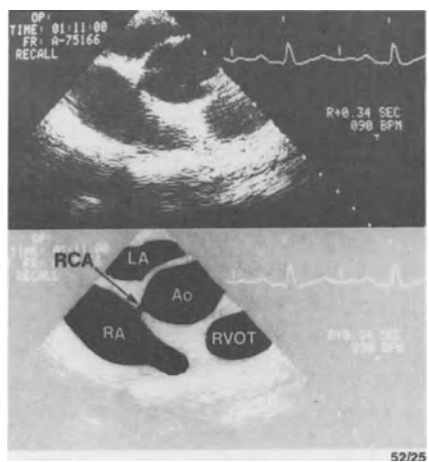
Figure 4. Transesophageal horizontal view showing ostium of right coronary artery (RCA). Ao: aorta. LA: left atrium. RA: right atrium. RVOT: right ventricular outflow tract.
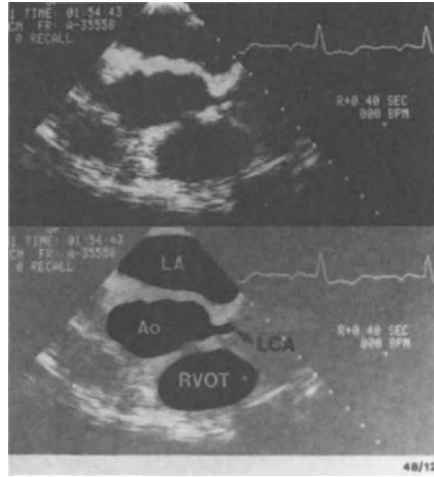
Figure 5. Ostium of left coronary artery (LCA) in transesophageal horizontal view. Left atrium (LA), aorta (Ao), and right ventricular outflow tract (RVOT) are also shown.

Figure 6. Transesophageal horizontal view at the level of the atrioventricular junction with left atrium (LA), mitral leaflets, left ventricle (LV) and left ventricular outflow tract (LVOT), interventricular septum, and right ventricle (RV).
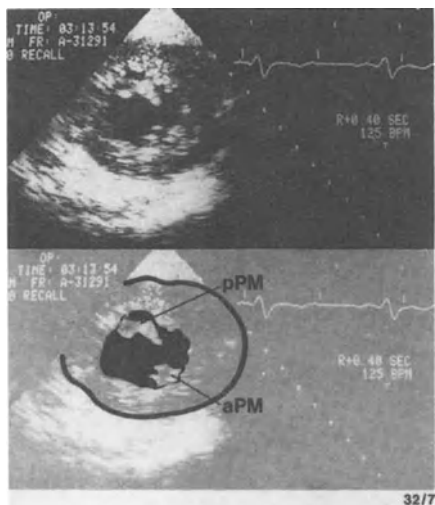
Figure 7. Transesophageal short-axis view of left ventricle at the level of the papillary muscles. aPM: anterior papillary muscle. pPM: posterior papillary muscle.
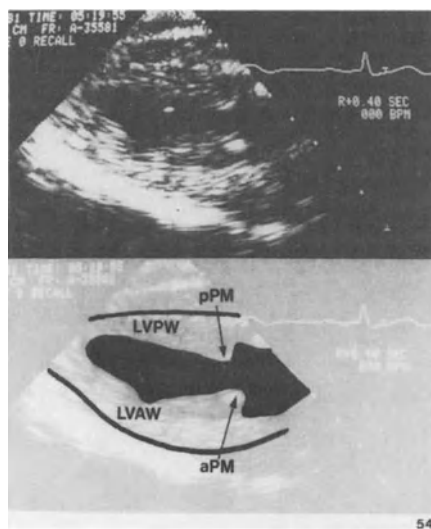
Figure 8. Transesophageal sagittal view of left ventricle at the level of the papillary muscles. Apical region to the left, mitral region to the right of figure. LVAW: left ventricular anterior wall. LVPW: left ventricular posterior wall. aPM: anterior papillary muscle. pPM: posterior papillary muscle.

scopic examinations. The gastroscope is introduced while the patient is lying in a supine position. The examination is done after the patient was fasted for about 8 hours. For sedation the patient usually receives 5 to 10 mg diazepam intravenously. Since fiber optics were replaced in this prototype, the probe is introduced blindly. An x-ray examination is performed in those patients where clinical history suggests a diverticulum of the esophagus.

IDENTIFICATION OF THE SITUS OF THE HEART

At a depth of about 40 cm from the patient's teeth the aorta ascendens at the level of the aortic root can usually be seen (Figure 2). Clockwise rotation of the endoscope will image the vena cava superior (Figure 3). By clockwise or counter-clockwise rotation of the probe at the level of the peripheral edge of the aortic cusps the origin of the right (Figure 4) or of the left (Figure 5) coronary artery can be identified. The left ventricular inflow and outflow tracts can be visualized by slightly advancing the gastroscope down the esophagus from the aortic root level and rotating counter-clockwise (Figure 6). At lower esophageal levels the transducer allows visualization of the left ventricle at the level of the papillary muscles (Figure 7) or of the apical region. By rotating the endoscope in a clockwise direction the different structures of the right heart can be seen. If the double array system is used, horizontal and sagittal cross-sections of the heart can be obtained from the same esophageal transducer position by activating the respective transducer array. A sagittal image of the left ventricle corresponding to the horizontal view of Figure 7 is shown in Figure 8.

Recently, efforts have been directed towards using this new technique as a monitoring device for the evaluation of left ventricular performance during surgery. The high resolution images allow monitoring of left ventricular function and size continuously during surgical procedures.

Transesophageal two-dimensional imaging of the heart adds a new dimension to the diagnostic application of cardiac ultrasonography as a complementory diagnostic tool or as an intraoperative monitoring device. Contours and motion of valves, cavities and great vessels can be easily identified by choosing the correct depth and transducer orientation within the esophagus. The proximity of the heart to the esophagus permits the use of high-frequency transducers, resulting in cardiac cross-sectional images of high spatial resolution. Interest in transesophageal cardiac imaging is presently increasing and various types of ultrasonic imaging devices for esophageal use have already been presented. All these devices suffered either from a rigid tip too large to allow use in man [8], or from mechanical vibrations [7], or from a very restricted field of view [8].

A miniaturized phased array transducer fixed to the distal end of a gastroscope has the advantages of being small in size and covering most parts of the heart within its 90° sector image.

Transesophageal two-dimensional images of the heart are generally less familiar

than those of transthoracic transducer locations. Since the long axis of the heart is oblique to the axis of the esophagus in the frontal as well as in the lateral plane and since the ultrasonic plane is either perpendicular or parallel to the esophageal axis, true long-axis views of the heart cannot be obtained with the present esophageal imaging system, whereas short-axis views at various left ventricular levels are possible with the horizontal phased array simply by transducer angulation. It is, however, important to examine the heart at angles oblique to the esophagus, i.e. parallel to the cardiac long axis, and we believe that this can be achieved with an esophageal phased array system which can be externally rotated about its normal axis.

REFERENCES

1. Frazin L, Talano JV, Stephanides L, Loeb HS, Kopel L, Gunnar RM: Esophageal echocardiography. Circulation 54:102–108, 1976.
2. Matsumoto M, Oka Y, Lin YT, Strom J, Sonnenblick EH, Frater RWM: Transesophageal echocardiography for assessing ventricular performance. NY State J Med 79:19–21, 1979.
3. Matsumoto M, Oka Y, Strom J, Frishman W, Kadish A, Becher R, Frater WM, Sonnenblick EH: Application of transesophageal echocardiography for continuous intraoperative monitoring of left ventricular performance. Am J Cardiol 46:95–105, 1980.
4. Hanrath P, Kremer P, Langenstein BA, Matsumoto M, Bleifeld W: Transösophageale Echokardiographie. Dtsch Med Wschr 106:523–525, 1981.
5. Kremer P, Hanrath P, Langenstein BA, Matsumoto M, Tams C, Bleifeld W: The evaluation of left ventricular function at rest and during exercise by transesophageal echocardiography in aortic insufficiency (abstr). Am J Cardiol 47:412, 1981.
5. Matsuzuki M, Matsuda Y, Yoshinobu I, Takahashi Y, Sasaki T, Toma Y, Ishida K, Yorozu T, Kumada T, Kusukawa R: Esophageal echocardiographic left ventricular antero-lateral wall motion in normal subjects and patients with coronary artery disease. Circulation 63:1085–1092, 1981.
7. Hisanaga K, Hisanaga A, Hibi N, Nishimura K, Kambe T: High speed rotating scanner for transesophageal cross-sectional echocardiography. Am J Cardiol 46:837–842, 1980.
8. DiMagno EP, Buxton JL, Regan PT, Hattery RR, Wilson DA, Suarez JR, Green PS: Ultrasonic endoscope. Lancet I:629–631, 1980.
9. Schlüter M, Langenstein BA, Polster J, Kremer P, Souquet J, Engel S, Hanrath P: Transesophageal cross-sectional echocardiography with a phased array transducer system-technique and initial clinical results. Br Heart H 48:67–72, 1982.
10. Souquet J, Hanrath P, Zitelli L, Kremer P, Langenstein BA, Schlüter M: Transesophageal phased array for imaging the heart. IEEE Trans Biomed Eng BME-29:707–712, 1982.

6. NONINVASIVE EVALUATION AND QUANTIFICATION OF REGIONAL MYOCARDIAL BLOOD FLOW

HEINRICH R. SCHELBERT, MARKUS SCHWAIGER, SUNG-CHENG HUANG, ANIL SHAH
and MICHAEL E. PHELPS

Radionuclide imaging with Tl-201 is widely used for evaluating regional myocardial perfusion. Its value for diagnosing ischemic heart disease and estimating its extent has been well established. However, the distribution of myocardial blood flow can be assessed with this technique only qualitatively, and measurements of regional myocardial perfusion in terms of ml/min/gm myocardium are not possible. Such measurements can conceivably be made with the recently developed positron emission computed tomography (Positron-CT) [1, 2]. This new imaging modality permits noninvasive measurements of indicator tissue concentrations. Cross-sectional Positron-CT images of the heart quantitatively reflect regional tracer tissue concentrations and hence are comparable to autoradiography. They offer the capability of measuring in vivo tissue activity concentrations which previously has been possible only by in vitro counting of tissue samples. Combined use of this new imaging device with tracers of blood flow is likely to permit noninvasive measurements of regional blood flow in the human heart.

We have extensively evaluated and characterized N-13 ammonia as such a tracer of myocardial blood flow [3, 4]. N-13 ammonia is administered intravenously and rapidly clears from blood into myocardium where it becomes trapped in proportion to myocardial blood flow. The tissue retention halftimes in myocardium average 2 to 3 hours. Therefore, distribution of N-13 activity in the myocardium at the time of imaging closely reflects the distribution of myocardial blood flow at the time of tracer injection. The net extraction of N-13 ammonia as the product of extraction fraction and blood flow is proportional to myocardial blood flow. As shown in Figure 1, this relationship is nonlinear. In the high flow range, increases in myocardial blood flow result in relatively small increments in N-13 tissue concentrations, yet flow changes within the range from 0 to 250 ml/min/100 gm are paralleled by proportionate and almost linear increases in myocardial N-13 tissue concentrations. Accordingly, within the physiologic range of blood flow, regional differences in perfusion are reflected by proportionate differences in tracer concentrations.
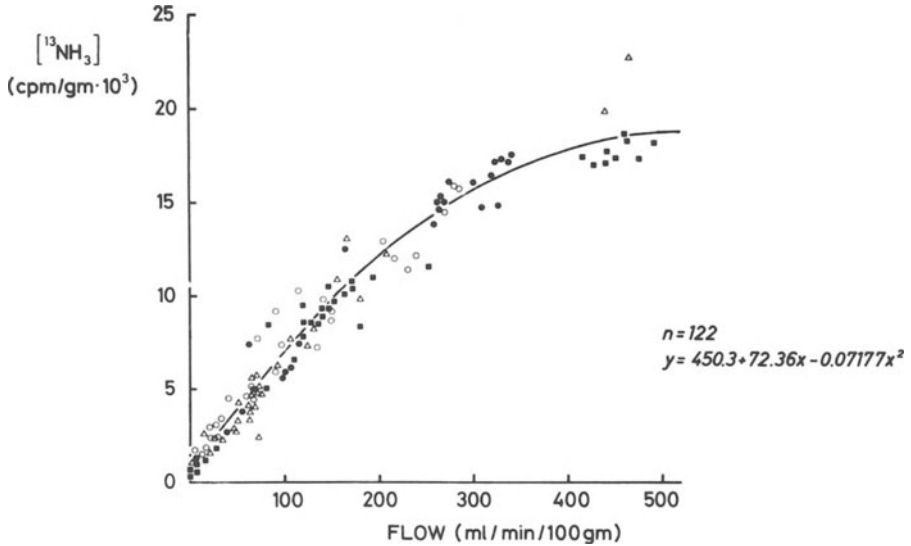
Figure 1. Comparison between regional myocardial blood flow and regional myocardial N-13 ammonia concentrations determined with in vitro counting in canine myocardium. Myocardial blood flow was measured using radioactive labeled microspheres. (With permission of American Journal of Cardiology.)

We have previously demonstrated the possibility of detecting mild, subcritical stenosis with Positron-CT and N-13 ammonia during drug induced hyperemia [5]. In these studies in chronically instrumented dogs, coronary stenoses of as little as 47% diameter narrowing were accurately identified. We subsequently employed the same approach in 32 patients with arteriographically documented coronary artery disease [6]. The findings in these patients were compared to those obtained in 13 normals who were young volunteers without clinical evidence of cardiovascular disease. Each participant was initially studied at rest with intravenous N-13 ammonia and cross-sectional imaging of the myocardial N-13 ammonia distribution. A second study was performed one hour later. After the N-13 activity had physically decayed, coronary hyperemia was induced with intravenous dipyridamole. A second dose of N-13 ammonia was injected and cross-sectional imaging of the myocardial N-13 activity distribution at the same levels through the heart was repeated. In the 13 normal volunteers, myocardial N-13 concentrations increased uniformly after dipyridamole and myocardial perfusion remained homogenous. By contrast, in 31 of the 32 patients with coronary artery disease, the myocardial distribution of N-13 activity became highly inhomogenous after dipyridamole and new or more extensive defects in regional N-13 concentrations were observed. A typical example is shown in Figure 2. Through quantitative analysis of the Positron-CT images, these new defects were caused by attenuated increases in N-13 concentrations in segments supplied by stenosed coronary arteries as compared to
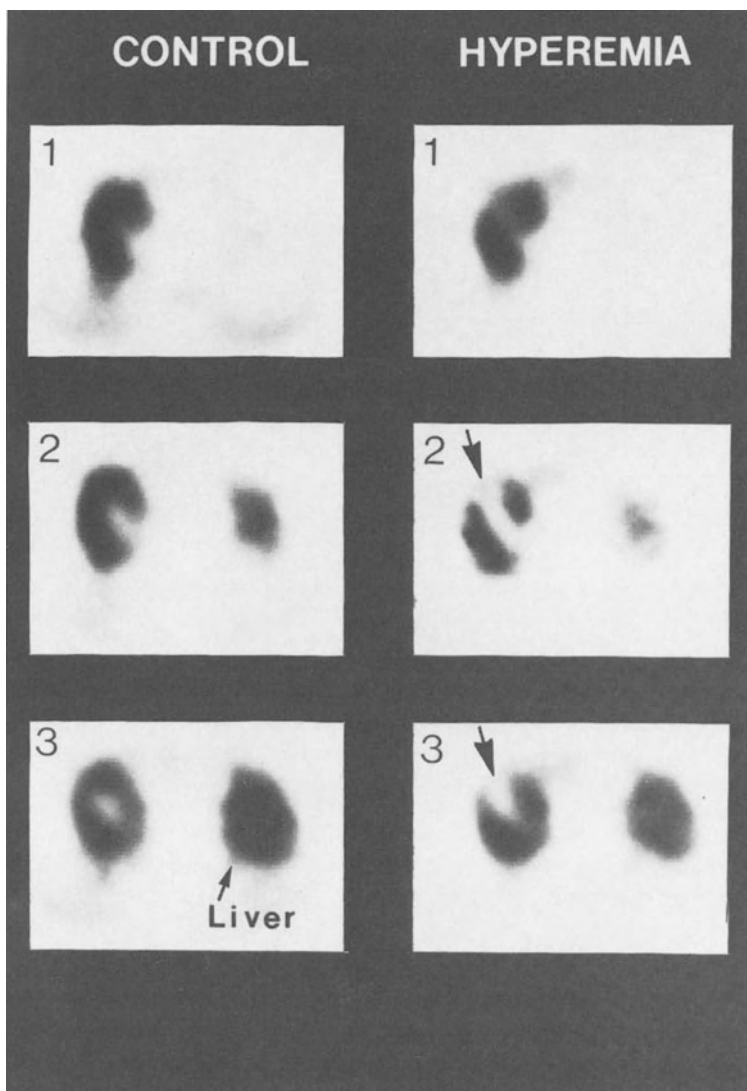
Figure 2. Control and hyperemic cross-sectional positron computed tomographic images of the myocardial N-13 ammonia distribution in a 67 year old woman with 100% stenosis of the proximal left anterior descending coronary artery. Level 1 is recorded through the high anterior and lateral wall, level 2 through the mid-left ventricle and level 3 through the mid to lower left ventricle. The control images reveal uniform N-13 activity throughout the left ventricular myocardium suggesting adequate collateral blood flow to the anterior wall at rest. However, in the hyperemic images, N-13 activity was greatly reduced in the anterior wall. N-13 activity increased from rest to hyperemia by 32% in the lateral wall and by 40% in the interventricular septum but by only 13% in the anterior wall.The appearance of a defect in the hyperemic images therefore does not indicate a decrease in blood flow from the control state to hyperemia but an attenuated response to pharmacologic coronary vasodilation.
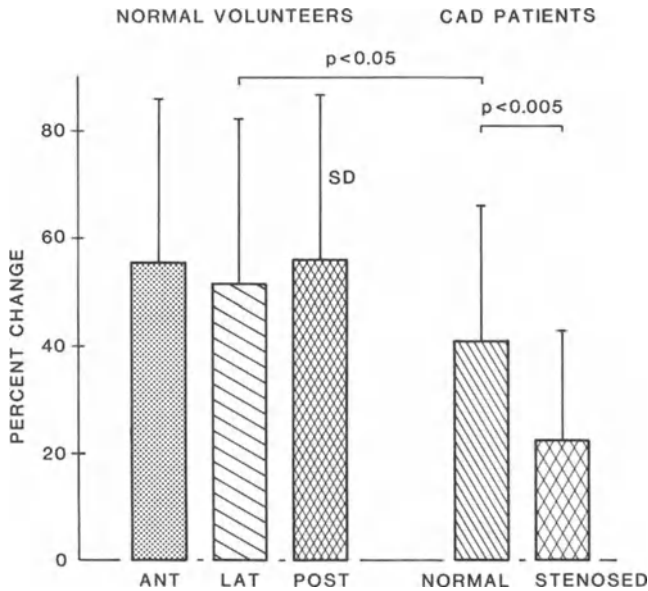
Figure 3. Increase in myocardial concentrations from the control state to dypridamole-induced coronary vasodilation. In the normal volunteers, the percent increase in N-13 concentrations was of similar magnitude in the anterior (ANT), lateral (LAT) and posterior (POST) wall and suggests similar hyperemic responses in the left anterior descending, left circumflex and posterior descending coronary arteries. In the patients with coronary artery disease (CAD), N-13 concentrations increased significantly less in myocardium supplied by stenosed vessels than in myocardium without arteriographically significant coronary artery lesions (normal). However, the percent increase in the "normal" segments was less than that in normal volunteers. p = probability; SD = standard deviation. (Permission from American Journal of Cardiology.)

control segments. In some instances, N-13 concentrations failed to increase at all or even declined from control to hyperemia. Hence, the flow increase in these segments was attenuated or even absent. Of interest was another observation: in myocardium supplied by apparently normal coronary arteries, the increase in N-13 concentrations from control to dipyridamole induced ischemia was less than in normal voluteers, suggesting the presence of coronary artery disease that was radiographically or anatomically not appreciated or was considered functionally insignificant (Figure 3).

As mentioned above, Positron-CT with N-13 ammonia after drug induced coronary hyperemia demonstrated in 31 of the 32 patients perfusion abnormalities that were not seen at control, resulting in an overall sensitivity for detection of coronary artery disease of 97%. More importantly, of the 58 coronary stenoses in this group of 32 patients, 52 or 90% were correctly identified by N-13 ammonia and Positron-CT during drug induced coronary hyperemia (Table 1).

Positron-CT imaging and N-13 ammonia was compared to T1-201 stress imag-

ing in 11 patients. All T1-201 studies were performed within 2 weeks of the Positron-CT study. In this patient subset, T1-201 stress scintigraphy correctly identified coronary artery disease in 10 patients and Positron-CT in all 11 patients. Because of the relatively small patient sample, this difference was statistically not significant. However, whereas T1-201 stress imaging correctly identified only 11 of the 19 diseased coronary arteries in the same patient sub-set, the tomographic approach correctly identified disease in 17 coronary arteries. This difference was significant and indicates the potential of Positron-CT and N-13 ammonia for assessing the extent of coronary artery disease. Coronary stenoses that remained undetected by Positron-CT usually involved the right coronary artery supplying the inferior wall which – with the current imaging devices – is difficult to visualize. Nevertheless, the results indicate that Positron-CT and N-13 ammonia significantly improved the sensitivity of detection of coronary artery disease and the noninvasive assessment of its extent.

We mentioned earlier the unique capability of Positron-CT for noninvasive measurements of regional indicator tissue concentrations. Because the properties of N-13 ammonia as a tracer of myocardial blood flow mimic to some extent those of radioactive microspheres, we hypothesized that the tracer may allow noninvasive quantitation of regional myocardial blood flow. Radioactive microspheres are widely used for measurements of regional myocardial perfusion in experimental animals. Microspheres are almost completely trapped and retained in myocardium in proportion to regional myocardial blood flow and rapidly clear from blood. N-13

Table 1. Summary of findings in normal volunteers and patients with coronary artery disease

	Number of patients	Patients with abnormal study	Total number of stenosed vessels	Number of stenosed vessels identified	Patients with all stenosed vessels identified	Sensitivity for detection of	
						CAD	Diseased vessels
A. Normal volunteers No coronary disease	13	0	0	0	0		
B. CAD Patients Single vessel disease	16	15	16	15	15	94%	94%
Double vessel disease	6	6	12	11	5	100%	92%
Triple vessel disease	10	20	30	26	6*	100%	87%
Total	32	31	58	52	26	97%	90%

* In each of the remaining 4 patients two stenosed vessels were detected.

ammonia is similarly trapped and fixed in myocardium in proportion to myocardial blood flow and its blood clearance is rapid. For example, within 5 min of injection, blood concentrations of N-13 ammonia are less than 5% of the peak concentration. The arterial input function is relatively clean and completed within a relatively short time.

Regional myocardial tissue perfusion can then be derived from tissue concentrations, the arterial input function and the withdrawal rate of arterial blood. Analogous to the microsphere technique, regional myocardial blood flow F is calculated by the equation $F = C_m \times F_a/C_a$, where C_m is the myocardial microsphere (or activity) tissue concentration (cpm/gm), F_a the withdrawal rate of arterial blood (ml/min) and C_a the activity in the arterial reference sample (cpm). The myocardial tissue concentration C_m is conventionally measured in vitro by well counting of tissue samples. With N-13 ammonia, C_m can be derived from the cross-sectional Positron-CT images. Regions of interest are assigned to the image and the derived counts ROI converted into counts per volume. Because of the relatively low spatial resolution of the current imaging device, true tissue tracer concentrations are underestimated because of the partial volume effect. This underestimation is related to object size [7], i.e. the thickness of the left ventricular wall, but can be corrected for if the regional wall thickness and the relationship between object size and count recovery are known [8]. Lastly, activity concentrations derived from the Positron-CT images are normalized to the activity concentrations in the arterial reference sample determined by well counting. Hence, C_m can be determined from the cross-sectional Positron-CT images by:

$$C_m = \frac{C_{PET} \cdot CF}{RC_{wt}}$$

where C_{PET} is the activity concentration derived from the ROI (cpm/cm^3), the calibration factor CF relating blood activity concentrations measured by well counting to those measured from the Positron-CT images, and the recovery coefficient RC_{wt} as a function of the left ventricular wall thickness wt. The latter value is derived from the relationship between recovered and true indicator concentrations established previously by Hoffman and Phelphs [7] and the left ventricular wall thickness determined by ultrasound. We successfully employed the microsphere approach in earlier animal experimental studies where microspheres labeled with positron emitting Ga-68 were administered into the left atrium and microsphere tissue activities determined in vivo with Positron-CT. These in vivo measurements were in good agreement with those determined simultaneously with gamma emitting microspheres and in vivo tissue counting [8].

The possibility to obtain similar measurements with N-13 ammonia as a tracer of MBF that can be administered intravenously was tested in chronically instrumented dogs. N-13 ammonia was administered intravenously and the myocardial N-13 ammonia concentrations determined by Positron-CT [9]. Beginning with the tracer injection, arterial reference blood was withdrawn at a constant rate for 2 min and
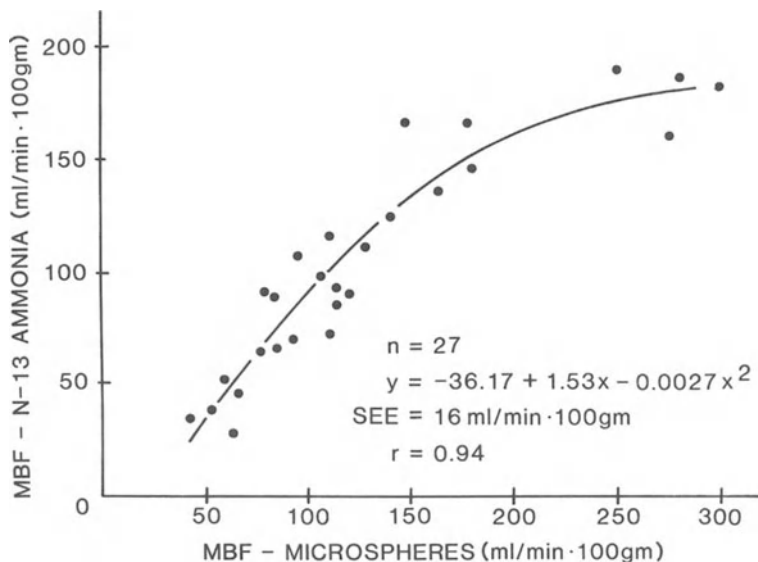
Figure 4. Comparison of myocardial blood flow measured by the arterial reference method with radioactive microspheres and by N-13 ammonia and Positron-CT in the canine myocardium.

tissue concentrations determined from the Positron-CT image acquired 3 min after tracer injection. Myocardial blood flow was also determined with the microsphere technique using 15μ radioactive labeled microspheres injected into the left atrium at the time of the N-13 ammonia administration [10]. Measurements of myocardial blood flow with the microsphere technique are compared in Figure 4 to those with the N-13 ammonia approach. The nonlinear relationship between the two measurements is consistent with our previous observations on N-13 ammonia (see also Figure 1). Yet, in the flow range up to approximately 200 ml/min/100 gm, the relationship is almost linear although N-13 ammonia measurements consistently underestimate regional myocardial blood flow by approximately 20 to 30%. This underestimation is because the extraction fraction of N-13 ammonia is less than 100%. Nevertheless, as demonstrated by the relatively small standard error of the estimate, the results indicate that noninvasive measurements of regional myocardial blood flow with this approach may in fact become possible.

More recently, Jones and co-workers [11, 12] succeeded in measuring local cerebral blood flow with 0–15 labeled water after inhalation of 0–15 labeled carbon dioxide. The same group of investigators expanded this approach by combining it with measurements of the local cerebral extraction fraction of oxygen thus making the measurement of the local cerebral metabolic rate of oxygen possible [12–15]. Using this method in patients with ischemic cerebrovascular disease, Frackowiak and co-workers [14] were able to assess the severity of ischemic cerebral insults and to more accurately predict their subsequent outcome. In these studies, regional
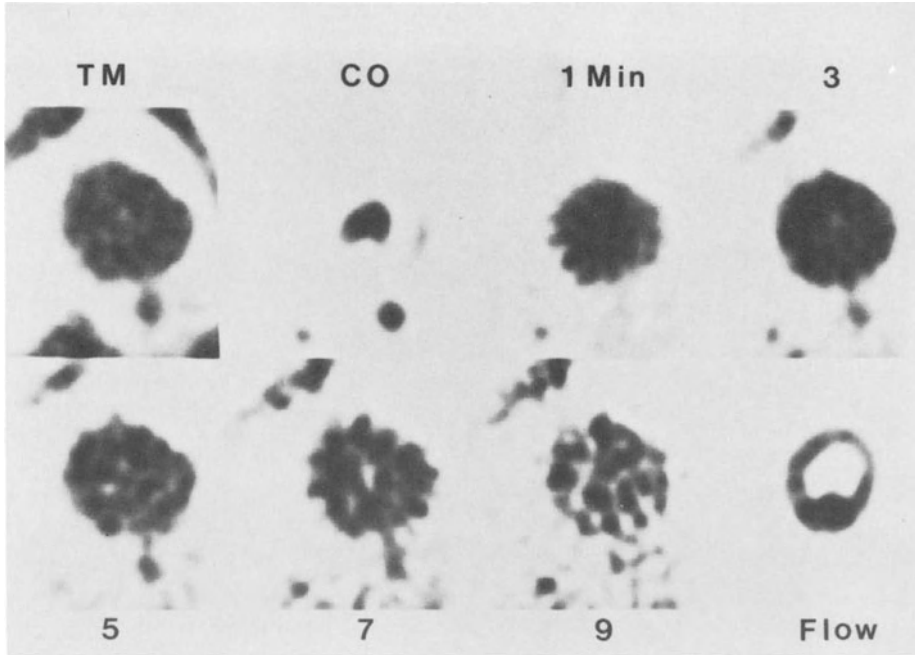
Figure 5. A typical example of an O-15 H$_2$O study for measurement of myocardial blood flow in the dog model. TM = transmission image using a Ga-67 mg ring source, CO = blood pool image following an inhalation of O-15 CO. These images are used to define the region of the left ventricular myocardium. Serial cross-sectional images are obtained at 1, 3, 5, 7 and 9 minutes following the intravenous bolus injection of O-15 water. At 1 minute the tracer is mostly within the blood pool and starts to diffuse into the myocardium, the latter images are characterized by the clearance of the tracer starting in the blood pool followed by the myocardium. Due to the short half time of O-15 (120 seconds), the late images are of noisy quality. From the projection data obtained for 10 minutes, the blood flow is determined by integrative analysis of the myocardial and blood time activity curves. The calculated flow values are displayed parametrically within the region of the myocardium as flow image.

oxygen metabolic rates were a far better predictor of tissue metabolism and subsequent clinical improvement than local cerebral blood flow.

Huang and co-workers [17–20] in our laboratory modified this method of cerebral blood flow measurements by administering a bolus of 0–15 labeled water intravenously. More recently, this approach has been adopted for blood flow measurements in myocardium. Measurements in the heart are complicated by a number of problems: unlike the brain, the heart is a thin walled and moving organ which complicates retrieval of true indicator tissue concentrations. This difficulty is further compounded by large pools of blood such as, for example, the cardiac chambers and the intramyocardial vascular space, both of which contain activity. This activity can lead to considerable cross-contamination of 0–15 activity between the blood pools and myocardial tissues. It appears however that these shortcomings

can largely be overcome by methods that allow corrections for activity cross-contamination or with the newer generation of high performance positron tomographs with improved temporal and spatial resolution. Preliminary animal experimental studies in our laboratory by Huang and co-workers [21] indicate that such measurements of local myocardial blood flow are indeed possible with oxygen-15 labeled water, serial Positron-CT imaging and arterial blood sampling. In these studies, blood pool images were obtained separately after inhalation of 0–15 labeled CO and were used to remove the activity contamination from the myocardial 0–15 water clearance data. From the corrected myocardial 0–15 water clearance data and the arterial input function, images of the regional myocardial perfusion were generated. Local perfusion values correlated well with those obtained by the radioactive microsphere technique as an independent reference. These observations – though preliminary – indicate that the 0–15 water technique can in fact be employed for accurate measurements of local myocardial blood flow (Figure 5).

At present, the practical use of this technique appears limited because of the relatively low spatial and temporal resolution of currently available whole body Positron-CT imaging devices. Yet, as new Positron tomographs are developed with higher resolutions and counting efficiency and will be available in the near future, the use of this technique appears feasible in man. Because of the short physical halftime of oxygen-15, this method offers the advantage of rapid serial measurements of myocardial blood flow. It also could be combined with measurements of regional myocardial oxygen extraction by the technique already established with Positron-CT in the brain.

While coronary artery disease and its extent can be identified noninvasively with qualitative radionuclide techniques with a relatively high degree of accuracy, it would seem that the external quantification of regional myocardial blood flow will have two major advantages: first, if tests can be devised that maximally and consistently increase coronary flow in a standardized fashion, these then would provide in combination with a noninvasive technique for the measurement of regional myocardial blood flow a means for quantifying coronary flow reserve as well as an impairment as the result of coronary artery disease. Accordingly, it might become possible to establish a quantitative index of the functional significance of coronary stenosis that could complement the anatomical information derived by coronary angiography. Secondly, the availability of a technique for measurements of regional myocardial oxygen metabolism may provide a new means to study tissue viability, as for example in ischemia. As recently demonstrated by Frackowiak and co-workers [22], in cerebral ischemia, regional oxygen extraction rates were better predictors of subsequent recovery than blood flow. Further, the availability of such a technique could be highly useful in evaluating the metabolic response to interventions currently used to improve function of ischemic tissue or to salvage injured myocardium.

48

REFERENCES

1. Phelps ME, Hoffman EJ, Mullani et al.: Application of annihilation coincidence detection to transaxial reconstruction tomography. J Nucl Med 16:210–224, 1975.
2. Phelps ME: Emission computed tomography. Semin Nucl Med 7:337–365, 1977.
3. Schelbert HR, Phelps ME, Hoffman EJ et al.: Regional myocardial perfusion assessed with N–13 labeled ammonia and positron emission computerized axial tomography. Am J Cardiol 43:209–218, 1979.
4. Schelbert HR, Phelps ME, Huang SC, et al.: N–13 ammonia as an indicator of myocardial blood flow. Circulation 63:1259–1272, 1981.
5. Gould L, Schelbert HR, Phelps ME, Hoffman EJ: Noninvasive assessment of coronary stenoses by myocardial perfusion imaging during pharmacologic coronary vasodilation. V. Detection of 47 percent diameter coronary stenosis with intravenous nitrogen-13 ammonia and emission computed tomography in intact dogs. Am J Cardiol 43:200–208, 1979.
6. Schelbert HR, Wisenberg G, Phelps ME, Gould KL, Henze E, Hoffman E, Gomes A, Kuhl BE: Noninvasive assessment of coronary stenoses by myocardial imaging during pharmacologic vasodilation. VI. Detection of coronary artery disease in man with intravenous N–13 ammonia and positron computed tomography. Am J Cardiol 49:1197–1207, 1982.
7. Hoffman EJ, Phelps ME: Quantitation in positron emission tomography. I. Effect of object size. J Comput Assist Tomogr 3:299, 1979.
8. Wisenberg G, Schelbert HR, Hoffman EJ, Phelps ME, Robinson GD, Selin CE, Child J, Skorton D, Kuhl DE: In vivo quantitation of regional myocardial blood flow by positron emission computed tomography. Circulation 63:1248–1258, 1981.
9. Shah A, Schelbert H, Schwaiger M, Henze E, Hansen H, Huang H: Regional myocardial blood flow assessed with N–13 ammonia and positron computed tomography in chronically instrumented dogs. J Nucl Med 23:P69, 1982.
10. Heymann MA, Payne BD, Hoffman JIE, Rudolph AM: Blood flow measurements with radionuclide-labeled particles. Prog Cardiovasc Dis 20:55–79, 1977.
11. Jones T, Chesler DA, Ter-Pogossian MM: The continuous inhalation of oxygen-15 for assessing regional oxygen extraction in the brain of man. Br J Radiol 49:339–343, 1976.
12. Jones SC, Reivich M, Greenberg JH: Error propagation in the determination of cerebral blood flow and oxygen metabolism with the inhalation of $C^{15}O_2$ and $^{15}O_2$. Acta Neurol Scand (suppl 72) 60:228–229, 1979.
13. Frackowiak RSJ, Lenzi GL, Jones T, Heather JD: The quantitative measurement of regional cerebral blood flow and oxygen metabolism in man, using oxygen-15 and positron emission tomography: Theory, procedure and normal values. J Comput Assist Tomogr 4:727–736, 1980.
14. Lammertsma AA, Jones T, Frackowiak RSJ, Lenzi GL: A theoretical study of the steady-state model for measuring regional cerebral blood flow and oxygen utilization using oxygen-15. J Comput Assist Tomogr 5:544–550, 1981.
15. Lammertsma AA, Frackowiak RSJ, Lenzi GL, Heather JD, Pozzilli C, Jones T: Accuracy of the oxygen-15 steady state technique for measuring rCBF and $rCMRO_2$: Tracer modeling, statistics, and spatial sampling. J Cerebr Blood Flow and Metabolism (suppl 1) 1:S3–S4, 1981.
16. Huang SC, Phelps ME, Hoffman EJ, Kuhl DE: A theoretical study of quantitative flow measurements with constant infusion of short-lived isotopes. Phys Med Biol 24:1151–1161, 1979.
17. Huang SC, Hoffman EJ, Phelps ME, Kuhl DE: Quantitation in positron emission computed tomography. 2. Effects of inaccurate attenuation correction. J Comput Assist Tomogr 3:804–814, 1979.
18. Huang SC, Phelps ME, Carson RE, Hoffman EJ, Plummer D, MacDonald N, Kuhl DE: Tomographic measurement of local cerebral blood flow in man with O-15 water. J Cerebr Blood Flow and Metabolism (suppl 1) 1:S31–S32, 1981.
19. Huang SC, Carson RE, Phelps ME: Measurement of local blood flow and distribution volume with

short-lived isotopes: A general input technique. J Cerebr Blood Flow and Metabolism 2:99–108, 1982.

20. Huang SC, Schwaiger M, Carson RE, Henze E, Hoffman EJ, Phelps ME, Schelbert HR: An O-15 water clearance method for quantitative regional myocardial blood flow measurements. J Nucl Med 23:P69, 1982.

II. QUANTIFICATION OF GLOBAL VENTRICULAR FUNCTION

7. PRESENT STATUS OF DIGITAL ANGIOCARDIOGRAPHY

PAUL H. HEINTZEN, RÜDIGER BRENNECKE AND JOACHIM H. BÜRSCH

1. INTRODUCTION

Conventional ("analog") angiocardiography and angiography of the coronary and peripheral circulation provide fundamental information about structure and function of the cardiovascular system. These techniques have reached a very high level of perfection.

The objective of this presentation is not only to outline
(a) *how* (and where) *digital* image processing techniques could yet evolve, but also:
(b) *why* and *where* digital angiocardiography can improve and/or complement subjective viewing of the passage of the contrast material and other heretofore practised quantitative angiocardiographic techniques.

2. DEVELOPMENT OF ANGIOCARDIOGRAPHIC METHODOLOGY

The essential steps in the development of angiocardiographic methodology should be reviewed briefly, since they reflect (not only) the historical evolution of these techniques but thereby demonstrate the complex interrelationship between the *medical goals* (and motivations), the physiological, mathematical and bioengineering *concepts* and the (fortunately simultaneous) technological *progress*, which gradually allowed the realization of these concepts and thus the achievement of some of the goals [1–11].

The main steps are considered the following:
(a) Imaging of the cardiovascular structures by *intravenous* contrast media injection and the use of the available *standard x-ray systems* (static pictures or very low temporal resolution).
(b) *Full size serial angiocardiography* by film changers (single or biplane, high spatial, low temporal resolution).
(c) Selective injection technique and percutaneous catheterization (right heart, left heart, coronary arteries).
(d) *Dynamic Cine- and Video*angiocardiography with high spatial- and temporal resolution image intensifiers.

QUANTITATIVE VIDEO ANGIOCARDIOGRAPHY
CONCEPTS AND REALIZATION
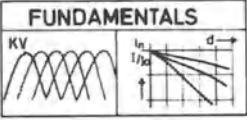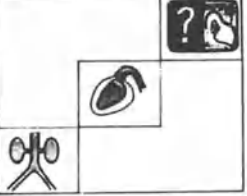
FUNDAMENTALS KV ln 1/d d→	TECHNICAL REQUIREMENTS FOR QUANTITATION X-RAY EQUIPM. LAMBERT-BEER	HIGH VOLTAGE STABILIZATION SYNCHRONIZ. I.I. GATING FILTERING SCATTER COMP.
VIDEODENSITOMETRY LV RV	QUANTITATION OF FLOW, CARD.OUTP EDV, ESV, EF VALVULAR REGURGITATION	LOGARITHMIC CONVERSION SHAPED WINDOW VDM with PULSED RADIATION
VIDEOMETRY INTERFACE **COMPUTER** VOLUME 2D/3D DIGITAL SHAPE CONTRAC IMAGE PATTERN PROC. DOCUMENT LV / RV LV / RV SUBTRACT. etc.	ACCURACY OF LV+RV VOLUME CAST STUDY CORRECTION FOR PHASE POSITION METHOD EXP. VALIDATION NORMAL VALUES CLINICAL APPL. GEOMETRY OF THE GROWING HEART	SPLIT SCREEN INTEGRATION OF REFERENCE DATA VOLUME CONSOLE COMPUTER INTERFACE SOFTWARE 4 BIT DIGITAL MATRIX
DIGITAL VIDEO ACG ?	BIOL. CONCEPTS CONTRAST-ENH. I.V. ANGIOCARD. MYOCARDIAL PERFUSION MUSCLE MASS FLOW DISTRIB. FUNCTIONAL IMAGING	8 BIT DIGITAL MATRIX "MODEM" SOFTWARE "ISAAC" µP-CONTROLLED X-RAY SYSTEM SOFTWARE

Figure 1. Survey on the evolution of digital videoangiocardiography from videodensitometry and videometry in our institution after having worked out the fundamentals for using the x-ray equipment as a measuring tool. Middle column: experimental and clinical concepts and efforts. Right column: bioengineering developments.

(e) Quantitative *Video*-(Cine) angiocardiography with (biplane) *electronic image* and reference *data* acquisition, processing storage, retrieval. Analog or partial *digital* parameter extraction.

X-ray equipment as "measuring tool".

(f) *Computerized processing of completely digitized image series*:

    a: successively obtained images (digital projection angiocardiography);

    b: simultaneously obtained images (computer tomography);

    c: combination of both (dynamic spatial reconstruction).

Figure 1 gives a survey on our efforts in this field starting in the mid-sixties. If one
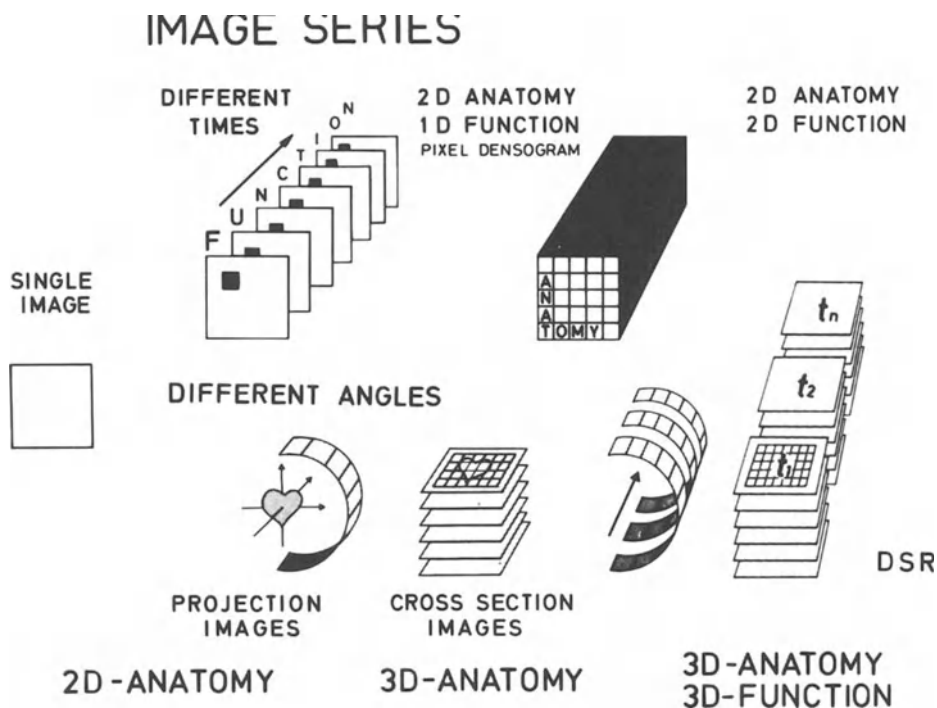
Figure 2. Comparison of the different modalities for generating and evaluating image *series*. Upper part: images taken *at different times* give insight into 2 D anatomy and function. With a comparable number of pictures taken at *different angles* (lower part) multiple cross sections of a static 3 D object can be obtained. It requires the same number of pictures and processed data for each image if a dynamic spatial reconstruction (DSR) of the beating heart should be achieved.

follows this evolution it is obvious that the *desire for quantitative angiocardiographic image analysis* was the strongest stimulus for the development of *digital* imaging techniques and computer processing of x-ray images – independent and before the advent of computer tomography [see 3, 4, 11–13].

The different modalities in digital processing of angiocardiographic or other image series are demonstrated in Figure 2. Projection images, taken under different angles (with moving structures at the same time or at least the same "phase") can be used to reconstruct (multiple) *cross sections* of an organ. The result still reflects static 2 or 3 D anatomy (lower part of Figure 2). From a comparable number of projection images *taken at different times* one gets insight into a "new dimension", namely "*function*" of the heart. To arrive at a clinically useful 3 D dynamic reconstruction of the beating heart, a huge, almost utopic data rate has to be processed, which is the purpose and the aim of the Mayo Clinic dynamic spatial reconstructor [DSR 3, 9, 10, 14, 15].

The principle of *d*irect, *d*ynamic *d*igital video-angiocardiographic (DDDVA) is
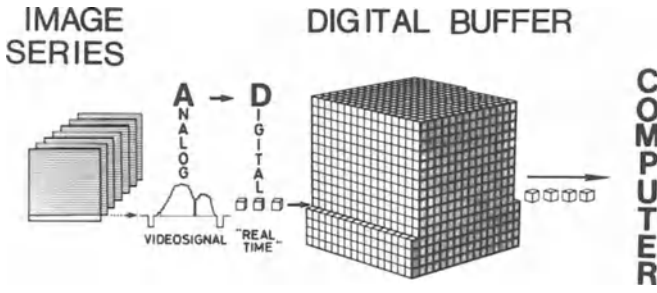
Figure 3. Graphic demonstration of the transformation of a linewise scanned videoimage series by A/D conversion into a "homogeneous" block of digitized data – temporarily stored into a digital buffer – and available for further operations as desired.

Figure 4. Graphic demonstration of the amount of imformation stored in a digitized block of data comparable to the average requirements in digital angiocardiography. Each picture element ("pixel") has 8 bits for gray level resolution. Each cube appears at the upper corner of the lower cube.
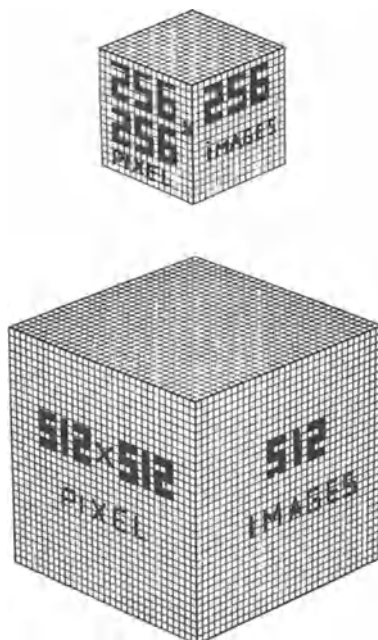
Figure 5. Comparison of the amount of information for handling a digitized image series with a spatial resolution of 256 × 256 picture elements ("pixels") and 256 images (e.g. about 50 fields per second for 5 seconds) and a resolution of 512 × 512 pixels for 50 frames per second, for 5 seconds.
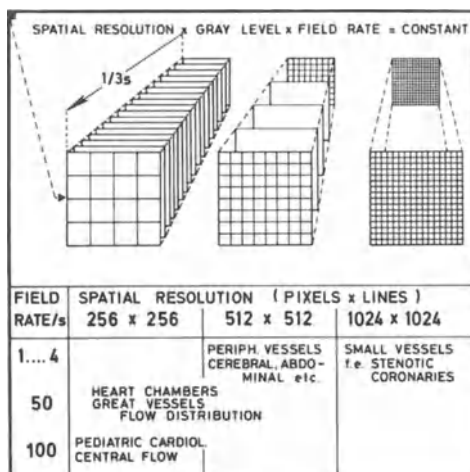
Figure 6. Demonstration of the "interchangibility" of spatial and temporal resolution for a given data rate (as the limiting factor of a given equipment). One has the choice between low spatial and high temporal or high spatial and low temporal resolution. Possible indications for the various options are given in the lower part of the picture.

outlined in Figure 3. The *linewise structure* of a video angiocardiographic image sequence is transfered by analog to digital conversion into a block of "homogeneous" data stored into a digital buffer which might or might not be part of the storage capacity of a digital computer. This process can be executed in real time. Each picture element ("PIXEL") represents the brightness information at a given picture site (location) and at a given time (picture number).

By this procedure a series of subsequent pictures is transformed into a block of simultaneously available data so that the *spatial and temporal information is interchangeable* and can be combined or mixed, as desired! The desired or required spatial and temporal resolution may vary widely in the various fields of possible radiological applications of digital imaging techniques. In cardiovascular radiology a spatial resolution of 256 × 256 or 512 × 512 and an image frequency of 1 to 50 fields per sec covers most of the needs.

A graphic representation of the order of information and the amount of data as related to the most commonly required resolutions is given in Figures 4 and 5. It is obvious, that the data rate is proportional to the product of the temporal and spatial and density resolution.

Figure 6 demonstrates the relationship between the various combinations of spatial and temporal resolution and the fields of useful application in cardiovascular radiology.

An ideal system should have the flexibility of allowing – for a given maximum data rate – a variable choice between spatial, temporal and (possibly) density resolution, according to the clinical or experimental problem under study.

As published earlier [16–21] single, "static" images and in particular image sequences may be objected to a number of image processing techniques, such as histogram modifications, filter operations (spatial, temporal) image restorations and other kinds of "manipulations" which can facilitate and improve the extraction of clinically relevant information by contrast enhancement, or by generating (synthetize) new image aspects and qualities.

The greatest benefit of digital image processing techniques in the field of cardiovascular radiology can be achieved not from digital processing of single, static images or just simple background subtraction operations, but from the flexible use of a whole image series due to the fact that *spatial and temporal information* can be combined and processed in variable modes. This however requires intelligent, experimentally elaborated and clinically relevant biological and engineering concepts.

This *simultaneous availability of all data* characterizes the "*anatomy*" of the cardiovascular system *and* the *changes* of structure and blood flow with time, i.e. "*function*" is the main reason for the specific advantages of digital over conventional angiocardiographic imaging techniques (Figure 7).

The possibilities of contrast enhancement and thereby the revival of *intravenous* contrast injection techniques in angiocardiography has certainly a number of useful clinical applications [19–26]. Probably its value is presently overestimated. Nev-
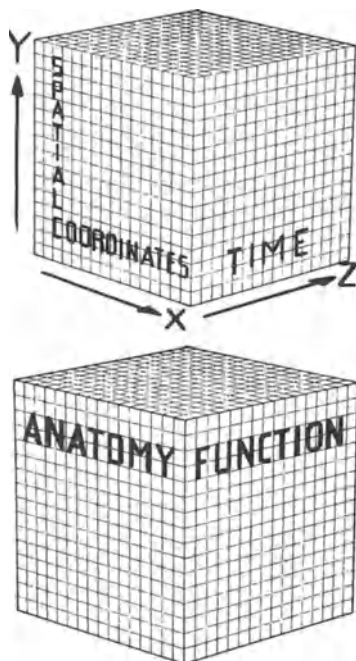
Figure 7. this graphic representation of a block of data obtained by digitizing a videoangiocardiographic image sequence should demonstrate the equalization of spatial and temporal coordinates and thereby the simultaneously available and mixable information about *anatomy* and *function*. This is one of the principle advantages of digital processing of image series.

ertheless these new aspects attracted and stimulated clinicians and manufacturers which resulted in the first commercially available systems for digital subtraction angiography in 1980/1981. This in turn is a prerequisite for the breakthrough of a method which otherwise remains often unnoticed for long periods.

3. SPECIFIC IMAGING TECHNIQUES

If the information from more than one picture of an image series (taken at different times) is combined, the result may yet only reflect anatomy. This is the case in dye filled cardiovascular structures after "background" subtraction.

There are, however, many modalities for digital image series processing – as demonstrated in Figure 8 – *where the information from a few or an increasing number of individual pictures is combined* (subtracted, summed up, mixed etc.) whereby these input pictures reflect the cardiovascular system *at different functional states*, e.g. at a given time interval (so called TID mode) or at specific instances of the cardiac cycle (i.e. endsystolic and enddiastolic pictures). Such operations can therefore be consid-

IMAGING TECHNIQUES
SIMPLE MODES

A   B   C   D   E

SIMPLE 'MASK' SUBTRACTION   TIME INTERVAL DIFFERENCE   ECG-(RESPIRATION)GATED SUBTRACTION COMBINATION + SUMMATION (ED or ES or all corresp. phases)   IMAGE SYNTHESIS

COMPLEX MODES

CIRCULATION TIMES

TEMP. SEGMENTATION

VOLUME PARAMETER

FLOW PARAMETER

EXTRACTION OF FUNCTIONAL PARAMETERS
FROM
MULTI-PIXEL-DENSOGRAMS
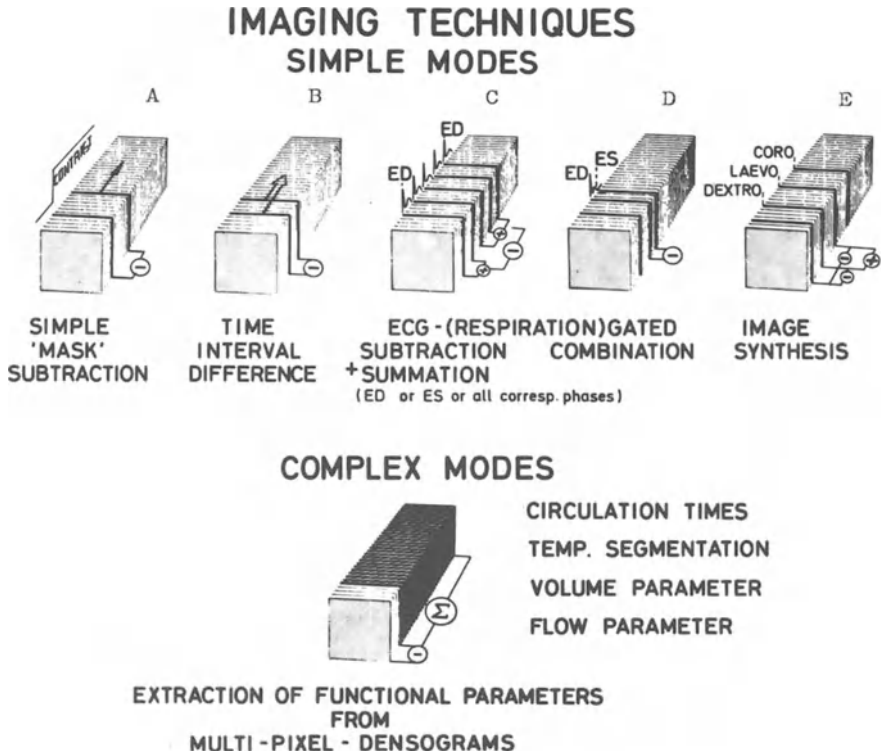
Figure 8. Survey on various techniques for extraction of clinically relevant information from angiocardiographic image series by combining in different ways the information of more than one picture from the series. The most common and simplest way is image subtraction. The most complex modes of digital image processing are using the information from the whole image series (lower part) for extraction of functional parameters from multi-pixel densograms.

ered already as simple types of "functional imaging".

Simple "masc mode subtraction" (Figure 8 A), which means subtraction without considering the cardiac phase, can be performed in real time. It gives satisfying results if motional artifacts can be kept small, for example in intravenous and intraarterial subtraction *angio*graphy of the peripheral circulation. (Most of the presently available equipment on the market allows this type of operation.)

If, however, digital subtraction techniques should be applied to the central circulation, *motional artifacts* are caused by the contraction of the heart and even more by the respiration. The "slow motion" artifacts of respiration can be reduced by subtracting images which are separated by a short time interval (TID mode) thus leaving only the more rapid changes of the contrast material distribution related to the heart motion and blood flow. The contrast itself is thereby reduced, which can be compensated in part by higher amplification after background subtraction.

Based on our experience, *ecg gated techniques* are almost always required to give
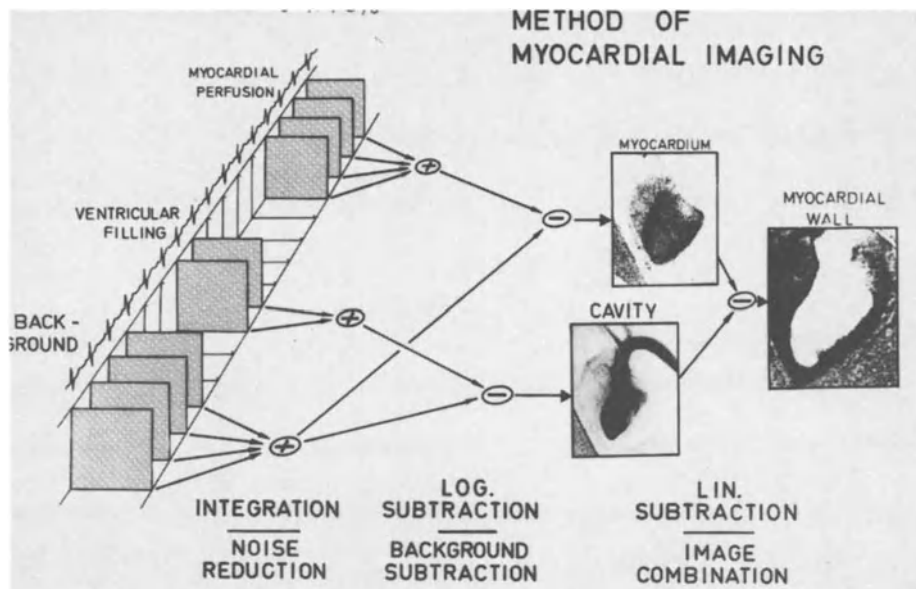
Figure 9. Demonstration of the method of myocardial imaging which is useful for the determination of LV muscle mass, wall thickness and thickening as well as for the detection of myocardial perfusion disturbances.

acceptable results from image subtraction if digital processing should be applied to the central circulation (Figure 8 C,D).

Respiration can cause motional artefacts, particularly in children. The method developed in our laboratory [19] allows the selection of pictures for subtraction from a series of "background" images taken over a whole respiratory and cardiac cycle before contrast injection in order to find those pictures by (on line) cross correlation techniques, which optimaly correspond to the actual contrast pictures. This ecg and respiratory gated subtraction is possible in real time with the *I*mage *S*equence *A*cquisition and *A*nalysis Computer ("ISAAC"), developed in our laboratories [20, 21, 26].

For functional studies of ventricular performance ecg gated endsystolic (ES) pictures can be subtracted from enddiastolic ones (ED) (Figure 8 C). The resulting subtraction images reflect the mode of contraction of the left ventricle as a 2 D correlate of stroke volume and ejection fraction (EF). From biplane pictures ventricular volumes and ejection fraction can be calculated as in conventional angiocardiography.

For specific studies of left or right ventricular function the radiation can also be triggered [27], from either the computer or a microprocessor which coordinates image generation, image acquisition, digitization, processing storage and retrieval [20, 21, 26].

In addition to the possible *reduction of contrast material* – which is needed for a given piece of information – the *radiation dose can also be reduced* in digital angiocardiography, be it intravenous or selective, depending on the diagnostic problem. Thus at least 4 left ventricular performance studies are possible (during rest and exercise) without increasing the patient's load [28].

Having the whole sequence of images stored in digital format enables any useful combination of pictures from various phases of the contrast passage to be used to synthetize composite images (Figure 8 E), whereby the background may be removed and the noise reduced before or parallel to image synthesis.

Combinations of dextro- and levocardiograms depicted in different gray levels or colours demonstrate the spatial relationship between the heart chambers and great vessels and thereby allow a clear delineation of the ventricular septum, in particular in the four chamber view [29].

For these studies, only a limited number of pictures from the whole series has to be processed. However, interactive search for those pictures which optimally fit to each other is required and can be done shortly after the procedure. This type of operation will probably not become a field for automatic real time digital image processing.

4. COMPLEX MODES OF FUNCTIONAL IMAGING.

4.1. Organ perfusion studies

These are possible by image integration and contrast enhancement during the passage of the contrast material through the capillary bed. One particular interesting aspect of digital angio*cardio*graphy is the study of the perfusion of the cardiac muscle itself, since it allows the determination of the left ventricular *muscle mass* and the detection of *perfusion defects* [24, 30–32].

For this purpose contrast enhancement is used by heart phase related integration and background subtraction during the capillary phase of the *coronary* circulation. This can be achieved by aortic, selective coronary or left ventricular dye injection. From the initial levocardiogram (LV injection) the internal surface of the left ventricular muscle wall is obtained. During the following perfusion of the heart muscle via the coronary arteries, contrast enhancement techniques allow the opacification of the myocardial wall and thereby the delineation of the epicardial surface. From this late picture the early levocardiogram is electronically subtracted, leaving only the left ventricular muscle shell opacified (Figure 9).

The left ventricular muscle mass can then be determined by subtracting the LV volume derived from the endocardial surface from the volume, obtained from the biplane epicardial contours of the left ventricle (LV), applying the established videometric methods. [33, 34]. The calculated muscle volume correlated very well
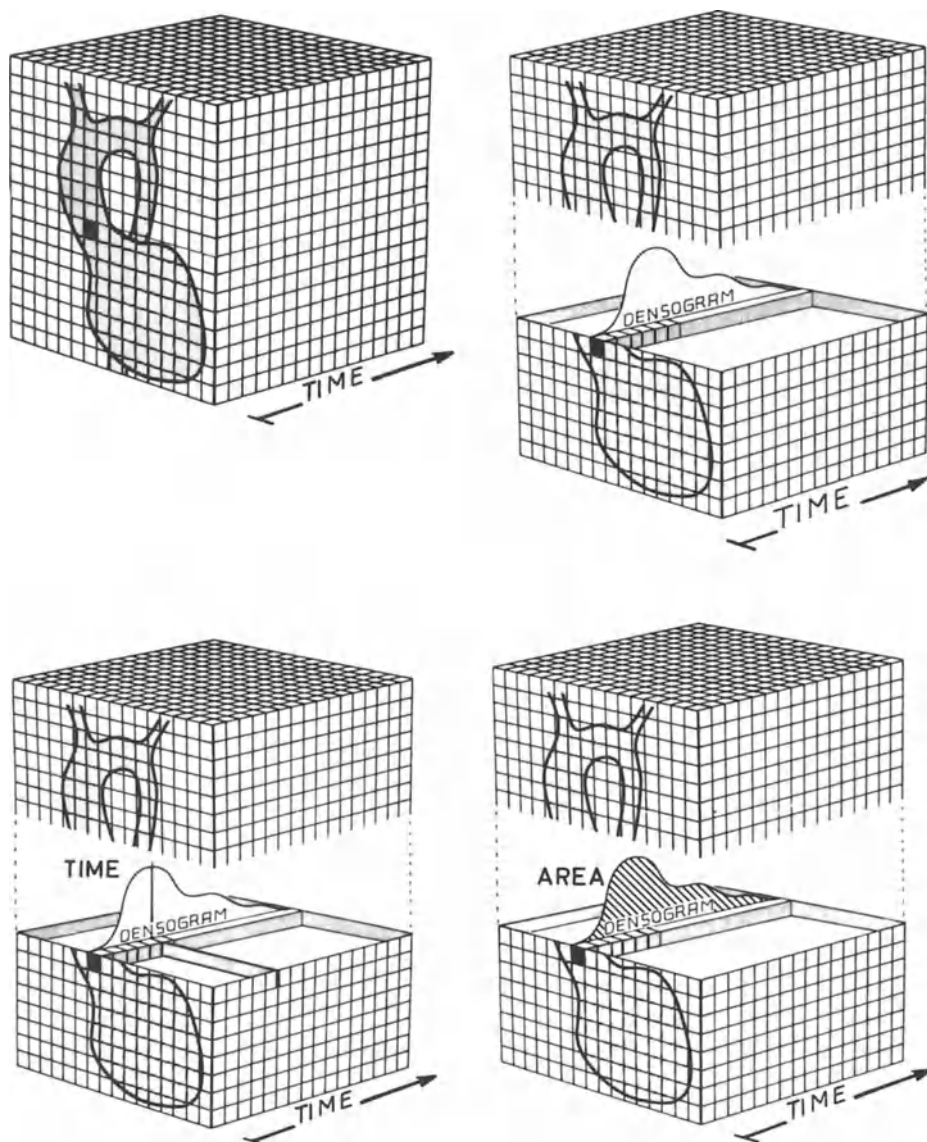
Figure 10. (a–d). Schematic demonstration that, in a digitized image series, each *pixel* can be considered as a videodensitometric window (a) so that the image changes with time constitute a matrix of pixel-densograms, (b) which can be evaluated in various ways applying some principles of the indicator dilution technique. From the pixel-densograms "functional" (-time)parameters (c) or volume parameters (area under the densogramm (d) can be obtained.

with the true LV muscle volume measured postmortem in pig hearts [30–32].

In addition, animal studies with experimentally created ventricular infarctions of known size have shown that variations in the wall thickness, wall motion and myocardial perfusion become detectable by this technique [32].

4.2. Blood flow distribution measurements

Within the block of data obtained after digitization of a complete image series, each picture element ("pixel") can be considered as a videodensitometric window so that all kinds of indicator dilution operation can be performed in the most complete way (Figure 8F).

From the whole density time curves functional parameters can be derived. This is demonstrated in Figure 10c for a *time parameter* (maximum of densogram or arrival time). This time value can be displayed providing a new picture quality which signalizes the progress of the contrast bolus within one image [35–38]. A 2D x-ray density display is thereby converted into a 2 D time value display either in gray levels, colours or numbers.

Such time parameters can be grouped considering the underlying anatomy and the physiological problem. For *flow distribution measurements* in the vascular tree, programs have been developed which allow a useful *"temporal segmentation"* of the contrast bolus so that its stepwise progression within a given time interval can be detected and displayed [36–38].

From the area under the same densogram (Figure 10d) another parameter can be derived representing the *depth* of the cardiovascular structure within the path of radiation, and thereby a measure of the *volume* of the vessel in a given region or segment of the vascular tree if all individual area-parameters are integrated.

Quantitative flow distribution measurements are possible in a branching vascular tree by a principle using *time* parameter extraction as described above *and* vascular *volume* parameters.

Since the isochrones obtained by temporal segmentation give a quantitative measure of the progress of the contrast bolus within a given part of the vessel, for example during a 60 millisecond interval, and the volume element between these isochrones is also known, the volume displacement in the vessel within a given time – i.e. the flow – at this site can be calculated. The relative flow rates in a branching vessel can be converted into absolute values, if the dimension of the vessel is determined by an independent (videometric) measurement at any site of the vessel. The calculated flow distribution can be indicated by numbers displayed with the (coloured) picture of the vascular tree [26, 37].

It is expected that this type of image analysis will be useful also for the study of the regional circulation in many other organs, and in particular for the investigation of quantitative functional aspects of the disturbed coronary circulation. Experimentally, studies about the usefulness and limitations of this methods are in progress.

5. CONCLUSION:

Digital x-ray imaging techniques evolved from the endeavour after quantitative data extraction from angiocardiograms could be realized stepwise according to the technological progress and the increasing awareness of its potential power.

At the present time it is still more an additional technique which can complement the high quality conventional angiocardiographic methods. In some instances it can already replace "more invasive" investigations – without being strictly "non invasive".

However, simple masc mode subtraction is only the "peak of the iceberg". The potential power of the method and the main reasons for the predicted expansion are:

(a) the flexibility of electronic, and in particular digital, data handling for image acquisition, processing, storage and retrieval and

(b) the possibility of arriving at completely new image qualities and information heretofore not available from the conventional radiographic imaging techniques.

As shown from our experimental studies "*quantitative* functional imaging" with various parameter extraction allows new insights into the structure and function of the cardiovascular system.

Since technology already provides the components for high quality digital x-ray imaging, and the knowledge is available, it can be predicted that – at least for angiocardiography – during the next decade digital (video?) electronic techniques will replace (and complement) roentgen cinematography in the same (overlapping) way that the latter has replaced full size angiocardiography. I am convinced that the evolving systems will not only be more flexible and powerful but also more economic.

The place for three-dimensional dynamic reconstruction of the cardiovascular system has still to be worked out and the superiority to be proved for the various pathological conditions. In any case we do not need "all dimensions" for "all" clinically relevant questions to be answered. We have to select the appropriate and available approach. In any case, it will be more and more "digital".

6. SUMMARY

A survey is given on the evolution of digital imaging techniques for the processing of angiocardiographic projection image series. The main advantage of this type of computerized angiocardiography is the fact that, in an image time series, structure and function of the cardiovascular system are represented by a homogeneous block of digitized data which can be combined and evaluated in a most flexible way. A very simple though attractive and clinically useful application of these technique is contrast enhancement by background subtraction and noise reduction. This allows

64

some diagnostic problems to be solved by intraveneous contrast injection and with less radiation.

Other more complex, specific and promising techniques are those for myocardial perfusion studies in coronary heart disease and muscle mass determination, as well as methods for blood flow measurements in branching vessels. Due to the flexibility of electronic digital data acquisition, processing, storage and retrieval (and the many new options for contrast enhancement, functional imaging and the generation of new image qualities) digital cardiovascular radiology is predicted to replace more and more conventional angiocardiographic techniques during the next decade.

REFERENCES

1. Doby T: Development of Angiography and Cardiovascular Catheterization. Publishing Sciences Group, Littleton, 1976.
2. Löhr HH, Gremmel H, Loogen F, Vieten H: Darstellung der Herzhöhlen, der Gefäßlumina und des Blutstromes. In: Diethelm L, Olsson O, Strand F, Vieten H, Zuppinger A (eds), Handbuch der Medizinischen Radiologie, Vol 10, Part 1, p. 314, Springer Verlag, 1969.
3. Wood EH, Sturm RE, Sanders JJ: Data processing cardiovascular physiology with particular reference to roentgen videodensitometry. Mayo Clin Proc 39:849–865, 1964.
4. Heintzen PH, (ed.) Roentgen-, Cine- and Videodensitometry. Fundamentals and applications for blood flow and heart volume determination. Thieme Stuttgart, 1971.
5. Bürsch JH: Quantitative Videodensitometrie. Grundlagen und Ergebnisse einer röntgenologischen Indikatormethode. Habilitationsschrift, Christian-Albrechts-Universität Kiel, 1973.
6. Heintzen PH, Bürsch JH (eds) Roentgen-Video-Techniques Thieme Stuttgart, 1978.
7. Cormack AM: Early two-dimensional reconstruction (CT scanning) and recent topics stemming from it. Nobel lecture Dec 8 (1979), J Comput Assist Tomogr 4:658, 1980.
8. Hounsfield GN: Computed medical imaging. Nobel lecture Dec 8 (1979) J Comput Assist Tomogr 4:665, 1980.
9. Wood EH: New vistas for the study of structural and functional dynamics of the heart, lungs and the circulation by noninvasive numerical tomographic vivisection. Circulation 56:506–520, 1977.
10. Robb RA: X-ray computed tomography: An engineering synthesis of multiscientific principles. Critical Reviews in Biomedical Engineering 7, 265–333, 1982.
11. Heintzen PH, Brennecke R, Bürsch JH, Hahne HJ, Lange PE, Moldenhauer K, Onnasch D, Radtke W: Quantitative analysis of structure and function of the cardiovascular system by roentgen-video-computer techniques. Proc Mayo Clin 57 (suppl):78–91, 1982.
12. Heintzen PH, Moldenhauer K, Lange PE: Three dimensional computerized contraction pattern analysis: description of methodology and its validation. Europ J Cardiol 1:229, 1974.
13. Heintzen PH, Brennecke R, Bürsch JH, Lange P, Malerczyk V, Moldenhauer K, Onnasch D: Automated videoangiocardiographic image analysis. Compter IEEE 8:55–64, 1975.
14. Robb RA, Lent AH, Gilbert BK, Chu A: The dynamic spatial reconstructor. J Med Syst 4:253–288, 1980.
15. Ritman EL, Kinsey JH, Robb RA, Gilbert BK, Harris LD, Wood EH: Three dimensional imaging of heart, lungs, and circulation. Science 210:273, 1980.
16. Brennecke R, Brown TK, Bürsch JH, Heintzen PH: Digital processing of videoangiographic image series using a minicomputer. Proc Comp Cardiol, IEEE Computer Society, Long Beach, pp 255–260, 1976.

17. Brennecke R, Brown TK, Bürsch JH, Heintzen PH: A system for computerized video-image preprocessing with applications to angiocardiographic roentgen-image series. In: Nagel HH (ed), Digitale Bildverarbeitung, Springer, Berlin-Heidelberg, New York, pp 244–262, 1977.
18. Brennecke R, Brown TK, Bürsch JH, Heintzen PH: A digital system for roentgen video image processing. In: Heintzen PH, Bürsch JH (eds), Roentgen-Video-Techniques, Thieme, Stuttgart, pp 150–157, 1978.
19. Brennecke R, Hahne HJ, Moldenhauer K, Bürsch JH, Heintzen PH: Improved digital real-time processing and storage techniques with applications to intravenous contrast angiography. Proc Comp Cardiol IEEE Computer Society, Long Beach, pp 191–194, 1978.
20. Brennecke R, Hahne HJ, Moldenhauer K, Bürsch JH, Heintzen PH: A special purpose processor for digital angiocardiography. Design and applications. Proc Comp Cardiol, Long Beach, IEEE Computer Society, pp 343–346, 1979.
21. Brennecke R, Hahne HJ, Heintzen PH: A multiprocessor system for the acquisition and analysis of video image sequences. In: Pöppl SJ, Platzer H (eds), Erzeugung und Analyse von Bildern und Strukturen, Springer, Berlin-Heidelberg-New York, pp 113–122, 1980.
22. Mistretta CA, Crummy AB, Strother CM, Sackett JF: Digital subtraction arteriography: an application of computerized fluoroscopy. Year Book Medical Publishers, Chicago, London, 1982.
23. Höhne KH: Digital image processing in medicine. In: Lindberg DAB, Reichertz PL (eds), Lecture Notes in Medical Informatics, Springer, Berlin-Heidelberg-New York, 1981.
24. Heintzen PH, Brennecke R, Bürsch JH: Computerized videoangiocardiography. In: Kaltenbach M, Lichtlen P (eds), Proc 3rd Symposium on Coronary Heart Disease, Thieme, Stuttgart, pp 116–121, 1978.
25. Heintzen PH, Brennecke R, Bürsch J: Computer quantitation of angiographic images. In: Miller HA, Schmidt EV, Harrison PC (eds), Non-invasive Cardiovascular Measurements, 167 Bellingham, WA: Society of Photo-Optical Instrumentation Engineers, pp 17–20, 1978.
26. Heintzen PH, Brennecke R (eds): Digital imaging in cardiovascular radiology. Int. Symposoum Kiel, 24–25 May 1982. Thieme, Stuttgart, 1983.
27. Wittmaack W, Brennecke R, Heintzen PH: Mikroprozessoreinsatz bei der Aufnahme von Videoangiokardiogrammen. Biomed Technik 25 (Ergänzungsband) pp 38–39, 1980.
28. Tobis J, Nalcioglu O, Henry W: Functional assessment of coronary stenosis using digital subtraction angiography. In: Heintzen PH, Brennecke R (eds), Digital Imaging in Cardiovascular Radiology, Thieme, Stuttgart, 1983 (in press).
29. Bogren HG, Bürsch JH, Brennecke R, Heintzen PH: Intravenous angiocardiography using digital image processing experience with axial projections in normal pigs and in pigs with experimentally generated left-to-right shunts. SPIE 314:287–293, 1981.
30. Radtke W: Die angiokardiographische Bestimmung des linksventrikulären Myokardvolumens mit Hilfe der digitalen Bildverarbeitung. Inauguraldissertation, Kiel, 1981.
31. Radtke W, Bürsch HJ, Brennecke R, Hahne HJ, Heintzen PH: Left ventricular muscle volume by digital angiocardiography. Invest Radiol (in press).
32. Bürsch HJ, Radtke W, Brennecke R, Hahne HJ, Heintzen PH: Assessment of myocardial perfusion by digital angiocardiography. In: Just, HJ (ed), Angiocardiography. Present status and future developments, Springer, Berlin-Heidelberg-New York, 1983 (in press).
33. Lange PE, Onnasch DGW, Farr FL, Heintzen PH: Angiocardiographic left ventricular volume determination. Accuracy, as determined from human casts, and clinical application. Europ J Cardiol 8:449–476, 1978.
34. Lange PE, Onnasch DGW, Farr FL, Heintzen PH: Angiocardiographic right ventricular volume determination. Accuracy, as determined from human casts, and clinical application. Europ J Cardiol 8:477–501, 1978.
35. Höhne KH, Böhm M, Erbe W, Nicolae GC, Pfeiffer G, Sonne B: Computer angiography: a new tool for x-ray functional diagnostics. Med Progr Technol 6:23–28, 1978.
36. Bürsch HJ, Hahne HJ, Brennecke R, Hetzer R, Heintzen PH: Funktions-Angiogramme als Er-

gebnis der densitometrischen Analyse digitalisierter Röntgenbildserien. Biomed Technik, Er-gänzungs 24:189–192, 1979.

37. Bürsch JH, Hahne HJ, Brennecke R, Grönemeyer D, Heintzen PH: Assessment of arterial blood flow measurement by digital angiography. Radiol 141:39–47, 1981.

38. Bürsch JH, Brennecke R, Heintzen PH: Digital angiocardiography Practical Cardiology 8:131–142, 1982.

8. QUANTIFICATION OF LEFT VENTRICULAR FUNCTION BY TWO-DIMENSIONAL ECHOCARDIOGRAPHY

RAIMUND ERBEL, PETER SCHWEIZER, JÜRGEN MEYER, WINFRIED KREBS AND SVEN EFFERT

INTRODUCTION

Two-dimensional echocardiography has overcome some of the major methodological limitations of M-mode echocardiography [1]. In addition the introduction of apical echocardiography by Silverman and Schiller [2] has opened up the possibility of imaging the left ventricle in long-axis in multiple projections. Usually the apical four- and two-chamber views are scanned. In these two cross sections of the left ventricle, aortic and mitral valves represent landmarks. Images of the left ventricle in the two-chamber view are very similar to cineventriculograms in the 30° right anterior oblique (RAO) projection. Therefore this scan plane was called "RAO-equivalent view".

Left ventricular volumes and ejection fraction were determined from apical two-dimensional echocardiograms and compared to cineventriculograms. Correlation coefficients ranged from 0.73 [3] to 0.98 [4]. Regression coefficients for end-diastolic volume ranged from 0.45 [5] to 0.94 [4], y-axis intercept from -3.7 ml [4] to 42 ml [6], and standard errors of estimate from 15 ml [7] to 45 ml [8]. For end-systolic volumes smaller standard errors of estimate were found, due to the smaller volume range (Table 1). Some authors reported higher regression equations [3, 9], some lower [4, 5, 6, 10], or even equal values [7] compared to end-diastolic volume. That means left ventricular volume is underestimated by two-dimensional echocardiography compared to cineventriculography.

Biplane volume determination from combined apical RAO-equivalent and 4-chamber views could not avoid underestimation of ventricular volume, as different authors could demonstrate [6, 11, 12]. It was obvious that even correlation coefficients and standard errors of estimate could not significantly improve because of methodological problems of either method [11, 12]. But the degree of underestimation of ejection fraction could be decreased [11].

The underestimation of ventricular volume was not dependent on whether mechanical [13, 14] or electronic sector scanners were used [5–7, 9–12]. Also, in respect to the resolution, no significant difference was found [15, 16].

In most studies patients with and without coronary artery disease were examined. Therefore different patient groups were analysed to evaluate influence on left ventricular volume determination by two-dimensional echocardiography. As Table

Table 1

Author	N	Algorithm	2dE planes	CVG projection	End-diastolic volume Regression equation	r	SEE (ml)	End-systolic volume Regression equation	r	SEE (ml)	Ejection fraction Regression equation	r	SEE (%)
Carr 1979	22	Area/length	RAO/4C	RAO/LAO	$y = 0,59x + 10,0$	0,93	—	—	—	—	$y = 0.89x + 4.8$	0.93	5.8
Erbel 1979	37	Simpson	RAO	RAO	$y = 0.70x + 20.6$	0.95	21	$y = 0.74x + 11.6$	0.97	11	$y = 0.75x + 12.0$	0.90	9.7
Folland 1979	35	Simpson	O /4C	RAO	$y = 1,02x + 34.0$	0.84*	43	—	0.86	32	$y = 1.01x + 4.0$	0.78	9.7
Parisi 1979	50	Simpson	O /4C	RAO	$y = 1.08x + 29.5$	0.82*	39	—	0.90	29	—	0.80	9.0
Schiller 1979	30	Simpson	RAO/4K	RAO/LAO	$y = 0.70x \quad 1.0$	0.80	15	$y = 0.70x \quad 2.0$	0.90	9	$y = 1.00x + 5.0$	0.87	7.6
Erbel 1980	50	Simpson	RAO	RAO	$y = 0.67x + 27.1$	0.94	22	$y = 0.70x + 14.7$	0.97	15	$y = 0.74x + 11.3$	0.91	6.0
Moynihan 1980	25	Simpson	O /4C	RAO	—	0.84*	45	—	—	—	—	0.80	10.0
Touche 1980	28	Area/length	4C	RAO	$y = 0.76x + 5.0$	0.92	44	$y = 0.75x + 13.0$	0.95	35	$y = 0.88x + 0.4$	0.92	7.5
Erbel 1981	38	Simpson	RAO/4C	RAO/LAO	$y = 0.68x + 3.0$	0.80	32	$y = 0.54x + 16.9$	0.87	23	$y = 0.67x + 17.1$	0.78	8.8
Erbel 1981	38	Simpson	RAO	RAO/LAO	$y = 0.74x \quad 0.2$	0.83	31	$y = 0.53x + 22.4$	0.84	25	$y = 0.57x + 22.3$	0.72	9.1
Gueret 1981	12	Area/length	RAO/4C	RAO	$y = 0.52x + 93.4$	0.73	40	$y = 0.86x + 21.8$	0.91	25	$y = 1.14x \quad 6.3$	0.97	3.7
Jenni 1981	42	Area/length	RAO/4C	RAO/LAO	$y = 0.94x \quad 33.7$	0.98	21	$y = 0.90x + 7.2$	0.97	17	$y = 0.80x + 9.4$	0.87	5.4
Kan 1981	30	Area/length	RAO	RAO/LAO	$y = 0.45x + 30.0$	0.84		$y = 0.41x + 15.0$	0.85		$y = 0.68x + 18.0$	0.91	
Starling 1981	30	Simpson	RAO/4C	RAO/LAO	$y = 0.58x + 40.0$	0.81	37	$y = 0.71x + 8.0$	0.92	28	$y = 0.98x + 2.0$	0.87	9.0
Starling 1981	70	Simpson	RAO/4C	RAO/LAO	$y = 0.66x + 42.0$	0.80	34	$y = 0.72x + 18.0$	0.88	27	$y = 0.76x + 12.0$	0.90	7.0
Erbel COCM	38	Simpson	RAO	RAO	$y = 0.62x + 12,3$	0.75	62	$y = 0.58x + 18.6$	0.84	49	$y = 0.62x + 8.7$	0.71	7.9
Erbel Valve Dis.	30	Simpson	RAO	RAO	$y = 0.65x + 10.3$	0.93	25	$y = 0.66x + 13.3$	0.94	25	$y = 0.62x + 16.1$	0.85	5.3
Quinones 1981	30	3 diameters	RAO/O	RAO	—			—			$y = 0.85x + 7.1$	0.91	7.4
Schnittger 1982	18	Area/length	4C	RAO	$y = 0.57x + 26.0$	0.85	14	—			—	—	—
Hahn 1982	25	Area/length	RAO/4C	RAO/LAO	$y = 0.83x + 9.6$	0.97	26	$y = 0.95x \quad 6.1$	0.94	27	$y = 0.98x + 9.9$	0.81	11.1

2dE = two-dimensional echocardiography (y), CVG = cineventriculography (x), O = 2dE parasternal cross-section, RAO-and 4-chamber views (RAO/4C), RAO-and LAO projection, * = regression equation 2dE (x), CVG (y), COCM = congestive cardiomyopathy, Valv. Dis. = Valvular Diseases.
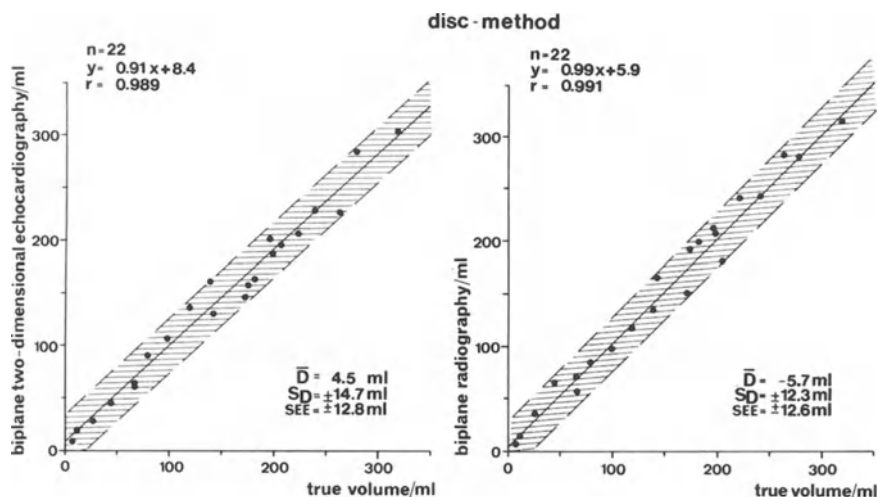
Figure 1. Correlation between directly determined, "true" or filling volume and indirectly measured volume by biplane two-dimensional echocardiography or radiography of asymmetric model hearts. D = mean difference ± standard deviation (S_D), SEE = standard error of estimate.

1 demonstrates, regression equations and correlations in patients with congestive cardiomyopathy and valvular heart disease were similar to those previously reported in patients with coronary artery disease [9]. That means that accuracy of volume determination by two-dimensional echocardiography is not dependent on underlying heart disease.

2. MODEL HEART STUDIES

In thin wall (1 mm) asymmetric model hearts, left ventricular volume determination was compared between directly measured "true" filling volume and indirectly measured two-dimensional echocardiographic and radiographic model heart volume. A disc method, area-length- and ellipsoid method for single and biplane volume calculation were used. For all calculation methods biplane estimation of volume was superior to single plane analysis. Only for the disc method – a modified Simpson's rule – could a linearity between the directly and indirectly determined volumes be found. For two-dimensional echocardiography the regression equation was given by $y = 0.91x + 8.4$, correlation coefficient, $r = 0.989$, standard error of estimate ± 12.8 ml, confidence limits 0.85, 0.98. For radiography regression the equation was $y = 0.99x + 5.9$, $r = 0.991$, standard error of estimate ± 12.6 ml, confidence limits 0.93, 1.06. Whereas "true" volume was not significantly underestimated by two-dimensional echocardiography, radiography overestimated "true" volume significantly. Between the two indirect methods a significant difference of 10.2 ± 21.1 ml was calculated. That means that a difference of about 10 ml
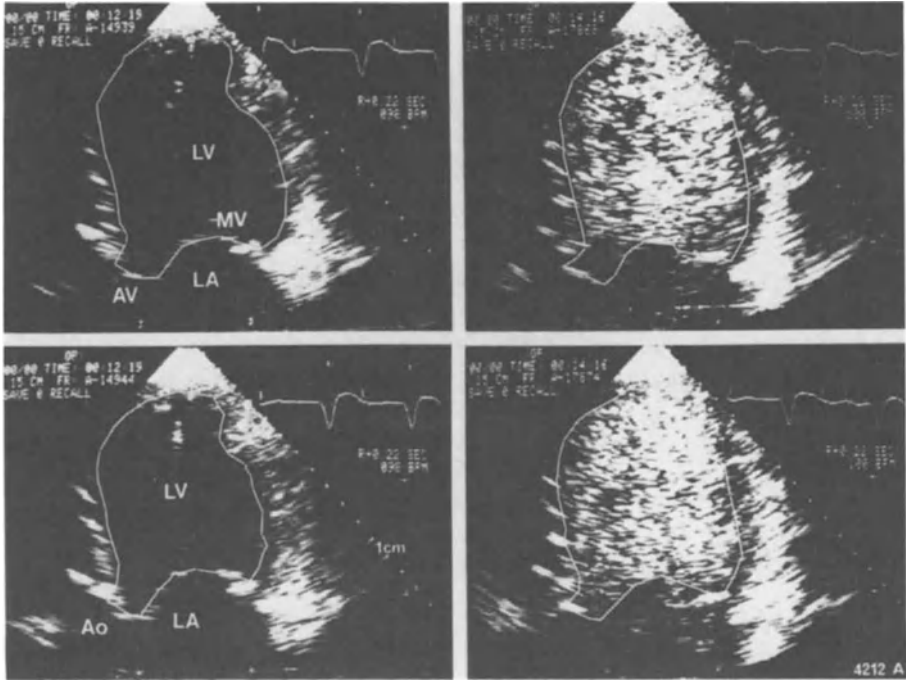
Figure 2. Apical two-dimensional echocardiogram in the RAO-equivalent view before (left side) and during (right side) cineventriculography at end-diastole and end-systole. LA/LV = left atrium/ventricle, Ao = Aortic root, MV = mitral valve. Endocardial border is outlined.

has to be expected because of methodological problems when comparisons between these two indect methods in patients are done (Figure 1).

3. ECHOVENTRICULOGRAPHY

In part, underestimation of left ventricular volume by two-dimensional echocardiography is explained by methodological difference observed in model heart studies. Differences in heart rate, blood pressure, and respiration phases, as well as possible influences of contrast agents were discussed as reasons for the systematic underestimation [9]. Therefore simultaneous recordings ot two-dimensional echocardiograms and cineventriculograms – echoventriculography – were performed to analyse left ventricular volume with both methods for the same heart beat. Radiographic contrast material served as a contrast agent for echocardiography as well. A typical example is shown in Figure 2. The injection of the contrast material filled the left ventricle with dense echoes; a clear outlining of left ventricular endocardial border was possible. The injection of contrast material resulted in a small increase of end-diastolic volume and stroke volume. With the fourth heart cycle left ven-
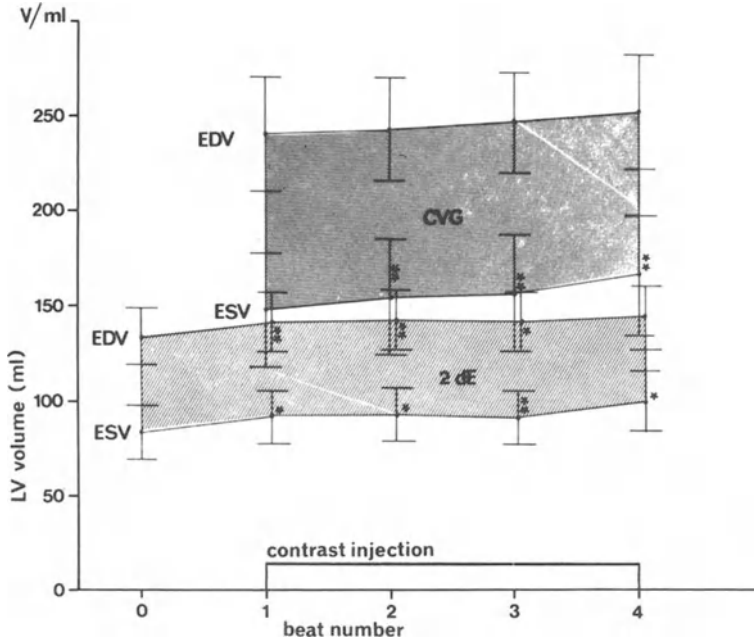
Figure 3. End-diastolic (EDV) and end-systolic volume (ESV) measured by cineventriculography (CVG) and two-dimensional echocardiography (2dE) for the first beat before and the four first beats during angiography.
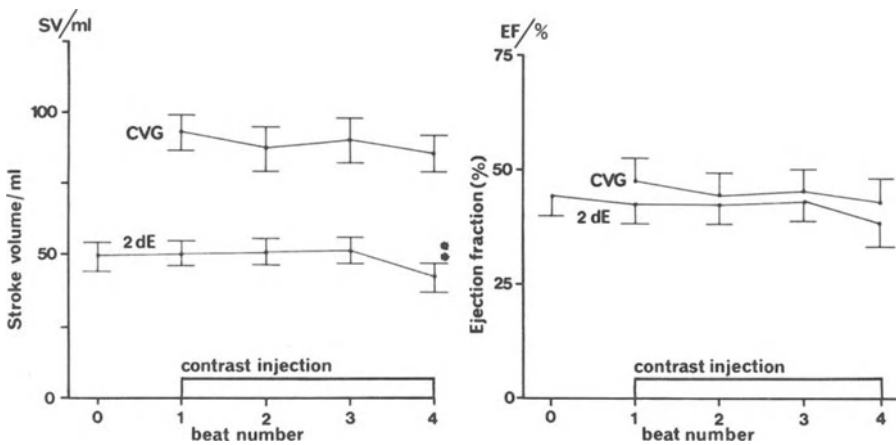
Figure 4. Stroke volume and ejection fraction of the left ventricle for the last beat before (0) and the first four beats (1–4) during contrast injection, cineventriculography (CVG), two-dimensional echocardiography (2dE). Both parameters decreased with the fourth beat, significantly for stroke volume determined by 2dE.
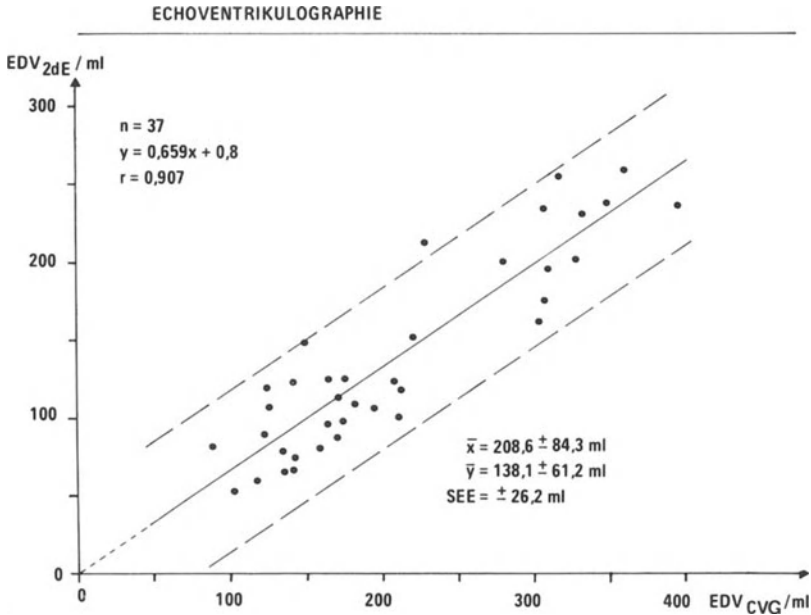
Figure 5. Correlation between cineventriculographic (CVG) and twodimensional echocardiographic (2dE) end-diastolic volume. $\bar{x}-$ = mean value, $\bar{y}-$ = mean value $\pm$ standard deviation, SEE = standard error of estimate.

tricular ejection fraction decreased significantly. This effect of the contrast material was observed with two-dimensional echocardiography and cineventriculography (Figures 3 and 4).

Analysis of left ventricular end-diastolic and end-systolic volume revealed a systematic underestimation of left ventricular volume as already observed in non simultaneous studies. For end-diastolic volume regression the equation was given by $y = 0.659x + 0.8$, $r = 0.907$, standard error of estimate ± 26.2 ml, for end-systolic volume by $0.571x + 17.8$, $r = 0.938$, standard error of estimate ± 18.6 ml (Figures 5 and 6). For ejection fraction regression the equation was $y = 0.606x + 13.0$, $r = 0.803$, standard error of estimate $\pm 9.1\%$. Mean value for two-dimensional echocardiography was $44.5 \pm 15.0\%$, for cineventriculography $52.0 \pm 19.9\%$. That means, despite simultaneous recordings of cineventriculography and echocardiography, left ventricular volume was underestimated by two-dimensional echocardiography.

Analysis of the position of the echo-transducer during cineventriculography revealed that the transducer was superiorly and anteriorly to the anatomic apex of the left ventricle (Figure 7) in 90% of our patients [18]. The mean angle between long axis of left ventricle and axial direction of echo beam measured $22.4 \pm 9.5°$ at end-diastole and $20.0 \pm 9.8°$ at end-systole ($n = 46$). These measurements were done during cineventriculograms in the 30° RAO-projection. In the 60° left anterior
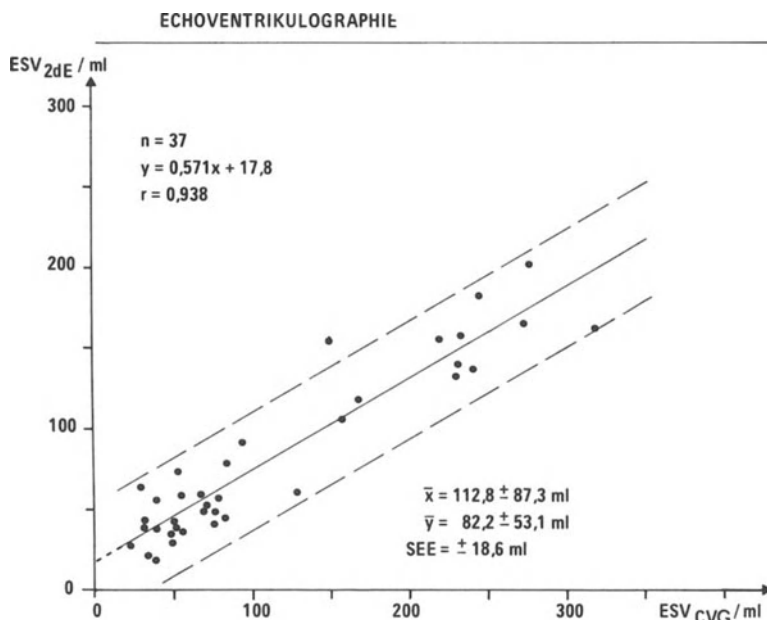
Figure 6. Correlation between cineventriculographic (CVG) and two-dimensional echocardiographic (2dE) end-systolic volume. Abbreviation see Figure 5.

oblique (LAO) 30° caudal-cranial projection, a mean angle of 33.1 ± 12.9° and 32.5 ± 12.7° was found, respectively.

Despite the transducer position being superiorly and anteriorly to the anatomic apex of the left ventricle, two-dimensional echocardiographic images showed that the left ventricle was scanned in the RAO-equivalent view in its whole contour and the long axis in the centre of the sector scan. Therefore two-dimensional echo-cardiographic image of the left ventricle represents in most patients a *tangential* cut of the heart resulting in underestimation of diameters, areas, and volumes of the left ventricle. Also underestimation of ejection fraction can be explained, because a tangential cut does not demonstrate the full contraction of a ventricle which is observed in the centre of the ventricle, as the tangential scan by M-mode in Figure 8 illustrates.

Other reasons of underestimation of left ventricular volume by two-dimensional echocardiography compared to cineventriculography have been discussed in detail previously [18]. Low lateral resolution and slice-thickness artifacts have to be mentioned [19, 20]. Differences in outlining left ventricular contour are important [18, 21]. Whereas for cineventriculograms outer borders of trabeculaes are followed, for two-dimensional echocardiography inner borders of the trabeculaes are out-lined. These differences could not be avoided by echoventriculography because it cannot be expected that microbubbles move inside the trabeculaes as contrast fluid
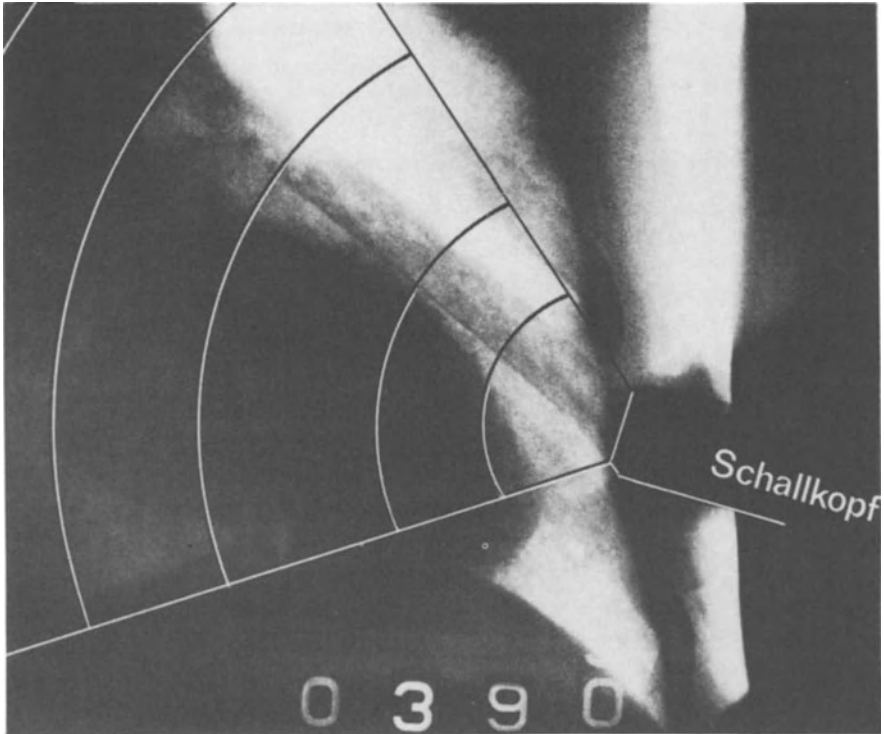
Figure 7. Cineventriculogram in the 30°RAO-view. On the screen the echo-transducer (Schallkopf) for simultaneous recording of two-dimensional echocardiogram in the apical RAO-equivalent view. Clearly illustrated is the position of the transducer superior to the anatomic apex. By fluoroscopic control a closer position to the apex of the left ventricle could not be achieved. Thus, a tangential cut of the ventricle could only be received.

does. It is concluded from these studies that underestimation of left ventricular contour is mainly due to a tangential cut of the heart, in part due to low lateral resolution, slice-thickness artifacts, and differences in outlining left ventricular endocardial border. Because of the large scatter of values for position of echo-transducer in respect to left ventricular apex, it seems to be impossible to predict for an individual patient the amount of underestimation. The fact that apical two-dimensional echocardiographic images represent tangential cuts of the heart have to be taken into account when three dimensional reconstructions of the heart are performed.

4. NORMAL VALUES

Correction of two-dimensional echocardiographically determined left ventricular volumes can be done with established regression equations, because correlation

coefficients were high and regression equations for different patient groups in one laboratory were comparable. Using this method important clinical results could be obtained in patients before and after coronary bypass surgery [22] and after re-cuscitation [23].

Because of the fact that high standard errors of estimate were found and that regression equations from one laboratory to the other differed significantly, and the large scatter of values which were found for the position of the echo-transducer in respect to left ventricular apex, it does not seem to be possible to predict under-estimation of ventricular volume by two-dimensional echocardiography for every individual patient. Therefore normal values for apical two-dimensional echocar-diography were calculated in 55 normal subjects, 35 men and 20 female. Mean age was 30.2 ± 6.0 and 26.2 ± 4.1 years respectively. Mean heart rate measured 72.5 ± 15.8 and $72.7 \pm 10.4 \, min^{-1}$, blood pressure $126.5 \pm 10.6/81.0 \pm 4.7 \, mmHg$ and $119.7 \pm 12.4/77.8 \pm 8.3 \, mmHg$. Left ventricular volume was determined in the RAO-equivalent and 4-chamber view for single plane measurements and in both combined planes for biplane calculations [24, 25]. Left ventricular volumes were calculated for body surface area. Normal values for the RAO-equivalent view are listed in Table 2. Indicated are mean values and standard errors of estimate. Tolerance limits separate the normal range from pathological values with a toler-ance coefficient of 95% covering a distribution of 90%. According to these tolerance limits classification of individual patients can be done.

No significant difference was found for normal values determined for RAO-equivalent and 4-chamber view, as well as for biplane measurements. Between men and women significant differences were found in respect to absolute values, but not for corrected values (that means for volume indices) [24, 25].

5. SENSITIVITY, SPECIFICITY, AND PREDICTIVE ACCURACY

In our laboratory the following tolerance borders are used: Cineventriculography: end-diastolic volume 205 ml, end-systolic volume 95 ml, stroke volume 72 ml, and ejection fraction 55%, two-dimensional echocardiography 155 ml, 70 ml, 43 ml, and 49% respectively. Based on these tolerance limits, sensitivity, specificity and pre-dictive accuracy for detection of left ventricular dysfunction were determined in 110 patients, 50 suffering from coronary artery disease, 38 from valvular heart disease, and 20 from dilatative cardiomyopathy [26]. For end-diastolic volume, sensitivity measured 83%, specificity 88%, and predictive accuracy 85%, for end-systolic volume 94, 86 and 86%, for stroke volume 39, 98 and 78%, and for ejection fraction 84, 98 and 98%. This means that impaired left ventricular function can be predicted by two-dimensional echocardiography with a high accuracy and sensitivity.

Table 2. Normal values for apical two-dimensional echocardiographic end-diastolic, end-systolic, stroke volume, and ejection fraction determination from RAO-equivalent and 4-chamber views (RAO/4C). Mean values $(\bar{x})$, standard deviation (SD), and tolerance borders with a tolerance coefficient of 95% covering 90% of the distribution

| | | End-diastolic volume index/ml/m^2 | | |
		RAO	Single-plane 4-chamber	Biplane RAO/4C
	$\bar{x}$	65.7	65.5	66.8
Male	SD	12.6	7.7	8.8
	T	87.5	78.8	82.0
	$\bar{x}$	59.3	62.0	60.7
Female	SD	11.4	10.8	12.5
	T	81.4	83.0	85.0

| | | End-systolic volume index/ml/m^2 | | |
		RAO	Single-plane 4-chamber	Biplane RAO/4C
	$\bar{x}$	27.4	27.2	26.9
Male	SD	7.2	5.2	5.2
	T	39.9	36.2	35.9
	$\bar{x}$	23.4	27.3	25.7
Female	SD	6.7	7.7	7.4
	T	36.4	42.2	40.1

| | | Stroke volume index/ml/m^2 | | |
		RAO	Single-plane 4-chamber	Biplane RAO/4C
	$\bar{x}$	37.1	38.3	39.9
Male	SD	8.0	5.5	7.0
	T	24.1	28.8	28.7
	$\bar{x}$	38.9	34.7	35.0
Female	SD	8.6	4.0	6.8
	T	23.4	26.9	21.8

Table 2 (continued)

		Ejection fraction/%		
		RAO	Single-plane 4-chamber	Biplane RAO/4C
Male	$\bar{x}$	58.5	58.7	59.2
	SD	7.1	5.9	6.0
	T	46.2	48.5	48.8
Female	$\bar{x}$	60.6	56.8	58.1
	SD	6.4	6.2	6.5
	T	48.2	44.8	45.5

6. REPRODUCIBILITY

Our studies revealed for beat-to-beat variability high values for explained variance calculated with a factor analysis program [27]. For RAO-equivalent view explained variance measured for end-diastolic volume was 95% and for end-systolic volume 96%, for stroke volume 88% and for ejection fraction 83%. Analysis of 5 instead of 3 consecutive heart beats revealed an increase of reliability of less than 1%. That means, for apical two-dimensional echocardiography, analysis of 3 consecutive heart cycles is sufficient; more heart cycles do not enhance accuracy.

Day-to-day variability was evaluated on three consecutive days in 16 subjects. It was found that an absolute change of at least 10–12 ml for ventricular volumes and 10% for left ventricular ejection fraction have to be assessed as a limit for significant serial alterations in individual patients to be able to differentiate between random and non random variations.

Intra-observer variability was small. No more than 5% intra-observer variability has to be expected for apical two-dimensional echocardiography as two-way analysis of variance and permutation tests revealed, except for the end-diastolic volume measured from RAO-equivalent views.

Inter-observer variability is strongly dependent on observer experience. Between experienced observers no significant differences were found for 4-chamber view and no significant differences for ejection fraction determined from RAO-equivalent views, but for end-diastolic, and end-diastolic volume as well as stroke volume in this scan plane, as permutation test demonstrated [27]. Thus, 4-chamber view showed a higher reproducibility than RAO-equivalent view.

7. PHARMACODYNAMICS

Comparison between two-dimensional echocardiography and cineventriculo-graphy before and after changes of ventricular function induced by positive in-otropic agent (Prenalterol), postextrasystolic potentiation, and heart rate were studied [28–30]. It could be demonstrated that regression equations before and after changes of ventricular function remained nearly unchanged. Therefore percentage changes of left ventricular volumes and ejection fraction of two-dimensional echo-cardiography and cineventriculography were comparable despite large differences in absolute values. That means, two-dimensional echocardiography can be used for pharmacodynamic studies if percentage changes instead of absolute changes are used.

8. CONCLUSIONS

Two-dimensional echocardiography can be used for left ventricular volume and ejection fraction determination with high sensitivity and specificity for detection of impaired left ventricular function. Analysis of 3 consecutive heart cycles should be performed. In serial studies a limits of 10% absolute change of ejection fraction has be assessed to differentiate between random and non random errors. Intra-observer variability is less than 5%. Inter-observer variability is strongly experience de-pendent. Percentage changes of left ventricular volumes and ejection fraction can be used for pharmacodynamic studies with two-dimensional echocardiography.

REFERENCES

1. Erbel R, Schweizer P: Diagnostischer Stellenwert der Echokardiographie bei der koronaren Herz-erkrankung – 1. M-mode Echokardiographie Z Kardiol 69:391–397, 1980.
2. Silverman NH, Schiller NB: Apex echocardiography. A two-dimensional technique for evaluating congenital heart disease. Circulation 57:503–511, 1978.
3. Gueret P, Corday E: Etide quantatitive de la function ventriculaire gauche per l'echocardiographie bidimensionelle. Arch Mal Coeur 74:329–33,6 1981.
4. Jenni R, Vieli A, Hess O, Anliker M, Krayenbuehl HP: Estimation of left ventricular volume from apical orthogonal 2–D echocardiograms. Eur Heart J 2:217–225, 1981.
5. Kan G, Visser CA, Lie KI, Durrer D: Left ventricular volumes and ejection fraction by single plane two-dimensional apex echocardiography. Eur Heart J 2:339–343, 1981.
6. Starling MR, Crawford MH, Sorensen SG, Levi B, Richards KL, O'Rourke RA: Comparative accuracy of apical biplane cross-sectional echocardiography and gated equilibrium radionuclide angiography for estimation of left ventricular size and performance. Circulation 63:1075–1084, 1981.
7. Schiller NB, Acquatella H, Ports TA, Drew D, Goerke J, Ringertz H, Silverman NH, Brundage B, Botvinick H, Boswell R, Carlsson E, Parmley WW: Left ventricular volume from paired biplane two-dimensional echocardiography. Circulation 60:547–555, 1979.
8. Moynihan PF, Parisi AF, Folland ED, Jones DR, Feldman CL: A system for quantitative evalua-

tion of the left ventricular function with two-dimensional ultrasonography. Med Instrum 14: 111–116, 1980.

9. Erbel R, Schweizer P, Meyer J, Grenner H, Krebs W, Effert S: Left ventricular volume and ejection fraction determination by cross-sectional echocardiography in patients with coronary artery disease: a prospective study. Clin Cardiol 3:377–383, 1980.

10. Touche T, Prasquier R, Merillon JP, Barthelemy M, Hanoun HC, Vervin P, Gourgon R; Mesure des volume ventriculaires gauches par echographie bidimensionelle a partir d'une coupe apicale. Arch Mal Coeur 73:691–700, 1980.

11. Erbel R, Schweizer P, Krebs W, Pyhel N, Meyer J, Effert S: Monoplane und biplane zweidimensionale echokardiographische Volumenbestimmung des linken Ventrikels. II. Untersuchungen bei koronarer Herzerkrankung. Z Kardiol 70:436–444, 1981.

12. Bommer W, Chum T, Kwan L, Neaman A, Mason DT: Biplane apex echocardiography versus biplane cineangiocardiography in the assessment of left ventricular volume and fraction: validation by direct measurements. Am J Cardiol 45:471, 1980.

13. Carr KW, Engler RL, Forsythe JR, Johnson AD, Gosink B: Measurement of left ventricular ejection fraction by mechanical cross-sectional echocardiography. Circulation 59:1196–1206, 1979.

14. Olshausen vK, Schuler G, Haueisen H, Leinberger H, Mehmel HC, Kübler W: Messung der L.V.-Ejektionsfraktion (LVEF) mittels zweidimensionaler mechanischer Apex-Echokardiographie (2DAE).

15. Helak JW, Plappert T, Muhammed A, Reichek N: Two dimensional echocardiographic imaging of the left ventricle: Comparison of mechanical and phased array systems in vitro. Am J Cardiol 48:728–735, 1981.

16. Latson LA, Cheatham JP, Gutgesell HP: Resolution and accuracy in two dimensional echocardiography. Am J Cardiol 38:106–110, 1981.

17. Erbel R, Krebs W, Henn G, Schweizer P, Richter HA, Meyer J, Effert S: Comparison of single-plane and biplane volume determination by two-dimensional echocardiography. I. Asymmetric model hearts. Eur Heart J (in press).

18. Erbel R, Schweizer P, Lambertz H, Henn G, Meyer J, Krebs W, Effert S: Echoventriculography – a simultaneous analysis of two-dimensional echocardiography and cineventriculography. Circulation (in press).

19. Schnittger I, Fitzgerald PJ, Daughters GT, Ingels NB, Kantrowitz NE, Schwarzkopf A, Mead CW, Popp RL: Limitations of comparing left ventricular volumes by two-dimensional echocardiography, myocardial markers and cineangiography. Am J Cardiol 50:512–519, 1982.

20. Goldstein A, Madrazo BL: Slice-thickness artifacts in gray-scale ultrasound. J Clin Ultrasound 9:365–375, 1981.

21. Joynt L, Popp RL: The concept of three dimensional resolution in echocardiographic imaging. Ultrasound in Med & Biol 8:237–247, 1982.

22. Erbel R, Schweizer P, Bardos P, Meyer J, Minale S, Messmer BJ, Effert S: Long-term control of left ventricular function after aortocoronary bypass surgery by two-dimensional echocardiography. In: Rijsterborgh H (ed), Echocardiology. Martinus Nijhoff, The Hague, Vol 9, pp 25–31, 1981.

23. Erbel R, Schweizer P, Lambertz H, Merx W, Meyer J, Effert S, Schoenmackers J: Prognostische Bedeutung der nicht invasiv bestimmten Ejektionsfraktion des linken Ventrikels bei reanimierten Patienten – Eine zweidimensionale echokardiographische Studie. Intensivmed 18:102–108, 1981.

24. Erbel R, Schweizer P, Meyer J, Effert S: Apikale zweidimensionale Echokardiographie. Normalwerte für monoplane and biplane Bestimmung der Volumina und der Ejektionsfraktion des linken Ventrikels. DMW (in press).

25. Erbel R, Schweizer P: Normal values for apical two-dimensional echocardiography. Ultrasound Med & Biol 8 (suppl 1):52, 1982.

26. Erbel R, Schweizer P, Meyer J, Effert S: Sensitivität und Spezifität der zweidimensionalen Echokardiographie zur Erkennung von Funktionsstörungen des linken Ventrikels. Z Kardiol 71:623, 1982.

27. Erbel R: Funktionsdiagnostik des linken Ventrikels mittels zweidimensionaler Echokardiographie. Habilitationsschrift, Aachen 1982.
28. Erbel R, Schweizer P, Lambertz H, Meyer J, Effert S: Kann die zweidimensionale Echokardiographie Änderungen der Ventrikelfunktion zuverlässig erfassen. Z Kardiol 71:154, 1982.
29. Erbel R, Schweizer P, Lambertz H, Voelker W, Meyer J, Effert S: Echoventricular analysis of prenalterol induced changes of left ventricular function. Circulation 64 (suppl IV):48, 1981.
30. Erbel R, Schweizer P, Lambertz H, Langen HP, Meyer J, Effert S: Einfluß der Herzfrequenz auf die Volumina und die Ejektionsfraktion des linken Ventrikels – eine zweidimensionale echokardiographische Studie. Verh Dtsch Ges Inn Med 88 (in press).
31. Erbel R, Schweizer P, Grenner H, Hofmann-Schneider E, Meyer J, Krebs W, Effert S: Zweidimensionale echokardiographische Bestimmung der linksventrikulären Volumina und der Ejektionsfraktion bei koronarer Herzerkrankung. Biomed Tech 24, Ergänzungsband, 82–83, 1979.
32. Folland ED, Parisi AF, Monihan PF, Jones DR, Feldman CL, Tow DE: Assessment of left ventricular ejection fraction and volumes by real-time, two-dimensional echocardiography. A comparison of cineangiography and radionuclide techniques. Circulation 60:760–766, 1979.
33. Parisi AF, Monihan PF, Feldman CL, Folland ED: Approaches to determination of left ventricular volume and ejection fraction by real-time two-dimensional echocardiography. Clin Cardiol 2: 257–263, 1979.
34. Quinones MA, Waggoner AD, Reduto LA, Nelson JG, Young JB, Winters WL, Ribiero LG, Miller RR: A new simplified and accurate method for determining ejection fraction with two-dimensional echocardiography. Circulation 64:744–753, 1981.
35. Barrett MJ, Jacobs L, Gumberg J, Hutton L, Meister SG: Simultaneous contrast two-dimensional echocardiography and contrast ventriculography: discrepancies in left ventricular volume. Am J Cardiol 47:453, 1981.
36. Roelandt J, Gorissen, Vletter WB, Meltzer RS: Contrast echocardiography: clinical applications. In: Schaper W, Gottwick MG (eds), Therapie der Arrthmien, Echokardiographie. Steinkopff, Darmstadt, pp 185–192, 1981.
37. Schnittger I, Fitzgerald PJ, Daughters GT, Ingles NB, Kantrowitz NE, Schwarzkopf A, Mead CW, Popp RL: Limitations of comparing left ventricular volumes by two-dimensional echocardiography, myocardial markers and cineangiography.
38. Hahn B, Bohn J, Strauer BE: Funktionsbeurteilung des Herzens mittles zweidimensionaler Echokardiographie. Z Kardiol 71:445–451, 1982.

9. IMAGING OF THE LEFT VENTRICLE BY CONTRAST ECHO-CARDIOGRAPHY

J. ROELANDT AND P.W. SERRUYS

The injection of biologically compatible solutions may produce a "cloud of echoes" in the blood which is otherwise echo free. The source of this echocardiographic contrast is microbubbles of air introduced during injection [1, 2]. Left ventricular catheter injections have been employed to identify left heart structures from M-mode echocardiograms [3, 4], to validate cardiac views imaged by two-dimensional echocardiography [5, 6], for the demonstration of small, intracardiac, left-to-right shunts and for the diagnosis of minimal degrees of aortic and mitral valve regurgitation [7, 8, 9].

Recently the possibility of transmitting echo contrast material across the capillary bed of the lungs to the left heart with pulmonary wedge injections [10, 11, 12] has been demonstrated. Some methodological and clinical aspects of left ventricular contrast echocardiography are reviewed. It should be realized, however, that most of this area is investigational.

METHODOLOGY OF LEFT VENTRICULAR CONTRAST ECHOCARDIOGRAPHY

Echocardiographic contrast studies of the left ventricle are performed in the catheterization laboratory. M-mode or two-dimensional techniques can be employed, each having its specific advantages and limitations for clinical problem solving and research.

Our experience with left ventricular echo contrast has been mainly with two-dimensional echocardiography. The long-axis and short-axis views from the parasternal transducer position as well as the four-chamber and long-axis views from apical transducer position are routinely recorded [6, 13]. The apical views are especially useful for quantitative left ventricular studies, since the entire left ventricle from apex to base can often be recorded. To create echocardiographic contrast, we routinely use a manual flush of the catheter with 5 to 10 ml of 5% dextrose in water. Indocyanine green dye may yield a better contrast effect because of its surfactant properties, which keep the microbubbles of air, resulting from the vigorous shaking during preparation, stabilized in the solution [2]. One millimeter of indocyanine green solution (5 mg/ml for adults) is injected into the catheter and manually flushed with 5 to 10 ml of physiologic saline or 5% dextrose in water [7].
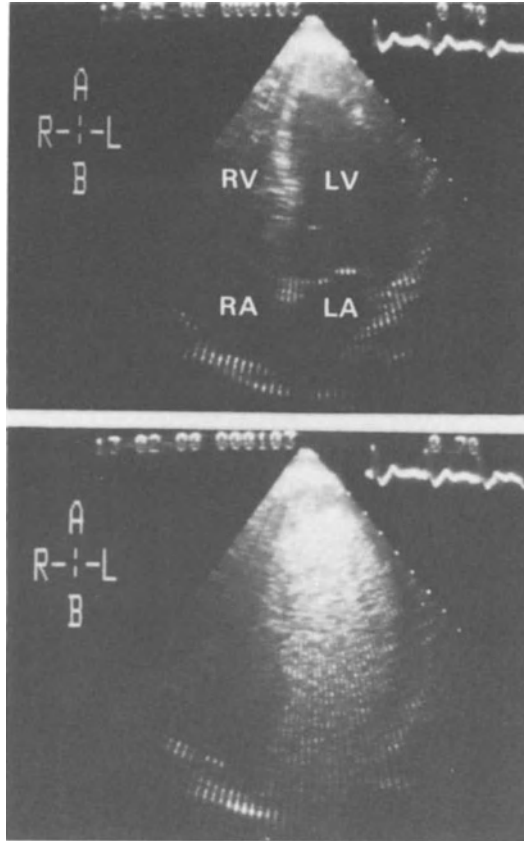
Figure 1. Stop-frame, apical four-chamber views obtained from a patient with a normal left ventricle immediately before (upper panel) and after pulmonary wedge injection of echocardiographic contrast (lower panel). The echo contrast fills both the left atrium (LA) and left ventricle (LV), of which the cavity contour becomes clearly delineated. A: apical; B: basal; L: left; R: right; RA: right atrium and RV: right ventricle. (With permission: Roelandt J et al: Contrast echocardiography of the left ventricle. In: Contrast Echocardiography, Roelandt J, Meltzer RS, Martinus Nijhoff, The Hague, 1982, pp 72–85.)

We have never observed any adverse patient reaction to direct left ventricular injections during echocardiographic contrast studies.

Bommer et al. [10] reported in 1979 that catheter injections in the pulmonary wedge position in dogs cause echocardiographic contrast on the left side of the heart. Reale et al [11] studied 43 patients with acquired or congenital heart disease and injected different echo-producing substances (indocyanine green dye, saline and carbon dioxide) via a balloon-tipped catheter in the pulmonary wedge position. Echocardiographic contrast was seen in the left ventricle in all patients studied. No complications or side effects were observed. We have studied 41 patients, using a Cournand 7F catheter alone in 27, a Swan-Ganz 7F catheter alone in 3 and both
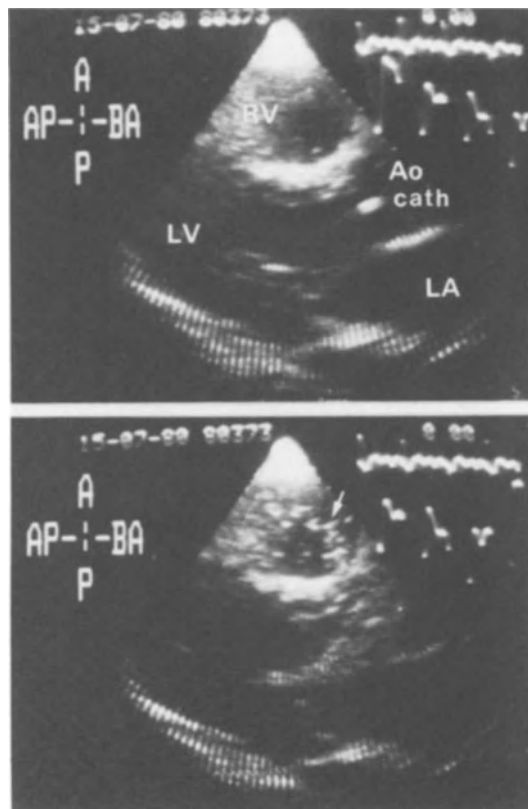
Figure 2. Parasternal long-axis views of a patient with a small ventricular septal defect before (upper panel) and after (lower panel) catheter injection of echo contrast in the left ventricular outflow tract. Echoes appear in the right ventricular outflow tract (arrow) proving the existence of a small left-to-right shunt. A: anterior; AP: apical; BA: basal; P: posterior; Ao: aorta; Cath: catheter; LA: left atrium; LV: left ventricle; RV: right ventricle. (With permission: Roelandt J et al: Contrast echocardiography of the left ventricle. In: Contrast Echocardiography, Roelandt J, Meltzer RS (eds), Martinus Nijhoff, The Hague, 1982, pp 72–85.)

catheters in 11, for pulmonary wedge injections [12]. Left ventricular echocardiographic contrast was seen in 3 out of 14 patients with the Swan-Ganz catheter and in 30 out of 38 patients when the Cournand catheter was used (Figure 1). We found that injection pressure proximal to the catheter had to be more than 40 kPa (300 mmHg) in order to obtain left side echocardiographic contrast.

Angiocardiographic studies with injections of Amipaque® further demonstrated that a complete occlusive wedge position of the catheter must be achieved. The latter finding probably explains the higher success rate with a Cournand catheter: its higher stiffness allows more complete occlusion. It is conceivable that the pressure applied during occlusive injections may allow deformation of the air

bubbles into a "dumbbell" shape resulting in their intact passage, rather than being retained by the "sieve" action of the capillary bed [14]. Apart from coughing, none of our patients had symptoms or worsening of their cardiopulmonary status related to the pulmonary wedge injections. Nonetheless, the method must still be considered as an experimental procedure until its safety has been finally established.

CLINICAL APPLICATIONS OF LEFT VENTRICULAR CONTRAST ECHOCARDIOGRAPHY

Demonstration of left-to-right shunts

Echo contrast flow patterns after left ventricular injection are helpful in identifying ventricular septal defects with left-to-right shunting and are at least as sensitive as indicator-dilution studies. Appearance of the echo contrast in the right ventricle or right ventricular outflow tract may be simultaneous with injection or be delayed by one cycle. The appearance time is dependent upon the timing of injection during the cardiac cycle and the position of the catheter in the left ventricle. A left-to-right shunt as small as 5% of the pulmonary flow may be detected [8]. We have experience with two patients in whom a ventricular septal defect was missed by oximetry and diagnosed by left ventricular contrast echocardiography (Figure 2). The method is useful for the demonstration of a left ventricular to right atrial shunt and the localization of small defects in the trabecular septum using the apical four-chamber view. Recently, Reale et al [11] have demonstrated the possibility of using pulmonary wedge injections for direct visualization of a left-to-right shunt at atrial or ventricular level, thus obviating left heart catheterization. They rightly concluded that the method could be used as a simple screening procedure during right heart catheterization to avoid invasion of the left heart in some patients. The toxicity of pulmonary wedge injections and the sensitivity of this approach as compared to oximetry and indicator dilution techniques need further evaluation.

Demonstration of valvular insufficiency

Systolic regurgitation of echo contrast material to the left atrium after left ventricular injection is indicative of mitral regurgitation. The method is sensitive and minimal amounts of regurgitation are readily detected [9, 15]. In moderate to severe degrees of mitral incompetence, the clearance time of the echo contrast form both the left atrium and left ventricle is considerably prolonged. Normally, echo contrast material remains from 4 to 10 cycles in the left ventricle and from 4 to 6 cycles in the left atrium. Uchiyama et al [16] were able to determine the site of regurgitation in two patients with mitral valve prolapse syndrome using the echo contrast techniques. Aortic regurgitation is demonstrated with a high degree of sensitivity by injecting echo contrast material in the aortic root and detecting its appearance in the left ventricle during diastole. The clearance time of the echo contrast from the left

ventricle is much prolonged (15 to 50 cycles). In some instances, the regurgitant pattern of echo contrast may be observed as a "shower of echoes" hitting the anterior mitral valve or interventricular septum. Clearance time cannot be used to quantify mitral or aortic regurgitation reliably. It may serve, however, to confirm or exclude its presence in patients in whom roentgenographic contrast studies are contraindicated due to pregnancy [17] or angiographic dye allergy.

EXPERIMENTAL APPLICATION OF LEFT VENTRICULAR ECHOCARDIOGRAPHY

Quantitation of left ventricular volume

Feigenbaum et al. [4] utilized left ventricular injections of indocyanine green dye to identify the endocardium from other echoes within its cavity. Even when using newer equipment, non-structural echoes often obscure the endocardial boundaries and make proper delineation of the left ventricular cavity difficult or even impossible [18]. It is conceivable that opacification of the left ventricular cavity with echocardiographic contrast would improve border recognition. Improved cavity delineation by echocardiographic contrast may increase the accuracy of left ventricular volume determination from two-dimensional images. All studies published so far on comparison of left ventricular volumes determined by angiocardiography demonstrate a systematic underestimation of volumes by the echo method. We therefore made recordings of the left ventricle in four views (parasternal long-axis and short axis views at mitral level; apical four-chamber and long-axis views) before and during left ventricular injections of dextrose 5% in water in 13 patients. Long-axis length and surface area within the endocardial contours were measured from stop-frame images independently from recordings with and without contrast using a lightpen system and a digital computer. These measurements were repeated by the same investigator one month later. Both long axis length and the surface area were significantly larger with contrast than without (p < 0.001). Thus, the use of echo contrast did improve the accuracy of these measurements. Measurements on contrast images did not improve the reproducibility, and even showed a higher intra-observer variability. This is not surprising as echo contrast improves border recognition in areas with non-structural echoes and endocardial drop-outs but obscures the endocardium in the areas where it is clearly visible during the baseline study. In another series of 18 patients we compared left ventricular volumes determined by angiocardiography with those measured from two-dimensional echocardiographic views (apical four-chamber view and apical long-axis view) before and during injections of echocardiographic contrast. The use of contrast improved the accuracy but did not alter the reproducibility (random error of measurement).
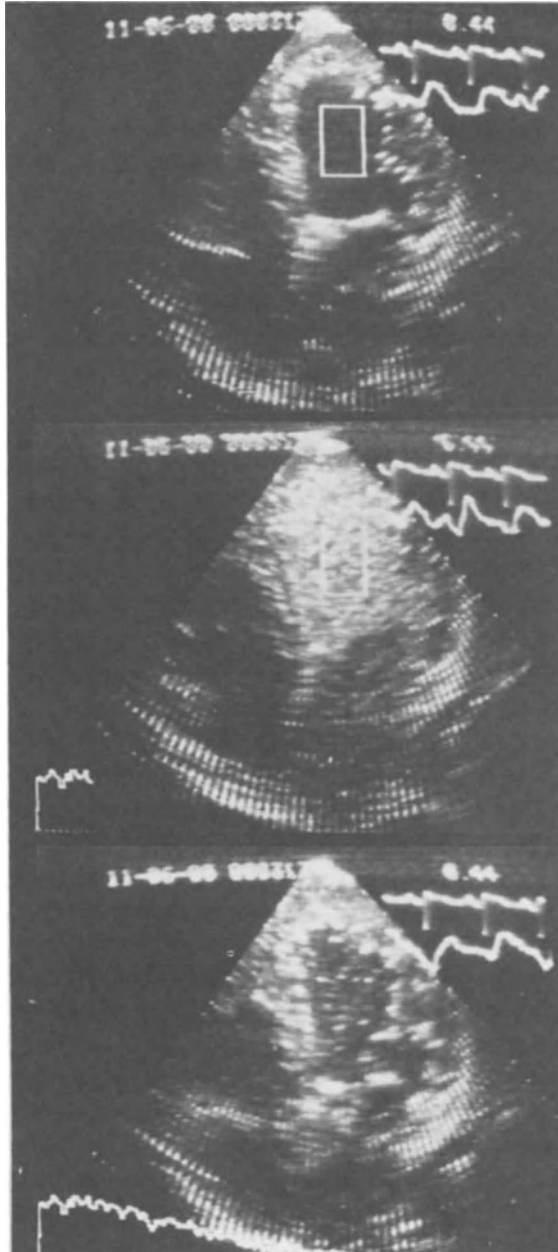
Figure 3. Apical four-chamber views with a rectangular sample area for measuring the videodensity designated within the left ventricular cavity (upper panel). During contrast studies, a curve of the cumulated videodensity is simultaneously displayed on the videoscreen (middle and lower panel). (With permission: Roelandt J et al: Contrast echocardiography in clinical practice. In: Progress in Medical Ultrasound, vol 3, Excerpta Medica, 1982, pp 183–216.)

Study of blood flow patterns

The non-contrast blood flowing from the left atrium into the left ventricle after its opacification with echo contrast allows us to observe transmitral blood flow. The negative contrast shadow delineates the functional mitral valve orifice while the anatomical orifice area is visualized during the baseline study. Intracavitary flow patterns produced by a mitral valve prosthesis can be followed after pulmonary wedge injections. Occasionally one may observe a vortex of echo contrast circulating within an ischaemic aneurysm in patients with coronary artery disease. Left ventricular contrast echocardiography may thus allow a new type of study on local flow, turbulence and stasis, which promises to become more useful in the future if transpulmonary echo contrast transmission becomes available.

Videodensitometric analysis of echocardiographic contrast

Bommer et al. [19] described in 1978 a method of obtaining dilution curves of echocardiographic contrast by videodensitometry. They focused an analog photometer upon the screen of the videomonitor over the middle of the right ventricular cavity during two-dimensional echocardiographic contrast studies. The dilution curves were reproducible on multiple echocardiographic contrast injections to an accuracy of 15%. The time course of decay made it possible to separate patients with normal from those with low cardiac output and/or tricuspid regurgitation. Echo-contrast indicator dilution curves of the left ventricle were subsequently performed in dogs using injections of 10 ml of a 1:100,000 concentration by volume of 30 micron diameter microballoons. Good correlations with cardiac output measurements were found [20]. We have used an image-processing computer to analyze video recordings of contrast injections in order to follow the decay of density after left ventricular and pulmonary wedge injections in 17 patients (Figure 3). A meaningful calculation of the area under the curve could not be made because of limitations due to video "overload" immediately after injection. In consequence, contrary to the studies by DeMaria et al [20], it seems that cardiac output measurements cannot be estimated reliably using routine contrast dilution techniques. The decay phase was found to be exponential and has characteristics of indicator-dilution curves, as predicted theoretically. Preliminary data indicate that R-wave gating may allow estimation of ejection fraction [21].

Hagler et al [22] used computer-based videodensitometric techniques to analyze video recordings of left ventricular contrast echocardiograms to quantitate left-to-right shunts. Time-density histograms were generated from the right and left ventricular cavities after injection of echo contrast in the left ventricle in 7 patients with a ventricular septal defect. Their results indicate the possibility of quantitating shunts with these techniques.

REFERENCES

1. Gramiak R, Shah PM: Echocardiography of the aortic root. Invest Radiol 3:356, 1968.
2. Meltzer RS, Tickner EG, Sahines TP, Popp RL: The source of ultrasonic contrast effect. J Clin Ultrasound 8:121, 1980.
3. Gramiak R, Shah PM, Kramer DH: Ultrasound cardiography: contrast studies in anatomy and function. Radiology 92:939, 1969.
4. Feigenbaum H, Stone JM, Lee DA, Nasser WK, Chang S: Identification of ultrasound echoes from the left ventricle by use of intracardiac injections of indocyanine green. Circulation 41:614, 1970.
5. Sahn DJ, Dilliams DE, Shackelton S, Friedman WF: The validity of structure identification for cross-sectional echocardiography. J Clin Ultrasound 2:201, 1975.
6. Tajik AJ, Seward JB, Hagler DJ, Mair DD, Lie JT: Two-dimensional real-time ultrasonic imaging of the heart and great vessels: technique, image orientation, structure identification and validation. Mayo Clin Proc 53:281, 1978.
7. Seward JB, Tajik AJ, Spangler JG, Ritter DE: Echocardiographic contrast studies. Mayo Clin Proc 50:163, 1975.
8. Pieroñ DR, Varghese J, Freedom RM, Rowe RD: The sensitivity of contrast echocardiography in detecting intracardiac shunts. Cathet Cardiovasc Diagn 5:19, 1979.
9. Kerber RE, Kioschos JM, Lauer RM: Use of ultrasonic contrast method in the diagnosis of valvular regurgitation and intracardiac shunts. Am J Cardiol 34:722, 1974.
10. Bommer WJ, Mason DT, DeMaria AN: Studies in contrast echocardiography: development of new agents with superior reproducibility and transmission through lungs. Circulation 59 and 60 (suppl II):II–17, 1979 (abstr).
11. Reale A, Pizzuto F, Giaffré PA, Nigri A, Romeo F, Martuscelli E, Mangier E, Scibilia G: Contrast echocardiography: transmission of echoes to the left heart across the pulmonary vascular bed. Eur Heart J 1:101, 1980.
12. Meltzer RS, Serruys PW, McGhie J, Verbaan N, Roelandt J: Pulmonary wedge injections yielding left-sided echocardiographic contrast. Brit Heart J 44:390, 1980.
13. Meltzer RS, Meltzer C, Roelandt J: Sector scanning views in echocardiography: a systematic approach. Eur Heart J 1:379, 1980.
14. Meltzer RS, Sartorius OEH, Lancée CT, Serruys PW, Verdouw PD, Essed CE, Roelandt J: Transmission of ultrasonic contrast through the lungs. Ultrasound in Med & Biol 7:377, 1981.
15. Amano K, Sakamoto T, Hada Y, Yamaguchi T, Ishimitsu T, Adachi H: Contrast echocardiography: application for valvular incompetence. J. Cardiography 9:697, 1979.
16. Uchiyama I, Isshiki T, Koizumi K, Ohuchi Y, Kuwako K, Umeda T, Machii K, Furuta S: Detection of the site and severity of mitral valve prolapse by real-time cross-sectional echocardiography with contrast technique. J Cardiography 9:689, 1979.
17. Meltzer RS, Serruys PW, McGhie J, Hugenholtz PG, Roelandt J: Cardiac catheterization under echocardiographic control in a pregnant woman. Amer J Med 71:481, 1981.
18. Roelandt J, Van Dorp WG, Bom N, Hugenholtz PG: Resolution problems in echocardiology, a source of interpretation errors. Amer J Cardiol 37:256, 1976.
19. Bommer W, Neef J, Neumann A, Weinert L, Lee G, Mason DT, DeMaria AN: Indicator-dilution curves obtained by photometric analysis of two-dimension echo-contrast studies. Amer J Cardiol 41:370, 1978 (abstr).

20. DeMaria AN, Bommer W, Riggs K, Dajee A, Miller L, Mason DT: In vivo correlation of cardiac output and densitometric dilution curves obtained by contrast two-dimensional echocardiography. Circulation (III–101) 1980 (abstr).
21. Bastiaans OL, Roelandt J, Piérard L, Meltzer RS: Ejection fraction from contrast echocardiographic videodensity curves. Clin Res 29:176, 1981 (abstr).
22. Hagler DJ, Tajik AJ, Seward JB, Mair DD, Ritter DG, Ritman EL: Videodensitometric quantitation of left-to-right shunts with contrast sector echocardiography. Circulation 57 and 58 (suppl II):II–70, 1978 (abstr).

10. QUANTIFICATION OF LEFT VENTRICULAR FUNCTION BY DOPPLER ULTRASOUND

KENT RICHARDS AND SCOTT CANNON

INTRODUCTION

Measurement of cardiac performance is a critical task in the evaluation of patients with cardiac disease. Because the heart's most important function is to deliver adequate blood flow to meet the metabolic needs of tissues, measurement of cardiac output is an important method of assessing cardiac performance. Unfortunately, resting cardiac output varies widely in normals and this normal range overlaps with that of individuals in which cardiac performance may be severely altered because of disease. Thus, evaluation of left ventricular performance must employ techniques which either pharmacologically or physically stress the heart, or which consider the independent roles of afterload, preload and contractibility on cardiac performance. The following discussion will emphasize the usefulness of non-invasive Doppler ultrasound in assessing systolic left ventricular performance. The role of parameters derived by combining ultrasonic imaging and Doppler will be stressed.

DOPPLER ECHOCARDIOGRAPHIC TECHNIQUES

Doppler echocardiography utilizes high frequency sound (usually 2–5 MHz) which is broadcast transcutaneously into the heart and great vessels. The frequency of ultrasound reflected from moving blood cells is shifted by an amount proportional to the velocity (V) of the moving blood. The Doppler frequency shift is the difference in frequency between the broadcast carrier signal and the reflected signal (F_R). Velocity may be calculated from the Doppler equation if Doppler frequency shift (F_D), speed of ultrasound and tissue (C_T), carrier frequency (F_c), and the cosine of the angle between the ultrasound beam and the blood velocity vectors ($\cos \theta$) are measured:

$$V = \frac{(F_D)\,(C_T)}{2\,(F_c)\,(\cos \theta)} \text{ (Figure 1.).}$$

If volume flow ($\dot{Q}$) is to be calculated, the cross-sectional area (A) of the vessel at the point at which the velocity measurement was made, must be known (Figure 2).
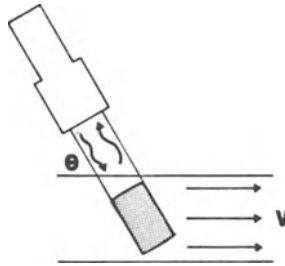
Figure 1. Ultrasound broadcast from the transducer encounters blood cells moving at velocity V within the sample volume (shaded) and is reflected back into the transducer. Doppler angel θ is shown.
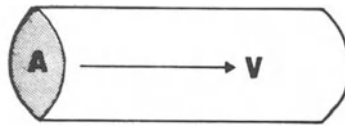
Figure 2. Volume flow (Q) may be measured if velocity (V) and cross-sectional area (A) of the vessel are known.

To estimate blood velocity accurately, the volume of blood sampled by Doppler must be representative of velocity patterns present across the entire cross-sectional area of the vessel. If volume flow is measured, it is assumed that the change in vessel diameter during systole is small. If serial measurements under different hemodynamic conditions are to be made, the velocity profile across the vessel cross-section is assumed to remain relatively constant; changes in vessel cross-sectional area must be measured for each hemodynamic situation.

Both images of Doppler flow data are required if volume flow, or changes in volume flow or velocity, are to be measured.

DOPPLER ECHOCARDIOGRAPHIC MEASUREMENT OF CARDIAC OUTPUT

An accurate, non-invasive method of monitoring beat-to-beat changes in cardiac stroke volume would be extremely useful in assessing cardiac function in critically ill patients as well as in those undergoing new therapeutic interventions. It would also provide objective information about the response to various diagnostic maneuvers (i.e. Valsalva) or the response to transient changes in cardiac rhythm (i.e. ventricular or atrial premature beats). Doppler echocardiographic techniques appear useful in each of these areas.
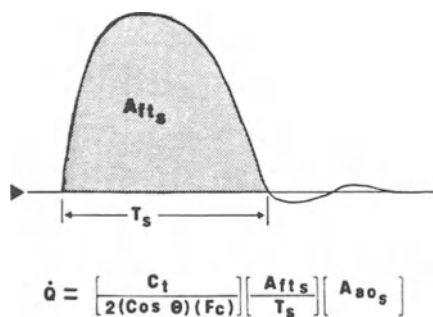
Figure 3. An analog Doppler tracing from the ascending aorta illustrates derivation of the systolic frequency-time area and systolic time. Time is on the X-axis and frequency shift on the Y-axis.

High quality Doppler echocardiographic recordings of blood velocity from the aorta have been reported by multiple investigators [1–4]. A good correlation between velocity calculated from ultrasonic Doppler echocardiographic techniques and that obtained using electromagnetic flowmeters has been demonstrated in instrumented animals [5–7]. Changes in the area under the systolic velocity-time curve (the integral of the systolic velocity signal) have correlated well with changes in stroke volume determined by invasive methods in experimental animals [5, 7] and man [8, 9]. The measurements in animal preparations appear valid whether induced by change in volume status or change in inotropic state [5, 7].

Cardiac output measurements in man require determination of aortic cross-sectional area at the level of the Doppler sample volume, as well as Doppler angle and the area under the Doppler frequency-time curve or mean Doppler frequency shift. Volume flow is directly proportional to the product of the speed of ultrasound in tissue ($C_T = 1.5 \times 10^5$ cm/sec), the systolic frequency-time area (A_{fts}) and the systolic aortic cross-sectional area (A_{AOs}), and inversely proportional to the product of the cosine of the Doppler angle (cos θ), frequency (F_c) and the sum of the time of systole for all frequency-time areas measured (T_s) (Figure 3).

In a series of 29 patients Darsee et al. [9] found a correlation coefficients of .96–.98 between thermodulation or Fick cardiac output and that obtained by Doppler techniques. Doppler measurements were made in the ascending aorta with the transducer at the suprasternal notch; the cosine of the Doppler angle was assumed to be one. Aortic cross-sectional area was measured at the aortic valve leaflets by M-mode echocardiographic technique.

A similar study by Magnin et al. [8] of 11 patients utilized a combined pulsed Doppler-phased-array ultrasonoscope. Because the parasternal window was used to measure ascending aortic velocity, accurate measurement of Doppler angle was important and was accomplished by superimposing Doppler beam and sample volume position on the two-dimensional echocardiographic image utilized to measure aortic cross-sectional area. A correction coefficient of .83 was observed be-
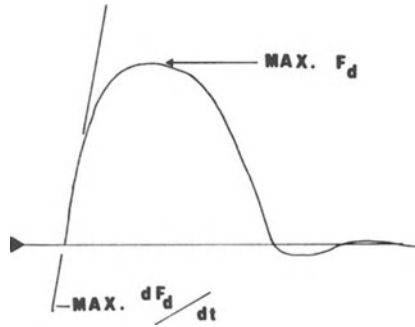
Figure 4. An analog Doppler tracing from its ascending aorta illustrates derivation of maximum blood acceleration (from maximum change in frequency per unit time, dF_d/dt) and maximum velocity (from maximum frequency, F_d).

tween simultaneous Fick and Doppler cardiac output. Considerable variability in the Doppler cardiac output occurred with changes in the parasternal window utilized; the authors attributed this primarily to difficulty in accurately measuring the three-dimensional angle required for velocity calculations.

Subsequent studies by Hoekenga et al [10] and Voyles et al [11] have utilized the suprasternal notch window to obtain ascending aortic Doppler signal. A correlation coefficient of .87 was noted between Fick and Doppler cardiac output in a series of 15 patients. Reproducibility of the suprasternal notch approach was demonstrated by observing less than 20% change in serial Doppler cardiac output measurements made by two separate technicians on ten resting patients.

The feasibility of performing Dopplercardiographic studies from the suprasternal notch during rest and upright bicycle exercise has been demonstrated by Greene et al [12]. Interestingly, a reduced increase in cardiac output was observed in patients with coronary artery disease when compared to normal controls. Their study suggests the possibility of using exercise Dopplercardiography as a means of evaluating left ventricular performance in patients with normal resting flow.

DOPPLER CARDIOGRAPHIC DETERMINATION OF MAXIMUM AORTIC VELOCITY AND ACCELERATION

The usefulness of maximum velocity and acceleration of ascending aortic blood flow as a method of assessing left ventricular contractility was first suggested by Rushner [13]. Kezdi et al [15] and Noble et al [14] have demonstrated a decrease in maximum acceleration during progressive left ventricular dysfunction induced in a canine model by acute coronary artery occlusion. A recent study by Van Den Bos et al [16] suggests that maximum blood acceleration is less influenced by changes in preload and afterload than are other ejection phase indices of ventricular contractility. During negative inotropic maneuvers, isovolumic indices (i.e. LV dp/dt) and maxi-

mum aortic blood acceleration move in parallel. Numerous authors have used both maximum aortic flow velocity and acceleration to assess left ventricular function in patients with coronary artery disease [17–19]. In a recent study by Klinke et al [20] changes in maximum velocity and acceleration were measured in 9 patients undergoing catheterization with a special electromagnetic flow probe; observations were made before and after propranolol injection. Their study demonstrated the expected decrease maximum dp/dt induced by administering the negative inotropic agent and illustrated the parallel changes in aortic flow acceleration and velocity. Important conclusions suggested by the authors included:

1. Usefulness of ascending aortic flow parameters – maximum velocity and acceleration – in assessing contractile state.
2. Parallel change between more classic indices of isovolumic function (maximum dp/dt) and ejection phase indices (stroke volume and stroke work), and maximum blood velocity and acceleration.

Though invasive validation of Doppler-derived aortic acceleration data has not been performed, comparison of invasive and non-invasive velocity-time records has been performed [6, 7]; correlations suggest that acceleration data should be available transcutaneously.

DOPPLER ECHOCARDIOGRAPHIC DERIVATION OF SYSTOLIC TIME INTERVALS

The ability to record systolic time intervals using non-invasive Doppler has been demonstrated by Rothendler et al [21]. Their technique utilized a Doppler ultrasound transducer over the temporal artery instead of the conventional carotid indirect pressure transducer. There was excellent correlation between conventional and Doppler-temporal artery derived left ventricular ejection time and pre-ejection period ($r = .99$). The major advantage in the technique is that it reduces artifact induced by motion. Because of this, Doppler-systolic time intervals may be obtained during moderate levels of exercise.

SUMMARY

The above literature suggest the clinical usefulness of Doppler in non-invasive evaluation of left ventricular performance. The data suggesting the use of ultrasonic Doppler and imaging in measuring changes in cardiac output are encouraging. Initial data concerning the usefulness of maximum aortic flow acceleration to evaluate left ventricular contractibility are exciting but require further investigation. The usefulness of systolic time intervals obtained during physical stress, likewise, awaits further research.

96

REFERENCES

1. Franklin DL, Schlegel W, Rushner RF: Bloof flow measured by Doppler frequency shift of back-scattered ultrasound. Science 134:564–569, 1961.
2. Light LH: Transcutaneous observation of blood velocity in the ascending aorta in man. J Physiol (Loud) 204:1P–2P, 1969.
3. Johnson SL, Baker DW, Lute RA, Dodge HT: Doppler echocardiography. Circulation 48:810–822, 1973.
4. Huntsman LL, Gams E, Johnson CC, Fairbanks E: Transcutaneous determination of aortic blood-flow velocities in man. Am Heart J 89:605–612, 1975.
5. Colocousis JS, Huntsman LL, Curreri PW: Estimation of stroke volume changes by ultrasonic Doppler. Circulation 56:914–917, 1977.
6. Steingart RM, Meller J, Barovick J, Patterson R, Herman MU, Teichholz LE: Pulsed Doppler echocardiographic measurement of beat-to-beat changes in stroke volume in dogs. Circulation 62:542–548, 1980.
7. Darsee JR, Mikolich JR, Walter PF, Schlant RC: Transcutaneous method of measuring Doppler cardiac output. Am J Cardiol 46:607–612, 1980.
8. Magnin PA, Stewart JA, Myers S, von Ramm O, Kisslo JA: Combined Doppler and phased-array echocardiographic estimation of cardiac output. Circulation 62:388–392, 1980.
9. Darsee JR, Walter PF, Nutter DO: Transcutaneous Doppler method of measuring cardiac output. Am J Cardiol 46:613–618, 1980.
10. Hoekenga DE, Greene ER, Loeppky JA, Mathews EC, Richards KL, Luft UC: A comparison of noninvasive Dopplercardiographic and simultaneous Fick measurements of left ventricular stroke volume in man. Circulation 62 III:199, 1980.
11. Voyles WF, Greene ER, Mirands IP, Reilly PA, Caprihan A: Observer variability in serial nonin-vasive measurements of stroke index using pulsed Doppler flowmetry. Biomedical Sciences In-strumentation 18:67–75, 1982.
12. Greene ER, Loeppky JA, Mathews EC, Hoekenga DE, Richards KL, Tuttle WC: Noninvasive Doppler stroke volume during rest and exercise. Proc of ACEMB 22:23, 1980.
13. Rushner RF: Initial ventricular impulse: a potential key to cardiac evaluation. Circulation 29:268–283, 1964.
14. Noble MIM, Trenchard D, Guz A: Left ventricular ejection in conscious dogs. Circ Res 19:139–147, 1966.
15. Kezdi P, Stanley EL, Marshall WK Jr, Kordenal RK: Aortic flow velocity and acceleration as an index of ventricular performance during myocardial infarction. Am J Med Sci 257:61–71, 1969.
16. Van Den Bos GC, Elzinga G, Westerhof N, Noble MIM: Problems in the use of indices of myocardial contractility. Cardiovaso Res 7:834–848, 1973.
17. Bennett ED, Else W, Miller G, Sutton GC, Miller HC, Noble MIM: Maximum acceleration of blood from the left ventricle in patients with ischemic heart disease. Clin Sci Mol Med 46:49–59, 1974.
18. Jenett D, Gake I, Mills C, Maver B, Thomas M, Shillingford J: Aortic velocity and acceleration measurements in the assessment of coronary heart disease. Eur J Cardiol 1:299–305, 1974.
19. Kolettis M, Jenkins BS, Webb-Peploe MM: Assessment of left ventricular function by indices drived from aortic flow velocity. Br Heart J 38:18–31, 1976.
20. Klinke WP, Christie LG, Nichols WW, Roy ME, Curry RC, Pepine CJ, Conti CR: Use of catheter-tip velocity-pressure transducer to evaluate left ventricular function in man. Circulation 61:946–954, 1980.
21. Rothendler JA, Schick EC, Ryan TJ: Derivation of systolic time intervals from Doppler measure-ment of temporal arterial blood flow. Am J Cardiol 47:68–72, 1981.

11. SCINTIGRAPHIC METHODS FOR QUANTIFYING GLOBAL LEFT VENTRICULAR FUNCTION*

HARALD SCHICHA

The global function of the left ventricle can be assessed by pressure and volume parameters. Volume parameters can be measured non-invasively by the following nuclear medicine procedures:
- measurement of minimal cardiac transit times,
- first pass radionuclide angiography (first pass RNA),
- multiple gated blood pool examination (multiple GBP).

MINIMAL CARDIAC TRANSIT TIMES

The minimal cardiac transit times are the differences of the appearance times in the various heart segments obtained after intravenous injection of a radioactive bolus. In patients with valvular heart disease and in patients with congestive heart failure the transit times are prolonged. The method proved to be very sensitive in detecting global cardiac malfunction, because in addition to the transit times of the ventricles, those of the atria and lung are also measured [1]. However, specificity is limited and repeated examinations in short time intervals are not possible.

For the detection and differentiation of cardiac diseases the assessment of regional function in addition to global function is essential. Moreover, abnormalities are observed frequently only during exercise. Therefore methods should be preferred which can assess global and regional function at rest as well as during exercise. For this purpose the first pass RNA and the multiple GBP are widely applied.

FIRST PASS RNA (Figure 1)

After injection of 10 to 20 mCi of $^{99\,m}$Tc as a bolus the first pass through the heart is registered generally in RAO position using a gamma camera with computer [2]. After flagging a region of interest of the whole heart, a double-peak curve is obtained. The first peak relates to the right (RH) and the second peak to the left
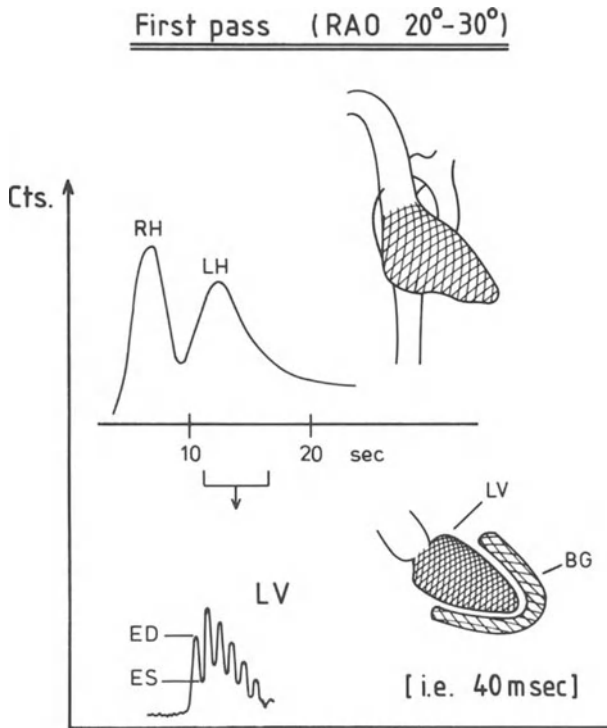
Figure 1. First pass RNA.

heart (LH). When imaging is performed during the first and the second peak, the right and the left ventricle can be separated. After background subtraction a high frequency curve from the right and the left ventricle (LV) can be generated. The count maxima represent the enddiastolic phase (ED) and the minima the end-systolic phase (ES). From these curves the right and left ventricular ejection fraction (RVEF, LVEF) can be calculated [3].

MULTIPLE GBP (Figure 2)

An ECG-gated count acquisition of the heart was first introduced by Hoffmann and Kleine in 1965 [4]. This principle was applied to the gamma camera by Strauss et al in 1971 [5]. Fifteen to 25 mCi ^{99m}Tc labelled albumin or red blood cells are injected. After 3 to 5 minutes the tracer is distributed equally within the circulation. The count acquisition by the gamma camera is directed by the patient's ECG via computer. The duration of several heart beats is measured by the computer and the heart cycle is then gated into 16 to 50 frames. The count acquisition is performed for 2 to 5 minutes to obtain adequate information for each single frame. Thus a

MULTIPLE GATED (LAO 30°-50°)
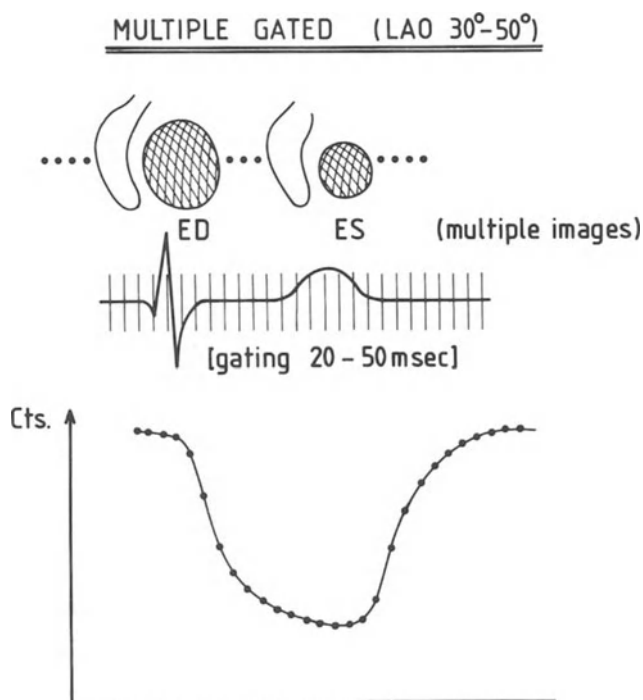
Figure 2. Multiple GBP.

representative heart cycle is generated which is the mean of several hundred beats. When imaged as a movie using an endless loop the impression of a beating heart is given. For quantitative evaluation the contour of the left ventricle should be flagged by multiple regions of interest according to its change during t'ıe heart cycle. This can be performed automatically. The resulting time-activity curve is equivalent to the volume changes of the left ventricle [6, 7, 8]. This can be performed for the right ventricle, too.

VOLUME PARAMETERS OF GLOBAL LEFT VENTRICULAR FUNCTION

Several volume and time-volume parameters can be derived quantitatively from the first pass RNA as well as from the multiple GBP (Figure 3). The most important parameter is the ejection fraction. The ejection fraction during the first third of systole (1/3EF) is considered to be more sensitive than the total one. Peak ejection rate, early diastolic filling rate and circumferential fiber shortening are also assumed to be sensitive parameters of global left ventricular function. Pre-ejection period, ejection time and rapid diastolic filling time can be measured, too. Ad-
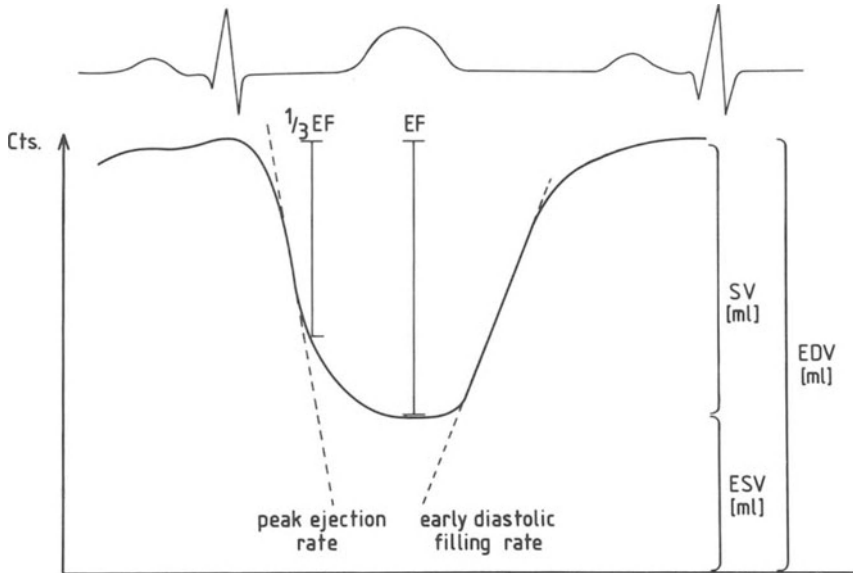
Figure 3. Volume and time-volume parameters of the activity curve.

Table 1. Comparison of first pass RNA and multiple GBP

	First pass	Multiple gated
Equipment	Gamma camera and computer	
Radionuclide	Tc–99m (Kr–81m, Au–195m)	Tc–99m
Bolus problems	Possible	No
positioning problems	Possible	No
Acquisition time	0.5–1 min	2–5 min
No of beat evaluated	3–6	150–600
time for evaluation	5–20 min	5–20 min
Separation of RV and LV	By geometry and by time	Only by geometry
Examination position	RAO 20°–30° anterior	LAO 30°–50° anterior LAO 60° 70°
Multiple positions	No	Yes
Multiple acquisitions (i.e. stepwise stress, drugs)	No	Yes
Absolute volumes (EDV, ESV, SV, cardiac output)	Yes	Yes
RVEF	Yes	Yes

ditionally absolute volumes can be calculated as the enddiastolic volume (EDV), the endsystolic volume (ESV) and the stroke volume (SV) in milliliters and the cardiac output (CO) in liters per minute. By comparing the output counts of the right and the left ventricle regurgitation fractions can be estimated.

Several questions arise:

1. Which are the advantages and disadvantages of the first pass RNA and the multiple GBP?
2. What is the accuracy of both methods compared to angiography?
3. How is their reproducibility?
4. Which are the advantages and the disadvantages compared to echocardiography?
5. What are the physiological and pathological reactions of the volume parameters of cardiac function? Which are the clinical indications for nuclear cardiac studies?

COMPARISON BETWEEN FIRST PASS RNA AND MULTIPLE GBP (Table 1)

For both methods a gamma camera with computer is necessary. It has to be noted that the quality and the versatility of the commercially available computer-software is very different and does influence accuracy and reproducibility of the results.

Up to now ^{99m}Tc is the most common radionuclide applied. In the case of multiple GBP albumin or red blood cells are labelled in order to obtain a tracer which stays predominantly in the circulation during the investigation.

The in-vivo labelling of red blood cells is easier, but the quality of the in-vitro labelling is superior. For the assessment of the right ventricular function also ^{133}Xe and ^{81m}Kr have been used. Whether the newly generator-nuclide ^{195m}Au will be superior and generally utilized for the first pass RNA, is dependent on the cost and on its availability.

For the first pass RNA a bolus injection is necessary. This requires a special injection technique. If the bolus is not sufficient or if regurgitation or severe pulmonary hypertension is present, evaluation may be impossible. These limitations are avoided by the multiple GBP.

The multiple GBP permits individual positioning of the gamma camera over the heart. This is not possible using the first pass RNA.

For the multiple GBP acquisition at least 2 minutes are required for each position. This may be critical in patients with severe exercise angina. The main advantage of the first pass RNA is the short acquisition time of about 20 to 30 seconds.

The evaluation of data can be performed automatically for the most part of both methods. The time needed is dependent on the complexity of evaluation and ranges between 5 and 20 minutes.

Using the first pass RNA separation of the right and left ventricle is possible by

$$EF_{GBP} = 0.2 + 0.94 \times EF_{Angio}$$
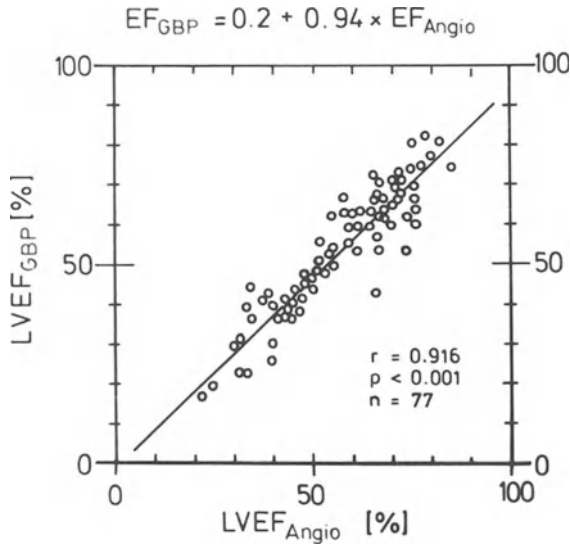
Figure 4. Comparison of LVEF measured by multiple GBP to biplane angiography (LVEF Angio) standard deviation = 5.2 ± 4.6%.

positioning of the camera as well as by the different time intervals, at which the bolus passes the right and the left ventricle. Therefore this method permits a nearly selective visualization of the left ventricle in RAO 30° position without overlap by the right ventricle. This makes it easy to compare the results with angiographic data. On the other hand the standard position for the multiple GBP is an individual LAO position generally between 30° and 50° in such a way that the right and left ventricle are separated clearly by the septal wall. This position is uncommon for angiography, which makes the comparison more difficult. Using the standard RAO 30° position the right and left ventricle cannot be separated. But additional imaging in the anterior and in the LAO 60° to 70° position is useful to assess wall motion abnormalities.

The most substantial advantage of the multiple GBP is that for about 4 hours

Table 2. Accuracy of LVEF measured by first pass RNA and multiple GBP in comparison with angiography

	First pass	Multiple gated
Number of studies	21	25
Number of patients	771	774
Correlation with angiography (r)		
Range	0.84–0.97	0.70–0.97
Mean	0.90	0.88

Table 3. Accuracy of absolute volumes measured by various nuclear methods

	Area-length	Various count methods
Number of studies	4	19
Number of patients	142	575
Correlation with angiography, Fick, thermodilution (*r*)		
Range	0.78–0.92	0.80–0.98
Mean	0.88	0.91

after application of the tracer any number of measurements can be performed. This includes multiple positions as well as multiple acquisitions at rest and during stepwise exercise. Also the effect of drugs and other interventions can be assessed easily during this time interval. On the contrary, using the first pass RNA with ^{99m}Tc, the number of measurements within a short time is limited. First pass and equilibrium methods can be combined.

The radiation exposure to the gonads by these studies utilizing ^{99m}Tc ranges between 200 and 400 mrad [9], which is about 1/2 to 1/5 of that of an x-ray urogram. Therefore repeated examinations are acceptable in most cases.

ACCURACY OF FIRST PASS RNA AND MULTIPLE GBP COMPARED TO ANGIOGRAPHY

A great number of studies has been performed to compare the nuclear methods with angiography. In 77 patients we found a correlation coefficient of 0.91 between multiple GBP LVEF and biplane angiographic LVEF (Figure 4). A summary of the literature data showes the following results (Table 2): comparing the first pass RNA with angiography the correlation coefficients ranges between 0.84 and 0.97 with a mean value of 0.90. For the multiple GBP the correlation coefficients ranged between 0.70 and 0.97 with a mean value of 0.88 which is not significantly different. Hence both methods show good correlation with angiography [2, 3, 5, 6, 10].

The right ventricular ejection fraction (RVEF) can also be obtained by both methods [3, 6, 10]. Comparing different nuclear methods the correlation coef-

Table 4. Reproducibility of nuclear cardiac studies

	r	+/−
LVEF	0.95–0.99	1–5%
Absolute volumes	0.90–0.99	1–12%

Table 5. Accuracy of LVEF measured with the nuclear stethoscope

Number of studies	5
Number of patients	337
Comparison with angiography or/and camera nuclear study (LVEF) (*r*)	
Range	0.54–0.92
Mean	0.77

ficients ranged between 0.95 and 0.98. When comparing the nuclear RVEF with the results of angiography, the correlation coefficient was somewhat lower ($r = 0.85$) which is probably due to the limitations of angiography for quantifying right ventricular function.

Absolute volumes of the left ventricle (Table 3) including end-diastolic volume, end-systolic volume, stroke volume and cardiac output have been measured by both methods with a good correlation either to angiography, to the Fick's principle or to thermodilution. The application of the area-length method yielded correlation coefficients ranging between 0.78 and 0.92 with a mean of 0.88. Recently various count-based methods have been developed. For those methods correlation coefficients ranged between 0.80 and 0.98 with a mean value of 0.91. Although the count-based methods are obviously more accurate, a standardized procedure has not been established up to now.

REPRODUCIBILITY (Table 4)

The reproducibility of nuclear cardiac studies has been investigated mainly using the multiple GBP. Those studies tested intraobserver-variance, interobserver-variance and the reproducibility of repeated acquisition within short time intervals. It could be demonstrated that using an automatic or semiautomatic flagging of the ventricular contours the reproducibility was much better compared to flagging by hand. With a short acquisition time of only 2 minutes, reproducibility was not decreased

Table 6. Comparison of echocardiography and radionuclide studies to angiography

	ECHO	Radionuclide
Number of studies	8	
Number of patients	412	
Correlation with angiography (LVEF) (*r*)		
Range	0.24–0.90	0.70–0.96
Mean	0.66	0.87
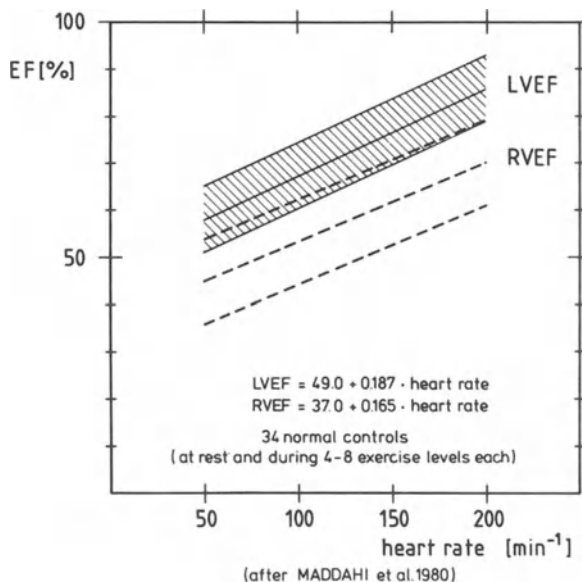
Figure 5. Normal range of RVEF and LVEF at different levels of exercise during graded ergometry.

essentially. For the LVEF a high reproducibility was obtained [6, 10]. The correlation coefficients ranged between 0.95 and 0.99 and the differences ranged between ±1 to 5 (absolute) %. For absolute volumes, various count-based methods showed also a good reproducibility with correlation coefficients ranging between 0.90 and 0.99, and with differences ranging between ±1 to 12 (relative) %.

THE "NUCLEAR STETHOSCOPE" (Table 5)

An inexpensive portable single probe detector has been developed to assess global cardiac function easily in intensive care units. First pass as well as multiple gated acquisitions can be performed [11]. In several investigations correlation coefficients of LVEF compared to angiography or to nuclear camera studies ranged between 0.54 and 0.92 with a mean value of 0.77. The positioning of the single probe detector is somewhat difficult. In patients with wall motion abnormalities the accuracy was rather poor. Nevertheless, reproducibility was high in these patients. Therefore the "nuclear stethoscope" may be useful especially for follow-up examinations in intensive care units.

COMPARISON BETWEEN NUCLIDE CARDIAC STUDIES AND ECHOCARDIOGRAPHY

Echocardiography has to be considered as a non-invasive procedure which may
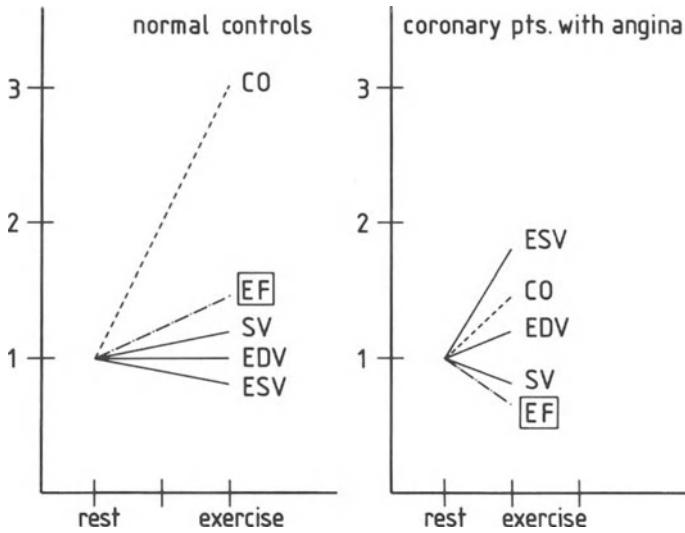
Figure 6. Response of the left ventricle to supine exercise. EF = ejection fraction, CO = cardiac output, SV = stroke volume, EDV = end-diastolic volume, ESV = end-systolic volume.

substitute nuclear cardiac function studies. Some investigations have been performed in order to compare echocardiography as well as nuclear cardiac methods to angiography (Table 6). Generally the accuracy and the reproducibility was superior using nuclear cardiac methods. On the other hand echocardiography covers numerous indications which cannot be covered by nuclear methods, e.g. in valvular and pericardial disease and in cardiomyopathy. The most important advantage of the nuclear cardiac study is that examination can be standardized and evaluations can be carried out automatically to a high degree. Moreover, studies at rest as well as during exercise can be evaluated regulary in more than 95% of cases. Therefore nuclear cardiac studies look superior in patients with ischemic heart disease. Nuclear cardiac methods and echocardiography should be considered to be supplementary methods [12].

RESPONSE OF THE LEFT VENTRICLE TO EXERCISE

In normal controls the RVEF as well as the LVEF increase during dynamic exercise [13] (Figure 5) which is the result of an increasing stroke volume and a decreasing end-systolic volume (Figure 6).

The LVEF increases during adequate exercise at least by 5 (absolute) % or at least by 10 (relative) % [3, 6, 10]. In patients with coronary artery disease a significant reduction of the LVEF during exercise angina is observed. In coronary patients without exercise angina, alterations of cardiac volumes are less pronounced during exercise. Therefore the LVEF may not change or may decrease only slightly.

The sensitivity of parameters of global function was found to vary between 45 and 95% for detecting coronary artery disease. This is probably due to significant differences in patient populations and to the mode and the level of exercise.

During the performing of exercise studies it has to be taken into account that the response of the left ventricle depends considerably on the mode of exercise and on special medications. The exercise response is different for dynamic exercise in the supine and erect position, or using the handgrip stress test, the cold pressure test, an afterload stress test or atrial pacing [14]. Additionally, drugs like nitrates, propranolol, isoproterenol or nifedipin may change the exercise response. Furthermore acute effects can vary from long-term effects. In coronary patients under long-term medication with betablockers the exercise response of the left ventricle can be normal [10].

INDICATIONS FOR NUCLEAR FUNCTION STUDIES

Regardless of the method used and of the mode of exercise performed, most important are a well defined standardized nuclear method and a sufficiently high exercise level. Before introducing any nuclear cardiac function study as a routine examination, it has to be validated by angiography.

There are numerous indications for nuclear cardiac exercise studies which can only be summarized briefly: for an initial examination they can help to establish, whether coronary artery disease is present and to differentiate between coronary artery disease and cardiomyopathy. For this purpose thallium scintigraphy also has to be considered. But even in patients with invasively proven heart disease, nuclear studies can be helpful to quantify the degree and the exercise response. Also the individual effects of drugs can be measured. Nuclear cardiac studies are most suitable for quantitative follow-up examinations. In this regard the limitations of invasive procedures are obvious. The effects of medical and surgical treatment can be controlled quantitatively including exercise tests.

Nuclear cardiac studies at rest and during exercise have been developed into a clinical routine examination during the last few years. The equipment is available in most of the nuclear medicine departments. Further improvement can be expected by technological progression, i.e. using the bifocal collimator or single photon emission tomography.

REFERENCES

1. Feinendegen LE, Vyska K, Schicha H, Becker V, Freundlieb C: The minimal transit times. Der Nuklearmediziner Suppl: 93–104, 1979.
2. Van Dyke D, Anger HO, Sullivan RW, Vetter WR, Yano Y, Parker HG: Cardiac evaluation from radioisotope dynamics. J Nucl Med 13:585–592, 1972.
3. Gordon DG, Ashburn WL, Slutsky RA: Assessment of ventricular function by first-pass radionuc-

lide angiography. In: Berman DS, Mason DT (eds), Clinical Nuclear Cardiology, pp 204–223, Grune & Stratton, 1981.

4. Hoffmann G, Kleine N: Eine neue Methode zur unblutigen Messung des Schlagvolumens am Menschen über viele Tage mit Hilfe von radioaktiven Isotopen. Verh Dtsch Ges Kreislaufforsch 31:93–96, 1965.

5. Strauss HW, Zaret BL, Hurley PJ, Natarajan TK, Pitt B: A scintigraphic method for measuring left ventricular ejection fraction in man without cardiac catheterization. Amer J Cardiol 28:575–580, 1971.

6. Berman DS, Maddahi J, Garcia EV, Freeman MR, Shah PK: Assessment of left and right ventricular function with multiple gated equilibrium cardiac blood pool scintigraphy. In: Berman DS, Mason DT (eds), Clinical Nuclear Cardiology, pp 224–284, Grune & Stratton, 1981.

7. Luig H, Bartella R, Carstens B, Domowitz S, Reuter R, Emrich D, Facorro L, Schicha H, Graf M, Karsch KR, Rentrop P, Kreuzer H: Nuklearmedizinische Bestimmung linksventrikulärer Volumenkurven ohne Untergrundkorrektur und ihre Validisierung durch direkten Vergleich mit biplan laevokardiographisch ermittelten Auswurffraktionen. Nucl Med 18:120–124, 1979.

8. Schicha H, Karsch KR, Rentrop P, Luig H, Kreuzer H, Emrich D: Vergleich verschiedener gated-blood-pool-Verfahren zur Bestimmung der linksventrikulären Ejektionsfraktion mit dem Angiogramm. In: Höfer R, Bergmann H (eds), Radioaktive Isotope in Klinik und Forschung, pp 75–82, Egermann, 1980.

9. Roedler HD, Kaul A, Hine GJ: Internal radiation dose in diagnostic nuclear medicine. Berlin, H. Hoffmann, 1978, p 103.

10. Pfisterer ME: Nuklearmedizinische Herzdiagnostik. Springer, 1982.

11. Wexler JP, Blaufox MD: Radionuclide evaluation of left ventricular function with nonimaging probes. Sem Nucl Med 9:310–319, 1979.

12. Hedde JP, Jennissen H, Hoeffken W, Blümchen G: Linksventrikuläre Herzfunktionsszintigraphie und Echokardiographie bei koronarer Herzkrankheit. In: Schmidt HAE, Rösler R (eds), Nuklearmedizin, pp 459–463, Schattauer, 1982.

13. Maddahi J, Berman D, Pantaleo N, Freeman M, Prause J, Forrester J, Swan HJC, Waxman A: What is the normal range for left and right ventricular ejection fraction at different levels of exercise? Findings of scintigraphic ventriculograpjy during graded ergometry in 34 normals. J Nucl Med 21:P5 (abstr), 1980.

14. Slutsky R: Response of the left ventricle to stress: effects of exercise, atrial pacing, afterload stress and drugs. Amer J Cardiol 47:357–364, 1981.

12. QUANTIFICATION OF LEFT VENTRICULAR FUNCTION BY COMPUTED TOMOGRAPHY

R. Rienmüller, A. Baumer, C.M. Kirsch and B.-E. Strauer

With the introduction of the third generation of CT-Scanners with scanning times of 1 to 6 seconds, CT became a well accepted method in the diagnostics of thoracic and mediastinal diseases. The CT changed and partly replaced some of the well established diagnostic procedures of the mediastinum [8, 10, 17]. To differentiate vascular from nonvascular structures in the mediastinum by CT it is mostly necessary to enhance the blood density by means of an intravenously applied contrast agent. By this means cardiac structures [5] like the interventricular septum, the myocardium, the heart chambers, the coronary arteries, the coronary sinus, the peri-epicardium and the subepicardial space will also become visible.

Having studied more than 530 patients with different cardiac diseases, CT of the heart seems to be not only of diagnostic value in constrictive pericardial diseases [4, 12], in different groups of cardiomyopathies [14] and in patients with primar and secondary cardiac tumors, but also in the follow-up of their specific treatment as a non-invasive method with reproducible results [14].

For diagnostic statements of CT studies of the heart it is not only necessary to analyse the morphological appearance of the above mentioned cardiac structures [7] and of the major heart vessels qualitatively, but it is also desirable to provide some quantitative data [14, 19].

The aim of this paper is to show the present capibilities of CT to assess quantitatively the left ventricular end-diastolic volume (EDV) and left ventricular muscle mass (LVMM) in absolute values and to quantify cardiac hemodynamics using ratios of the heart chambers and of the major heart vessels respectively. A comparison with angiocardiographic (HK) data will be presented.

PATIENTS AND METHODS

We studied more than 530 patients with different cardiac diseases. Of these patients, we selected those for whom (in addition to our CT studies) angiocardiographic data were available. Regardless of the diseases we selected only those data for a comparative study which were obviously technically inconstestable in both methods. The mean time difference between the CT- and HK-studies was 3 days.
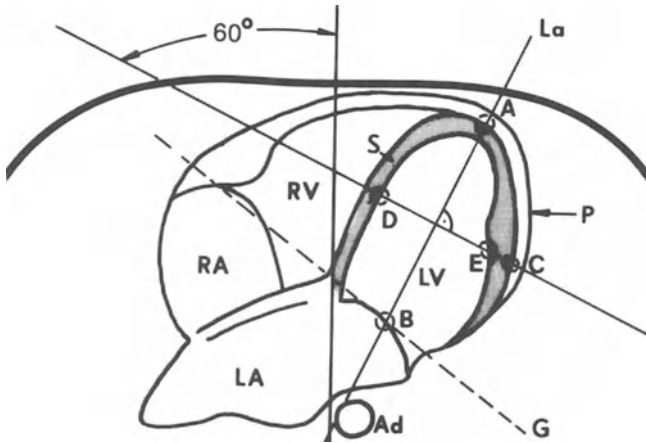
Figure 1. Outline of a CT-scan of the heart with the maximum circumference of the left ventricle. AB: long axis; CD: transverse axis; S: interventricular Septum; P: pericardium; RV: right ventricle; LV: left ventricle; RA: right atrium; LA: left atrium; Ad: descending aorta; G: line through the atrio-ventricular grooves.

Equipment and procedures of cardiac CT

In our CT study we used a 4.8 second Somatom II (Firma Siemens). The patients were examined in a supine position and suspended inspiration. They were scanned contiguously from the left diaphragma to the aortic arch performing 16 to 40 scans per patient with a scan-layer thickness of 8 mm. The necessary amount of contrast agent (65% Solution of Methylglucamine-ioxithalamat, Telebrix 300®, Fa. Byk-Gulden) ranged between 50–150 ccm. Some consideration of cardiac CT images:

1. Using our CT unit without gating we get a reconstructed CT image of a beating heart over a period of 4.8 sec. This means during one CT scan the heart performs 5–10 strokes. Nevertheless, due to the image reconstruction principle the CT images of the heart look well defined.
2. After intravenous contrast enhancement of the blood anatomical details of 5–3 mm become visible, assuming the density of the surrounding tissue is sufficiently different. In a non-moving object, details of maximum 1.5 mm will be detectable.
3. In contrast to angiographic, echocardiographic and nuclear medicine studies using CT without gating, it is not possible to analyze the motion of the heart.
4. Acute changes of cardiac dynamics at the time of scanning are not detectable.
5. However, it is possible to visualize the results of longer lasting changes in cardiac hemodynamics having caused morphological changes of the heart and its major vessels.
6. Any measured distance AB_m in a CT image of the heart is a function of the real distance AB_r the heart rate (HR), the stroke volume (SV), the applied hard- and software (HSW) and the partial volume effect (PVE) [14].

$$AB_m = f\ (AB_r,\ HR,\ SV,\ T_{CT},\ HSW,\ PVE)$$

Quantitative assessment of the enddiastolic volume in CT

We select the very cardiac scan in which the left ventricle shows its maximum circumference and draw the long axis through the apex and the middle of the left ventricle (LV) parallel to the septum (Figure 1). The end-point A of the long axis is determined by the outside contour of the left apex. The end-point B one gets by drawing a connecting line between both of the atrioventriculare grooves. The vertical line above the middle of the long axis is the transverse axis. Its end-point C is determined by the outside-contour of the postero lateral wall of the left ventricle. The end-point D is at the inside of the septum of the LV [13].

Similar to angiocardiographic methods for calculating the left ventricular volume, the above mentioned long and transverse axis is used to calculate the enddiastolic volume by applying the so called two axis method and the formula $V = II/6 \cdot L \cdot M^2$. We suppose, that the shape of the left ventricle is of elliptical configuration – an assumption which is conclusively proved by Arvidsson, Greene, Dodge and others [1, 3, 6].

Quantitative assessment of the left ventricular muscle mass in CT

Assuming the left ventricle to be of rotational elliptical shape we calculate the left ventricular muscle mass in CT as the difference of the outside and the inside contours of the left ventricle [14, 19].

Quantitative assessment of cardiac dynamics

Some quantitative assessment of the results of chronic changes of cardiac hemodynamics are possible by calculating the ratios of left ventricle/left atrium, the right ventricle/right atrium and of the major heart vessels as ratios of the corresponding parts of the descending aorta/inferior vena cava and of the descending aorta/ superior vena cava.

In detail we select the very cardiac scan in which the left ventricle and left atrium or right ventricle and right atrium respectively are of their maximum size. Then, using indentical technical CT parameters, we measure the circumference of the left and right ventricle and the maximum transverse axis of the corresponding left or right atrium and calculate the ratios. For calculating the ratios of the major heart vessels we select the cardiac scan where the inferior vena cava and the corresponding descending aorta can be detected simultaneously. Then we measure the circumferences of both vessels and calculate their ratios. Similarly we select that cardiac scan in which the superior vena cava, ascending aorta, pulmonary truncus and the
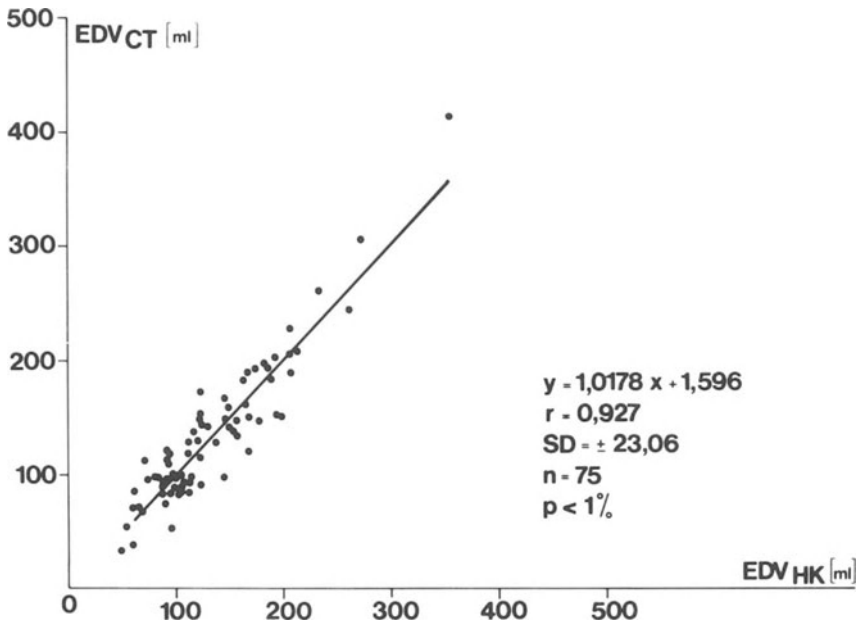
Figure 2. Comparison of the enddiastolic volumes of the left ventricle calculated from CT and angio-cardiograms.

corresponding part of the descending aorta are also detectable simultaneously. The calculation of the ratios followed the measurements of the circumferences of these vessels.

Procedures in cardiac catheterisation

Left ventricular angiocardiogramms were obtained by intraventricular injection of 40 to 60 ccm of contrast agent (Urografin® 76% using a contrast injector) in a 30° RAO projection. Only the angiogramms of the first to third heart cycle following a contrast injection were used, assuming there was no extrasystolic or postextra-systolic heart action [18]. The calculation of the left ventricular volumes were performed according to a modification of the two axis method of Dodge.

The left ventricular muscle mass was calculated as the difference between the left ventricular total volume and the enddiastolic volume, including the specific weight of the heart muscle mass as described by Hugenholz [9] and Simon [15].

RESULTS

Assessment of the enddiastolic volume in CT

Using the above method we compared the enddiastolic volumes of 75 patients, regardless of their cardiac diseases. The selection of the patients was performed under the premises that the CT as well as the HK images were technically sufficient. Figure 2 shows the results of the comparison of the enddiastolic volume calculated from CT- and HK-images in healthy individuals and in patients with various cardiac diseases. There is a linear correlation $y = 1,0178\,x + 1,596\,(P < 1\%)$. With a correlation coefficient $r = 0,93$. The 95% interval of confidence for r ranges between 0.89 to 0.95. The standard deviation is ± 23 ccm.

Results of the enddiastolic volume calculated by CT in various cardiac diseases

Table 1 shows the results of the enddiastolic volume calculated from CT images only in 123 patients with various diseases. All of the patients had undergone angiocardiography. Five patients did not present pathologic findings in HK; 9

Table 1. EDV calculated from ST in healthy persons and in patients with different cardiac diseases

Diagnosis	Number of patients	Mean EDV value (ml)	$\bar{x} + a$ 95% IC[j]	Significance of the differences of EDV[k, l]		
Normal[a]	5	92	± 21	○	●	
n. HF[b]	9	90	± 23			
HF[c]	14	149	± 58			
art.RR[d]	20	120	± 16			△
sec.CM[e]	12	134	± 23	○		
CHD[f]	29	134	± 16		●	
CHD with An.[g]	12	185	± 44		●	△
CCM[h]	13	248	± 57		●	△
HCM (O,N)[i]	9	105	± 21			

[a] Patients with no pathology in angiocardiography.
[b] Inborne heart failure.
[c] Aquired heart failure.
[d] Systemic hypertension.
[e] Secondary cardiomyopathy (WHO/ISFC).
[f] Coronary heart disease.
[g] Coronary heart disease and left ventricular aneurysm.
[h] Dilative cardiomyopathy (WHO/ISFC).
[i] Hypertrophic obstructive (○) and non obstructive (N) cardiomyopathy (WHO/ISFC).
[j] IC: Interval of confidence.
[k,l] △, ●: 95% significance of the differences of EDV in different groups of patients.
○: 90% significance of the differences of EDV in different groups of patients.
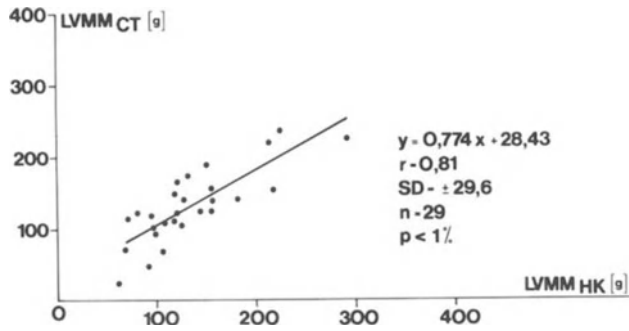
Figure 3. Comparison of the left ventricular muscle mass calculated from CT and angiocardiograms.
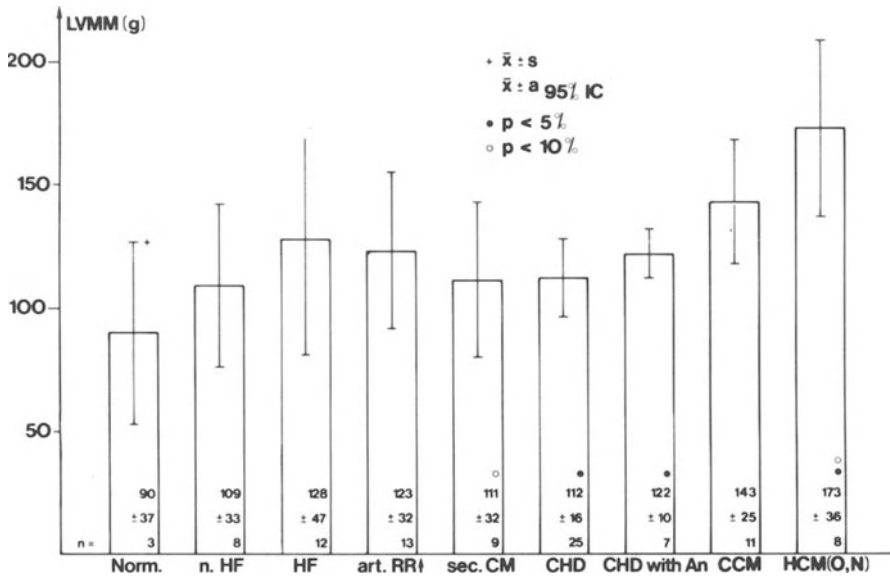
Figure 4. Left ventricular muscle mass calculated by CT images in 96 patients with various cardiac diseases. Norm: patients without pathologic findings in angiocardiography; n.HF: congenital heart failure; HF: heart failure; art.RR: systemic hypertension; sec.CM: secondary cardiomyopathy; CHD: coronary heart disease; CHD with An: coronary heart disease with aneurysm of the left ventricle; CCM: dilative cardiomyopathy; HCM: hypertrophic, obstructive-O, non-obstructive N, cardiomyopathy.
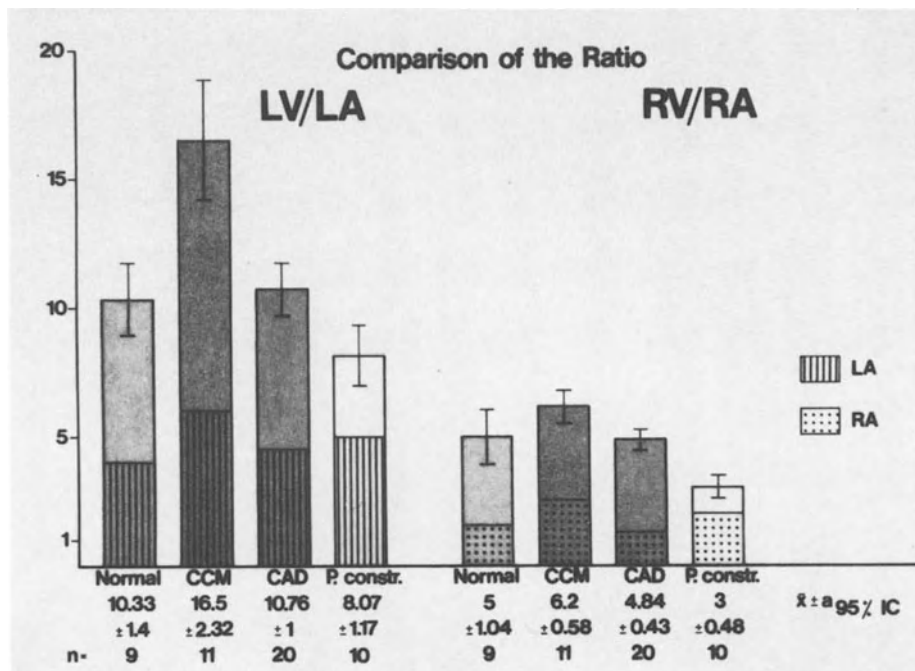
Figure 5. Comparison of the ratios of the left ventricle/left atrium and right ventricle/right atrium. LV: left ventricle; LA: left atrium; RV: right ventricle; RA: right atrium; Normal: patients without pathologic findings in angiocardiography; CCM: dilative cardiomyopathy; CAD: coronary heart disease; P.constr.: constrictive pericarditis; n: number of patients; IJ: interval of confidence.

patients had congenital and 14 patients aquired heart failure; 20 patients were suffering from systemic hypertension of different stages; 13 patients had dilative, 9 hypertrophic and 12 secondary cardiomyopathies (WHO/ISFC); 41 patients had coronary artery diseases, 12 of them with a left ventricular aneurysm.

Assessment of the left ventricular muscle mass in CT

Comparison of the results of the assessment of the left ventricular muscle mass in CT and HK follows.

In 29 patients we compared the weight of the left ventricle muscle mass with both of the methods and again found a linear relation (Figure 3): $y = 0.774\,x + 28.43$ ($P < 1\%$) with a certain underestimation of the left ventricular muscle mass in CT. The correlation coefficient $r = 0.81$ and its 95% interval of confidence is 0.64 to 0.91. The standard deviation is ± 29.6 g.
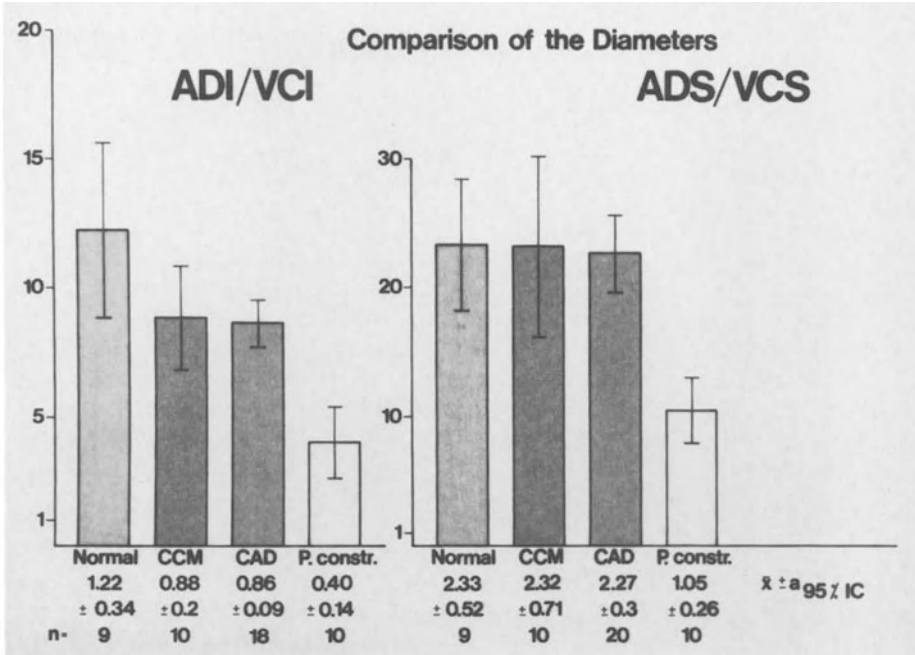
Figure 6. Comparison of the ratios of diameter of the descending aorta/inferior vena cava and of descending aorta/superior vena cava.

Results of the left ventricular muscle mass calculated by CT in various cardiac diseases

Figure 4 shows the left ventricular muscle mass calculated by CT images only in 96 patients with various cardiac diseases. All the cardiac diagnoses were confirmed by angiocardiography. Three patients did not present any pathologic findings in HK; 8 patients had congenital and 12 acquired heart failure; 13 patients had systemic hypertension of different stage; 32 patients had coronary artery diseases of different stages, 7 of them with a left ventricular aneurysm; 11 patients had dilative, 8 hypertrophic and 7 secondary cardiomyopathies (WHO/ISFC). Figure 4 shows the mean values and their 95% interval of confidence. The points and circles shows the 90% of 95% differences of the values of the left ventricular muscle mass between the various group of patients.

Quantitative assessment of chronic changes of cardiac dynamics in CT

Chronic pressure and/or volume changes in the pulmonary and/or systemic circulation can be followed by changes in the shape, size, position and relation of the heart chambers and the major heart vessels which are detectible by CT. We calculated the
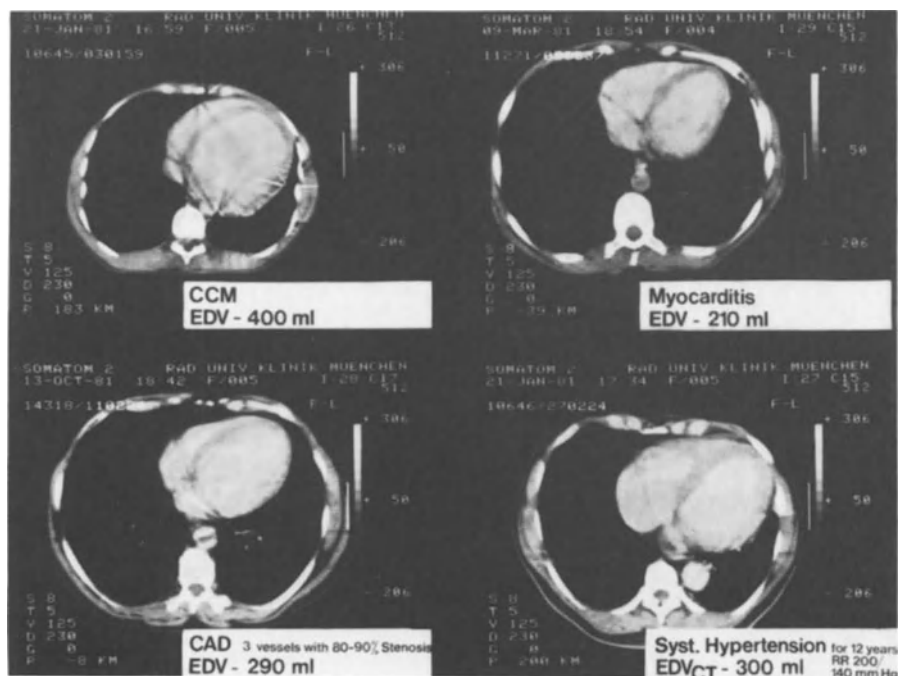
Figure 7. CT-scans in 4 patients with various cardiac diseases with the maximum circumference of the left ventricle.

ratios of the LV/LA and of the RV/RA in 50 patients. 10 were normals, 11 had dilative cardiomyopathy, 20 coronary artery diseases and 10 had constrictive pericarditis. All the diagnoses were proven by angiocardiography. Figure 5 displays the mean values of LV/LA and RF/RA ratios and their 95% interval of confidence – the highest for the group of dilative cardiomyopathies and the lowest for the constrictive pericarditis. The relative size of the ventricles compared to the corresponding atria are just qualitatively drawn.

Figure 6 shows the mean values of the ratios between the diameters of descending aorta (inferior part) (ADI) and the corresponding inferior vena cava (VCI) and between the descending aorta (superior part) (ADS) and of the corresponding superior vena cava (VCS) and their 95% interval of confidence. It is obvious that the ratios ADI/VCS are the highest for healthy persons and the lowest for the group of patients with constrictive pericarditis. The ratios ADI/VCI in patients with dilative cardiomyopathies and coronary artery diseases are not sufficiently distinguishable from normals.

In the comparison to the ratios ADS/VCS only the group of patients with constrictive pericarditis are different from normals. Patients with dilative cardiomyopathy and coronary artery disease show approximately the same values.
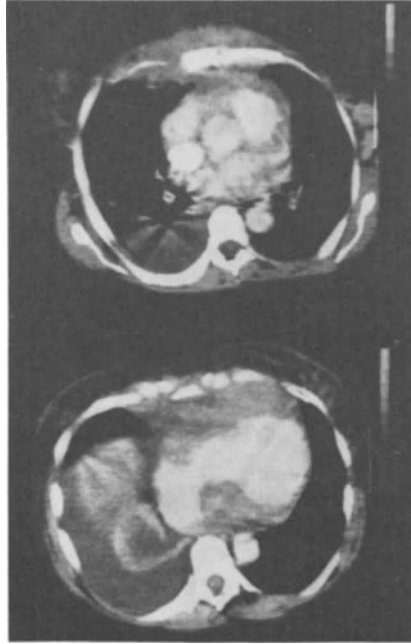
Figure 8. (a) CT scan at the level just above the basis of the heart of a patient with the history of Hodgkin disease before therapy. (b) CT scan at the level of the middle of the heart.

DISCUSSION

Even without gating, CT studies of the heart show cardiac structures which are different or similar in their size, shape, position and relation in dependence of the underlying cardiac diseases and the results of their chronic hemodynamics changes.

These morphological changes visible in CT are dependent on the underlying cardiac diseases with their changes of the volumes and/or pressure loads in the total or a part of the circulatory system. Figure 7 shows the CT scans of four hearts in which the left ventricle shows its maximum circumference. In the upper left there is a dilated left ventricle of a rounded shape in a patient with a dilative cardiomyopathy and with an enddiastolic volume of 400 ccm.

The upper right image shows the heart of a patient with clinically proven myocarditis. The left ventricle is also enlarged and of elliptical shape. The enddiastolic volume was 210 ccm.

In the lower left image there is the CT scan of a patient with coronary artery disease (3 vessels disease). Again the left ventricle is enlarged and of elliptical shape. The enddiastolic volume was 290 ccm. There is also a thinning of the arterior wall of the left ventricle due to an infarction. The last image in the lower right shows the heart of a patient with systemic hypertension for about 12 years (RR 200/140 mmHg max).
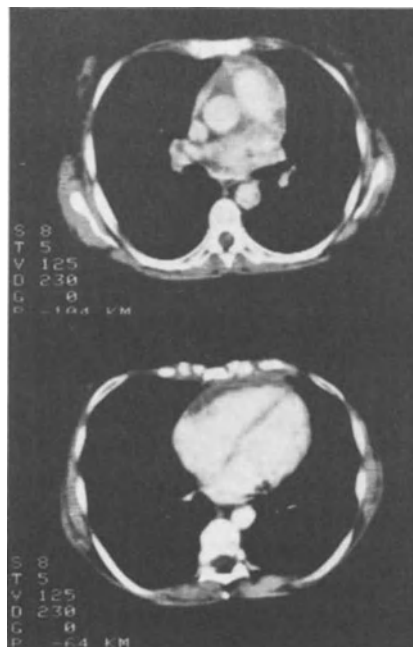
Figure 9. (a, b). CT scans of the same patient at the same levels after successful chemotherapy.

The left ventricle is also dilated but a hypertrophy of the septum and of the myocardial wall is also visible. The enddiastolic volume was 300 ccm.

Even if "we cannot state in quantitative physical terms the reason why images without significant artifacts can be obtained of structures which are moving to the extent the myocardium does" as stated by Carlsson et al [2], all the four CT images of the heart show expected shape and size of the left ventricle and of the surrounding structures.

Figure 8 shows two CT scans of a patient with a history of Hodgkin disease with a tumor mass in the left atrium bulging into the left ventricle and in the direction of the right atrium and right ventricle. There is also a tumor mass in front of the right ventricle infiltrating the pericardium and the anterior chest wall (Figure 8a, b). After successful chemotherapy (Figure 9b) there is no tumor mass in the left atrium. The tumor in front of the right ventricle became smaller and the heart chambers are now of normal shape, size, position and relation to each other.

Due to the cardiac inflow and outflow reduction the superior vena cava is enlarged (Figure 8a) in comparison to the descending aorta and changed to normal size at the end of the successful treatment (Figure 9a).

These examples of CT scans of the heart performed on a routine basis of 5 different patients show the present quality of non-gated CT images. However, if used in the clinical diagnostic procedures, it is also neccessary to quantify at least

some of the visible cardiac structures.

The above mentioned assessment of the enddiastolic volume of the left ventricle yield a value of the size of the left ventricle. Our values of the enddiastolic volume and left ventricle muscle mass calculated in patients with various cardiac diseases correspond to the known values of the angiocardiography and thus allow their application in the daily cardiac diagnostics [19]. There is no question that, as long as we cannot perform gated CT images of the heart from the diaphragm to the aortic arch contiguously, or as long as we do not have a CT machine available with scanning times in the order of some milliseconds, it will not be possible to assess acute changes of the volumes or the movement of the myocardial walls [11, 16].

Although it is sometimes difficult to measure the circumferences of the chambers and the major heart vessels in CT images, the calculated ratios support the qualitative assessment of the chronic cardiac hemodynamics. Problems can occur, caused by motion, partial volume effect [2] or by highly inhomogenous thoracic structures, when the sampling theorem is hurt. Furthermore, scanning of cardiac structures or vessels in an oblique projection can enlarge or reduce the real size.

SUMMARY

According to our experience (having studied more than 530 patients with a variety of cardiac diseases) we think that a carefully performed cardiac CT as well as a careful analysis of the position, size, shape and relation of all the cardiac structures and of the heart tissues makes it possible to arrive at diagnostic statements close to those obtained by angiography, echocardiography and nuclear medicine studies. Finally it is possible to quantify the enddiastolic volume and the left ventricular muscle mass with an accuracy comparable to invasive methods.

REFERENCES

1. Arvidson H: Angiocardiographic determination of left ventricular volume. Acta Radiologica, Vol. 56, Fasc. 5, November 1961.
2. Carlsson E, Lipton MJ, Berninger WM, Doherty P, Redington RW: Selective left coronary myocardiography by computed tomography in living dogs. Invest Radiol 12(6):559–562, 1977.
3. Dodgé HT, Sandler H, Ballew DM, Lord JD: The use of biplane angiocardiography for the measurement of left ventricular volume in man: Am Heart J 60:776, 1960.
4. Doppman JL, Rienmüller R, Lissner J, Cyran J, Bolte H-D, Strauer B-E, Hellwig H: Computed tomography in constrictive pericardial disease. J Comput Assist Tomogr 5(1):1–11, 1981.
5. Lackner FR, Simon M, Grube E, Thurn P: Computer-Kardio-Tomographie (CKT) Methodik and Ergebnisse der morphologischen Analyse. Elektormedia, Heft 3, 1978.
6. Greene DG, Carlisle R, Grant C, Bunnell JL: Estimation of left ventricular volume by one-plane cineangiography. Circulation 25, 1967.
7. Guthaner DF, Wexler L, Harell G: CT Demonstration of cardiac structures. AJR 133:75–81, 1979.
8. Heuser L, Lackner K, Felix R, Mödder U, Friedmann G: Erweiterung der thoracalen Diagnostik

durch die Computertomographie. Röntgenol 31:135–144, 1978.

9. Hugenholtz PG, Kaplan E, Hull E: Determination of left ventricular wall thickness by angio-cardiography. Amer Heart J 78:513, 1969.

10. Lackner K, Brecht G, Janson R, Scherholz K, Lützeler A, Thurn P: Wertigkeit der Computer-tomographie bei der Stadieneinteilung primärer Lymphknotenneoplasien. Fortschr Röntgenstr 132(1):21–30, 1980.

11. Lipton MJ, Hayashi TT, Boyd D, Carlsson E: Measurement of left ventricular cast volume by computed tomography. Radiology 127:419–423, 1978.

12. Moncada R, Baker M, Salinas M, Demos RC, Churchill R, Love L, Reynes C, Gunnar RM: Diagnostic role of computed tomography in pericardial heart disease; congenital defects, thicken-ing, neoplasms, and effusions. Am Heart J 103, 1982.

13. Rienmüller R, Lissner J, Kment A, Bohn J, Strauer B-E, Hellwig D, Erdmann E, Cyran J, Steinbeck G, Höss D, Höfling B: Das enddiastolische Volumen des linken Ventrikels in der Computer-tomographie im Vergleich zur Herzkatheterventrikulographie. Computertomographie Heft 2, Band 1, 62–67, 1981, Georg Thieme Verlag Stuttgart.

14. Rienmüller R, Lissner J, Bohn J, Maier H, Nitsch J, Strauer B-E: Computer tomography studies on cardiac geometry. In: Digital Video image Techniques in Cardiovascular Radiology. International Symposium and Tutorial, Kiel 1982, Georg Thieme Verlag. In press.

15. Siemers PT, Higgins ChB, Schmidt W, Ashburn W, Hagan P: Detection, quantitation and contrast enhancement of myocardial infarction utilizing computerized axial tomography: comparison with histochemical staining and ^{99m}Tc-pyrophosphate imaging. Investigative Radiology 13(2), 1978.

16. Skiöldebrand CG, Lipton MJ, Redington RW, Berninger WH, Wallace A, Carlsson E: Myocardial infarction in dogs, demonstrated by non-enhanced computed tomography. Acta Radiologica, 22(1), 1981.

17. Sommer B, Doppman JL, Stelter W, Mayr B, Rienmüller R, Lissner J: Der diagnostische Stellen-wert der Computertomographie bei mediastinalen Erkrankungen in Abhängigkeit von deren Lokalisation. Computertomographie 1, 1981, In Druck.

18. Strauer B-E: Hypertensive Heart Disease. Springer Verlag, Berlin-Heidelberg-New York, 1980.

19. Strauer B-E, Büll U, Rienmüller R: Nicht-invasive Diagnostik von Herzerkrankungen – Fragen des Kardiologen an den Radiologen. In: IV. Radiologische Woche, München 1980, Schnetztor Verlag GmbH, Konstanz 1982.

III. REGIONAL WALL MOTION IN MYOCARDIAL ISCHEMIA

13. EARLY CHANGES IN TRANSMURAL ISCHEMIA: AN OVERVIEW ON DETECTION CAPABILITIES OFFERED BY ECHOCARDIOGRAPHIC AND NUCLEAR TECHNIQUES IN MAN*

A. DISTANTE, O. PARODI, D. ROVAI, P. MARZULLO, E. PICANO, E. MOSCARELLI, W. BENCIVELLI AND A. L'ABBATE

INTRODUCTION

The approach to the diagnosis of ischemic heart disease in its acute manifestations has deeply changed over the last few years, since multiple evidence has been collected on the role of functional and often transient factors in the pathogenesis of ischemic attacks [1].

Although clinical history, ECG and enzymes still represent milestones in the screening phase of acute coronary patients, it is becoming more and more important to provide evidence of myocardial ischemia independent from ECG, which does not always show conclusive diagnostic alterations. "Independent evidence" could be reached by means of other non-invasive techniques, such as those offered by echocardiology and nuclear cardiology. For a long time echocardiographic and nuclear techniques have been considered less than adequate techniques for studying coronary patients and specifically myocardial ischemia, which is known to be not only a transient but also a regional phenomenon. Some of these limitations have also been overcome with the notion that echocardiography and nuclear medicine as well as ECG provide much more information if performed during ischemic attacks than basally.

Over the past few years at the Clinical Physiology Institute we have paid much attention to the extraordinary potentialities intrinsic to nuclear and ultrasonic techniques in the detection of acute myocardial ischemia and in the definition of its site and extension.

Our experience on this issue, based mainly on data collected in Prinzmetal patients during attacks of angina at rest and ST segment elevation, can be summarized in the observation hereinafter reported [2, 3].

SIGNS OF MYOCARDIAL ISCHEMIA

A. Echocardiographic techniques

The usefulness of echocardiography in acute myocardial ischemia stems from the
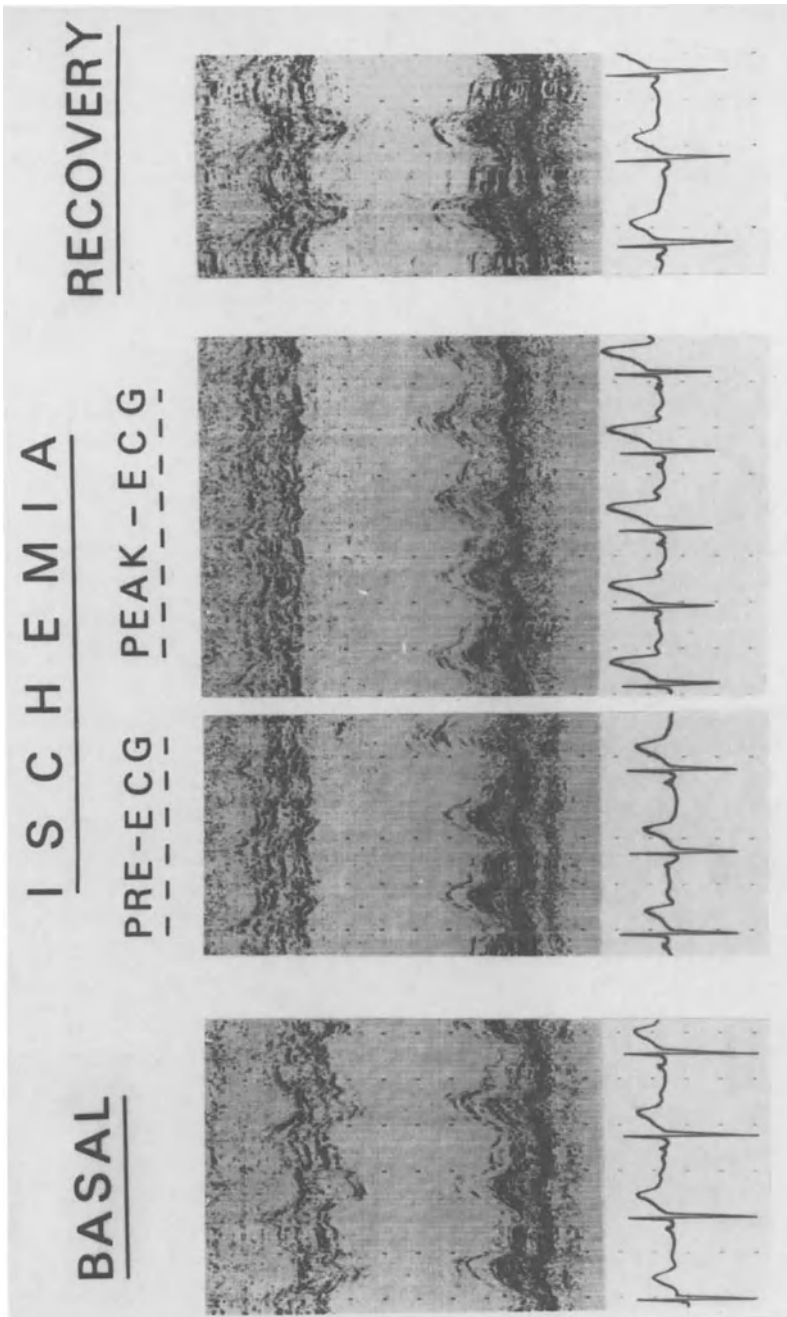
*Figure 1.*Original M-mode recordings documenting a full sequence of induced myocardial ischemia as related to electrocardiographic appearance of ST segment changes. It is clearly seen that mechanical changes in the septal wall do occur before ECG changes indicative of myocardial ischemia. The sequence of mechanical impairment of the ischemic septal wall is characterized by a progressive decrease both in systolic thickening and in wall motion, which become totally abolished at the peak ECG phase (ST segment elevation).

Mechanical impairment is fully reversible as shown in the recovery phase: moreover, the previously ischemic wall demonstrates a "rebound phenomenon" consisting of an overshoot in motion and of systolic thickening (With kind permission of American Heart Journal.)
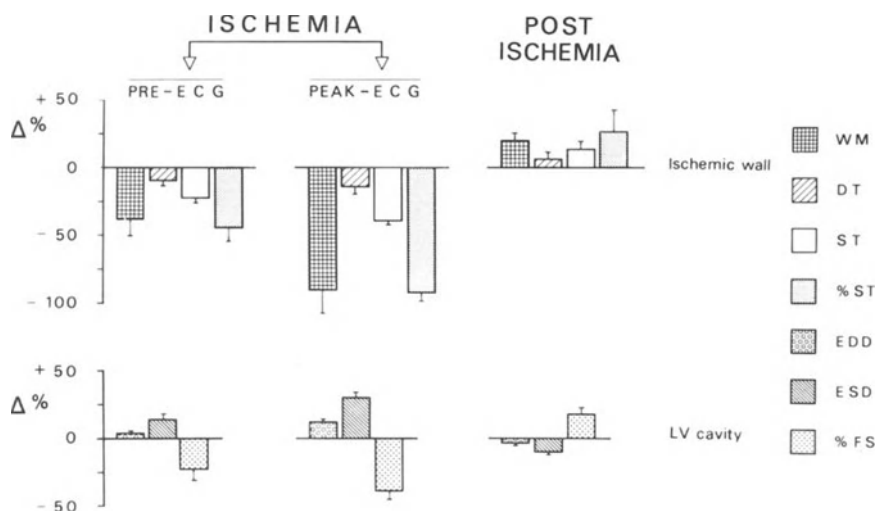
Figure 2. Histograms (mean ± SEM) showing percentual variations (%) from the basal state relative to the main echocardiographic parameters during different phases ("Pre-ECG"; "ECG"; "Post-ECG"). The presented values are referred to eleven episodes of myocardial ischemia with ST segment elevation induced by ergonovine maleate. WM = wall motion; DT = end diastolic thickness; ST = end systolic thickness; %ST = % systolic thickening; EDD = end-diastolic diameter; ESD = end-systolic diameter; % FS = % fractional shortening. (With kind permission of American Heart Journal.)

experimental evidence that ischemia transiently affects both the geometry and the function of cardiac structures.

(a) *Regional impairment of contractility indices* (decrease in percentual systolic wall thickening, in wall motion and in percentual fractional shortening). These parameters have been shown to be realiable expressions of regional contractility. In agreement with several experimental studies, their impairment occurs in man also as a very early phenomenon of myocardial ischemia when related to the apperance of ECG changes and anginal pain (Figures 1 and 2).

(b) *Regional wall thinning* (decrease in end-diastolic wall thickness). this sign, during anginal attacks at rest, could be due to a primary reduction in coronary blood flow with a consequent decrease in intramyocardial blood content of the ischemic area. Experimental studies have shown that coronary blood flow and intravascular blood content represent dynamic variables influencing wall thickness, which decreases following the occlusion of the coronary artery. An additional factor, which might explain the thinning of the ischemic wall, could be represented by the regional dilatation of the ventricle which would cause stretching and reciprocal sliding of the fibers.

(c) *Left ventricular enlargement* (increase in end-diastolic dimensions). Such a
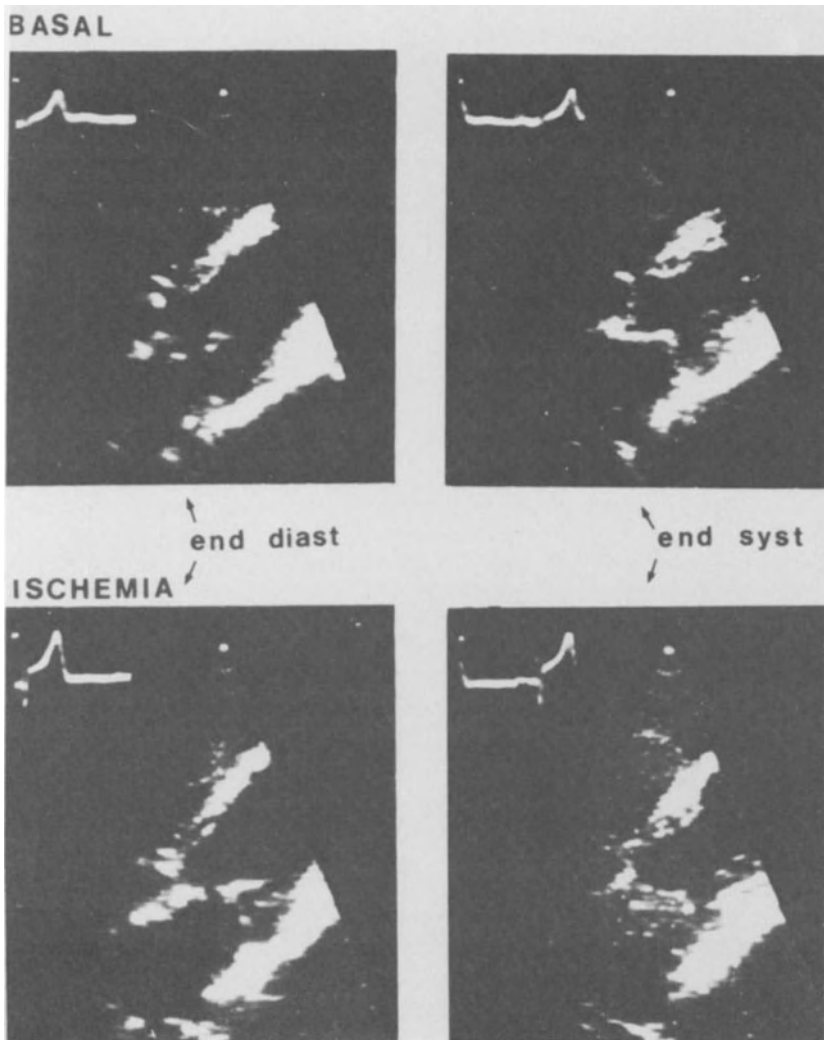
Figure 3. Two-dimensional echocardiograms obtained from the subxifoid approach during basal condition (BASAL) and during an episode of spontaneous myocardial ischemia with ST segment elevation (ISCHEMIA). On the top, the two spots were recorded during end-diastole while the two spots on the bottom during end-systole. It is clearly evident that, in the basal state, the interventricular septum has a normal thickening from diastole to systole; during ischemia however only the proximal part of the septum thickens while the distal portion does not change at all from diastole to systole.

Such a difference in mechanical function of the two different portions of the septum produces, during systole, a sharp anatomical demarcation between the ischemic and the non ischemic wall (step sign). (Distante et al: Mises à jour cardiologiques, 11:455, 1982. With kind permission.)
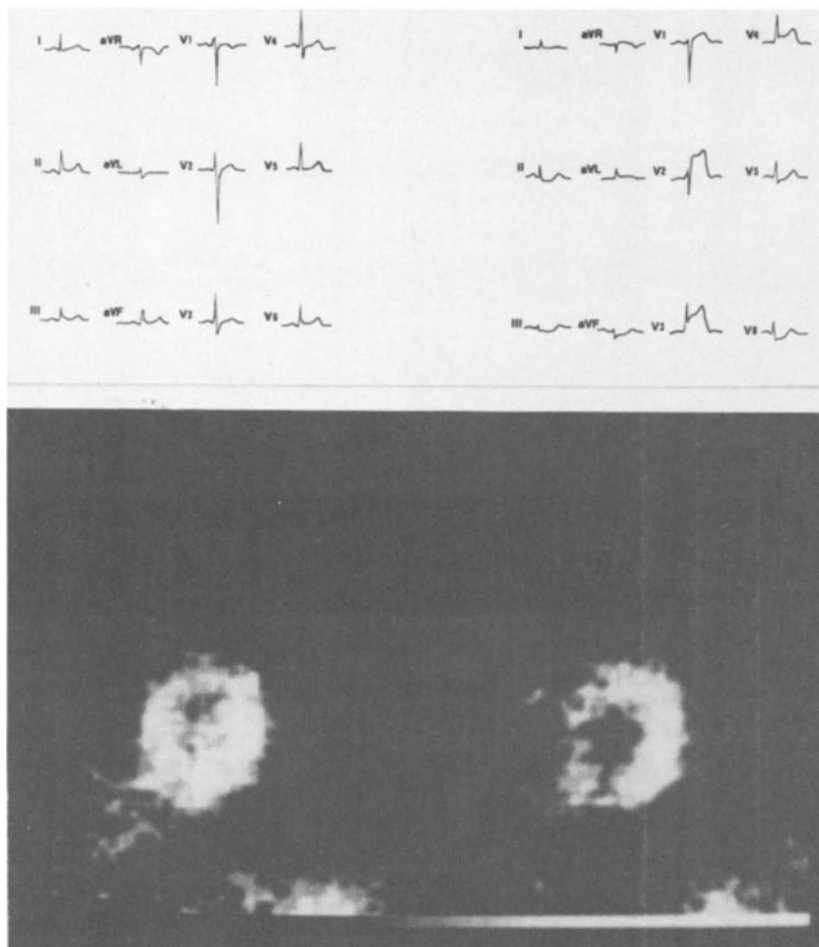
Figure 4. ^{210}Tl scintigraphy obtained during transient ischemia in the LAO 40° projection (right panel) and in control conditions 4 hours later (left panel). ECG during ischemia shows ST segment elevation in the anterior leads. In the corresponding image a severe and apparently transmural perfusion defect is evident in the septal wall which appears within normal limits in the control scintigram. ECG changes were not accompanied by anginal pain.

change parallels the decrease in contractility indices and the thinning of the ischemic wall, and could be partially explained by the incomplete left ventricular emptying and by the increase of left ventricular end-diastolic pressure. As observed also in chronic ischemic heart disease with significant pump impairment, left ventricular cavity may appear geometrically distorted (Figure 3).

(d) *Rebound phenomenon* (increase in contractility indices and wall thickness, decrease in left ventricular end-diastolic and end-systolic diameters). This transient
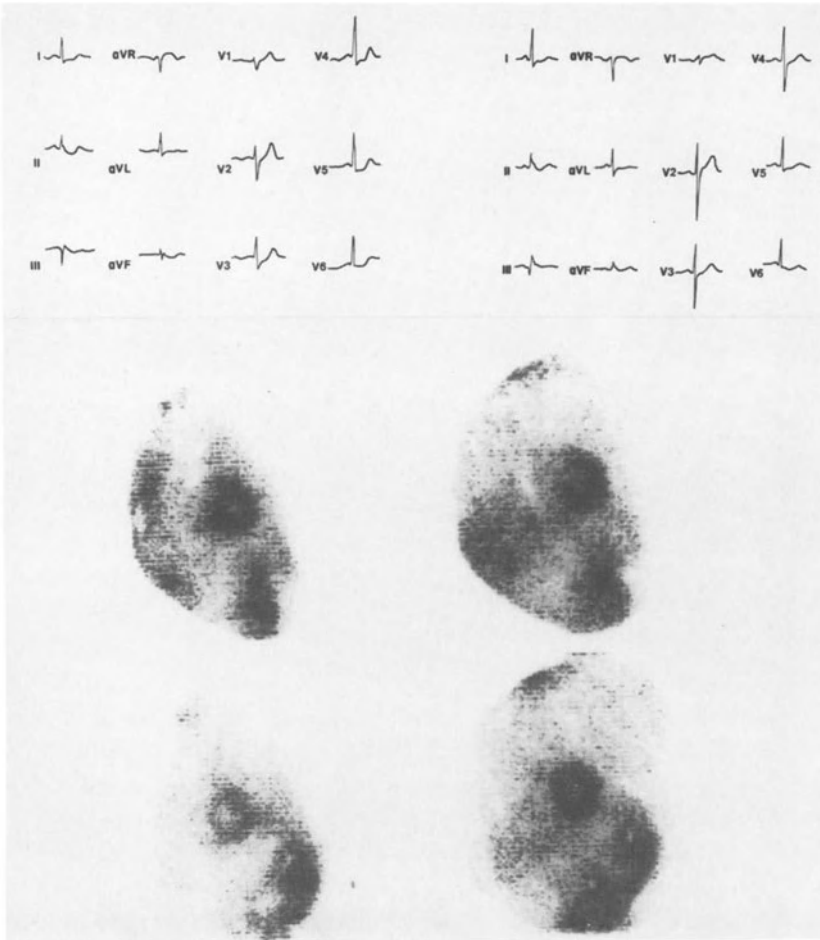
Figure 5. ^{201}Tl scintigraphy obtained a few minutes following tracer injection (left panel) and 4 hours later (right panel), in AP projection (upper images) and in LAO 40° (lower panels). Although ECG clearly demonstrates lateral ischemia, only a transient septal perfusion defect is detectable. The defect appears to be not transmural.

The scarce correlation between site of ECG changes and hypoperfused myocardial walls is a common finding in angina at rest characterized by ST segment depression.

overshoot of ventricular function, which has been linked to reactive hyperemia, occurs in the recovery phase of myocardial ischemia; it has already been shown in experimental animals after a brief period of coronary occlusion followed by the re-opening of the vessel, a situation very similar to the coronary spasm resolution in man.

B. Radioisotopic techniques

(a) *Regional wall motion abnormalities and left ventricular cavity enlargement as detected by Blood Pool Gated scintigraphy.* The monitoring capabilities inherent to this technique have allowed demonstration that impairment of contractility not only preceeds the ECG alterations and anginal pain, but also can occur in absence of symptoms (silent ischemia). To this purpose, however, echocardiographic monitoring – although cumbersome in some patients – must be used for an accurate assessment of the sequence of events. Qualitative (cine-mode) as well as quantitative (ejection fraction, phase analysis) indices may be obtained in different clinical conditions.

An alternative approach to the study of acute ischemia is provided by the use of a single collimator probe (Nuclear Stethoscope); with this technique – although no imaging is available – it is possible to monitor, with a higher temporal resolution, the changes in end-diastolic, end-systolic volumes and ejection fraction occurring during attacks of myocardial ischemia (4)

(b) *Reversible perfusion defects on ^{201}Thallium myocardial scintigraphy.*

Thallium scintigraphy is diagnostic of myocardial ischemia when it shows a transient uptake defect in images obtained within a few minutes following the tracer injection [5]. This defect should disappear after a certain time, for the re-distribution of the isotope has elapsed (usually from some minutes to a few hours after the same injection) (Figure 4).

Scintigraphic pattern is different in angina at rest with ST segment elevation and ST depression (Figure 5); in the first case, a transmural, severe and localized perfusion defect is usually detectable, while in the second case such a defect appears to be apparently limited to the subendocardial layers, although less severe but more extensive ̄6].

The major limiting factors in the use of this technique are the limited imaging qualities of the tracer, the interference of metabolic factors, and the unpredictable effect of reactive hyperemia. Moreover, being a "one sample" technique, the Thallium injection must be triggered by some independent sign of ischemia, thus preventing the use of the technique in the assessment of the sequence of events.

TIME SEQUENCE OF ECHOCARDIOGRAPHIC AND RADIOISOTOPIC SIGNS OF ISCHEMIA

The above described signs of ischemia are detectable with utmost evidence at peak ECG ischemic changes; these are, however, some of the pathophysiologic changes which characterize transient ischemic attacks. However, at least in patients with ST segment elevation during pain, contractility impairment of the ischemic wall is detectable – by Echocardiography and Blood Pool Gating – before onset of ECG

alterations. Such changes are of the same kind, but less pronounced than those present at peak ECG changes. When ischemia is over, pain disappears and ECG is back to normal; a transient functional overshoot in contractility of the previously ischemic wall (with values significantly increased as compared to the basal state) is detected by Echocardiography and Blood Pool Scintigraphy. Such rebound effect in Prinzmetal angina is linked to reactive hyperemia, very likely triggered by the release of coronary vasospasm: ^{201}Tl can show, in these cases, an increase in tracer uptake as compared to basal.

The occurrence of phenomenon such as the "contractile rebound" after ischemia can appear in contrast to the reported echocardiographic persistent segmental wall motion abnormalities in patients with unstable angina [7]. These data, on the contrary, may well describe two opposite patterns of a spectrum. On one side, when ischemia is less severe or lasts a short time, reperfusion might trigger the over-recruitment of contractile units which ischemia had "switched off" (so a contractile overshoot becomes evident, meaning that ischemia "hits and runs") [8]. At the other end of the spectrum, severe ischemic episodes, either too long or too many, might cause a more prolonged post-ischemic dysfunction: in this case, ischemia "hits and stuns", and echocardiography can act as the detector of presence and entity of myocardial stunning.

CONCLUSIONS

A combined use of echocardiographic and radioisotopic techniques allows a fairly accurate detection of presence, site and extent of transient myocardial ischemia. The major drawbacks of each technique are also the biggest aces of the other: spatial and temporal resolution, cost and manpower, for nuclear techniques; limited spatial imaging, qualitative reading, restriction by acoustic window for echocardiography. Their complementary use can give a remarkable amount of additional information on acute transient myocardial ischemia, both on the pathophysiological and on the clinical side.

REFERENCES

1. Maseri A: Pathogenetic mechanisms of angina pectoris: expanding views. Thomas Lewis Lecture. Br Heart J 43:648, 1980.
2. Distante A, Rovai D, Picano E, Moscarelli E, Palombo C, Morales MA, Michelassi C, L'Abbate A: Transient changes in left ventricular mechanics during attacks of Prinzmetal angina: an M-mode echocardiographic study. Am Heart J 1983 (in press).
3. Distante A, Rovai D, Picano E, Moscarelli E, Morales MA, Palombo C, L'Abbate A: Two dimensional echocardiography in Prinzmetal Angina. Journal of American College of Cardiology, March 1983 (abstract) (in press).
4. Davies GJ, Bencivelli W, Parodi O et al: ECG gated blood pool imaging tailored to study transient changes in left ventricular contractility. IEEE Computers Society, Computers in Cardiology, 295, 1981.
5. Maseri A, Parodi O, Severi S et al: Transient transmural reduction of myocardial blood flow, demonstrated by thallium-201 scintigraphy, as a cause of variant angina. Circulation 54:280, 1976.
6. Parodi O, Marzullo P, Galli M et al: Different pattern of contractility and perfusion in resting angina with ST segment elevation and depression. Am J Cardiol 49:1046, 1982.
7. Nixon JV, Brown CN, Smitherman TC: Identification of transient and persistent segmental wall motion abnormalities in patients with unstable angina by two dimensional echocardiography. Circulation 65:1497, 1982.
8. Braunwald E, Kloner RA: The stunned myocardium: prolonged, post ischemic ventricular dysfunction. Circulation 66:1146, 1982.

14. REGIONAL WALL MOTION DURING STRESS TESTING: A COMPARISON BETWEEN ATRIAL PACING AND ISOMETRIC HAND GRIP

R.W. Brower, H.J. ten Katen, A.H.A. Bom and P.W. Serruys

INTRODUCTION

Both the use of isometric hand grip and atrial pacing have been advocated as a means for stressing the heart so as to reveal functional disturbances not apparent at rest in patients with ischaemic heart disease. There remains uncertainty, however, concerning their relative strengths in eliciting a response. The isometric handgrip test (IHGT) usually elevates blood pressure and heart rate simultaneously with possibly direct inotropic stimulation via catecholamine release. In patients with coronary artery disease, peripheral resistance has been shown to increase, while in normal resistance is less affected. The atrial pacing stress test (APST) increases the minute work of the heart while shortening the diastolic filling period for the coronary circulation. In patients with already compromised coronary perfusion this stress can induce myocardial ischemia. Furthermore, it has been argued that the first post-pacing beat, provided the Q-Q interval can be controlled to equal that at rest, would most directly reflect normal chronotropic conditions after the onset of pacing induced stress. By analogy, if the primary stress of the IHGT in a population with chronic coronary artery disease is after-load elevation with or without in-otropic effects, the heart rate should be controlled to most directly document the consequences. Thus, this study was undertaken to compare the response in patients with coronary artery disease to these two stress tests where the effect of heart rate was eliminated.

While the aim of this work is towards a better understanding of the APST and IHGT, the practical application is also important. It would be most desirable to have available completely non-invasive means of measuring heart function as well as stressing the heart. The IHGT would be especially attractive in this regard if it could be shown to be an effective stress test in terms of those quantities easily measured non-invasively.
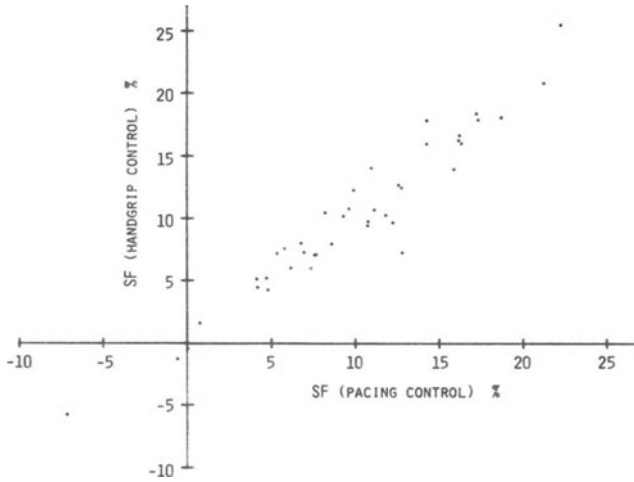
Figure 1a. Reproducibility of shortening fraction measurements from marker pairs at rest. Data were taken from the control period prior to the APST and IHGT, about 20 minutes apart. The standard error of the estimate is 1.64 percentage points which is taken as a practical estimate of the reproducibility of shortening fraction.
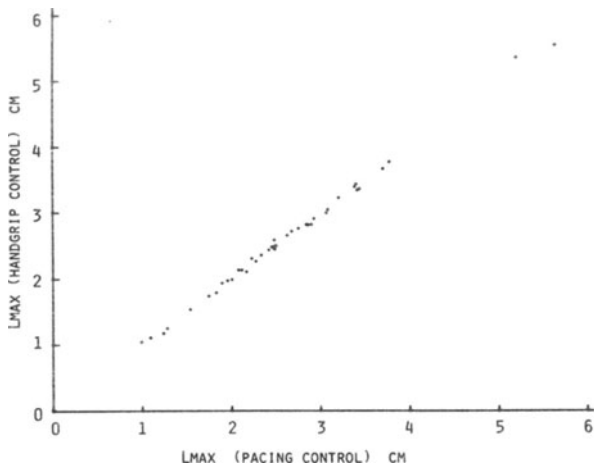
Figure 1b. Reproducibility of maximum marker separation, Lmax, as in Figure 1a. The standard error of the estimate is 0.51 mm.

METHODS

Patient material

Twenty adult patients were studied one year after coronary artery bypass graft surgery. The mean age was 51 yr, range 30 to 64 yr. Sixteen patients were in NYHA I and four in class II. In total 48 grafts were placed (2.4 grafts/patient) of which 73% were patent at one year. The mean ejection fraction was 0.61 ± 0.12 (range 0.32 to 0.77); six patients had an EF below the normal limit of 0.55. Cardiac index was 3.30 ± 0.67 L/min/m^2 (mean $\pm$ SD).

At the time of surgery, 41 epicardial marker pairs were placed in bypass perfused regions on the left ventricle. In 73% of regions grafts were patent and contributing to the total perfusion, while in the remaining 27%, the pertinent coronary artery could be at least partially visualized via collaterals or flow through the native diseased coronary artery. The test regions thus represent a spectrum in adequacy of perfusion and this is reflected in the range of regional shortening fraction measured as well as their response to stress testing.

Protocol

All medication was discontinued 36 hours before catheterization which was performed without pre-medication. All hemodynamic data and marker motion reported here were obtained prior to angiography.

The maximal handgrip pressure was determined at a paced heart rate (HR) 10 to 15 BPM above rest values. Control measurements were made at rest. The patient was then asked to sustain 50% of maximum over a two minute period. Registration of LV pressure and marker motion was obtained during the last 20 seconds.

The atrial pacing stress test was performed by incrementing the HR 20 BPM every minute until a maximum of 180 BPM, or until the ECG was positive, or the patient reported angina. Marker motion was recorded at basal HR, at maximum paced HR, and for the first post-pacing beat upon cessation of pacing. HR for the first post-pacing beat was controlled by the pacemaker set at the rest rate.

We measured the absolute marker separation using biplane projections and calculated the shortening fraction occurring during the ejection period. Thus, measurements from the same region were obtained for both stress tests. Dyskinesia was quantified by a negative shortening fraction.

RESULTS

Reproducibility

Control measurements of marker motion were made prior to the atrial pacing and

isometric handgrip stress test 20 minutes apart. The mean heart rate was 79 ± 11 BPM and 91 ± 10 BPM (mean ± SD) respectively. The 12 BPM difference reflects the policy of performing the hand grip measurements with atrial pacing 10 BPM above rest values in order to over-ride the chronotropic effect of handgrip.

The relation between the two control measurements for shortening fraction (SF) and maximum marker separation (Lmax) is shown in Figures 1a and 1b respectively. Mean shortening fraction was 9.90 ± 6.1 and 10.0 ± 6.3 (units percent shortening). The regression equation has a correlation coefficient of 0.964 with a standard error of the estimate of 1.64 for 41 measurements. The standard error of the estimate is taken as a practical estimate of the reproducibility of the measurement of shortening fraction.

The mean maximum marker separation, Lmax, for the two control measurements was 2.61 ± 0.94 cm and 2.61 ± 0.94 cm with a correlation coefficient of 0.999 and standard error of the estimate of 0.051 cm. The value of 0.051 cm is 2% of the mean separation, which we take as the reproducibility of the measurement of marker separation.

Pacing

The results of the atrial pacing stress test (APST) on HR, SF, and Lmax are shown in Table 1 (Meas. I & II). The HR increase was on average 70 BPM from a basal rate of 80 BPM. In response, SF decreased by 2 percentage points ($P < 0.001$), while Lmax decreased by 0.8 mm (-3% of control). That is, on average SF and Lmax both decreased significantly, but by a factor only slightly in excess of the reproducibility of the measurement. The hemodynamic measurements during pacing followed a pattern consistent with previous reports (Table 2, Meas. I & II). Peak LV pressure showed a small, but significant ($P < 0.0002$) decline of 12 mmHg, and end diastolic pressure fell by 6.7 mmHg ($P < 0.0001$), peak rate of change of LV pressure increased from 1570 ± 330 mmHg/s to 2060 ± 510 mmHg/s ($P < 5 \times 10^{-6}$), and Vmax increased from 48 ± 9.5 s^{-1} to 66 ± 14.5 s^{-1} ($P < 10^{-5}$).

Post-pacing

The heart rate for the first post-pacing beat, determined from the R–R interval of the paced ECG, was virtually identical to the control rate (Tables 1 and 2, Meas. III). The post-pacing SF increased from control by 1 percentage point, while Lmax increased from control values by 0.3 mm on average. Thus, while there was a statistically significant increase in both SF and Lmax, the change was not great. In spite of considerable individual variability in SF and Lmax there was a consistent response.

Multivariate analysis showed that the post-pacing shortening fraction change ($\triangle$ SF = SF post-pacing − SF control) could be predicted from the response of marker motion during pacing.

$$\triangle SF = -1.33 \quad + 0.48 \times (SF\ pacing - SF\ control$$
$$- 58 \times (Lmax\ pacing - Lmax\ control)/Lmax\ control$$
$$+ 4.31 \times (T\ post\text{-}pacing - T\ pacing)$$
$$R = 0.84$$

where T represents the RR interval in s.

This finding is best illustrated in Figure 2 which shows the measured SF change compared with that predicted by the above regression equation. This SF change is positively correlated with the change in SF during pacing, and negatively correlated with the fractional change in Lmax. The change in the RR interval (postpacing − pacing) has a weaker positive influence on the shortening fraction change. On average both SF and Lmax decrease during pacing, but are not highly correlated with each other ($R = 0.292$). This is an essential point in explaining the heretofore unpredictability of the post-pacing beat. It is primarily the combined response of SF and Lmax during pacing which predicts how the first post-pacing beat will behave. SF post-pacing will be maximized when, during pacing, SF increases and Lmax decreases. Likewise SF post-pacing will be minimized when SF decreases during pacing and Lmax increases.

The hemodynamic measurements post-pacing are summarized in Table 2. Peak

Table 1. Summary of marker measurements in 20 patients (41 marker pairs)

Variable	Measurement	Mean	SD	P
HR	I	77	11	–
	II	148	17	10^{-6}
	III	80	15	NS
	IV	89	10	–
	V	91	13	NS
SF	I	9.90	6.09	–
	II	7.88	6.70	0.001
	III	10.89	7.54	0.02
	IV	10.04	6.28	–
	V	9.61	6.34	NS
Lmax	I	2.61	0.94	–
	II	2.53	0.92	2×10^{-6}
	III	2.64	1.92	2×10^{-5}
	IV	2.61	0.94	–
	V	2.63	0.96	NS

SF = shortening fraction, Lmax = maximum marker separation. All statistical comparisons employed the Students paired t-test with respect to the appropriate control or rest values. NS means no significant difference at the 0.01 level of significance. Measurements: I = control at rest, II = maximum pacing rate, III = first post pacing beat (HR controlled), IV = control for IHGT (HR controlled 10 BPM above rest), V = IHGT (HR controlled 10 BPM above rest).

LV pressure increased by 20 mmHg over control levels ($P < 0.0001$) while EDP showed a non-significant increase of 2.7 mmHg. Peak dP/dt increased 820 mmHg/s ($P < 10^{-6}$), and Vmax increased by 15 s^{-1} ($P < 10^{-6}$) over control values.

Hand grip

Because the right atrium was paced at 10 to 15 BPM above rest levels during the isometric handgrip test (IHGT) to override the chronotropic effect of the test, there

Table 2. Summary of hemodynamic measurements during the APST and IHGT

Variable	Measurement	Mean	SD	P
HR	I	78.6	11.3	–
	II	149.3	19.9	10^{-6}
	III	82.8	15.9	NS
	IV	91.3	10.7	–
	V	93.6	12.6	NS
Peak *P*	I	134	25.2	–
	II	122	21.0	0.0002
	III	154	28.2	0.0001
	IV	138	25	–
	V	165	29.8	5×10^{-6}
EDP	I	16.1	7.0	–
	II	9.4	5.5	5×10^{-6}
	III	18.8	6.6	NS
	IV	13.1	4.9	–
	V	19.3	6.6	5×10^{-6}
Peak dP/dt	I	1570	330	–
	II	2060	510	5×10^{-6}
	III	2390	410	10^{-6}
	IV	1760	375	–
	V	1920	504	0.003
Vmax	I	48	9.5	–
	II	66	14.5	10^{-5}
	III	63	11.6	10^{-6}
	IV	52	10.2	–
	V	49	9.8	0.003

Measurement: I = control at rest, II = maximum pacing rate, III = first post pacing beat (HR controlled), IV = control for IHGT (HR controlled 10 BPM above rest), V = IHGT (HR controlled 10 BPM above rest). P = probability computed from Student's paired t-test, NS = no significant difference at the 0.01 level. All comparisons with respect to appropriate control measurement.
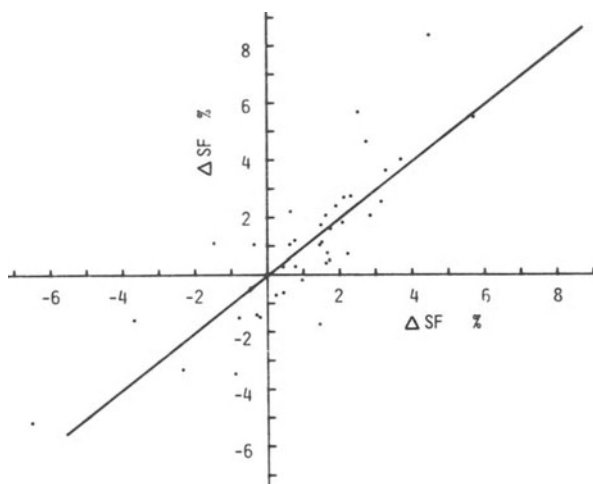
Figure 2. The measured shortening fraction change (first post pacing beat − control) vs that predicted from multivariate analysis incorporating measurements made during the atrial pacing stress test. This suggests that all the information contained in the first post-pacing beat is also available in the APST.

was no significant change in HR of 90 BPM. On average SF remained unchanged, as did Lmax.

Multivariate regression with the variables identified as most predictive during the APST also failed to reveal any outstanding correlations, neither did step-up analysis using the entire set of measured variables reveal any significant correlations. We can only conclude that the IHGT, in the absence of the usual heart rate response, is not a sufficient stress to the heart to be reflected in changes in either myocardial dimension or fractional shortening.

On the other hand, there were clear hemodynamic changes during the IHGT. Peak LV pressure increased by 27 mmHg ($P < 5 \times 10^{-6}$). This was accompanied by an increase in LV EDP by 6.2 mmHg ($P < 5 \times 10^{-6}$). There was a less impressive and conflicting change in the contractility indices: Peak dP/dt increased by 160 mmHg/s ($P < 0.003$) while Vmax, which is less load dependent, fell by 3 s^{-1} ($P < 0.003$) to a level identical with that during rest prior to the APST. Thus, during the IHGT the most significant response was found for peak LVP and EDP, but there was relatively little change in the contractility indices in response to the conflicting demands of the stress and loading conditions.

DISCUSSION

During atrial pacing, the left ventricle normally responds with an increase in all contractility indices, such as peak dP/dt and Vmax, and a decrease in end-diastolic

pressure (EDP). A decrease in contractility and/or an increase in EDP is associated with the onset of ischaemia. Ventriculographic studies [2] show that the LV volume decreases during pacing; stroke volume also decreases nearly inversely with heart rate, so that cardiac output is maintained. The decrease in EF is not as great as that of SV, as EF is partially compensated by the decrease in EDV. It is therefore expected that the normal response of the epicardial markers would be a decrease in both Lmax and SF. The results reported above confirm these expectations. Nevertheless, there is a great deal of variability as would be expected in so heterogenious a group of patients one year after bypass grafting. Following the abrupt reduction in the pacing rate the Q–Q interval (and heart rate) returned to near rest values, but SF and Lmax increased slightly. There was considerably individual and regional variability in this response.

In spite of this variability in the change in shortening fraction with respect to control values, this change could be individually predicted from the response obtained during pacing (Figure 2). Furthermore, the change in SF and Lmax during pacing were independent predictors of this response. This implies a decoupling of the dimension change and shortening fraction change during stress testing. That is, there may be three classes of abnormal response: a decrease in SF of more than normal and/or a constant or increase in Lmax.

One can only speculate at this point on the physiological mechanism which would allow a decoupling of the SF and Lmax response in ischaemic heart disease. This may be due to an imbalance in the utilization of reserve mechanisms. Nevertheless, the existence of such a possibility is now documented.

There is nearly universal agreement that the dominant effect of isometric hand grip (IHGT) is an increase in systemic arterial pressure. There is less agreement over the mechanisms involved or their relative importance in normal man compared to the patient with ischaemic heart disease. Savin et al [1] found that the blood pressure increase in patients after bypass surgery was attributable to an increased peripheral resistance with no significant changes in ventricular dimensions, EF, or velocity of shortening, in spite of a significant increase in HR. In a denervated group of patients the HR response was absent, but otherwise an essentially similar response was noted. Ishise [2], on the other hand, studied normals and hypertensives and concluded that the after load elevation was due to an increase in cardiac output with little change in peripheral resistance. There were no significant changes in LV dimensions for the normotensives. These results are consistent with the hypothesis that normals respond to IHGT by increasing CO, while patients with coronary artery disease respond by increasing peripheral resistance. Indeed, models based on the interplay between alpha and beta sympathetic activity, and parasympathetic activity have been proposed by Savin et al [1].

The response to the induced afterload increase in stroke work, end diastolic pressure and volume, and contractility has been classified by several investigators [3, 4, 5, 6] as follows: the normal response is an increase in stroke work with minimal elevation in preload; the abnormal response is an unchanged or decreased stroke

work with elevation in preload. Contractility does not appear to change greatly for either type of patient.

In our group of 20 patients, 12 showed a 4 mmHg or more rise in EDP while in 8 it was 3 mmHg or less. Multivariate correlation between the change in Vmax vs the change in EDP and peak P failed to reveal any significant correlations. Correlation analysis with the change in peak dP/dt as the independent variable, however, did reveal a significant correlation with the change in peak pressure ($R = 0.82$) but not EDP. Therefore, the response of EDP is not predictive of the response of contractility to IHGT. The correlation of peak dP/dt with peak P, but not that of Vmax with peak P, reflects their different sensitivities to load effects; Vmax is generally considered to be less load dependent.

There were no significant changes in ventricular dimensions or in shortening fraction during IHGT, nor did multivariate regression analysis reveal any more subtle patterns in the IHGT response predictable from the APST response.

Previous reports on the value of the IHGT as a stress test focused primarily on LV pressure or pressure derived indices. Our results are largely consistent with these findings even with the HR maintained constant. The dominant effect was afterload elevation. There were less clear changes in the contractility indices: peak dP/dt increased while Vmax was decreased. It is likely, therefore, that the increase in contractility described previously was in large part a secondary effect of a heart rate increase. In this study SF and Lmax generally failed to respond to the stimulus of afterload elevation, with constant heart rate, even in those patients who demonstrated a manifestly abnormal APST. When IHGT does result in ischaemia, as has been reported in the literature, a mechanism involving a heart rate increase must therefore be suspected. While we do not dismiss the IHGT as a non-invasive stress test, its use does appear contraindicated for follow-up involving the measurement of myocardial dimensions. Direct atrial pacing, while an invasive procedure, appears to be more powerful in detecting functional abnormalities as a result of ischaemia not apparent at rest.

REFERENCES

1. Savin WM, Alderman EL, Haskell WL, Schroeder JS, Ingels NB, Daughters GT, Stinson EB: Left ventricular response to isometric exercise in patients with denervated and innervated hearts. Circulation 61:897–901, 1980.
2. Ishise S: Hemodynamic and left ventricular alterations in response to isometric handgrip exercise. Jap Circulation J 42:411–416, 1978.

3. Krayenbuehl HP, Rutishauser W, Schoenbeck M, Amend I: Evaluation of left ventricular function from isovolumic pressure measurements during isometric exercise. Am J Cardiol 29:323–330, 1972.
4. Helfant RH, DeVilla MA, Banka VS: Evaluation of left ventricular performance in coronary heart disease: use of isometric handgrip stress test. Catheterization and Cardiovascular Diagnosis 2:59–67, 1976.
5. Ludbrook P, Karliner JS, O'Rourke RA: Effects of submaximal isometric handgrip on left ventricular size and wall motion. Am J Cardiol 33:30–36, 1974.
6. Stefadouros MA, Grossman W, Shakawy, ME, Witham AC: The effect of isometric exercise on the left ventricle volume in normal man. Circulation 49:1185–1189, 1974.

15. DIGITAL IMAGING OF THE LEFT VENTRICLE
BY PERIPHERAL CONTRAST INJECTION
DETECTION OF IMPAIRED GLOBAL AND REGIONAL
LEFT VENTRICULAR FUNCTION

P. Spiller, T. Fischbach, J. Jehle, A. Lauber, B. Pölitz and F.K. Schmiel

In the last few years digital image processing of intravenous angiograms has become an accepted diagnostic tool for visualization of peripheral arterial vessels. On the contrary, there are only a few studies analyzing cardiac function with this technique [1, 2, 3, 4], because of technical problems, but primarily due to difficulties resulting from voluntary or involuntary motions of the patients.

Digital image processing consists of two steps: at first static high contrast background structures are eliminated by subtracting a mask image from the contrasted images. Additionally the resulting difference image is contrast enhanced. It is evident that the quality of the difference image considerably depends on the selection of the mask image. The more congruous the background structures are in both the mask and the contrasted image, the better must be the visualization of those structures which are filled with contrast medium. A nearly total elimination of background structures is rather easily achieved in intravenous cineangiographies of the peripheral arteries.

Digital image processing of the cardiac chambers, on the contrary, is complicated by considerable changes of the background structures caused by the contraction of the heart and the motion of the lungs. Since intravenous digital angiocardiography was considered to be helpful to study left ventricular function not only at rest, but also during exercise, the aim of the present work was to test the accuracy of the method in clinical studies in man. The main objectives of the paper therefore are:

1. to describe the digital image processing system used,
2. to review our experiences with different mask modes, and
3. to prove the reliability of intravenous digital subtraction angiocardiography for quantitative evaluation of left ventricular function at rest and during exercise.

Figure 1 depicts the hardwired processing system by which the image subtraction is performed in real time. At first the videosignal of the mask image is A/D converted (8 bit, 5 MHz) and stored as a matrix of 256 × 256 pixels in an image memory. The mask image is dynamically subtracted from the digitized current image sequence by
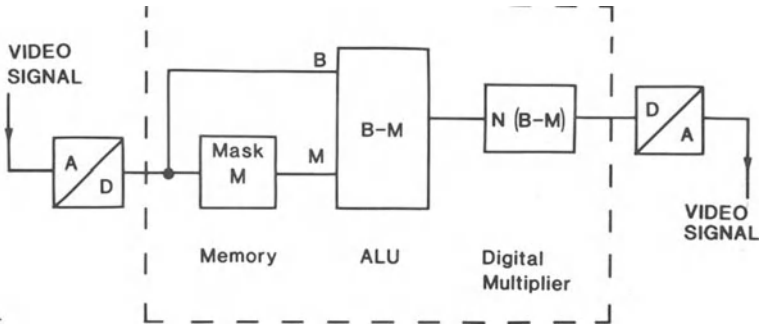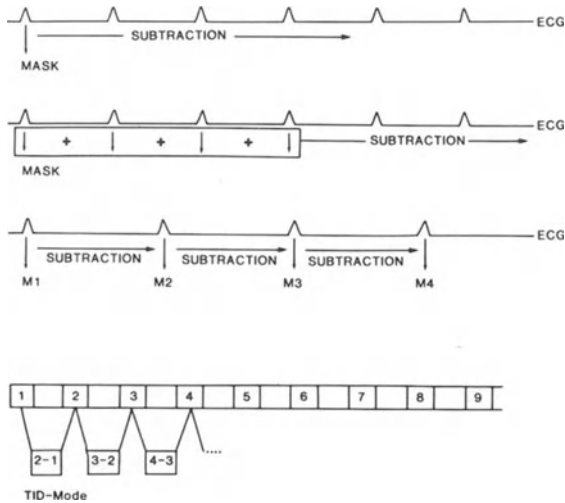
Figure 1.

Figure 2.

means of an arithmetic and logical unit – a so-called ALU. The output of the ALU provides a dynamic difference image which can be digitally amplified and reconverted into a normal video signal by a D/A-converter. In contrast to commercially available systems, the system designed by our group is relatively small and portable. It has the advantage that it can be used, for example, combined with a small C-arm unit in the coronary care unit.

Figure 2 illustrates the different mask modes which we examined in this study. One of the simplest modes means storing one ECG-triggered mask image and subtracting it from all subsequent images. From our experience non-triggered mask images lead to poor visualizations of the cardiac chambers, which can rarely be evaluated quantitatively. The next mode includes a mask image averaged from several frames of the same phase of the cardiac cycle obtained from consecutive beats. Our system allows ECG-triggered averaging of 2 to 128 beats. The third

Figure 3a.
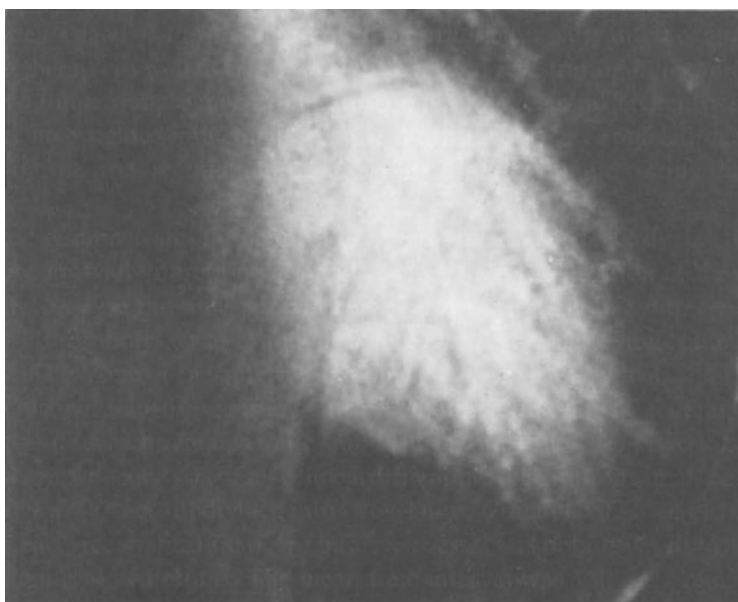
Figure 3b.
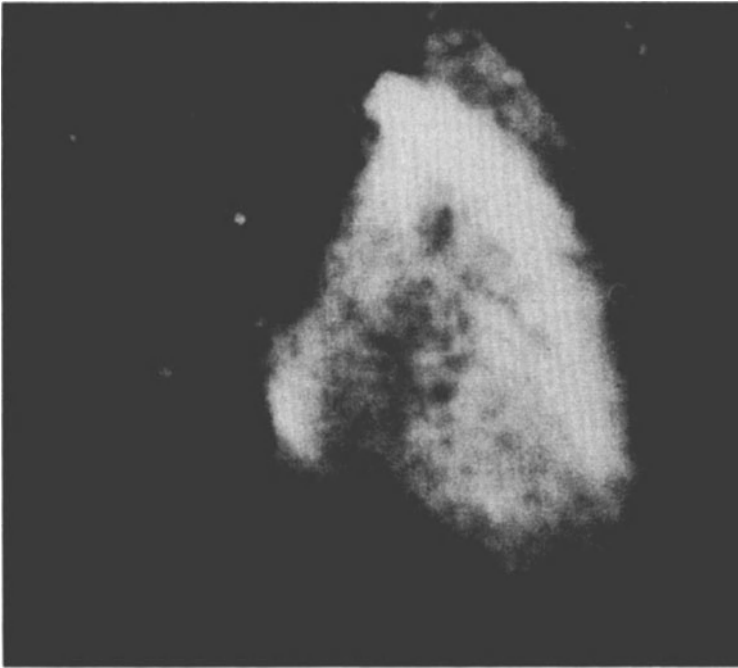
Figure 4.

mode illustrates the subtraction of a mask image which is updated each R-wave throughout the entire angiographic frame sequence. The last mode – the so-called TID-mode or time-interval-difference mode – includes the subtraction of a mask image which is updated at fixed time intervals of some 10 ms. Contrary to the first two modes, the last two use mask images which are obtained from the contrast phase.

Some examples of selecting an adequate mask are demonstrated in Figures 3a and b and Figure 4. Figure 3a depicts an unprocessed image of the left ventricle obtained by injecting 40 ml of contrast medium into the vena cava. The ventricular borders can barely be seen. Figure 3b shows the same, but processed and enhanced image. The mask image has been obtained by averaging some images of the pre-contrast phase. The ventricular borders are readily visible. In Figure 4 the TID-

Table 1. Quantitative evaluation

Mask mode	Rest	Excercise
Pre contrast averaged	18/20	17/20
TID	20/20	20/20
TID (ED/ES)	18/20	17/20
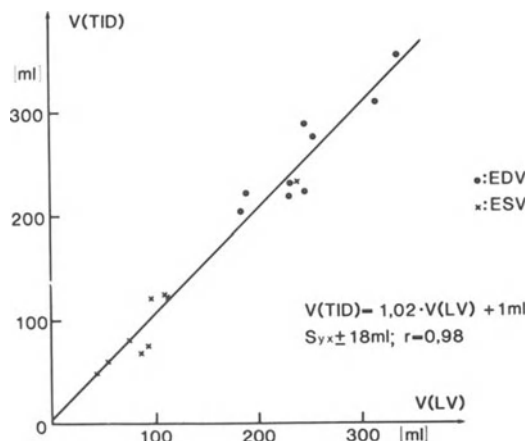
Figure 5.
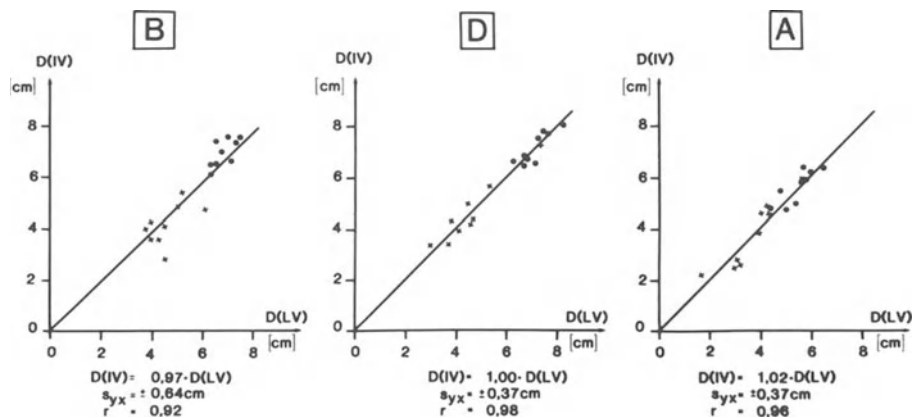
Figure 6.

mode – i.e. subtraction of a mask from the contrast phase – was chosen. The endocardial outline of the left ventricle can clearly be identified in all regions.

The advantage of the TID-mode is that – due to the close temporal relation of mask and unsubtracted image – the effect of patient motion is minimized. One essential disadvantage, however, is that in patients with regional hypo- or akinesia the border outlines of the left ventricle can be visualized only insufficiently. This can easily be explained: the TID-mode consists of subtracting two succeeding images of the contrast phase from each other. The chamber outlines only become visible if the two images are different, i.e. if the ventricle changes its configuration between them. In the case of akinesia the lack of motion results in a lack of visualization.

Table 1 summarizes the number of the obtained angiocardiograms which could be evaluated quantitatively by means of three different mask modes. The most
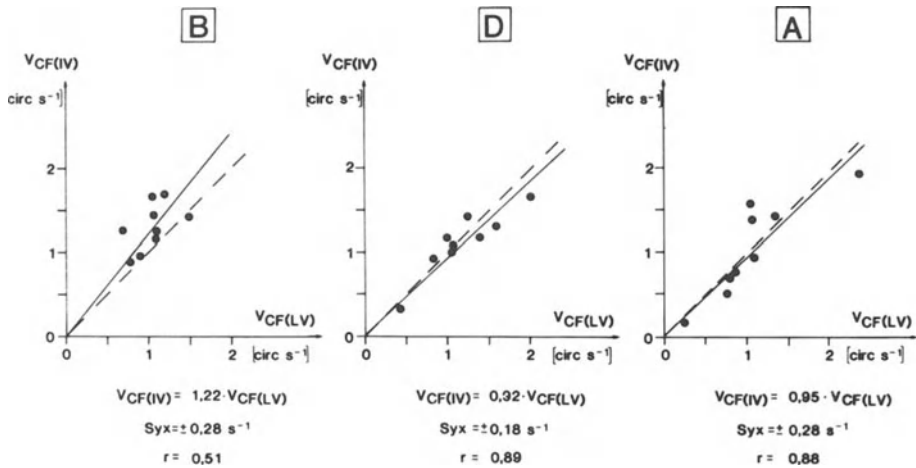
Figure 7.

effective mode was the TID-mode, which allowed outline of left ventricular borders at rest and during exercise in all 20 cases examined. Using the first mode – with a mask averaged from the pre-contrast phase – and the third one – a modified TID-mode with both endsystolic and enddiastolic images from the same cardiac cycle – only 17 and 18 cineangiograms, respectively, could be evaluated quantitatively. On the whole, the examples and Table 1 reveal that each mask mode has its specific advantages and limitations.

To prove the accuracy of the dimensional left ventricular data obtained by intravenous digital subtraction angiocardiography, a comparison with direct left ventricular angiocardiograms was performed. The reliability of measurement was tested by correlating corresponding dimensional data determined from both examinations. Digital subtraction was performed using the time-interval-difference mode. The angiograms had been performed at rest during the same routine heart catheterization. 40 ml of contrast material (Urografin 76%) were injected with a flow rate of 15 to 20 ml/s into the superior or inferior vena cava as well as into the left ventricle. Contrast images were recorded on videotape and cinefilm, respectively. The cinefilms were transformed into a videosignal and then processed. Left ventricular dimensions were determined at enddiastole and endsystole to calculate left ventricular volumes and diameters.

In Figure 5 left ventricular volumes determined from intravenous digital subtraction angiocardiography are correlated to values obtained from left ventricular angiography with direct injection of contrast material. The enddiastolic and endsystolic volumes show a good correlation. The standard deviation of the residuals amounts to ± 18 ml on average.

From the same examinations the correlations of the enddiastolic and endsystolic diameters in the basal (B), equatorial (D) and apical (A) region of the left ventricle
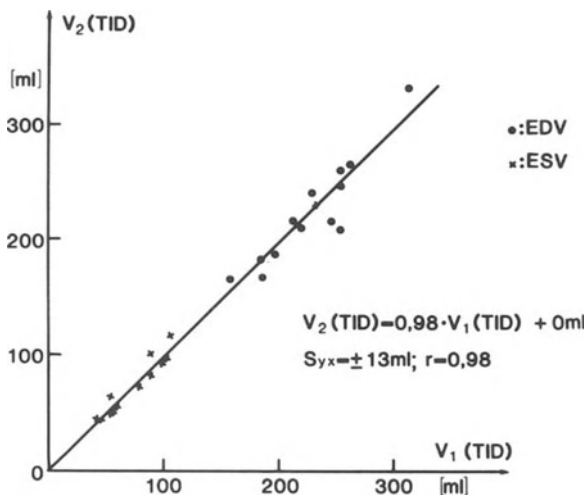
Figure 8.

are depicted in Figure 6. All regression lines are near to the lines of identity, the standard deviation of the residuals range between 3.7 and 6.4 mm. The corresponding circumferential fiber shortening rates, determined as parameters of regional function, also reveal a close correlation (Figure 7). The poor correlation of the basal (B) diameters and circumferential fiber shortening rates result from difficulties in recognizing the ventricular borders in that region where the left atrium is superimposed.

To test the reliability of intravenous digital subtraction angiocardiography *during exercise*, measurements regarding the reproducibility were performed.

In Figure 8 left ventricular volumes determined from two evaluations of the same intravenous angiocardiogram are correlated. For processing, the time-interval-difference mode was used. The regression line is near to the line of identity, the standard deviation of the residuals amounts only to $\pm$ 12 ml.

CONCLUSIONS

1. Left ventricular angiocardiograms of good diagnostic quality can be obtained by intravenous injection of contrast material and subsequent digital image processing by a portable hardwired system.

2. The selection of the mask image considerably influences the quality of the difference image. The TID-mode permits quantitative evaluation of intravenous angiocardiograms at rest and during exercise in all cases examined. This mode is limited, however, in patients with local left ventricular akinesia.

3. The accuracy and reproducibility of functional parameters of the left ventricle, obtained by intravenous digital angiography are comparable to those de-

termined from angiocardiograms with direct injection of contrast medium. Digital subtraction angiography allows a quantitative analysis of global and regional ventricular function at rest and during exercise. It must be emphasized, however, that it is an at least semi-invasive technique.

REFERENCES

1. Bogren HG, Bürsch J, Brennecke R, Heintzen P: Intravenous angiocardiography using digital image processing experience with axial projection in normal pigs. Invest Radiol 17:216–223, 1982.
2. Higgins CB, Norris SL, Gerber KH, Slutsky RA, Ashburn WL, Baily N: Quantitation of left ventricular dimensions and function by digital video subtraction angiography. Radiology 144: 461–469, 1982.
3. Kruger RA, Mistretta CA, Houk TL, Riederer SJ, Shaw CG, Goodsitt MM, Crummy AB, Zwiebel W, Lancaster JC, Rowe GG, Flemming D: Computerized fluoroscopy in real time for noninvasive visualization of the cardiovascular system. Radiology 130:49–57, 1979.
4. Vas, Ran, Diamond GA, Forrester JS, Withing JS, Swan HJ: Computer enhancement of direct and venous-injected left ventricular contrast angiography. Am Heart J 102:719–728, 1981.

16. COMBINED CARDIAC CINEANGIOGRAPHY AND PERIPHERAL DIGITAL SUBTRACTION ANGIOGRAPHY

K. BACHMANN, H.D. BETHGE AND P. MARHOFF

Intravenous angiography, introduced as early as 1939 by Roob and Steinberg [11], is making a comeback. With the advance of high resolution image intensifiers, television fluoroscopy and digitalization at hand, digital subtraction angiography of extracranial, abdominal and peripheral arteries can be performed ambulatorily by transvenous power injection. High quality imaging as a prerequisite of routine use has been demonstrated not only for digital vascular imaging but also for digital subtraction angiography of the left ventricle [3, 4, 5, 6, 7, 8, 10, 11, 12, 13].

Basically, the method of digital vascular imaging offers high quality imaging with the minimum of contrast material at the site of interest. But in our experience this advance in angiography is, in patients with multiple atherosclerotic lesions, reduced by the so-called "non-invasive" transvenous route because multiple injections of 30–40 cc contrast material are needed to achieve such a high quality. On the other hand, catheterization is no longer the problem it was in the days of Roob and Steinberg [11] and the question arises as to why digital subtraction angiography is not used as part of the invasive procedure and in combination with cineangiography. The majority of our candidates for invasive procedures are patients suspected of having, or already diagnosed as having, coronary heart disease. Total cineangiography has demonstrated that 64.8% of these patients have concomitant obstructive peripheral artery disease and thus we have to deal with the generalized type of atherosclerosis [1, 2]. This was the reason why we introduced "total cineangiography" regardless of whether symptoms of peripheral or coronary artery disease disabled the patient.

There exists more argument for combining cardiac cineangiography and peripheral digital subtraction angiography. After opacification of the left ventricle there is a run-off of contrast material into the arterial system, enough for simultaneous digital vessel imaging in the supraaortic, abdominal, pelvic or femoral area. Thus digital subtraction angiography performed simultaneously with ventriculography could substantially reduce both the amount of contrast material and fluoroscopic exposure of conventional "total cineangiography".

For combined cineangiography and digital subtraction angiography two x-ray image intensifier fluoroscopic systems are in place. One is a 27/17 cm image intensifier mounted on a C-arm (Angioskop®, Fa. Siemens AG) and the other a 33/25/17 cm image intensifier which is working independently, either in the con-

Figure 1. On the left hand side the conventional part of the twin system is shown, comprising image intensifier plus TV-system and cine camera. TV-images can be stored on video tape and later reviewed. Cine film has to be processed before viewing. The right hand side shows the second large field (33 cm) image intensifier with TV-camera and digital subtraction unit with an additional monitor for viewing the subtraction image, either as dynamic display (50 frames per second) or stop-action display. For patient annotation on hardcopy an alphanumerical keyboard is provided. The command module serves for setting the proper processing modes and parameters for digital subtraction.

ventional or the digital subtraction mode (Figure 1).

The digital image processing unit (Angiotron®, Fa. Siemens AG) is connected to the output of a high-resolution, high line rate TV-system (Videomed H®, Fa. Siemens AG) that is operated in a 50 frames per second 624 lines per frame mode for this purpose. TV images are digitized and integrated in a proper way so as to achieve both high signal-to-noise ratio and adequate display of dynamic data. Of two digital image stores one is used for storing the "mask" image (image containing no contrast-medium), whereas the other serves during real time observation for integration purposes, and finally for storing the "filling" image (image containing the optimum filling phase). When subtracting these images from one another the subtraction image that results is amplified and displayed on a proper monitor. Simultaneously with processing, the original video data can be stored on a high bandwidth (10 MHz) Video tape recorder for replay at any time, and reprocessing through the subtraction unit as often as wanted. For hardcopies a 100 mm camera (Videospot H®, Fa. Siemens AG) is used. Since image quality is mainly determined by contrast and noise, optium conditions are maintained at kV_p settings from 60 to 70 kV and input dose rates to the image intensifier of around 500 $\mu R/s$. For the ease of operation an automatic dose rate control is provided.

With both image intensifiers in place, left ventriculography is combined with

serial digital imaging of the supraaortic and cerebral vessels, the abdominal aorta including the renal arteries or the pelvic arteries. Because left ventricular angiography is routinely performed twice, before and after sublingual intake of ISDN, two to three areas of interest can be visualized simultaneously by digital subtraction angiography. The contrast material injected in the left ventricle is 20–30 cc with a flow of 4–8 cc per second. This is sufficient for digital imaging of the abdominal and pelvic area. Digital supraaortic vascular imaging is achieved with 8–12 cc and a flow of 4–6 cc/sec.

Because catheterization of the descending aorta with the Sones catheter causes no problem for the angiographer and adds no risk to the patient, down-stream injection into the descending aorta is added in patients for digital subtraction angiography of the femoral arteries, and in patients who need more than those two or three digital imagings performed simultaneously with the ventricular angiogram. The technique of intraaortic contrast material injection has the advantage of a further reduction of contrast material and concomitant increase in image quality. This ultra-low-doses digital subtraction angiography is extremely useful in patients with a generalized type of atherosclerosis who need, in addition to coronary angiography and ventriculography, a great number of peripheral, abdominal or supraaortic angiograms. Furthermore, digital subtraction angiography is still available when we have to deal with severely ill patients and patients with renal failure.

The Sones catheter can easily be advanced into the abdominal aorta as far as the femoral artery. Having started in 1972, this catheterization technique has been used in more than 4000 patients without any serious complications. It has turned out to be the ideal approach, too, for low-dose-high-quality digital vascular imaging. As compared with the transvenous power injection, regardless of whether the cubital or femoral vein is used, only 1/3 to 1/10 of contrast material is required, and in combination with left ventricular angiography no additional contrast material is needed at all. This provides the option of a large number of series, each of them of good quality. Thus, with less contrast material, higher vascular imaging quality is achieved, providing the option of increasing the number of single injections far beyond the limit set for the transvenous approach.

In our experience it is not the catheterization technique but the contrast material which has to be taken as the main potential risk factor in angiography. This has prompted us to replace "total cineangiography" by the combination of cine coronary angiography and ventriculography with digital vascular imaging using the same catheterization technique which has proven itself to be both safe and reliable in more than 4000 patients. Thus digital imaging reduces the number of objections to "total cineangiography", particularly those which focus on the amount of contrast material.

The low-contrast-high-quality digital subtraction angiography has, however, been used in intraluminal dilatation of peripheral, abdominal and extracranial arteries. Up to now we have performed cine-coronary-angiography and ventriculography in combination with digital vascular imaging (total angiography) in 121
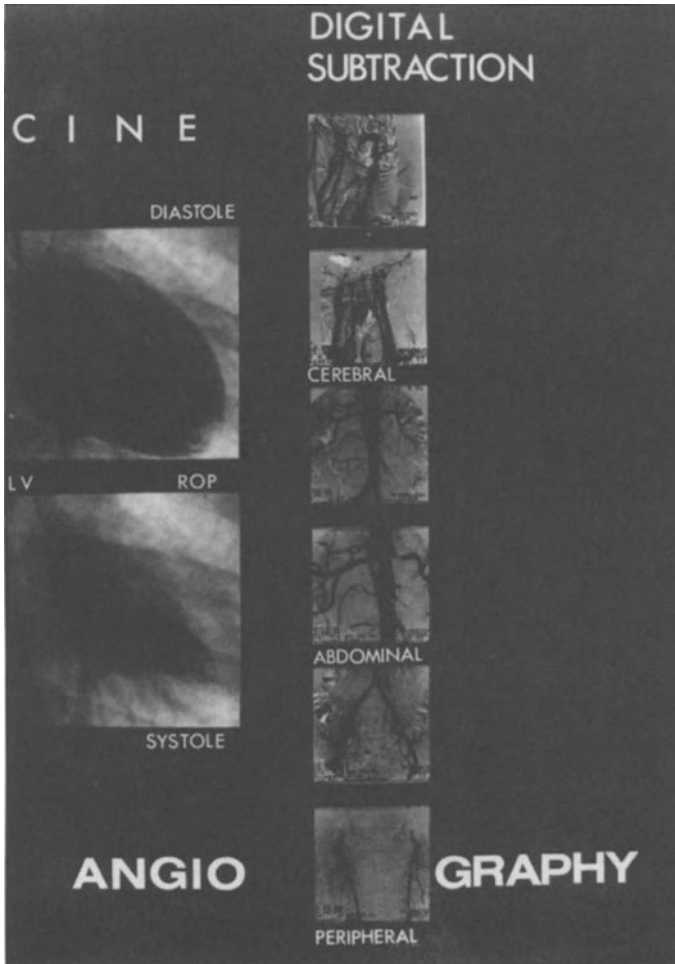
Figure 2. Using "run-off" contrast material from left ventricular cine angiography (CA) for digital cerebral, abdominal and peripheral subtraction angiography (DSA).

patients with coronary heart disease or supraaortic, abdominal or peripheral obstructive arterial disease without a single complication. Examples of digital subtraction angiography in sequence to left ventriculography and after direct intraaortic injection are given in Figures 2 and 3.

CONCLUSION

A system for combined cineangiography and digital subtraction angiography is described which can be used routinely for "total angiography" with a minimum of
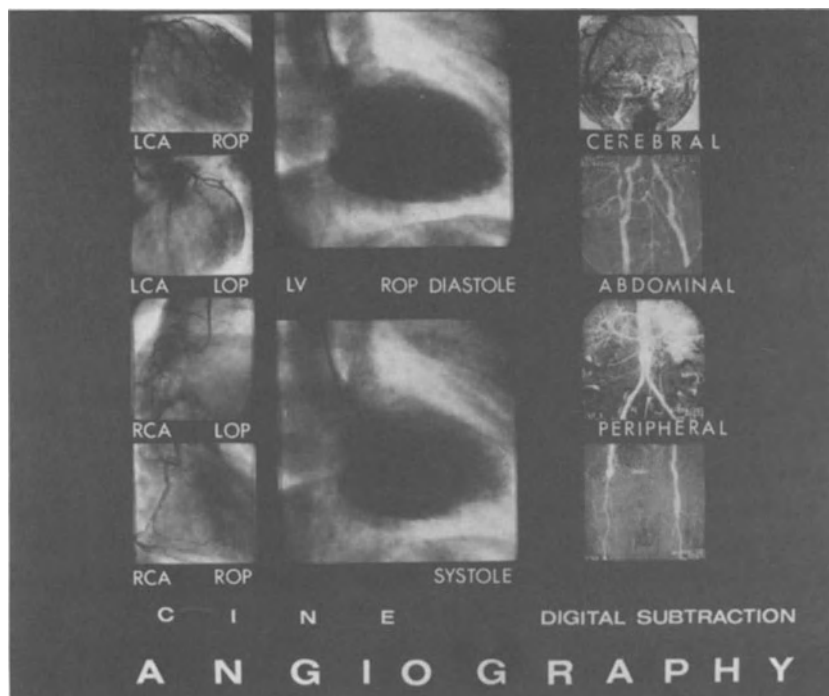
Figure 3. Combination of cine coronary angiography and left ventriculography with direct digital subtraction angiography (DDSA) of cerebral, abdominal and peripheral vessels.

contrast material and x-ray exposure, using "run-off contrast-material" after ventriculography for sequential opacification of cerebral, abdominal, pelvic and femoral arteries.

The future trend in digital subtraction angiography should not lead us back to the days of Roob and Steinberg [11]. We greatly appreciate the pioneer work done by Mistretta and coworkers [9, 10] (but we do not share their conclusion "that digital vascular imaging will suffice to reduce the number of conventional catheterization procedures"). The patient should have the option of best quality imaging with a minimum of contrast material and lowest x-ray exposure. This can be achieved by using the combination of cineangiography and digital subtraction angiography or direct digital vascular imaging. Thus digital vascular subtraction angiography is a step forward towards "total angiography" of patients regardless of whether they have symptoms of coronary heart disease or obstructive peripheral artery disease. Furthermore, direct digital imaging still provides angiography for the severely ill patient when conventional angiography including the transvenous approach is too high a risk.

REFERENCES

1. Bachmann K: Total cineangiography. In: Lichtlen P (ed), Coronary Angiography and Angina Pectoris. Gg. Thieme Verlag, Stuttgart, 1976.
2. Bachmann K, Raab G, Niederer W: Combined coronary and peripheral angiography. 1982.
3. Bethge HD, Bachmann K, Raab G: Transbrachiale, transluminale Dilatation von supraaortalen, abdominellen und peripheren Arterien (BTD). Dtsch Ges Thorax-, Herz-, Gefäßchirurgie, Bad Nauheim 1983.
4. Brennecke R, Brown TK, Bürsch J, Heintzen DH: Computerized video-image processing with application to cardioangiographic roentgen image series. In: Nagel HH (ed), Digital Image Processing, Springer, New York, 1977.
5. Heintzen PH, Brennecke R, Bürsch J: Present status of digital angiography. Int Symp: Advances in Non-invasive Cardiology, Aachen 1982.
6. Kruger RA, Mistretta CA, Houk TL, Riederer SJ, Shaw CG, Goodsitt MM, Crummy AB, Zwiebel W, Lancaster JC, Rowe GG, Flemming D: Computerized fluoroscopy techniques for non-invasive imaging of the cardiovascular system. Radiology 130:49, 1979.
7. Ludwig JW, Engels BCH: Digitale Gefäßabbildung (DVJ). Röntgenstrahlen 46:12, 1981.
8. Martin EC: Low-contrast angiography with digital subtraction technique. Medicamundi 27:14, 1982.
9. Mistretta CA, Ort MG, Cameron JR, Crummy AB, Moron PR: Multiple images subtraction technique for enhancing low contrast periodic ojects. Invest Radiol 8:43, 1973.
10. Mistretta, CA: Digital vascular imaging. Medicamundi 26:   , 1981.
11. Roob GP, Steinberg I: Visualization of this chambers of the heart, the pulmonary circulation and the great vessel in man. AJR 1–17, 1939.
12. Stark E, Harth P, Walther M, Kollath J, Riemann H: Die digitale Subtraktionsangiographie – eine wertvolle Hilfe bei der Diagnose von Gefäßkrankheiten. Internist 23:388, 1982.
13. Seyferth W, Marhoff P, Zeitler E: Digitale Subtraktionsangiographie (DSA), diagnostischer Stellenwert und Risiko. Electromedica 2:60, 1982.
14. Seyferth W, Dilbat G, Zeitler E: Digitale Subtraktionsangiographie (DSA), klinische Erfahrungen nach 1000 Patientenuntersuchungen (abstr). ZF Kardiologie 71:603, 1982.
15. Spiller P, Jehle J, Lauber A, Pölitz B, Schmiel FK: Digital imaging of the left ventricle by peripheral contrast injections – detection of impaired global and regional left ventricular function. Int Symp Advances in Non-invasive Cardiology, Aachen 1982.
16. Vas R, Diamond GA, Forrester JS, Whiting JS, Pfaff MJ, Levisman JA, Nakano FS, Swan HJC: Computer-enhanced digital angiography: correlation of clinical assessment of left ventricular ejection-fraction and regional wall motion. Amer Heart J 104:732, 1982.

IV. TECHNICAL ASPECTS OF PRECORDIAL ECG-MAPPING

17. TECHNICAL ASPECTS OF PRECORDIAL ECG-MAPPING

R. HINSEN, J. SILNY, G. RAU, R. VON ESSEN, W. MERX AND S. EFFERT

### 1. SUMMARY

The method of ECG-mapping is a high resolution ECG approach that has been demonstrated to provide additional information about the electrophysiological events in the heart. Multiple thoracic leads are recorded in order to analyze local potential changes on the body surface. Recent advances in electronic technology have enabled the development of practical clinical mapping systems. For the evaluation of body surface mapping in the clinical routine use we developed a completely self-contained clinical mapping system that contains all hardware/software components necessary for acquisition, processing, representation and documentation of surface maps. Amplifiers as well as microcomputer, floppy disk storage, printer and graphic CRT-terminal are mounted on a very compact trolley that can be easily wheeled to different measurement applications. In our system, 48 thoracic leads plus standard leads I, II, and III are sampled simultaneously using multiplexing techniques and direct memory access.

After preprocessing and automatic analysis the system provides comprehensive measurement reports, including plots of the representative complexes, printed values of the measured amplitudes and time intervals, graphs of the course of all computed parameters throughout the test etc. Using the described system we evaluated the diagnostic performance of ECG-mapping in comprehensive clinical studies.

2. INTRODUCTION

In the clinical practice the cardiac electric field is generally studied by recording and analysing local potential changes as functions of time (Figure 1). There remains a lot of information about the electrophysiological events in the heart that cannot be obtained by this method. The precise study of the cardiac electric field requires the knowledge of the potential distribution at numerous thoracic points as obtained by "body surface mapping". This high resolution approach has been demonstrated to provide additional information useful for diagnosis and monitoring of heart disease [6, 8]. Up to 256 thoracic measurement points are used for the calculation of the total surface potential distribution around the thorax (Figure 2).

Standard Leads (Wilson V1 - V6)
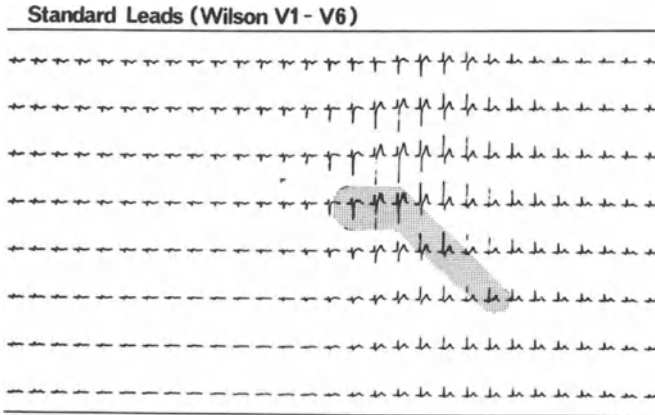
Figure 1. Computer plot of multiple ECG signals as functions of time. The position of each plotted signal corresponds to its position in the electrode array. The shaded area indicates the thoracic location of the six Wilson-leads.
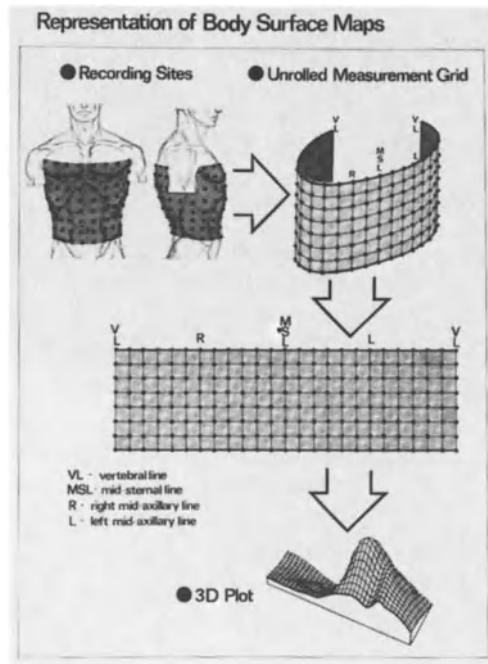
Figure 2. Recording sites of multiple ECG-leads and representation of the momentous spatial potential distribution as 3D plot. The equally spaced measurement grid is cut at the vertebral line and unrolled for representation.
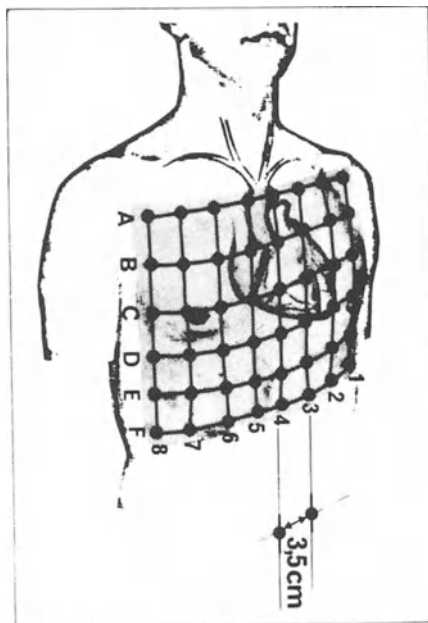
Figure 3. Multiple electrode array in position on the thorax. 48 electrodes are connected to a flexible plate.

3. A METHOD FOR CLINICAL ECG-MAPPING

3.1. System-Hardware

For comprehensive clinical studies we had to reduce the number of electrodes. Studies of Barr et al [1], Lux et al [4] and others reported that minimized lead systems with 24 to 35 electrodes were sufficient to obtain the clinical significant information content. In our institute we are also working on this problem in experimental and theoretical studies. Based on our present data we estimate that less than 50 optimally placed thoracic electrodes – adapted to the individual case – are sufficient for the registration of the clinical significant ECG information content. In most cases the immense technical overhead of a system with a greater number of input channels can be avoided.

Because the number of positions of thoracic electrodes has still to be discussed and no lead system has been established as a standard up to now, we use a grid of maximal 256 equally spaced measurement points for the calculation of the total potential distribution around the thorax (32 columns with 8 electrodes). We have implemented several acquisition modes:
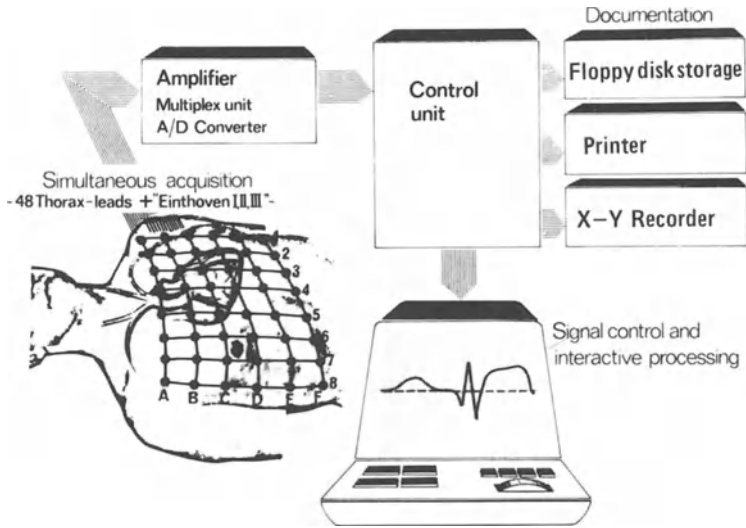
Figure 4. Diagrammatic representation of the main components of the mapping system.

1. We record a 48-electrodes lead system (6 columns with 8 electrodes, equally spaced in a 3.5 × 3.5 cm grid (Figure 3)), in several adjacent positions on the thorax sequentially. Special software merges the different records into one surface map.
2. Minimized lead systems with non-equally spaced electrode positions are used. Software modules transform these data to our standard grid.
3. Only certain "regions of interest" are analysed, e.g. for monitoring of ischemia and necrosis in patients with myocardial infarction [2, 3], and for ergometer stress tests [7].

Our standard lead system is shown in Figure 3. All electrodes are connected to a flexible synthetic plate. It takes only a few seconds to attach the electrode array to the patient's thorax or to remove it. However, a lot of technical problems had to be solved concerning data acquisition and processing. Figure 4 shows our hardware configuration. A control unit based on a microprocessor supervises the whole system and initializes the necessary functions. 48 thoracic leads as well as standard leads I, II, III are amplified in an amplifier unit. There is a separate amplifier channel for each lead. The amplified leads are connected to a multiplex unit and digitized in an analog/digital converter. Each channel is acquired with 500 samples per second. The digitized data are stored on a floppy disk storage. All leads are sampled simultaneously. To manage the high throughput-rate the analog input channel as well as the floppy disk controller have been realized as direct memory access controller.
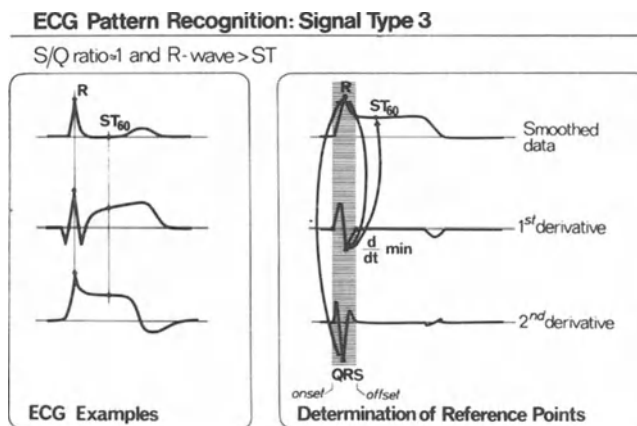
Figure 5. One example of several implemented pattern recognition algorithms. Reference points are determined in the smoothed signal as well as in its first and second time derivative.

All hardware components are mounted on a very compact trolley. It contains amplifiers, microcomputer, floppy disk storage, graphic display and printer. This stand-alone system allows the registration, preprocessing, analysis and representation of surface maps under clinical conditions. We reduced the number of control elements to a minimal necessary set of buttons that is placed on a specially designed panel [5].

3.2. Preprocessing and computer analysis

After the sampling period, a quality control of the recorded ECG signals can be performed by accelerated display of all signals on the CRT screen. In an alternative mode the system automatically controls signal quality and marks ECG intervals of lower quality. Software routines for removing line frequency interferences and baseline drifts have been implemented. If there is too much noise on single channels, the noisy data can be replaced by means of interpolation techniques. The signal is then estimated from an average of the signals at the four nearest points.

Mapping data are averaged and evaluated off-line. For this purpose we have implemented a lot of software modules in our system. The first step of evaluation is the calculation of a representative heart action of all ECG complexes in the sampling interval in order to reduce respiratory artifacts and muscle activities.

The representative heart complexes of all monitored leads are passed to a pattern recognition module that determines reference points. For rapid and accurate estimation of reference points we have implemented different ECG pattern recognition routines for the different types of – more or less deformed – QRS complexes. Figure 5 shows one example of several implemented ECG pattern recognition algorithms.
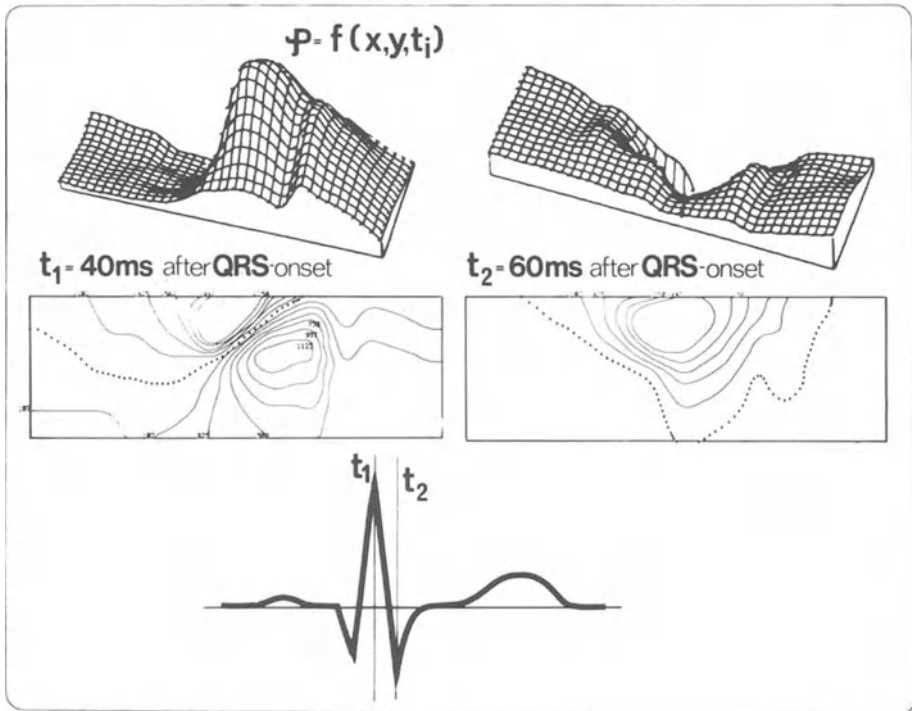
Momentaneous Thoracic Potential Distribution

Figure 6. Display of ECG-Mappings as 3D maps and isopotential maps for preselected instances within the heart complex.

Reference points are determined in the smoothed ECG signal as well as in its first and second time derivative. In borderline cases a chain is performed to the interaction module. In this module, characteristic ECG points are determined interactively by displaying the ECG signal on the CRT terminal and positioning graphic markers. All relevant measurement parameters are calculated after the separation of the ECG waves. Typical parameters are: Sum-values of R-wave amplitudes, Q-wave amplitudes and ST-segment elevation in all leads of a "region of interest" (e.g. monitoring of myocardial infarction [2] or QT-intervals and ST-segment depression (e.g. stress tests for diagnosis of coronary heart disease [7]).

The trend of ST-segment elevation is evaluated as an indicator of reversible myocardial ischemia, and Q-wave development and R-wave reduction as indicators of irreversible myocardial damage.

3.3. Display of ECG-maps

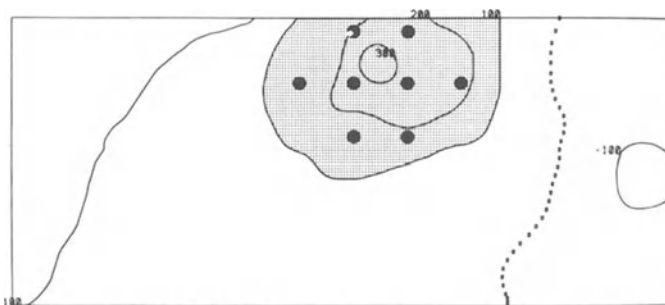The sampled signals are displayed as functions of time $f(x_i, y_i, t)$. For exact quanti-

Figure 7. The precordial potential distribution at an interval of 60 ms after the S-wave is used to define the number and positions of the permanent monitoring electrodes.

tative and qualitative analysis, the momentous potential distributions are displayed as isopotential maps or as perspective 3D maps (see Figure 6). Interpolation between measurement points is performed with spline functions. Series of 3D-maps or Iso-maps are calculated for selected times within the representative heart complex and displayed on the built-in CRT-display. The perspective is calculated for a predetermined point of sight (2 angles). Hidden lines of the three dimensional potential distribution are eliminated. Monitoring parameters (sum values) are plotted as trend curves.

4. CONTINUOUS ON-LINE ECG-MAPPING

Our clinical studies with the 48-electrode array demonstrated that it is possible to further reduce the number of monitoring electrodes and we developed a method for continuous on-line mapping in patients with acute myocardial infarction. In a first
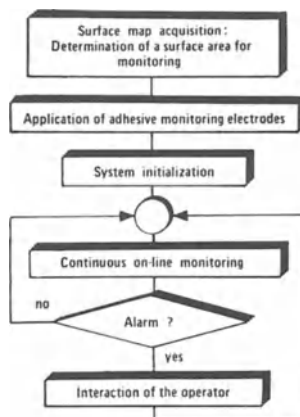

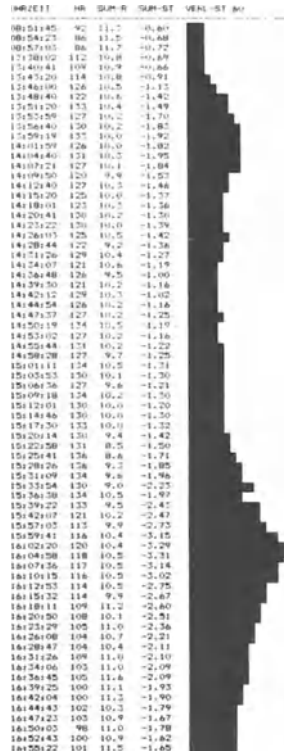*Figure 8.* Flow chart of continuous on-line mapping.

164

Figure 9. The built-in printer of the mapping system shows the course of the measured parameters (sum of ST-segment amplitudes). This patient with acuty myocardial infarction had two phases of recurrent ischemia.

step we register a multiple lead surface map of the precordial potential distribution and define the number and positions of the permanent monitoring electrodes. We use the momentous isopotential map at an interval of 60 ms after S-wave to define a "region" on the thorax surface for monitoring. In our preliminary studies with this method we used 8 electrodes and placed them around the centre of the determined region (Figure 7).

Figure 8 shows a flow chart of the system operation. After the determination of a surface area for monitoring we attach the adhesive monitoring electrodes to the thorax. Before starting continuous on-line monitoring the system must be initialized for the measurement problem. After that, continuous on-line monitoring is performed until alarm conditions are fulfilled. During continuous on-line monitoring all representative complexes and trend curves of the monitored parameters are immediately displayed. Figur 9 shows an original measurement print-out (course of ST-segment sum-values) of a patient with acuty myocardial infarction. The trend curve indicates two phases of recurrent ischemia.

REFERENCES

1. Barr R, Spach MS, Herman-Giddens GS: Selection of the number and positions of measuring locations for electrocardiography. IEEE Trans Biomed Eng: 18:125–138, 1971.
2. Hinsen R, von Essen R, Silny J, Merx W, Rau G, Effert S: Monitoring of myocardial ischemia and necrosis in acute myocardial infarction. Computers in Cardiology, pp. 71–76. Long Beach, California: IEEE Computer Society, 1979.
3. Hinsen R, Budde R, von Essen R, Merx W, Silny J, Rau G, Effert S: Continuous on-line ECG-mapping in patients with acute or impending myocardial infarction. Computer in Cardiology, pp. 197–200, Long Beach, California: IEEE Computer Society, 1981.
4. Lux RL, Smith CR, Wyatt RF, Abildskow JA: Limited lead selection for estimation of body surface potential maps in electrocardiography. IEEE Trans Biomed Eng 25:270–276, 1978.
5. Rau G: Ergonomische Überlegungen bei der Gestaltung komplexer medizinischer Instrumentierung unter Einsatz von Mikroprozessoren. Biomed Technik 24:Sup 10–15, 1979.
6. Taccardi B, de Ambroggi L, Viganotti C: Body surface mapping of heart potentials. In: Nelson CV and Geselowitz DB (eds), The Theoretical Basis of Electrocardiology, pp 436–466, Clarendon Press, Oxford, 1976.
7. Von Essen R, Hinsen R, Spruss KH, Silny J, Merx W, Meyer-Erkelenz JD, Rau G, Effert S; Automated mapping of ECG surface potentials in detection of ischemia during stress test. Computers in Cardiology, pp. 41–45. Long Beach, California: IEEE Computer Society, 1980.
8. Yamada K: Body surface isopotential map: past, present and future. Jap Circ J 45:1–14, 1981.

18. ABILITIES AND LIMITATIONS OF PRECORDIAL MAPPING IN ACUTE MYOCARDIAL INFARCTION

R. von Essen, W. Merx, S. Effert, R. Hinsen, J. Silny and G. Rau

In more than 90% of all patients acute myocardial infarction can be recognized by the 12 leads standard ECG. Only in few cases is it necessary to increase the number of electrodes for diagnostic purposes as, for instance, in dominant right heart infarction. For detailed analysis of the electrocardiographical development of myocardial infarction and for the evaluation of therapeutical influence on infarct size, however, multiple leads exceeding the number of 12 standard leads have shown themselves to be useful. The first investigations concerning these topics were done in animal experiments by Maroko, Braunwald and co-workers in the late sixties using epicardial leads [1, 2, 3] and showed the good correlation between ST-segment elevation after LAD occlusion, CK content of myocardium and histological findings in the ischemic area. The close correlation between epicardial and precordial ECG changes in anterior myocardial infarction made this method also applicable to man [4].

"Limitation of final infarct size" was the slogan of the seventies and a lot of interventions and treatments, either reducing myocardial oxygen demand or improving oxygen supply of the ischemic area, were studied. During the first years, attention was focused especially on the ST-segment changes. A rapid decrease of ST-segment elevation was estimated as beneficial to infarct size. One example is shown in Figure 1. Though the significant influence of the β-blocker metoprolol on the ST-segment elevation compared to placebo can be recognized, a significant influence on final infarct size could not be proved (from our double-blind study concerning the effect of metoprolol on infarct size in acute myocardial infarction [5]. Analysis of the spontaneous course of ST-segment elevation in some cases already reveals a rapid decrease of ST-segment elevation during the first hours after onset of infarction without any specific therapy (Figure 2) as seen here in four of our patients. Thus, interest turned more to the changes in Q-, R- and S-waves. Our short-term investigations of ECG alterations using 48 precordial leads and calculation of the sum of all precordial Q- and R-wave amplitudes and ST elevation demonstrate that a potentially reversible ischemia (indicated by the ST-segment elevation) seems to change into an irreversible myocardial damage (indicated by the development of Q-waves and reduction or complete loss of R-waves) during the first 6 to 8 hours [6, 7]. After these initial ECG alterations, the further course could be divided into two different types: one group of patients had no further changes in Q-
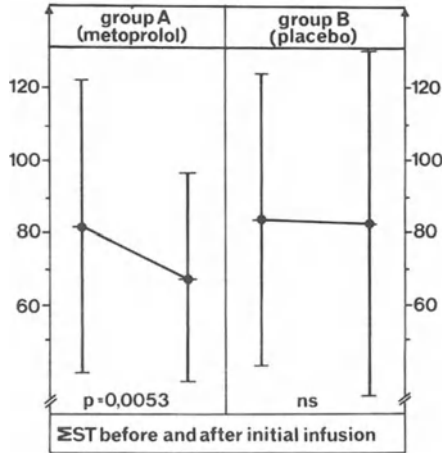
Figure 1. Influence of β-blocker infusion on ST-segment elevation compared to placebo in patients with acyte myocardial infarction.

and R-waves and ST-segment elevation. CK-MB serum curves corresponded to those of an uncomplicated infarction. The other group had ECG and enzymatic signs of an extension of infarction with a new increase of ST-segment elevation, a further development of Q-waves and reduction of R-waves and a second peak of MBCK (Figure 3 and 4). Thus, precordial mapping gives an insight into the dynamic of the development of myocardial damage. At this point it should be
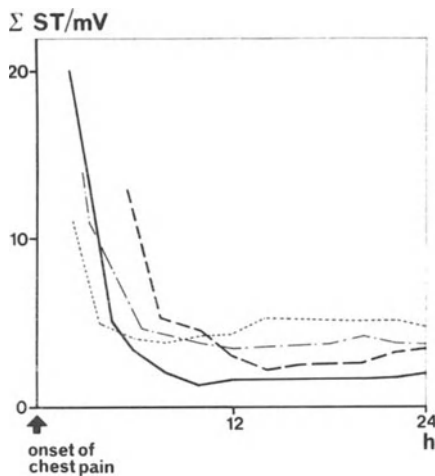

Figure 2. Spontaneous decrease of ST-segment elevation in four patients with anterior myocardial infarction without any treatment influencing infarct size ($\sum$ ST = sum of precordial ST-segment elevation using a 48 lead system).
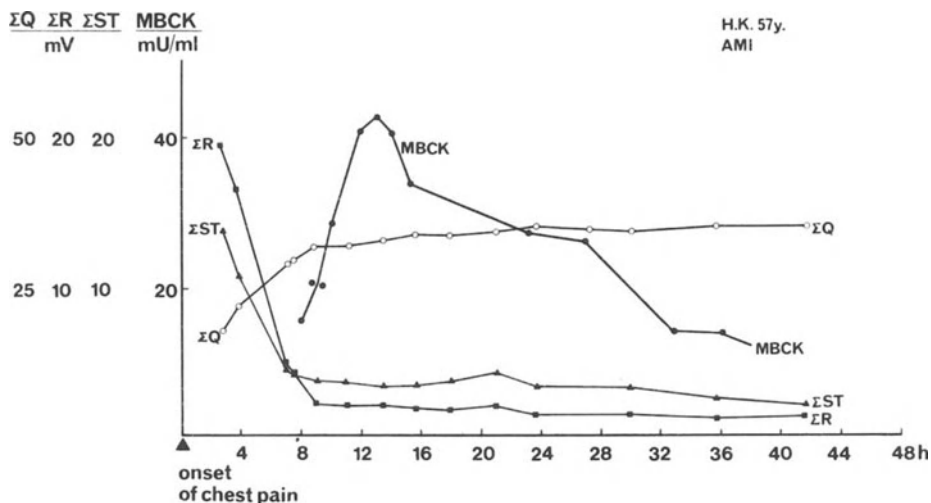
Figure 3. Representative patient with uncomplicated myocardial infarction. After initial decrease of ST-segment elevation and R-wave reduction and increase of Q-waves, there are no further changes indicating extension of necrosis. This is confirmed by a MB-CK serum curve compatible with an uncomplicated infarct.
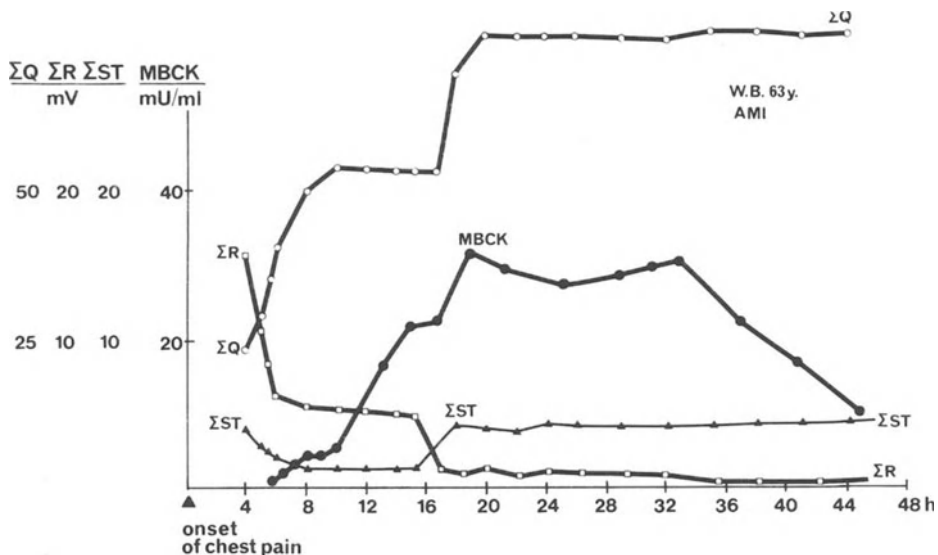

Figure 4. Representative patient with extension of myocardial infarction. 15 hours after onset of chest pain, a second increase of ST-segment elevation, a new increase of Q-waves and a further reduction of R-waves (accompanied by angina) can be seen. A delayed second peak of MB-CK indicates extension of necrosis.
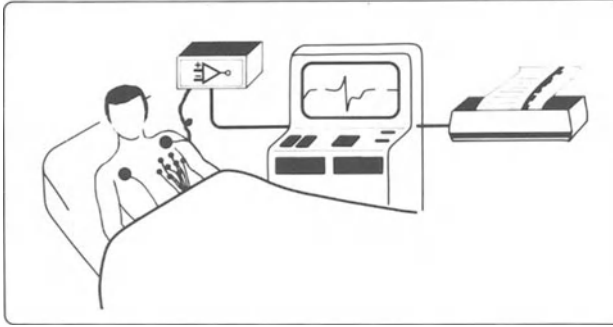
Figure 5. Schema of our monitoring system with the attached electrodes, amplifier and A/D-converter, mobile minicomputer and database unit, scope and plotter.

mentioned, that our investigations in patients with acute infarct and successful thrombolysis revealed that Q-waves and R-wave loss are, in parts, reversible and not identical to necrosis.

As a new ST-segment elevation is the earliest objective sign of ischemia, the consequence was to monitor ST-segment shifts in patients with high risk of re-
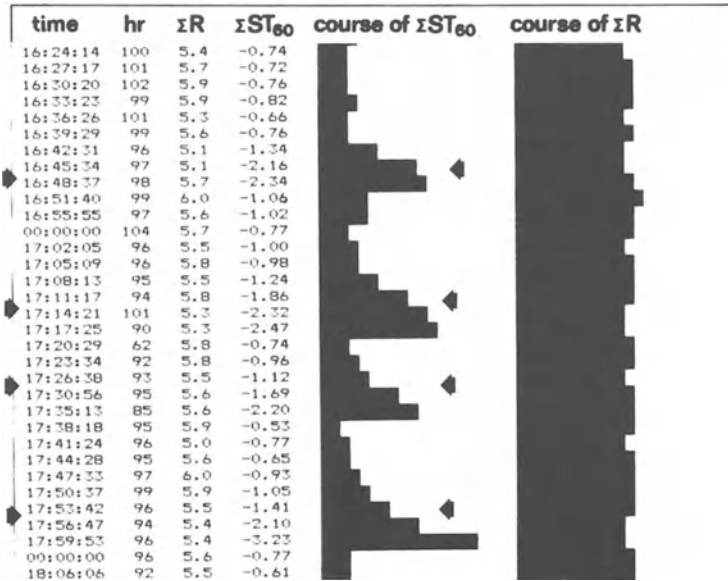
G.P., 62 y. m.

time	hr	ΣR	ΣST$_{60}$	course of ΣST$_{60}$	course of ΣR
16:24:14	100	5.4	-0.74		
16:27:17	101	5.7	-0.72		
16:30:20	102	5.9	-0.76		
16:33:23	99	5.9	-0.82		
16:36:26	101	5.3	-0.66		
16:39:29	99	5.6	-0.76		
16:42:31	96	5.1	-1.34		
16:45:34	97	5.1	-2.16		
16:48:37	98	5.7	-2.34		
16:51:40	99	6.0	-1.06		
16:55:55	97	5.6	-1.02		
00:00:00	104	5.7	-0.77		
17:02:05	96	5.5	-1.00		
17:05:09	96	5.8	-0.98		
17:08:13	95	5.5	-1.24		
17:11:17	94	5.8	-1.86		
17:14:21	101	5.3	-2.32		
17:17:25	90	5.3	-2.47		
17:20:29	62	5.8	-0.74		
17:23:34	92	5.8	-0.96		
17:26:38	93	5.5	-1.12		
17:30:56	95	5.6	-1.69		
17:35:13	85	5.6	-2.20		
17:38:18	95	5.9	-0.53		
17:41:24	96	5.0	-0.77		
17:44:28	95	5.6	-0.65		
17:47:33	97	6.0	-0.93		
17:50:37	99	5.9	-1.05		
17:53:42	96	5.5	-1.41		
17:56:47	94	5.4	-2.10		
17:59:53	96	5.4	-3.23		
00:00:00	96	5.6	-0.77		
18:06:06	92	5.5	-0.61		

Figure 6. Histogram of a 62-year-old patient with impending infarction and repetive attacks of severe ischemia, documented by new ST-elevations. Ischemias could be stopped within few minutes by nifedipine → .
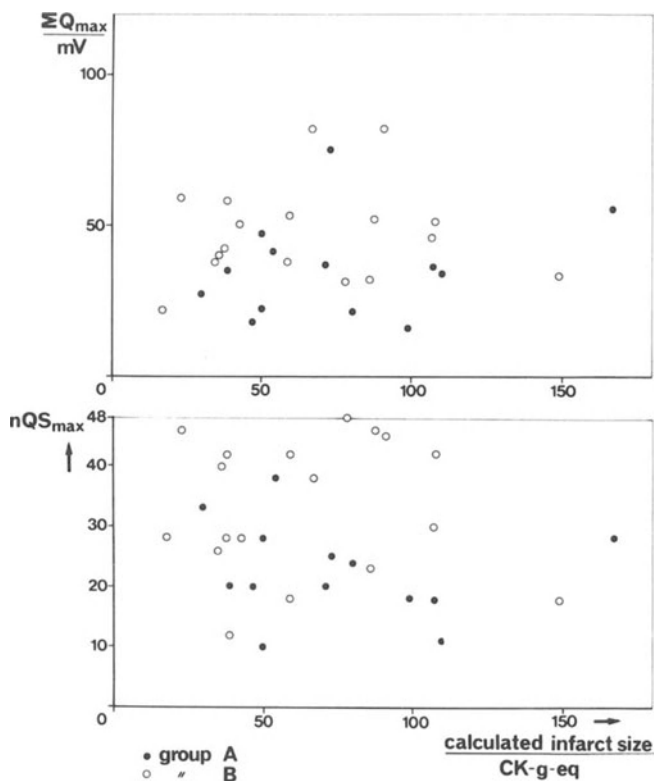
Figure 7. There was no correlation ($r < 0,5$) between precordial Q-wave amplitudes ($\sum Q$) and number of precordial QS complexes = leads without R-waves (nQS) compared to calculated infarct size from CK serum cruves (g.eq). The maximum of $\sum Q$ and nQS during the furst 48 hours after onset of infarction was used. Group A = patients with uncomplicated infarcts (see Figure 3). Group B = patients with extension of infarcts (see Figure 4).

ischemia and in those with impending infarction. A computerized system was devised, able to monitor up to 16 electrodes simultaneously (Figure 5). The selection of electrodes was based on a preceding 48 electrodes mapping. In anterior and inferior infarction different strategically placed electrodes are used, located in and around the centre of the ischemic area. The sum of the ST-elevation and of the R-waves are calculated in 3 minute intervals and plotted as a histogram. Figure 6 shows the histogram of a patient with impending infarction and repetitive attacks of severe ischemia, documented by new ST-elevation. Ischemia could be stopped within few minutes by nifedipine. Our first experiences in 50 patients monitored for 24 to 48 hours demonstrate that this method is a useful tool to recognize ischemias at once and to improve therapy for avoiding ischemic attacks or extension of infarcted myocardium [8].

All hopes to quantify infarct size exactly by means of precordial mapping have not yet been fulfilled. Our investigations could find no correlation between ECG

changes (number of precordial leads with ST-segment elevation, number or amplitudes of Q-waves, precordial R-wave amplitudes or number of precordial QS-complexes) and infarct size calculated from CK or MBCK (Figure 7). However, recently Selvester et al [9] reported the pathological validation of computer model criteria and infarct size and location. The correlation between a segment subdivision of the left ventricle and ECG signs of infarction using a score-system allowed in patients with first myocardial infarction, and in absence of ECG criteria of hypertrophy or bundle branch block a good quantification, which could be proved by pathological findings [9].

CONCLUSION

For diagnostic purposes precordial mapping is useful only in a few cases. Detailed analysis of the ECG using multiple leads gives an insight into the dynamic process from reversibly ischemic myocardium to irreversible damage. It enables us to differentiate between uncomplicated and complicated infarcts. The investigations have improved our knowledge of the time course of the infarct and have influenced our decision as to how long after onset of infarct does thrombolysis make sense. A continuous on-line monitoring of multiple leads promises to increase our knowledge of ischemia and improve therapy for avoiding ischemic attacks. To date, ECG does not allow exact quantification of infarct size even when using multiple leads.

REFERENCES

1. Maroko PR, Kjekshus JK, Sobel BE, Watanabe T, Covell JW, Ross J, Braunwald E: Factors influencing infarct size following experimental coronary artery occlusion. Circulation 43:67–82, 1971.
2. Maroko PR, Libby P, Sobel BE, Bloor CM, Sybers HD, Shell WE, Covell JW, Braunwald E: Effect of glucose-insulin-potassium infusion on myocardial infarction following experimental coronary artery occlusion. Circulation 45:1160–1175, 1972.
3. Braunwald E, Maroko PR: The reduction of infarct size – an idea whose time (for testing) has come. Circulation 50:206–209, 1974.
4. Muller JE, Maroko PR, Braunwald E: Evaluation of precordial electrocardiographic mapping as a means of assessing changes in myocardial ischemic injury. Circulation 52:16–21, 1975.
5. v Essen R, Merx W, Neis W, Ritz R: Wirkung von Metoprolol auf die Infarktgröße beim akuten Myokardinfarkt. Dtsch med Wschr 107:1267–1273, 1982.
6. v Essen R, Merx W, Effert S: Spontaneous course of ST-segment elevation in acute anterior myocardial infarction. Circulation 59:105–112, 1979.
7. v Essen R, Merx W, Dörr R, Effert S, Silny J, Rau G: QRS mapping in the evaluation of acute anterior myocardial infarction. Circulation 62:266–276, 1980.
8. v Essen R, Hinsen R, Louis R, Merx W, Silny J, Rau G, Effert S: On-line monitoring of multiple precordial leads in high risk patients with coronary artery disease. Computers in Cardiology IEEE, Seattle 1982 (in press).
9. Selvester RH, Ideker RE, Wagner GS: Pathological validation of computer model criteria for infarct size/location. Computers in Cardiology IEEE, Seattle 1982 (in press).

19. DETECTION AND QUANTIFICATION OF ACUTE MYOCARDIAL INFARCTION BY TWO-DIMENSIONAL ECHOCARDIOGRAPHY

P. Schweizer, R. Erbel, W. Merx, J. Meyer, W. Krebs and S. Effert

1. INTRODUCTION

The immediate and long-term prognosis of patients with acute myocardial infarction depends largely on the site and extent of the infarcted myocardium. Recently, clinical and experimental studies have demonstrated that two-dimensional echocardiography can visualize wall motion abnormalities in acute myocardial infarction and can be used to quantify the extent of ischemia. The practicability of those methods could be of special interest to estimation of changes secondary to t-therapeutic interventions [1, 2, 3, 4].

For several reasons the following quantitative echocardiographic studies in acute myocardial infarction were carried out using long axis apical two chamber views: in our experience this section plane can be obtained with a success rate of over 85%, even in critically ill patients. This is in contrast to the success rate of parasternal views which can be obtained only in about 65% [2, 5, 6]. Left ventricular regional and global function can be studied from the same section plane. Furthermore, the apical two chamber view permits visualization of anterior, apical and inferior parts of the left ventricle, resembling cineangiographic right anterior oblique projection [7].

2. SENSITIVITY AND SPECIFICITY OF THE METHOD

To test the sensitivity and specificity of the method, studies were first of all carried out in 39 patients with acyte myocardial infarction immediately before cineangiography and coronary arteriography were performed. There were 24 anterior wall infarctions and 15 inferior wall infarctions. Two chamber apical cross sections were compared with 30°–RAO cineangiographic projections in a quantitative manner. The control group consisted of 32 normal persons.

Borrowed from cineangiography, the following quantitative method was applied. It was presumed that the two-dimensional cross sections used were comparable to the cineangiographic views: the inner boundaries of the left ventricle were traced with a light pen system in endsystole and enddiastole and were transferred to a videometry unit with digital computer and corresponding computer periphery.
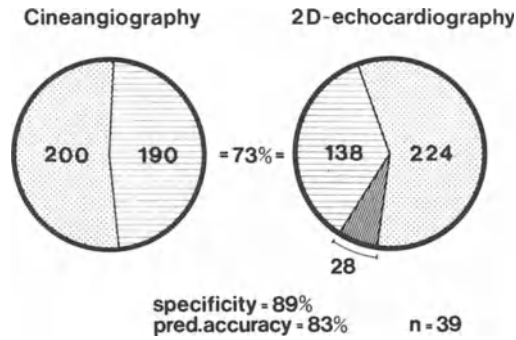
174

Figure 1. Correlation between echocardiographically and cineangiographically detected wall motion abnormalities in 390 area segments of the left ventricle from 39 patients with acute myocardial infarction.
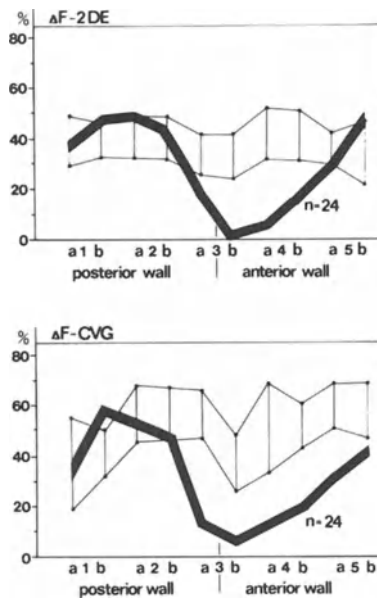

Figure 2. Plots of regional contraction in area segments ($\triangle$ F%) for the 24 patients with anterior wall infarction. Correlation between two-dimensional echocardiography (above) and cineventriculography (below). The normal contraction range is represented by the tolerance limits (lower limits) and the mean values (upper limits) and was established in 32 persons.
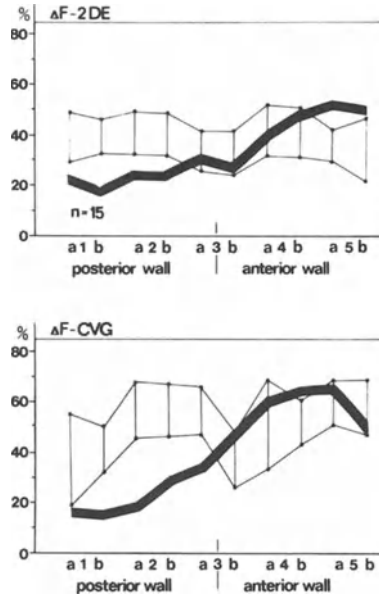
Figure 3. Regional contraction abnormality in 15 patients with inferior wall infarction. Schematic representation similar to Figure 2.
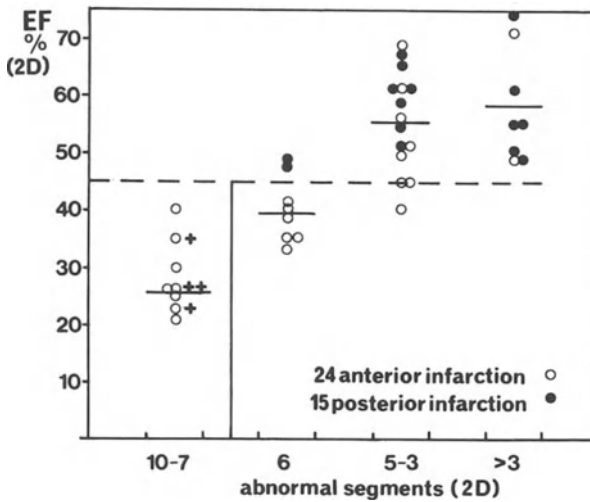

Figure 4. Regional and global left ventricular function in 39 patients with acute myocardial infarction. A high risk group with severe contraction abnormalities and reduced ejection fraction can be identified with echocardiography. In this high risk group 4 patients died during early hospitalization.

Volumes were calculated according to the Simpson's rule.

Regional contraction was quantified as follows: the center of gravity of the endsystolic outline was derived by the computer. 12 radials from this center intersected the systolic and diastolic perimeters each forming an angle of 30°. Two basal segments near the valvular region were excluded from analysis. A systolic fractional area change was measured for each of the ten remaining area segments. In order to differentiate between normal and disturbed wall motion, tolerance limits were established with 32 normals.

Figure 1 is a schematic representation of the total results obtained with 39 patients. Starting from 390 segments, 190 segments were abnormal with cineangiography and 164 segments proved to be abnormal with two-dimensional echocardiography. 28 segments were false positive with the latter method. Thus the total sensitivity was 73%, whereas the specificity was 89% and the predictive accuracy was 83%.

Plots of regional contraction for the 24 patients with anterior wall infarction versus those of 32 control persons are depicted in Figure 2. On the left hand side can be seen the echocardiographic data and on the right hand side the cineangiographic data. The lower border of the field of normal range, represented by the limit of tolerance, is more pronounced with cineangiography than with two-dimension echocardiography. Concerning the cross sectional echocardiographic detection of anterior wall motion abnormalities, the sensitivity was 80% (the exact correspondence in each subsegment), whereas the specificity was 87%.

In contrast, the mean changes in fractional area change of the 15 patients with inferior wall infarction are summarized in Figure 3. The sensitivity of two-dimensional echocardiography for the detection of inferior wall motion abnormalities was 67% with a specificity of 85%. There are of course some discrepancies between the echocardiographic and cineangiographic method, which first of all are due to the fact that the apical view does not cover all of the ventricular wall seen with cineangiographic right anterior oblique projection [7].

Nevertheless, in our hands this method proved to be very informative in respect to the localization of the infarction and in respect to the prognosis and outcome of the patients. Two-dimensional echocardiographic ejection fraction was plotted against the amount of pathological segments determined with two-dimensional echocardiography in each patient. From global and regional function a subgroup of patients could be identified, having bad ejection fraction and large zones of contraction abnormality. In this high risk group 4 patients died of pump failure during the early stage of infarction (Figure 4).

3. ASSESSMENT OF THERAPEUTIC INTERVENTIONS

Two-dimensional echocardiography seemed also to be a reliable means to assess the effect of therapeutic interventions in sequential studies, where each subject served
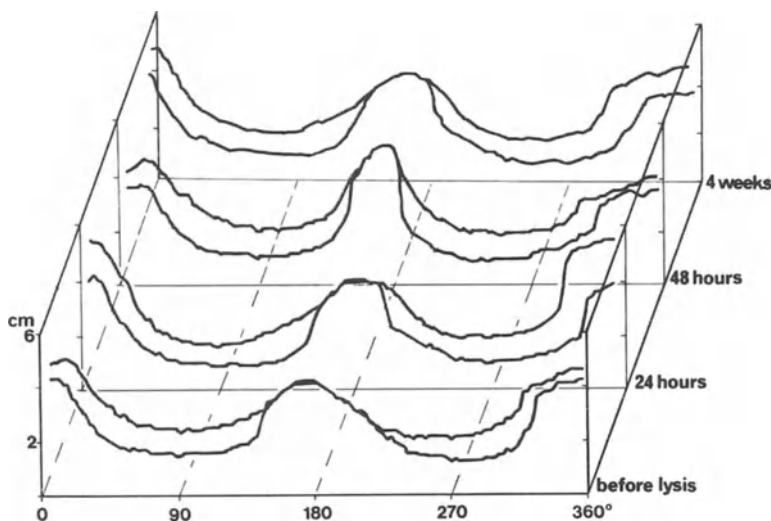
Figure 5. Radial plots of the endsystolic and enddiastolic left ventricular contour, i.e. the percentage radial shortening of the systolic and diastolic perimeters against the radial angle 0–360°. Demonstration of a large akinetic zone during the acute stage of infarction, which begins to improve on the first day after streptokinasis therapy.

as his own control. Such a study was performed in acute myocardial infarction to determine whether the extent of regional motion abnormality may be influenced by early successful intracoronary thrombolytic recanalization of the occluded vessel.

42 patients aged 41 to 74 years fulfilled the criteria for early intracoronary streptokinase therapy as well as the criteria for repeated registration of technically adequate two-dimensional echocardiograms. Global and regional left ventricular function were investigated immediately before the intracoronary application of steptokinasis, on the first, second and third day after infarction and during the third to fourth week.

Figure 5 demonstrates the changes of wall motion disturbance during the course of an anterior wall infarction with early successful recanalization of the infarcted vessel. In this case the time interval between the beginning of symptoms and the success of thrombolysis was exactly 180 min. During the acute stage of infarction a larger akinetic zone of the anterior and apical wall is visible, which – in this case – shows a distinct improvement in contraction on the first day of acute myocardial infarction and which remains quite stable during the follow up period.

After complete analysis of all echocardiographic registrations in all patients the collective was further subdivided into two groups. *Group A* consisted of 16 patients in which early recanalization of the infarcted vessel was obtained within 4 hours of the beginning of symptoms. The mean time interval was 180 ± 32 min. *Group B* consisted of 26 patients, in which thrombolysis was successful only later than 4 hours, the mean interval being 315 ± 56 min or in which the intervention with
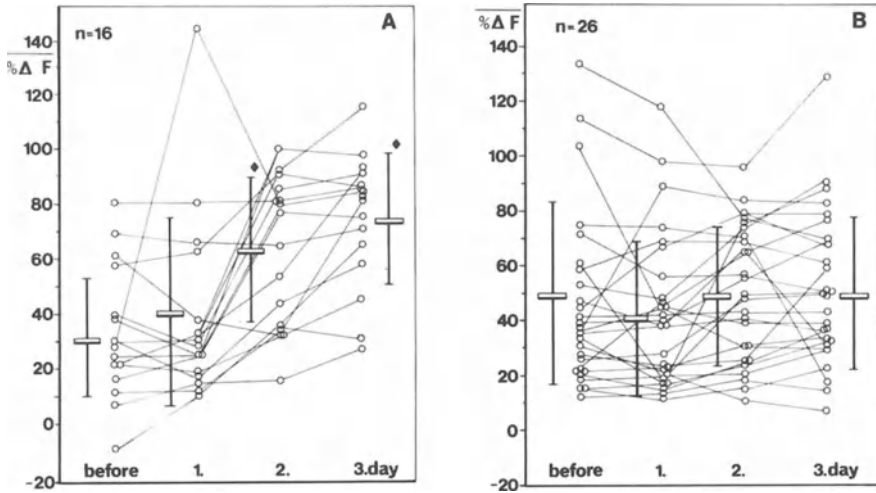
Figure 6. Changes of wall motion abnormality during the first three days of myocardial infarction. Only in group A, with short time interval between the beginning of symptoms and recanalization, is there a significant improvement in wall motion relative to the control value.

streptokinasis remained ineffective; this was the case in 6 patients. The fractional area changes of those segments, which proved to be pathological during the investigation in comparison to tolerance limits, were summed up for each follow up period and for each patient.

The changes of wall motion abnormality during the first three days of myocardial infarction are depicted in Figure 6. In *group B* the sum of regional fractional areas being pathological during the follow up study was 49% before therapy and did not show any significant alteration during the first three days. In *group A*, in contrast, with a short time interval between the beginning of symptoms and recanalization, there was a significant improvement in wall motion relative to the control value. The sum of the fractional areas being 33% at the beginning showed further improvement up to 75% at the third day of investigation.

During the late follow up period (i.e. during the 3rd to 4th week after acute myocardial infarction) in the 26 patients of group B there was again no significant alteration despite intensive variation of individual values. In contrast, in the 16 patients of group A, an additional small but significant increase in wall motion could be measured.

According to this significant change in regional function, which was only observed in group A, only in this group of 16 patients could a slight change in global function be observed. The ejection fraction significantly increased from 47 ± 8% to 54 ± 8%. The global left ventricular function in group B, with a worse control value of 43% ± 10%, did not show any significant change during the follow-up period (EF: 44 ± 10% after 4 weeks).

4. SUMMARY AND COMMENT

Our data demonstrate that two-dimensional echocardiography has a fair sensitivity and specificity to localize and quantify wall motion abnormalities. An underestimation of the angiographically measured wall disturbance is due to the tangential cut of the heart from apical cross sectional views. In combination with the echocardiographically determined global function, the method has further the capability to predict the early prognosis of patients with acute myocardial infarction.

During therapeutic intervention with streptokinasis a significant improvement in regional and global function of those patients undergoing very early reperfusion could be observed. These latter findings share some limitation, of course, because no direct estimation of myocardial vitality is possible from quantitation of regional left ventricular function alone. Segmental wall motion abnormalities can be associated with both myocardial ischemia and infarction [8, 9].

REFERENCES

1. Weiss JL, Bulkley BH, Hutchins GM, Mason SG: Two-dimensional echocardiographic recognition of myocardial injury in man: comparison with postmortem studies. Circulation 63:401, 1981.
2. Schweizer P, Erbel R, Merx W, Krebs W, Erckelenz F v, Lambertz H, Effert S: Wall motion abnormalities in acute myocardial infarction. Correlation between two-dimensional echocardiography and cineangiography. Europ Heart J (Suppl) 2:108, 1981.
3. Eaton LW, Weiss JL, Bulkley BH, Garrison JB, Weisfeldt ML: Regional cardiac dilatation after acute myocardial infarction. Recognition by two-dimensional echocardiography. New Engl J Med 300:57, 1979.
4. Meltzer RS, Woythaler CN, Buda AJ, Griffin GC, Harrison WD, Martin RP, Harrison DC, Popp RL: Two-dimensional echocardiographic quantification of acute, isolated myocardial infarction by two-dimensional echocardiography. Am J Cardiol 47:1020, 1981.
5. Visser CA, Kan G, Lie KI, Becker AE, Durrer D: Apex two-dimensional echocardiography. Alternative approach to quantification of acute myocardial infarction. Br Heart J 47:461, 1982.
6. Wyatt HL, Meerbaum S, Heng MK, Rit J, Gueret P, Corday E: Experimental evaluation of the extent of myocardial infarction. Recognition by two-dimensional echocardiography. Circulation 63:597, 1981.
7. Erbel R, Schweizer P, meyer J, Grenner H, Krebs W, Effert S: Left ventricular volume and ejection fraction determination by cross sectional echocardiography in patients with coronary artery disease. Clin Cardiol 3:377, 1980.
8. Rentrop P, Blanke H, Karsch KR, Rutsch W, Schartl M, Merx W, Dörr R, Mathey D, Kuch K: Changes in left ventricular function after intracoronary streptokinase infusion in clinically evolving myocardial infarction. Am Heart J 102:1188, 1981.
9. Falsetti HJ, Marcus ML, Kerber RE, Skorton DJ: Quantification of myocardial ischemia and infarction by left ventricular imaging. Circulation 63:747, 1981.

20. DETECTION AND QUANTIFICATION OF ACUTE MYOCARDIAL INFARCTION BY MYOCARDIAL SCINTIGRAPHY

P. PROBST, O. PACHINGER, H. SOCHOR AND E. OGRIS

INTRODUCTION

Detection and quantification of acute myocardial infarction were some of the most important goals in cardiology in recent years, since, in both acute and old myocardial infarction, morbidity and mortality are related to the extent of myocardial damage [1, 2, 3]. Furthermore, this has become particularly important because of new attempts for the treatment of acute infarction in the early stage [4]. In order to evaluate the success of therapeutic interventions it is necessary to get an estimate of infarct size as soon as possible. An ideal method should differentiate between normal myocardium, jeopardized tissue (which means myocardium that basically might be saved by interventions) and necrotic irreversibly damaged muscle. This has been shown experimentally by special staining methods in vitro, but so far not in vivo [5].

Apart from ECG, various methods for estimation of infarct size are currently used: (1) depletion of myocardial creatine and creatine-MB (CK) depletion, (2) assessment of regional ventricular function by echocardiography and isotope studies of ventricular function and (3) radionuclide methods delineating normally perfused myocardium or necrotic tissue. Since these radionuclide techniques are noninvasive and can be used rather easily in the intensive care setting, this paper will deal with radioisotope methods for the assessment of myocardial infarction [6, 7, 8, 9, 10, 11].

RADIONUCLIDES IN USE

Two major approaches are currently used to delineate normal and/or damaged myocardium. "Cold spot scanning" techniques will define abnormal areas by a defect in the normal distribution of an agent taken up by normally perfused and viable myocardium. Of all substances – mainly potassium analogs – thallium 201 has turned out to be the isotope of choice for this approach, mainly due to its good correlation with myocardial blood flow and to the inverse relationship of Tl–201 uptake [12]. Demonstration of lesions in a positive contrast technique theoretically yields advantages due to possible higher target-to-non-target ratios for detecting infarcted areas as "hot-spots". Almost all infarct avid tracers have been Tc–99m

Table 1

"Hot spot" scanning	Infarct scanning (use of infarct avid radiopharmaceuticals)
(1) Hg-203 labelled	Chlormerodrin fluorescin
(2) Tc-99^m labelled sulfhydril containing	
substances	DMA (dimercaptosuccinic acid)
	Penicillamin
	Thioglycerol
Other substances	
	Tetracyclin
	Glucoheptonate
	DTPA (diethyltriaminepentaacetat)
	POP (polyphosphate)
	PYP (pyrophosphate)
	MDP (methylendiphosphonate)
(3) I-131 labelled AB to	Myosin
	Myoglobin
	Mitochondria
(4) Ga-67 citrate Ln-111 leucocytes	Substances labelling inflammatory infiltrat

labelled but unfortunately the mostly used Tc–99m pyrophosphate is also taken up by bone and this reduces the signal to noise relation. In a given infarct a cold lesion detected by non-uptake of Tl–201 is usually also well defined by a substantial increase of Tc–99m pyrophosphate in the same area. The superposition of these 2 scintigrams should add up to a complete scan of the myocardium [13, 14, 15, 16, 17].

Tables 1 and 2 depict a listing of substances which have been used, which are still in use and which are under investigation for hot spot or cold spot scanning. Out of

Table 2

| "Cold spot" scanning	Myocardial scintigraphy
(1) K-43, Cs-129, Rb-81, Tl-201	Potassium analogs
(2) I-123 labelled FA	HDA (heptadecanoic acid)
PPA (phenylpentadecanoic) acid)	
(3) C-11, F-18, N-13, O-15, Ga-68	Radiopharmaceuticals labelled with
	positron emitters
	C-11 Palmitate
	C-11 Carbonmonoxyde
	F-18 Dog (desoxyglucose)
	N-13 Ammonia
(4) Tc-99^m, In-113, Cr-51, I-131	Labelled particles
(5) Tc-99^m labelled substances	DMPE (dimethylphosphinoethane)
	BMTA (betamethylomegaphenyl-tetradecanoicacid)
(6) Te-123^m labelled substances	TeHDA (tellurheptadecanoic acid)

Table 3. Comparison of Tl-201 and PYP for scanning of acute myocardial infarction

	Tl-201	Tc-99^m PYP
Mechanism of accumulation	Perfusion Na/K ATPase	Uptake in damaged myocardium
Contrast pattern	Negative	Positive
Highest sensitivity	6^h	24–48^h
Decr. sensitivity	24^h	6^d
False negative	Small infarcts NTM infarcts RV-INF.	Small infarcts (<3g) NTM infarcts No residual flow
False positive	Unstable AP Previous MI Ischemia	Unstable AP Persistent after previous MI Any calcification Aneurysm Cardioversion

the many substances which have been used for hot spot scanning, only the pyrophosphate are routinely in clinical use [12, 18]. But there are promising developments, as with labelled antimyosin, labelled antibodies or myoglobin [19]. There are also some advances in labelling inflammatory infiltrates. Up to now only animal experiments have been performed with these new substances. Out of the isotopes which are used for cold spot scanning, clinical practice has focused on thallium-201 [20]. This isotope has a low gamma energy which leads to a low radiation exposure of the patient and has a half life long enough to allow commercial distribution and repeated examination. It accumulates in the normal myocardium related to myocardial blood flow; analogs of free fatty acids labelled with single photon emitters (I-123 HDA) deliver a different kind of information. Lacking the facilities of positron imaging these fatty acid analogs can be considered the "poor man's" metabolic imaging [21]. Although some promising work has been presented more recently, showing a possible use of these isotopes for better definition of the functional status of the myocardium in acute and chronic ischemia by giving information about the relation of perfusion and metabolic demands, these techniques are not currently used as a standard diagnostic approach on a routine basis

Table 4. Tl-201 in acute myocardial infarction

Advantages	Disadvantages
Highly sensitive (<6^h)	Expensive
Localisation	Availability
DD necrosis-ischemia	Quantification in acute stage
In non diagnostic EKG	
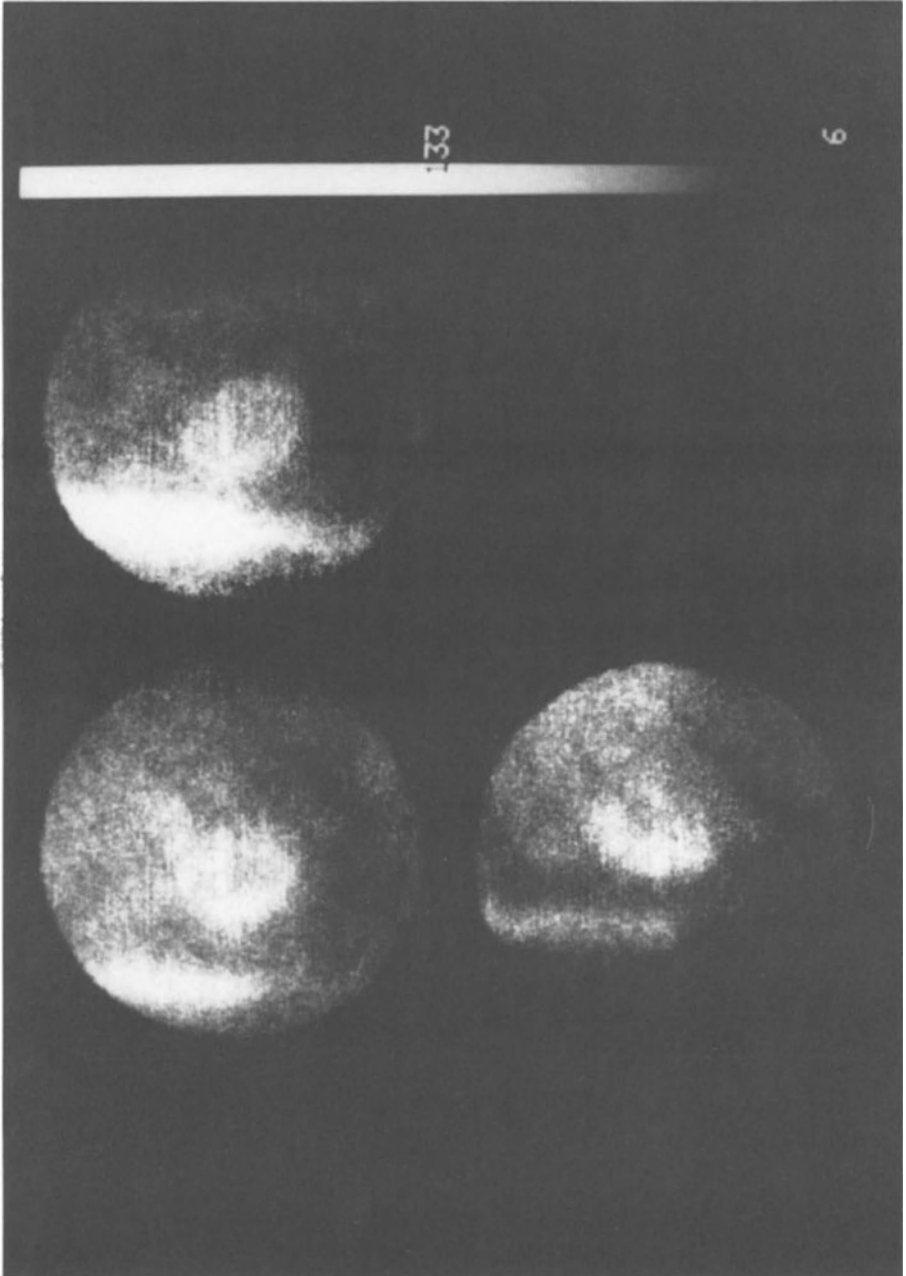
Figure 1. Technetium-99m stannous pyrophosphate scan of a patient with extensive myocardial infarction showing a "doughnut" pattern as a poor prognostic sign.

[22, 23]. The most promising substances – positron emitters – are also listed in the table. Unfortunately these are only available for few centers with a cyclotron nearby and a positron imaging device. This situation is most likely to remain for the near future. Nevertheless (as is also discussed in this book), only positron techniques allow true quantification of perfusion and metabolism at the present time [24, 25]. Substances listed under point 4 are used by intracoronary administration and will not be discussed in this paper. Therefore this review will focus on one representative technique of the hot spot scanning group, Tc–99m–pyrophosphate, and on one of the cold spot methods, imaging with thallium–201 (10, 13, 16, 17, 18, 26).

COMPARISON OF PYROPHOSPHATE IMAGING AND THALLIUM–201

While thallium uptake is mainly dependent on perfusion and the function of the membrane ATP-ase system, pyrophosphates are accumulated in damaged myocardium (Table 3). Therefore thallium–201 shows a negative and pyrophosphate a positive contrast. The sensitivity of thallium 201 is high within the first 6 hours, of pyrophosphate between 24 and 48 hours. Sensitivity for Tl–201 decreases after 24 hours, for pyrophosphate imaging after 6 days [12, 15]. False negative results with thallium–201 can be seen in small infarcts, in non-transmural infarcts and in right ventricular infarction. With pyrophosphate we may get false negative results in small infarcts (less than 3 grams is thought to be a limit), in non-transmural infarction and if there is not enough residual flow to the infarcted area. False positive results with thallium–201 are seen in unstable angina pectoris, previous old myocardial infarction and ischemia. With pyrophosphate false positive results can be obtained also in unstable angina pectoris or after previous myocardial infarction with persistent accumulation. Any calcification can cause an accumulation of pyrophosphate (calcified valves, thrombi, pericarditis). Aneurysms and cardioversion can also give positive pyrophosphate scans.

Figure 1 shows an example of a positive pyrophosphate scan with a large anterior wall myocardial infarction showing a higher accumulation of the radiopharmaceutical at the border of the infarct zone. This "doughnut pattern" is supposed to be a poor prognostic sign. The accumulation of pyrophosphate in the ribs and in the sternum leads to a higher background. Pathophysiologic factors for the concentration of this tracers in damaged myocardium are the presence of some residual flow to the damaged muscle ($10–40\%$ of the control normal values), calcium accumulation in the damaged myocardial cells and the presence of irreversibly injured myocardial cells [11, 12, 15].

Advantages of Thallium–201 are its high sensitivity in the first 6 hours from the beginning of symptoms. An exact localisation, especially in non-diagnostic ECG, can be obtained and by sequential imaging differential diagnosis of necrosis and ischemia is possible. The former disadvantage resulting from the fact that thal-

Table 5. Tc 99^m PYP in acute myocardial infarction

Advantages	Disadvantages
Cheap	Long time interval
Easy to obtain	Background
Highly sensitive	Poor quantification
RV-infarction	Poor specificity

lium–201 is a cyclotron product and therefore still expensive has been improved by a rather wide spread distribution net. The main limitations however are due to its biological behavior. Although thallium–201 uptake is mainly determined by myocardial blood flow, cellular extraction and the status of the cell membrane can alter the amount of uptake independent of flow. Furthermore, in hyperemia thallium–201 uptake underestimates blood flow and overestimates flow and very low ranges. For a wide flow range it offers a good relationship with blood flow and is still the imaging agent of choice for delineating myocardial perfusion abnormalities. Sensitivity in acute myocardial infarction has been reported by Wackers et al [14] to be 100% within the first 6 hours, 76% within 24 hours and 73% after 48 hours. Ritchie et al have shown sensitivities of 85% within the first 7 days and of 70% after that time period [27]. The same authors have shown a sensitivity of 95% in anterior wall myocardial infarction and 73% in inferior myocardial infarction. Specificity for the detection of acute myocardial infarction, however, is low since not only necrosis shows a defect but also persisting ischemia and old scars. In addition it was shown that there is a decrease of defect size within the first few hours of acute infarction due to reduction of ischemia of the border zone. Therefore there is a decrease of defect size without on actual decrease of infarct zie [14, 28].

The advantages of pyrophosphate are that it is cheap, easy to obtain and that it is highly sensitive. It has also the property to visualize right ventricular infarction. One of the main disadvantages is the long time interval after infarction until the scan becomes positive. This precludes its use for the estimation of infarct size

Table 6. Indications for myocardial imaging in acute myocardial infarction

Suspected MI
    EKG non diagnostic
    Enzymes non diagnostic

Localisation
DD unstable angina – AMI
Prognosis: Tl 201: Defect size
                Intact Myocardium
          Tc 99^m PYP: Doughnut pattern
                Persist. pos.

Table 7. Imaging procedures and imaging devices

(1) Planar imaging   (Scintillation Camera)
(2) Tomographic imaging
    2.1.   Limited angle tomography
        7-pinhole collimator rotating slant-hole collimator
    2.2.   Transaxial tomographic approaches
        SPECT (single photon emission computerized tomography)
        PCT (positron computerized tomography)

reduction due to any intervention [29]. Some data are available reporting on early post-interventional uptake in damaged myocardium after intracoronary application after intracoronary selective thrombolysis [4, 30]. Other disadvantages of the tracer are the high background, the poor quantification possibilities and the rather low specificity [12, 26].

INDICATIONS FOR INFARCT SCINTIGRAPHY

Retrospective analysis of main reasons for imaging in acute infarction in the coronary care unit revealed that the main indication was infarct diagnosis and infarct size estimation. In addition patients with non-interpretable ECG, suspected myocardial infarction (positive enzymes, negative ECG) were studied. Also, for differential diagnosis of ischemia versus infarcted tissue and unstable angina pectoris versus myocardial infarction, these isotopes techniques were applied. Therefore the following indications for infarct scanning have been accepted: (1) Suspected myocardial infarction if the ECG is non-diagnostic or the enzymes are not diagnostic. (2) Unclear localization. (3) Differential diagnosis of unstable angina pectoris in acute myocardial infarction using sequential scanning. (4) Infarct size estimation as a prognostic indicator.

As Perez-Gonzales et al [31] have shown more recently that scintigraphic infarct size, determined both by Tc–99m pyrophosphate and Tl–201, could successfully separate a higher risk group of patients from the ones with better prognosis. Early scintigraphic parameters appeared more accurate than any other laboratory indicator for determining late prognosis. Perfusion abnormalities $>35\%$ of the ven-
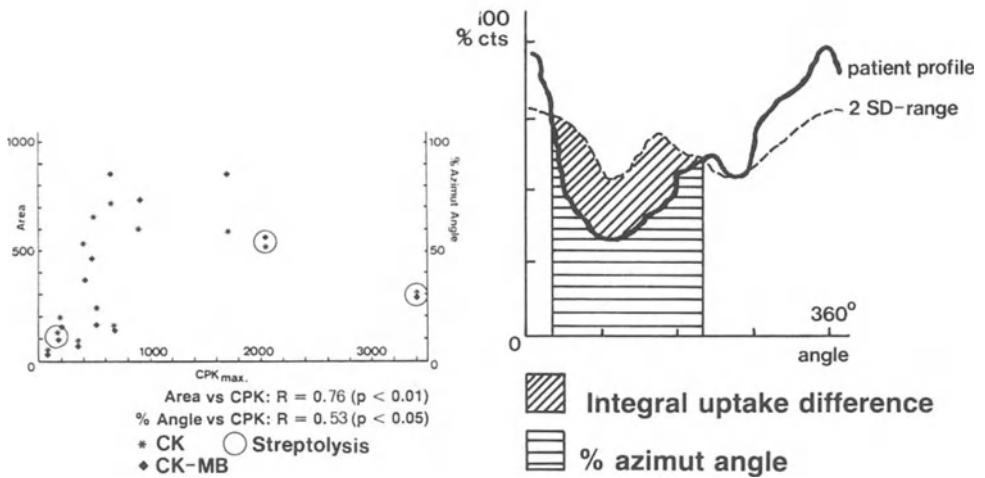
Table 8. Sensitivity of Tl-201: planar imaging vs. 7-pinhole tomography

	Planar qualitative	Planar quantitative	Tomo qualitative	Tomo quantitative
Pat. with previous MI (N = 26)	88%	92%	92%	96%
Pat. with previous MI and additional reversible ischemia (N = 46)	72%	76%	87%	91%

Defect size definition in 7-PH tomography

Area vs CPK: R = 0.76 (p < 0.01)
% Angle vs CPK: R = 0.53 (p < 0.05)
* CK ○ Streptolysis
◆ CK-MB

Integral uptake difference
% azimut angle

Figure 2. Infarct size estimation by seven-pinhole Tl–201 scintigraphy. Right panel: defect size estimation by circumferential profile analysis between intersection points of individual patient profile with lower limit of the 2 SD range of the normal population. Defect size is expressed as % circumferential angle and as integral uptake area. Left panel: Correlation of enzymatic parameters (CK, CK-MB) with scintigraphically determined infarct size. A significant correlation was found. Patients indicated as streptolysis-patients were not taken for regression analysis.

tricular area were significantly more often accompanied by non-survival [32, 33, 34, 35].

IMAGING PROCEDURES AND IMAGING DEVICES

Table 7 shows several methods currently in use for myocardial imaging. Concerning quantification of infarct size there was a great hope that tomographic approaches would lead to a significant improvement [36]. The advantages of lower background, higher contrast, improved semiquantitative analysis and improved localization capabilities can be applied for infarct imaging. In a comparative study of planar imaging and 7-pinhole imaging in our institution a slightly increased sensitivity for detection of myocardial infarction was found (Table 8). For the diagnosis, "infarct" tomographic techniques by 7-pinhole tomography could not significantly increase sensitivity. In 30% of the patients, however, additional information concerning size or localization of the infarct was obtained. When comparing the peak CPK in acute infarction with scintigraphically determined thallium–201 defect size by 7-pinhole tomography using a circumferential profile approach [37, 38, 39], a
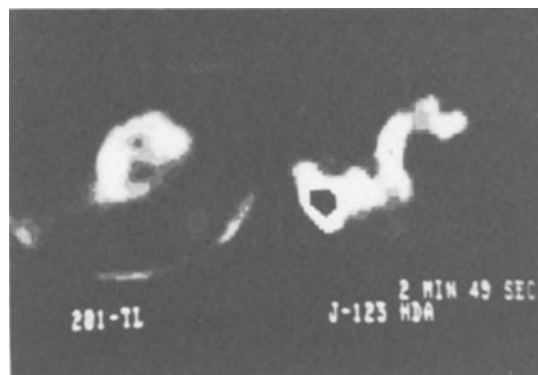
Figure 3. 201–Tl Scan and 123 I-fatty acid extraction image in a patient with successful lysis of an occlusion of the right coronary artery. The 201 Tl defect size appears smaller than the disturbed metabolic activity.

significant correlation of $r = 0.76$ was found. Defect size was expressed as percent angle of total circumference and as integrated uptake area of the individual patient's profile under the normal distribution (Figure 2). Several authors have shown that this quantitative technique was able to demonstrate significant differences in Tl–201 defect size before and after streptolysis, and in comparison with patients with unsuccessful or unattempted lysis in acute myocardial infarction [23]. A quantification in absolute terms, however, is still not possible [40, 41].

These findings are in good concordance with more recently published data of Tamaki et al [42], obtaining tomographic data from a transaxial tomographic technique using a rotating gamma-camera, showing also significant correlations of CK-MB depletion and scintigraphically defined infarct volume being superior over planar determination infarct size ($r = 0.89$ for tomography, $r = 0.73$ for planar imaging). Nevertheless, there are significant problems in attempts for quantification: difficulties in reconstructing three-dimensional infarcts from planar scans, poor resolution (more than 3 gram infarcted myocardium necessary) and overlying structures of the thorax.

Defect size is also dependent on the radiopharmaceutical which is used for definition of the "area of risk". When comparing Tl–201 and fatty acids analogs (I-123 HDA) we could see significant differences in defect size in patients who had undergone successful streptokinase therapy with restoration of antegrade coronary flow. The majority of them (70%) had smaller defects in the Tl–201 scan as compared to a much larger metabolic impairment in the fatty acid study. This might be due to a persistent metabolic damage of myocardial tissue as compared to the restored flow demonstrated by the small thallium-perfusion defect [23, 43]. Therefore the choice of the substance will also influence the sizing criterion. However, useful information about the functional status might be detected by these rather new techniques. One of the main problems for tomographic reconstruction is

190

absorbtion, especially when using the low energy isotope Tl–201. Hopefully new isotopes with higher gamma energies will also increase tomographic accuracy [36].

FUTURE ASPECTS

Clinicians would expect from these isotope methods a 3-dimensional representation of infarcted myocardium as soon as possible in the course of infarction [44, 45]. In addition quantification of infarction in terms of gram infarcted tissue would be desirable. There are promising aspects in positron emitting substances. Unfortunately these are confined only to a few centers with cyclotrons nearby and with special instrumentations. Furthermore we could expect the development of new radionuclides with similar behaviour to thallium but labelled with technetium which might lead to better images and may be used with tomography. Development of better algorithms for background and absorption correction in tomography can also be expected. What has been achieved so far is the fact that we already have techniques at hand which delineate jeopardized myocardium in a much more physiologic way than just enzymes or ECG registrations. The prognostic information obtainable from these methods could be usable as guidelines for identification of high-risk subgroups of patients, because data available suggest that these isotope studies might be superior to other methods for prediction of the course of individual patients and could be clinically applied to guide treatment in the individual infarct patient.

REFERENCES

1. Hillis LD, Braunwald E: Myocardial ischemia. N Engl J Med 296:971, 1034, 1093, 1977.
2. Geltman EM, Ehsani AA, Campbell MK, et al: The influence of location and extent of myocardial infarction on long-term ventricular dysrhythmic and mortality. Circulation 60:805, 1979.
3. Sobel BE, Bresnahan GF, Shell WE, et al: Estimation of infarct size in man and its relation to prognosis. Circulation 46:640, 1972.
4. Rentrop P, Blanke H, Karsch K, et al: Selective intracoronary thrombolysis in acute myocardial infarction and unstable angina pectoris. Circulation 63:307, 1981.
5. Fishbein MC, Meerbaum S, Rit J, et al: Early phase acute myocardial infarct size quantification: validation of the triphenyl tetrazolium chloride tissue enzyme staining technique. Am H J 101:593, 1981.
6. Norris RM, Whitlock RML, Barratt-Boyes C, et al: Clinical measurement of myocardial infarct size. Modification of a method for the estimation of total creatine phosphokinase release after myocardial infarction. Circulation 51:614, 1975.
7. Bleifeld W, Mathey D, Hanrath P, et al: Infarct size estimated from serial serum creatine phosphokinase in relation to left ventricular hemodynamics. Circulation 55:303, 1977.
8. Nixon JV, Narahara KA, Smitherman TC, et al: Estimation of myocardial involvement in patients with acute myocardial infarction by two-dimensional echocardiography. Circulation 62:1248, 1980.
9. Rigo P, Murray M, Strauss HW, et al: Left ventricular function in acute myocardial infarction evaluated by gated scintigraphy. Circulation 50:678, 1974.

10. Strauss HW, Harrison K, Langan JK, et al: Thallium 201 for myocardial imaging. Relation of thallium 201 to regional myocardial perfusion. Circulation 51:641, 1975.

11. Parkey JP, Bonte FJ, Meyer SL, et al: A new method for radionuclide imaging of acute myocardial infarction in humans. Circulation 50:540, 1974.

12. Pitt B, Thrall JH: Thallium–201 versus technetium-99m pyrophosphate myocardial imaging in detection and evaluation of patients with acute myocardial infarction. Am J Cardiol 46:1215, 1980.

13. Bailey IK, Griffith LSC, Rouleau J, et al: Thallium–201 myocardial perfusion imaging at rest and during exercise: comparative sensitivity to electrocardiography in coronary artery disease. Circulation 55:79, 1977.

14. Wackers FJT, Sokole EB, Samson G, et al: Value and limitations of thallium–201 scintigraphy in the acute phase of myocardial infarction. N Engl J Med 295:1, 1976.

15. Henning H, Schelbert HR, Rig etti A, et al: Dual myocardial imaging with technetium-99m pyrophosphate and thallium-201 for detecting, localizig and sizing acute myocardial infarction. Am J Cardiol 40:147, 1977.

16. Zaret BL, DiCola VC, Conabedian RK, et al: Dual radionuclide study of myocardial infarction. Relationships between myocardial uptake to potassium-43 technetium-99m stannous pyrophosphate, regional myocardial blood flow and creatine phosphokinase depletion. Circulation 53:422, 1976.

17. Willerson JT, Parkey RW, Stokely EM, et al: Infarct sizing with technetium-99-m stannous pyrophosphate scintigraphy in dogs and man. Relationship between scintigraphy and praecordial mapping estimates of infarct size in patients. Cardiovasc Res 11:291, 1977.

18. Poliner LR, Buja LM, Parkey RW, et al: Clinic-pathologic findings in 52 patients studied by technetium-99m stannous pyrophosphate myocardial scintigraphy. Circulation 59:257, 1979.

19. Khaw BA, Gold HK, Leinbach RC, et al: Early imaging of experimental myocardial infarction by intracoronary administration of I-131 labelled anticardiac myosin (Fab)$_2$ fragments. Circulation 53:1137, 1978.

20. Pohost GM, Zir LM, Moore RH, et al: Differentiation of transient ischemia from infarcted myocardium by serial imaging after a single dose of thallium 201. Circulation 55:294, 1977.

21. Freundlieb Ch, Höck A, Vyshak, et al: Myocardial imaging and metabolic studies with (17-123-I)-Iodoheptadecanoic acid. J Nucl Med 21:1043, 1980.

22. Sobel BE, Weiss ES, Welch MJ, et al: Detection of remote myocardial infarction in patients with positron emission transaxial tomography and intravenous C-11-palmitate. Circulation 55:853, 1977.

23. Pachinger O, Sochor H, Ogris E, et al: Assessment of the functional result of intracoronary streptokinase therapy in acute myocardial infarction by thallium scintigraphy and metabolic studies. J Nucl Med 23:P 4 (Abstr).

24. Geltmann EM, Bielle D, Welch MJ, et al: Characterization of nontransmural myocardial infarction by positron emission tomography. Circulation 65:747, 1982.

25. Schelbert HR, Phelps ME, Hoffman EJ, et al: Regional myocardial perfusion assessed with N-13 labelled ammonia and positron emission computerized axial tomography. Am J Cardiol 43:209, 1979.

26. Sharpe DN, Botvinick EH, Shames DM, et al: The clinical evaluation of acute myocardial infarction size with 99m technetium pyrophosphate scintigraphy. Circulation 57:307, 1978.

27. Ritchie JL, Zaret BL, Strauss HW, et al: Myocardial imaging with thallium 201: A multicenter study in patients with angina pectoris or acute myocardial infarction. Am J Cardiol 42:345, 1978.

28. Niess GS, Logic JR, Russell RO, et al: Usefulness and limitations of thallium-201 myocardial scintigraphy in delineating location and size of prior myocardial infarction. Circulation 59:1010, 1979.

29. Maddahi J, Ganz W, Geft I, et al: Assessment of efficacy of intracoronary thrombolysis in envolving myocardial infarction by thallium-201 scintigraphy. J Nucl Med 23/94, 1982.

30. Schofer J, Stritzke P, Kuck KH, et al: Dual intracoronary myocardial scintigraphy site Tl-201 and

Tc 99m pyrophosphate predicts myocardial salvage immediately after successful intraar. thrombolysis. Circulation 66:II–335, 1982.

31. Perez-Gonzalez J, Botvinick EH, Dunn R, et al: The late prognostic value of acute scintigraphic measurement of myocardial infarction size. Circulation 66:960, 1982.

32. Holman LB, Chisholm RJ, Braunwald EW, et al: The prognostic implications of acute myocardial infarct scintigraphy with 99m Tc pyrophosphate. Circulation 57:320, 1978.

33. Silverman KH, Becker LC, Bulkley BH, et al: Value of early thallium-201 scintigraphy for predicting mortality in patients with acute myocardial infarction. Circulation 61:996, 1980.

34. Olson HG, Lyons KP, Aronow WS, et al: Follow up technetium-99m stannous pyrophosphate myocardial scintigrams after acute myocardial infarction. Circulation 56:181, 1977.

35. Bulkley BH, Silverman K, Weisfeldt ML, et al: Pathologic basis of thallium-201 scintigraphic defects in patients with fatal myocardial injury. Circulation 60:785, 1979.

36. Budinger TF: Physical attributes of single photon tomography. J Nucl Med 21:579, 1980.

37. Vogel RA, Kirch D, LeFree M, et al: A new method of multiplanar emission tomography using a seven pinhole collimator and an anger scintillation camera. J Nucl Med 19:648, 1978.

38. Francisco DA, Collins SM, Go RT, et al: Tomographic thallium-201 myocardial perfusion scintigrams after maximal coronary artery vasodilatation with intravenous dipyridamole – comparison of qualitative and quantitative approaches. Circulation 66:370, 1982.

39. Sochor H, Pachinger O, Ogris E, et al: Imaging performance of thallium 201 pinhole tomography in comparison with planar imaging: value and limitations. In: Höfer R, Bergman H (eds), Radioaktive Isotope in Klinik und Forschung, 15, pp 493, Verlag H. Egermann, Vienna, 1982.

40. Ritchie JL, Williams DL, Caldwell JH, et al: Seven pinhole emission tomography with thallium 201 in patients with prior myocardial infarction. J Nucl Med 22:107, 1981.

41. Morrison J, Coromilas J, Munsey D, et al: Correlation of radionuclide estimates of myocardial infarction size and release of creatine kinase-MB in man. Circulation 62:277, 1980.

42. Tamaki S, Nakajima H, Murakami T, et al: Estimation of infarct size by myocardial emission computed tomography with thallium-201 and its relation to creatine kinase-MB release after myocardial infarction in man. Circulation 66:994, 1982.

43. Simoons ML, Wijns W, Bela Kumaran K, et al: The effect of intracoronary thrombolysis with streptokinase on myocardial thallium distribution left ventricular function assessed by blood pool scintigraphy. Am J Cardiol 49:973, 1982.

44. Keyes JW, Jr, Leonard PF, Brody SL, et al: Myocardial infarction quantification in the dog by single photon emission computed tomography. Circulation 58:227, 1978.

45. Keyes JW, Jr, Brady TJ, Leonard PF, et al: Calculation of viable and infarcted myocardial mass from thallium-201 tomograms. J Nucl Med 22:339, 1981.

21. TRANSMISSION COMPUTED TOMOGRAPHY IN ACUTE MYOCARDIAL INFARCTION

ROBERT HERFKENS, BRUCE BRUNDAGE, PAUL KRAMER, JAMES GOLDSTEIN
AND MARTIN LIPTON*

INTRODUCTION

The attenuation of roentgen radiation by different tissues is the basis for images recorded on film as well as those obtained during fluoroscopy. Computed tomography involves the reconstruction by computer of attenuation profiles. The theory underlying this concept was developed and applied by Godfrey N. Hounsfield and Alan M. Cormack; for this research they received the 1979 Nobel Prize [1, 2]. Their work resulted in the first available commercial CT head scanner in 1972 in England [3]. The impact of this development in neuroradiology was dramatic and is well-documented – invasive neuroradiographic procedures have subsequently decreased by over 40%. There is an even greater need for reconstruction of the anatomy of the heart throughout the cardiac cycle in health and disease. Compared with stationary organs like the brain, imaging of the heart presents a far greater challenge. The use of CT for diagnosing heart disease is still in its infancy. Nevertheless, clinically useful cardiac applications have already emerged and new developments are progressing rapidly. It is the purpose of this chapter to outline the present clinical status of cardiac CT for diagnosing acute myocardial infarction and to discuss the advantages and limitations of this modality.

ISCHEMIC HEART DISEASE

Ischemic heart disease, also known as coronary artery disease, is the prime killer of men over the age of 35 and of all adults over the age of 40 in the United States. More than one million people die annually in this country from heart disease, some 55% of all deaths. Each year 1.2 million Americans sustain their first heart attack and despite our best efforts, at least one third die within a month. Only 50% are unable

to return to their previous employment and require disability support. Thus, coronary artery disease, by virtue of its incidence and nature, is perhaps the most urgent medial problem of our time [4]. It is the primary reason for patients seeking advice from their physicians, the largest single cause of days spent in the hospital, and the principal diagnosis on most hospital discharge sheets. The total direct cost of heart disease is approximately 12 billion dollars each year. The indirect costs in terms of lost productivity, family hardships, etc., are incalculably higher. A major portion of the 12 billion dollar outlay is spent on the various diagnostic techniques currently used.

The above statistics tend to indicate the relative inadequacy of presently available diagnostic methods to detect heart disease until it has progressed to a late stage. More than 100 million electrocardiograms are performed annually, but a heart attach is often the first confirmation of advanced disease. The sequence of events leading to heart attack is usually gradual, occurring over a number of years. Thus, there should be ample opportunity for early diagnosis with a sufficiently sensitive diagnostic procedure. The established modalities of echocardiography and isotope imaging contribute greatly to the routine management of ischemic heart disease, but they seldom provide all the necessary diagnostic information required for adequate patient management, and like aniography, these methods have fundamental limitations of their own. Despite remarkable advances in the development of these noninvasive imaging techniques, the diagnostic gold standard remains traditional cardiac catheterization with haemodynamic recording and angiocardiography. Invasive procedures, however, are not ideal because they are costly, require patient hospitalization and carry the risk of complications and are not warranted routinely following acute infarction. These disadvantages preclude their use for widespread patient screening. Angiocardiography is also limited for more fundamental reasons. It is not three-dimensional and is primarily an anatomic study which cannot directly quantitate regional myocardial perfusion. It cannot measure myocardial wall thickening, nor can it identify left ventricular mass with any degree of precision. The prospect, therefore, of developing a noninvasive imaging modality capable of obtaining all the required diagnostic information – preferably during one diagnostic examination – is an extremely desirable goal. It was this philosophy which excited the interest of our group and was the motivation to explore and develop computed transmission tomography (CT) for cardiac diagnosis.

COMPUTED TRANSMISSION TOMOGRAPHY

The physician is presented with a cross-sectional digital image which is stored in the scanner's computer, and provides the opportunity for image manipulation, analysis and direct quantitation. CT also has considerably greater density resolution of 0.5–1.0% compared with 5–10% obtained with conventional x-ray film/screen systems. The spatial resolution of CT is notably superior to nuclear medicine

imaging and, unlike echocardiography, CT scanning is not restricted or impeded by air in the lungs or by the rib cage. All present commercial CT scanners were designed only for the head and body where motion artifacts are limited to patient movement and peristalsis, hence relatively long exposure times are acceptable. Cardiac imaging has special requirements because not only must cardiac structure be demonstrated, but also cardiac motion requires evaluation.

The scanner used for cardiac studies at UCSF is a General Electric CT/T 7800 series rotary fan beam whole body scanner, modified to provide a 2.4 second exposure for a 360° angle of reconstruction. This instrument also has the capability to perform 525° overscans from which either 2 360° or 3 180° (plus fan angle) reconstructed images with some overlap are possible. A delay of approximately one second occurs before the next rotation is performed in the opposite direction. Tomographic sections of 1 cm thickness are usually selected. This scanner has been described in detail elsewhere [5]. Scanners with similar exposure times designed by other companies are also now being evaluated in several other centers. CT provides excellent images for structural diagnostic interpretation and has the added advantage of cross-sectional tomography. However, only recently has attention been focused on a second major capability of CT scanning: its ability to provide quantitative and numerical assessment of various aspects of normal and diseased processes in the body. This ability is fundamental to an instrument that acquires precise digital data of the attenuation properties of tissues within a three-dimensional distribution of very small volume elements (the CT image). Since the precise geometrical location of each picture element (pixel) is known, CT can be used to accurately measure sizes of anatomic structures. Furthermore, the value of the attenuation (CT number) within each pixel reflects the tissue density at that point. Since CT scans can be repeated relatively rapidly in time, dynamic aspects of changes in density and size can be studied. Such quantitative studies have a variety of important clinical applications and can often be used to obtain information not available from any other technique.

ACUTE MYOCARDIAL INFARCTION

An exciting and potentially one of the most useful prospects for CT imaging of the heart is the recognition and quantification of myocardial infarction by contrast enhancement. Multiple transverse slices at either 0.5 cm or 1 cm intervals from the apex to the base of the heart permits imaging of the entire ventricular myocardium. Infarcted tissue can be delineated with small intravenous boluses (20 ml) or drip infusion of 1.5 ml/kg of contrast medium as an area of lower density than normal myocardium (Figure 1). It may be possible to estimate the area and size of infarction by measuring such contrast deficient areas on each of the CT scans. Differences in infarcted tissue density compared to non-infarcted myocardium have been demonstrated in excised dogs' hearts, presumably because of edema. These early studies

were all limited to postmortem hearts and models [6–12]. The development of improved instruments and more rapid exposure times, together with contrast medium enhancement has made possible cardiac imaging in vivo [13–15].

The region of infarction can be demonstrated in beating dog hearts, first as a zone of decreased myocardial perfusion, and then delayed enhancement may be observed in 15–30 minutes. The perimeter of the infarction is enhanced by a as yet not completely explained delayed uptake of the contrast agent. The center of the infarctionremains relatively contrast free, at which time the contrast medium has usually washed out of adjacent normal myocardium (Figure 1).

CT CORRELATIVE STUDIES IN DOGS

Doherty, et al [15] reported a study comprising 28 mongrel dogs. Myocardial infarcts were produced by coronary ligation via a left thoracotomy in 23 animals and 5 dogs were normal controls. Anterior infarcts were produced in 16 dogs by ligating the proximal left anterior descending coronary artery just distal to the first septal perforator, and posterior infarcts were produced in 7 dogs by ligating the circumflex coronary artery distal to the origin of the first marginal branch. Eight dogs were imaged within 12 hours of infarction. Four of these were scanned at hourly intervals after ligation for 6 hours. The others were first scanned between 24 and 72 hours. Nine were imaged at least twice and three were imaged four times over four months. In the dogs in whom CT and pathologic infarct sizes were compared ($n = 8$), all the infarcts were 24–48 hours old. After the dogs were sacrificed with an overdose of pentobarbital, the hearts were removed and the left ventricle was dissected free from the rest of the heart. It was then sliced in rings 1 cm thick from apex to base. The rings of myocardial tissue were stained with nitroblue tetrazolium, the regions that did not take up the stain were traced on transparent paper and the area was calculated by planimetry. In two cases after the scans had been completed, the dogs were frozen in position used for scanning in order to preserve their anatomic relationships, and were then cut into 1 cm thick transverse slices with a band saw.

The distribution of contrast material at tissue level was also determined from the post-mortem distribution of ^{131}I-labeled contrast medium injected 10 minutes before sacrifice. This was correlated ($n = 4$) with a microsphere determination of blood flow and with measurement of thallium-201 (1.5 mCi 10 minutes before sacrifice) and technetium-99m pyrophosphate uptake (10 mCi 45 minutes before sacrifice).

The ring where the infarct was most prominent on nitroblue tetrazolium staining was further sliced into sections through normal tissue to infarct border and into the infarct center, so that the endocardial layers were separated from the epicardial layers. Samples were placed in 10% buffered formalin solution and counted in a Hewlett-Packard gamma spectrometer. Window settings were selected to corre-
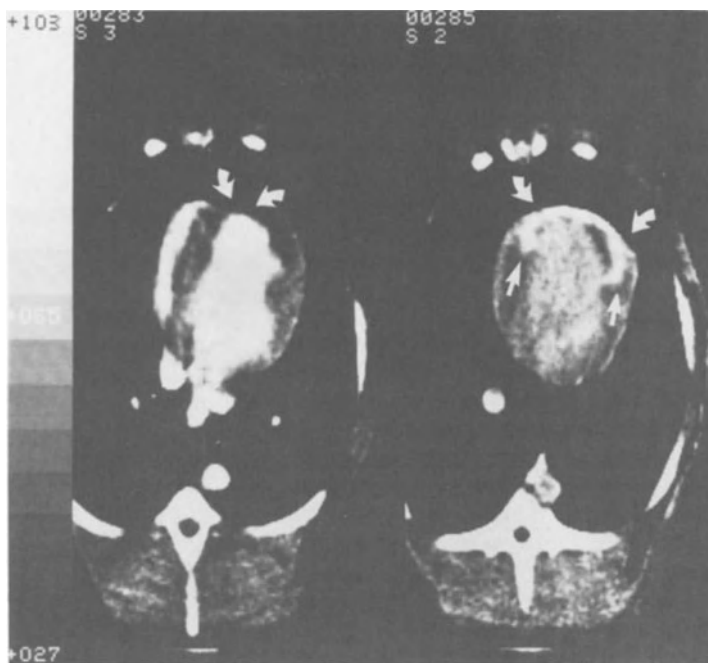
Figure 1. Early and late contrast medium enhancement in an acutely infarcted dog: non-gated recon-structions. This figure shows two 4.8 second 1 cm thick scans following an intravenous bolus of 20 ml of contrast medium at the level of the ventricular cavities in a dog with a heart rate of 114 beats per minute. This animal has a 2 day old anteroseptal myocardial infarction produced by permanent ligation of the left anterior descending coronary artery. The left panel shows contrast enhancement of both ventricles between which is seen the less enhanced ventricular septum, continuous with the free left ventricular myocardial wall. The area which appears to be less well opacified represents the myocardial infarction. The scan on the right was obtained 10 minutes later at the same anatomical level without further contrast medium injection. The area of the infarct is now dramatically profiled by marked contrast medium enhancement relative to surrounding healthy myocardium, which is less enhanced due to normal washout.

spond to the peak energies for each radionuclide, and appropriate correction for scattered radiation and decay were performed. Results were expressed as counts/min per 0.1 g of tissue. After counting, selected samples from the border zone and infarct center were processed in a conventional manner for histology and sections were stained with hematoxylineosin. The presence of infarction was documented by light microcopic examination of the sections.

RESULTS IN DOGS

When dogs with homogenous transmural myocardial infarcts were imaged during and after contrast infusion, three classes of tissue could be distinguished by the
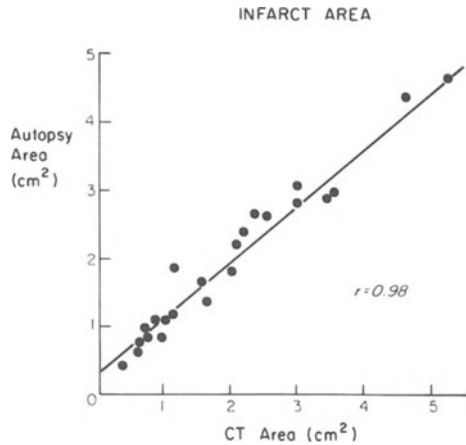
Figure 2. Correlation of the cross-sectional areas of homogenous transmural infarcts determined by computed tomography and pathology. Twenty-three individual slices from eight dogs with infarcts 24–48 hours old are shown. The correlation coefficient $r = 0.98$. Reproduced from Circulation 63:597 (1981), Figure 6.

kinetics of contrast uptake and washout. The normal myocardium opacified at a rate approximately 50% lower than the ventricular cavity. The infarct center showed only slight enhancement compared with the normal myocardium. Surrounding the infarct was a border zone that opacified, during infusion runs, at a rate similar to normal myocardium. However, the washout time constant was approximately six times larger than that of normal myocardium. Figure 2 shows the good correlation that was found on comparison of the area of the unenhanced myocardium determined from the CT image data taken during infusion with that obtained post-mortem ($r = 0.976$, $y = 0.861\ x\ (+\ 0.33)$. The smallest area of infarction in the slices measured 0.35 cm² from a dog whose total infarct weight was 1.3 g. ECG gated scans were also performed in 7 animals with infarction and in 5 normal controls using the method described by Berninger et al [16]. Wall motion abnormalities were detected in all the infarct animals at the site of the infarct and were not seen in the normals. The gated scans, compared qualitatively with the ungated scans, showed better image quality due to the fact that motion artifacts which were prominent in dogs whose noninfarcted myocardium was hyperkinetic, were reduced (Figure 3). Gating did not significantly increase the resolution of the infarct region, presumably because it was almost statis throughout the cardiac cycle. CT gating studies are now also being performed in other centers [17–19].

PATHOLOGY OF DOG INFARCTS

Histologically, the infarct centers consisted of a homogenous population of cells
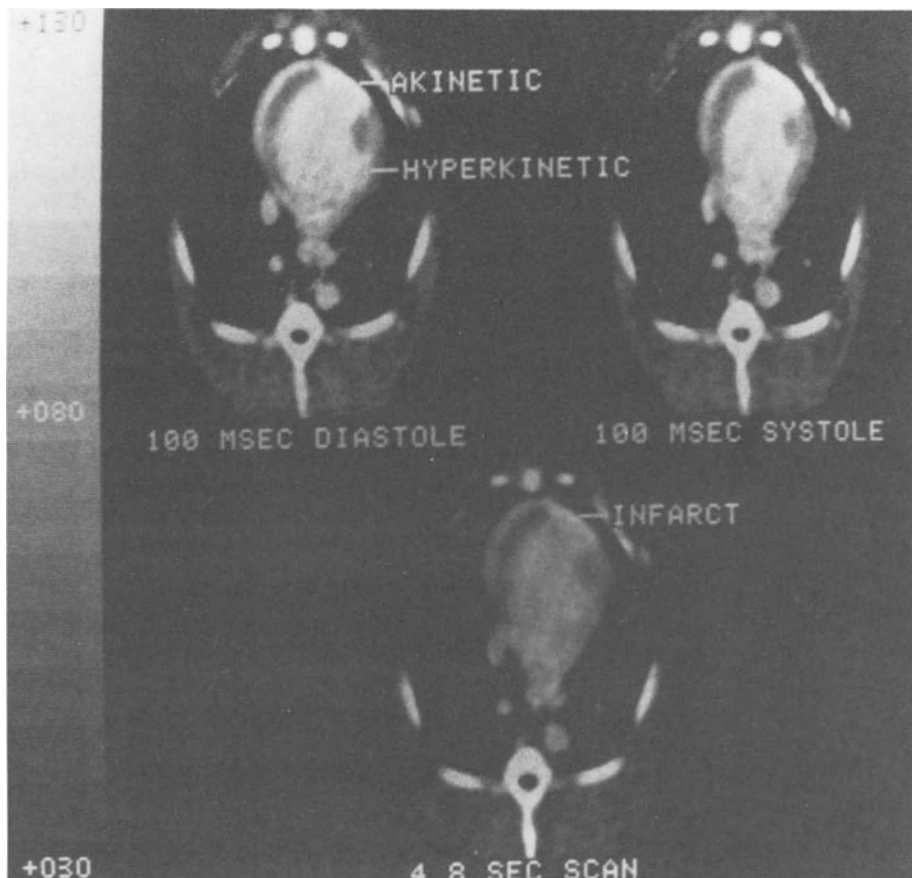
Figure 3. End diastolic and end systolic gated images of an animal with a chronic anterior infarct. A high rate of infusion of contrast medium was used initially to enhance the infarcted area followed by a continuous infusion at a lower rate. The infarcted region is akinetic. The left ventricular wall posterior to the papillary muscle is hyperkinetic. Reproduced from J. Computer Assisted Tomography 32:155, 1979.

that showed poor staining and relaxed myofibrils with hypereosinophilic cyto-plasm, whereas the border zone showed foci of normal cells interlaced with a pleomorphic group of cells. These cells showed a variable degree of myofibril disruption, frequent contraction bands, and some has basophilic cytoplasm. There was a greater degree of neutrophil infiltration in the border than in the center. The highest concentration of ^{131}I-labeled contrast medium and technetium-99m pyro-phosphate occurred in the tissues that histologically contained predominantly border zone tissue, both at the lateral boundaries of the infarct and in the epicardial layers. Compared with normal tissue, the maximum ratios were 6:1 and 25:1 for the ^{131}I and pyrophosphate, respectively. In the endocardial samples where the zone of sharp reduction occurred, the distribution of contrast behave more like thallium
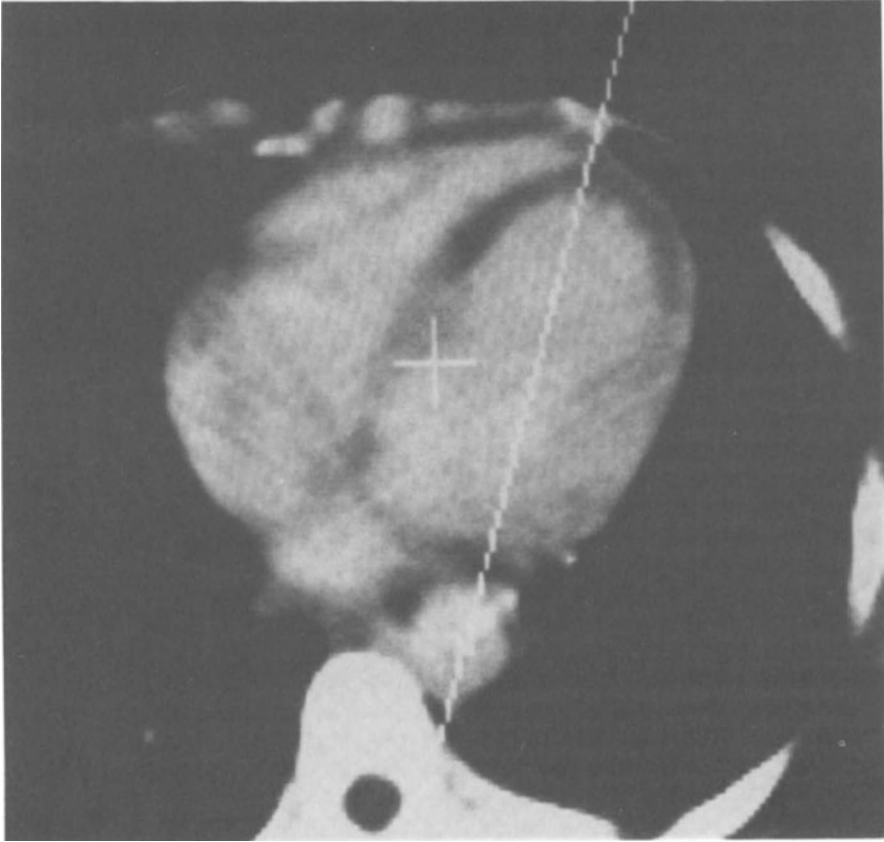
Figure 4(a). A non-gated CT scan from a series taken through the ventricular cavities following an intravenous infusion of 1.5 mg/kg body weight of Conray 400 in a patient with an acute (approximately 3 days old) antero-septal myocardial infarction. The infarcted region is depicted as the dark horseshoe-shaped area of myocardium. Note that the remaining normal myocardium is contrast enhanced and in part forms a border around the infarct zone. The dotted line was selected by the physician so that the CT computer can reconstruct this oblique (almost sagittal) projection, as shown in Figure 4B.

than pyrophosphate, which consistently tended to penetrate deeper into the infarct center. Using excitation analysis to detect the presence of iodine, Higgins et al [20] showed that the maximum ratio between normal and infarcted myocardium was 8:1 and occurred 180 minutes after injection, in agreement with our "in vivo" data.

These investigations have now been extended to human studies. The prognosis of patients sustaining myocardial infarction depends primarily upon left ventricular recovery and function. This is related closely to the extent of ischemic injury. Recent developments and emphasis on interventions aimed at limiting the infarction and associated necrosis are dependent upon techniques capable of identifying and quantitating infarct size. Preliminary results in humans studied at our Institute by contrast enhanced CT durin the past three years show some promise in this direction.
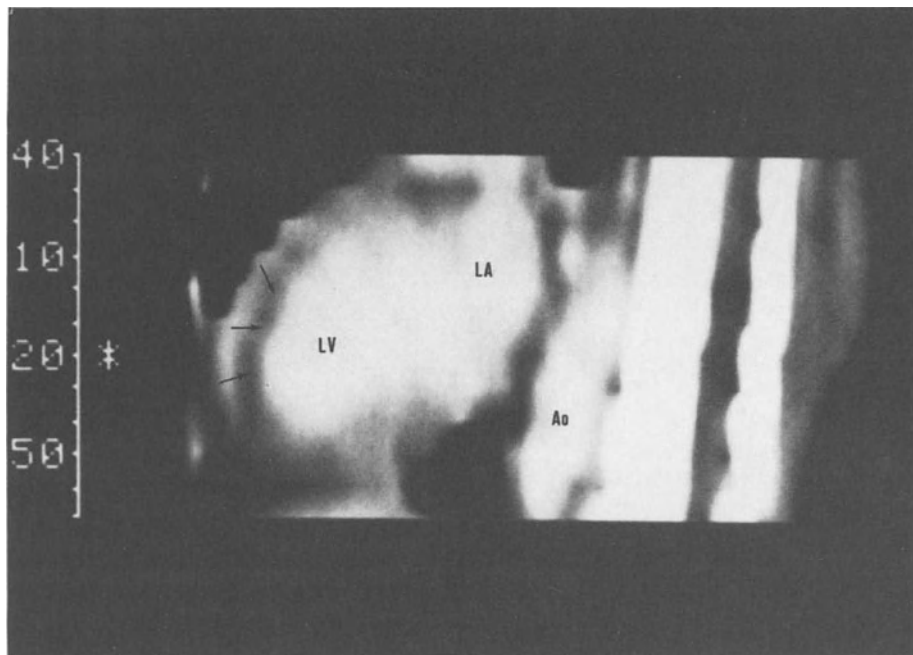
Figure 4(b). Shows a CT computer reconstruction in a steep oblique (almost lateral plane) through the left ventricle and aorta. This plane corresponds to the line depicted in Figure 4(a). The computer selects pixels along this plane from 1 cm thick CT scans obtained at multiple contiguous levels – optimally obtained while the patient holds respiration static. The infarct size in longitudinal extent can be appreciated as the ark, almost black, band (arrows) along the left side of the image with adjacent densely enhanced left ventricular cavity (LV) profiled. The region of the left atrium (LA) is seen further to the right and behind this the descending aorta (AO). → = infarct; LV = left ventricle; Ao = aorta; LA = left aorta.

The diagnosis of acute infarction was based on the classically established methods of history, ECG findings and enzyme criteria in our patient population. Contrast media containing a high concentration of iodine (e.g. Conray 400, or Renografin 76) was infused intravenously in a dose of 1.5 ml/kg during a ten minute period. CT scanning was performed at contiguous 1 cm levels from cardiac apex to base during the end of the infusion. The patients were instructed to suspend respiration during the scans.

The CT appearances of a typical infarct is illustrated in Figure 4(a) and (b). Display options are available for transforming a series of sequential scans into coronal, oblique or, as shown in Figure 4(b), sagittal sections. Delayed enhancement seen routinely in the animal studies was very seldom found in patients. The explanation is uncertain, but many factors, including contrast volume, the administered pharmaco-kinetics of contrast agent, as well as species variation in collateral pathways may be influential. Quantitative CT methods used to measure infarct size are currently being evaluated. The major problem in both static and
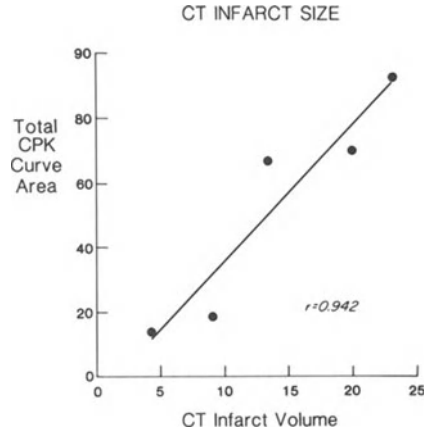
Figure 5. Shows the correlation of infarct volume estimated from CT scan data with the total myocardial enzyme (CPK) curve area. Although only a few points are plotted, the relationship appears very promising. The correlation coefficient $r = 0.94$.

dynamic sizing applications is the method used for defining the edge or boundary of the structure of interest. Methods including the half-height CT number contour, point of steepest descent, and histogram boundary selection have been considered. A preliminary analysis of infarct size using planimetry of each slice and summing the slices in 5 patients is illustrated in Figure 5. Infarct size shown here appears to correlate with the corresponding CPK enzyme curve areas. This, however, is a small patient series. Many blood sample enzyme measurements are, of course, required to determine the shape of the enzyme curve in each patient; such a prospective study is in progress at UCSF. Validation studies of this type are essential but not simplistic either in logistics or coordination. Our preliminary results indicate that present CT scanners are quite capable of demonstrating antero-septal lesions using the perfusion defect originally seen in the dogs (11 of 13, i.e. 80–90% were recognized by CT). However, there are limitations in scanning the inferior wall, and infarction here was usually overlooked [21]. Prospects, however, are good for improving these results. CT procedural techniques can be modified, and improvements continue in CT technology and instrumentation. It should be noted that CT also has the potential to measure wall thickness, and with ECG gating, wall dynamics. Associated intraventricular thrombus can also be identified as illustrated in the example shown in Figure 6. The sensitivity appears to be similar to that of two-dimensional echocardiography, but preliminary work suggests that CT may be more specific, particularly in the apical region of the left ventricle [22].

Since CT development is still at a very early stage compared with the long development periods required for other imaging techniques such as cinecardio-angiography, it is apparent that the future potential for cardiac CT is great [23, 24]. The first prototype cardiac CT scanner designed at UCSF is nearing completion

[25]. The impact of this multislice millisecond CT instrument is awaited with great anticipation and enthusiasm.

REFERENCES

1. Hounsfield GH: Nobel Prize Acceptance Speech, Medical Physics. 7:283, 1981.
2. Cormack AM: Nobel Prize Acceptance Speech, Medical Physics. 7:277, 1980.
3. Hounsfield GH: Computerized transverse axial scanning (tomography): Part 1, description of system, British Journal of Radiology 46:1016, 1973.
4. Braunwald (ed) Protection of the ischemic myocardium. Circulation (Supp I), 53:1, 1976.
5. Berninger WH, Redington RW, Leue W, Axel L, Norman D, Brundage B, Carlsson E, Herfkens R, Lipton MJ: Technical aspects and clinical applications of CT/X, a dynamic CT scanner. J of Comput Asst Tomogr 5:206, 1981.
6. Ter-Pogossian MM, Weiss ES, Coleman RE: Computed tomography of the heart. Am J of Roentgenology 127:79, 1976.
7. Alfidi RJ, Haaga J, Meaney TF, MacIntyre WJ, Gonzalez L, Tarar R, Zelch MG, Boiler M, Cook SA, Jelden G: Computed tomography of the thorax and abdomen: a preliminary report. Radiology 117:257, 1977.
8. Gray WR, Jr, Parkey RW, Buja LM, Stokely EM, McAllister RE, Bone FJ, Willerson JT: Computed tomography: in vitro evaluation of myocardial infarction. Radiology 122:511, 1977.
9. Powell WR, Jr, Wittenberg J, Maturi RA, Kinsmore RE, Miller SW: Detection of edema associated with myocardial ischemia by computerized tomography in isolated, arrested canine hearts. Circulation 55:99, 1977.
10. Adams DF, Hessel SJ, Judy PF, Stein JA, Abrams HL: Computed tomography of the normal and infarcted myocardium. Am J of Roentgenology 126:786, 1976.
11. Lipton MJ, Hayashi TT, Boyd DP, Carlsson E: Ventricular cast volume measurements by computed tomography. Radiology 127:419, 1978.
12. Higgins CB, Sovak M, Schmidt W: Uptake of contrast materials by experimental acute myocardial infarction: a preliminary report. Investigative Radiology 13:337, 1978.
13. Lipton MJ, Body DP: Models for dynamic CT imaging of the heart and brain, AUR Symposium. In: Milne Inc (ed), Research Methods in Radiology, Praeger Scientific, 1983 (in press).
14. Carlsson E, Lipton MJ, Berninger WH, Doherty P, Redington RW: Selective left coronary myocardiography by computed tomography in living dogs. Investigative Radiology 12:559, 1977.
15. Doherty PW, Lipton MJ, Berninger WH, Skioldebrand CG, Carlsson E, Redington RW: The detection and quantitation of myocardial infarction in vivo using transmission computed tomography. Circulation 63:597, 1981.

16. Berninger WH, Redington RW, Doherty P, Lipton MJ, Carlsson E: Gated cardiac scanning in normal and experimentally infarcted canines. J of Comput Asst Tomogr 32:155, 1979.

17. Lackner VK, Thurn P: EKG-gesteuerte kardiocomputertomographie. Fortsch Rontgenstr 132:169, 1980.

18. Lackner K, Thurn P: Computed tomography of the heart: ECG-gated and continuous scans. Radiology 140:413, 1981.

19. Lipton MJ, Naple S, Brundage B, Tyberg J, Boyd D, Redington R: Electrocardiograph gated CT for regional myocardial motion analysis. Circulation 64(IV):220, 1981.

20. Higgins CR, Sovak M, Schmidt W, Siemers PT: Differential accumulation of radiopaque contrast material in acute myocardial infarction. Am J Cardiol 43:47, 1979.

21. Goldstein JA, Lipton MJ, Kramer PH, Brundage BH: Evaluation of acute myocardial infarction by contrast enhanced computed tomography. Clinical Research 30(1):10A, 1982.

22. Goldstein J, Lipton M, Schiller N, Ports T, Brundage B: Evaluation of left ventricular aneurysms with contrast enhanced computed tomography and two-dimensional echocardiography. Clinical Research 30:10A, 1982.

23. Lipton MJ, Higgins CB: Evaluation of ischemic heart disease by computerized transmission tomography. Radiologic Clinics of North America 18(3):557, 1980.

24. Brundage BH, Lipton MJ: The emergence of computed tomography as a cardiovascular diagnostic technique. (Editorial) Am Heart J 103(2):313, 1982.

25. Boyd DP, Gould RG, Quinn JR, Sparks R, Stanley JH, Hermannsfeldt WB: A proposed dynamic cardiac 3-D densitometer for early detection and evaluation of heart disease. IEEE Trans Nuclear Science NS-26:2724, 1979.

V. TISSUE ANALYSIS

22. TISSUE QUANTIFICATION BY ULTRASOUND. TECHNICAL ASPECTS

ROBERT C. CHIVERS

1. INTRODUCTION

Cardiology has a distinct place in the development of diagnostic ultrasound, for two reasons. Firstly, cardiology as a speciality has almost exclusive use of one of the modes of ultrasonic diagnosis – the M-mode (1954) which followed the development of the B-mode (1952) by just two years [1], and secondly it was the cardiologists Asberg [2] and Bom [3] who pioneered motional imaging that has proved so valuable to those using B-mode for other investigations (scanning). The development of the A-scan was based on a simple physical model of partial reflection of an ultrasonic pulse at a change of the acoustic impedance of the propagation medium. Considerable effort was expended in electronic development to emphasise those features of the returning echo train that were consistent with this model. The image produced thus tended to be a *differential* one, which limited its quantitative interpretation.

The subsequent developments in ultrasonic diagnostic techniques have very largely tended to be technological rather than scientific because of the speed of developments in the electronics industry that have very dramatically increased the sophistication of the instruments that can be economically produced [4]. However, the B-scans produced were bistable, only outlining the structures present and giving little or no information on what was between the large echo producing interfaces. This was of no disadvantage in M-mode scanning where the display indicates relative distances as a function of time from which the parameters of movement, displacement, velocity and acceleration may be derived.

Approximately ten years ago [5] a fundamental change took place in the philosophy of ultrasonic diagnosis with the extension of the simple interface model to include the many small echoes that were detected between those of the major interfaces but not displayed. The postulate was that these were caused by scattering of the waves by small scale inhomogeneities in the tissue. This produced two new directions of endeavour – the development of grey-scale machines in which these textural features play an important diagnostic role, and the whole field of tissue characterization. The two are clearly related: in the former we are interested in finding the display which permits optimal differential diagnosis of a particular pathology, in the latter for quantitative ultrasonic indices which can be related to

histological and pathological classifications. Eventually these two may merge, but at the present the links between them are tenuous. Before discussing them, the ultrasonic parameters that may be appropriate will be outlined.

2. ULTRASONIC PARAMETERS

The parameters which may be used to describe the way in which an ultrasonic wave propagates through tissue are [6]:
- acoustic velocity $C = (\rho\beta)^{-\frac{1}{2}}$ where ρ is the density and β the compressibility of the tissue
- characteristic acoustic impedance $Z = \rho c$
- absorption coefficient α_A
  (an index of the ultrasonic energy lost by conversion to other forms of energy)
- scattering cross section per unit volume α_s
  (an index of the ultrasonic energy redirected out of the propagating beam)
- attenuation coefficient $\alpha_T = \alpha_s + \alpha_A$
  (an index of the total energy lost per unit distance as the pulse propagates).

It is difficult to adopt a systematic approach to the problem of relating these to a particular histology or pathology, partly because of the physical variability that may exist within a particular pathological classification. In addition it may be a combination of these parameters, or their dependence on some other variable such as temperature, that gives the most sensitive discriminatory test. However, following a suggestion of Fields and Dunn [7], O'Brien [8] has reviewed the literature on the variation of velocity and attenuation looking for general trends. His conclusion was that as the complexity of the tissue increases, both velocity and attenuation increase, with the collagen content increasing and the water content decreasing. For a material such as heart muscle which may have well defined fibre directions, the velocity, scattering and attenuation may all be anisotropic (i.e. depend on the direction of the fibres in relation to that of the ultrasonic beam).

Measurements taken in the laboratory from only a guide to the in vivo situation, not only because of the problem of the condition of the tissue, but also because the two parameters most usually measured in the laboratory – velocity and attenuation – can only be estimated with pulse-echo systems, and even then the signal processing required is quite sophisticated (as is discussed in Section 5 below). An alternative to the approach based on ultrasonic parameter measurements is that of quantification of the display itself.

3. QUANTITATIVE ANALYSIS OF DISPLAYS

The traditional M-scan picture has intrinsic in it not only a display of motion but also of reflectivity. For thin structures, the reflectivity is related not only to the

boundary impedance changes that the structure produces, but also to the thickness of the structure itself and to its orientation with respect to the ultrasonic beam. The identification of the relative contributions of these effects is difficult. If the structure is extended, in addition to the echoes caused by the impedance changes at the interfaces, there may be the small scale "scattering" echoes of the extended model discussed in Section 1. Working from a commercial scanning device quantitative indices can be derived both for the reflectivity of the interfaces and for the scattering properties. Thus Friedman et al [9] have shown that left main carotid artery disease can be distinguished (in two dimensional echo cardiography) from epicardial fat or calcification associated with aortic and mitral valve disease (all of which produce high level echoes). This is achieved by careful adjustment of the gain of the the display and by the choice of a particular type of display characteristic, both of which may be quantified. Similarly, quantitative indices may be derived for the textural features associated with scattering [10]. The main problems with these approaches, though, are that they tend very often to depend on the signal processing and transducers used to make the display, and are essentially empirical (and thus hard to optimise).

4. LABORATORY MEASUREMENTS ON HEART TISSUES

The information available in the literature on ultrasonic velocity and attenuation in tissues has been collated by Goss et al [11]. Such listings need to be interpreted with care [12] since much data is on different animals, the conditions of the tissues are often unspecified and the experimental technique may have been subject to errors such as the phase-cancellation artefact identified in 1975 [13], the implications of which have still not been well defined [5, 14].

Of the parameters given in Section 2, only the velocity, scattering and attenuation of cardiac tissue appear to have been significantly investigated. The methods of measuring scattering have been discussed by Reid [15], but there are a wide range of techniques for measurement of velocity and attenuation, nearly all of which involve having the source and the detector of the ultrasound on opposite sides of the specimen, thus making them inapplicable for in vivo work. Apart from using conventional approaches for measuring values averaged over small volumes, there are two techniques available for more detailed investigation – ultrasonic computer assisted tomography and ultrasonic microscopy. The former [16] is similar to its x-ray predecessor except that in addition to reconstructions related to attenuation from the amplitudes of the pulses, the time delays may also be reconstructed to give maps of "velocity". Acoustic microscopy [17] may give extremely good resolution of the texture of both velocity and attenuation, but the better the resolution, the higher the frequency needed and the thinner the specimen used. At 100 MHz, for example, a 500 μm thick sample is used and measurements may be made over an area 70 μm square [17]. Neither computer-assisted tomography nor microscopy

appear to have been used extensively to date for cardiac tissue, although the latter indicates significant velocity changes for infarcted tissues, and anisotropy of heart muscle [17].

Measurements of attenuation for cardiology appear to have been pioneered by Lele and his coworkers [18, 19] who discovered the frequency dependence of attenuation to be indicative of myocardial infarction. They have also shown the impedance of infarcted myocardium to be lower than that of healthy tissue [19]. The former result has been confirmed and extended by Miller and his coworkers [20] who have performed a series of meticulous investigations [21–25]. Using a creatine kinase analysis as an index, a good correlation has been found in dogs between the severity of myocardial infarction and the slope of the attenuation with frequency [21], both increasing together. The production of ischaemia in dogs appears to result in a significant decrease in the attenuation of the ischaemic region in the first 24 hours, but after 3 days it is significantly higher as it is for infarcts. Thus variations of attenuation may be an early index of ischaemia [22].

It appears that the increased attenuation is due to a collagen increase, and that although collagen appears to be the main factor causing an increase in the infarcted tissue, it accounts for only approximately 15% of the attenuation in normal tissue [23]. Oedema may also contribute to the increased attenuation.

Scattering measurements have been reported by Reid and Shung who indicate an apparent isotropy of scattering for heart tissue at 5 MHz [26] and an approximately fourth power dependence on frequency [27]. Mimbs and his colleagues have shown there to be an increase in the ultrasonic backscatter in ischaemic tissues (of dogs and rabbits) [24] and found a strong dependence of this backscatter on collagen content. Investigation of the backscattering of myopathic regions [25] showed some increase although fibrotic regions showed more greatly increased backscattering compared to the normal at 2.25 MHz in rabbits. Thus alterations do occur in the properties of reflected sound in cardiomyopathy which could be used for early detection although more investigation may be needed to optimise the index used.

Scattering measurements may also be used to give an index of structural spacing in tissues and one report [28] indicates an increase in the fibre bundle spacing from 90–110 μm before infarction to 200–220 μm after.

5. IN-VIVO MEASUREMENTS

Little work appears to have been described in vivo. Gore et al [29] have used an autocorrelation function approach on a normal heart showing significant changes between end-systole and end-diastole techniques, indicating a potential for monitoring muscle contractility. The group at Washington University, Missouri (Miller, Mimbs et al) have performed measurements in dogs (open chest) in vivo and shown that backscattering in ischaemic regions increases significantly and may be measured in vivo if the heart is accessible. In recent years a number of techniques

have been described in the literature for estimating values of, for example, imped-ance [30], velocity [31], attenuation [32], and scattering [33] from pulse-echo data. These do not yet appear to have been used greatly in cardiology. One of the most important features is the compromise inherent in any of these techniques as to the validity of the assumptions involved. Invalidity of these assumptions will cause differences between parameter values measured by conventional laboratory trans-mission methods and those estimated from pulse-echo techniques. The application of results obtained in vitro to the in-vivo situation are thus liable to need careful proving before they can be reliably used. In addition to the fact that there are limitations involved in estimating velocity and attenuation data by pulse-echo methods, there are the problems of the overlying tissues, the cardiac motion, and the orientation of the tissues being investigated [34]. A powerful data acquisition and manipulation system is required. More information on digital processing and applications will be found in the next three papers.

There is clearly a great potential for investigation in this area of tissue quantifi-cation but for it to be effective it must be directed by specific important clinical questions. One incidental question that arises is whether or not it may be wise to move the normal frequency range of M-scans out of the region in which the attenuation characteristics of ischaemic and normal tissue are almost the same [20].

REFERENCES

1. Wells PNT: Biomedical Ultrasonics, p. 509, Academic Press, London, 1977.
2. Asberg A: Ultrasonic cinematography of the living heart. Ultrasonics 5:113–117, 1967.
3. Bom N, Lancee CT, Van Egmond RC: An ultrasonic intracardiac scanner. Ultrasonics 10:72–76, 1972.
4. Chivers RC: Some scientific and technical aspects of medical ultrasonics. J Med Eng Tech 5:128–133, 1981.
5. Chivers RC: Tissue characterization. Ultrasound Med Biol 7:1–20, 1980.
6. Hill CR: Ultrasonic attenuation and scattering by tissues. In: de Vlieger M et al (eds), Handbook of Clinical Ultrasound, John Wiley, Chichester, 1978.
7. Fields S, Dunn F: Correlation of echographic visualizability of tissue with biological composition of physiological state. J Acoust Soc Am 54:809–812, 1973.
8. O'Brien WD: The relationship between collagen and ultrasonic attenuation and velocity in tissue, In: Ultrasonics International 1977, pp. 194–205, IPC Guildford, 1977.
9. Friedman MJ, Sahn DJ, Goldman S, Eisner DR, Gittinger NC, Lederman FL, Puckette CM, Tiemann JJ: High predictive accuracy for detection of left main carotid artery disease by antilog signal processing of two-dimensional echocardiographic images. Am Heart J 103:194–201, 1982.
10. Chivers RC: Quantitiative image indices in ultrasonic diagnostics of inhomogeneous materials, Archives of Acoustics (Warsaw) 6:147–162, 1981.
11. Goss SA, Johnston RL, Dunn F: Comprehensive compilation of empirical ultrasonic properties of mammalian tissues, J Acoust Soc Am 64:423–457, 1978.
12. Chivers RC, Parry RJ: Ultrasonic velocity and attenuation in mammalian tissues. J Acoust Soc Am 63:940–953, 1978.
13. Marcus PW, Carstensen EL: Problems with absorption measurements of inhomogeneous solids, J Acoust Soc Am 58:1334–1335 (L), 1975.

14. Aindow JD, Chivers RC: Experimental assessment of phase fluctuations of ultrasonic waves propagating in tissue models and tissues, Ultrasound Med Biol 8 (Supp. 1):1(A), 1982.
15. Reid JM: The scattering of ultrasound by tissues, In: Linzer M (ed), Ultrasonic Tissue Characterization, Special publication 453, pp. 29–47, NBS Washington, 1976.
16. Greenleaf JF, Johnson SA: Algebraic reconstruction of spatial distributions of refractive index and attenuation in tissues from time of flight and amplitude profies, ibid 1976, 109–119.
17. Yuhas DE, Kessler LW: Acoustic microscopic analysis of myocardium In: Linzer M (ed), Ultrasonic Tissue Characterization II, Special publication 525, pp. 73–84, NBS Washington, 1979.
18. Namery J and Lele PP: Ultrasonic detection of myocardial infarction in dog, IEEE 1972 Ultrasonics Symposium, pp. 491–494, 72 CHO 708–8SE, 1972.
19. Lele PP, Mansfield AB, Murphy AI, Namery J, Senapati N: Tissue characterization by ultrasonic frequency dependent attenuation and backscattering, In: Linzer M (ed), Ultrasonic Tissue Characterization, Special publication 453, pp. 167–196, NBS Washington, 1976.
20. Miller JG, Yuhas DE, Mimbs JW, Dierken SD, Busse LJ, Weiss AN, Sobel BE: Ultrasonic tissue characterization: correlation between biochemical and ultrasonic indices of myocardial injury, In: de Klerk J, McAvoy B (eds), Proc IEEE Ultrasonic Symposium, Cat No 1120–450, Annapolis, p. 33, 1976.
21. Mimbs JW, Yuhas DE, Miller JG, Weiss AN, Sobel BE: Detection of myocardial infarction in vitro based on altered attenuation of ultrasound, Circulation Res 41:192–198, 1977.
22. Mimbs JW, O'Donnell M, Miller JG, Sobel BE: Changes in ultrasonic attenuation indicative of early myocardial ischaemic injury, Am J Physiol 236:H340–344, 1979.
23. O'Donneij M, Mimbs JW, Miller JG: The relationship between collagen and ultrasonic attenuation in myocardial tissue, J Acoust Soc Am 65:512–517, 1979.
24. Mimbs JW, O'Donnel M, Bauwens D, Miller JG, Sobel BE: The dependence of ultrasonic attenuation and backscatter on collagen content in dog and rabbit hearts, Circulation Res 47:49–58, 1980.
25. Mimbs JW, O'Donnell M, Miller JG, Sobel BE: Detection of cardiomyopathic changes induced by doxorubicin based on quantitative analysis of ultrasonic backscatter, Am J Cardiol 47:1056–1060, 1981.
26. Sigelmann RA, Reid JM: Scattering of ultrasound by biological tissues, In: Reid JM, Sikov MR (eds), Interaction of Ultrasound and Biological Tissues, p. 245. Washington, Bureau of Radiological Health Publication FDA-73-8008, 1973.
27. Reid JM, Shung KK: Quantitative measurements of scattering of ultrasound by heart and liver, In: Linzer M (ed), Ultrasonic Tissue Characterization II, Special publication 525, pp. 153–156. NBS, Washington, 1979.
28. Dines KA, Weyman AE, Franklin TD, Cuddeback JK, Sanghvi NJ, Avery KS, Baird AI, Fry FJ: Quantitation in changes in myocardial fibre bundle spacing with acute infarction using pulse echo ultrasound signals, Circulation 60: (Supp.II) p. 17, 1979.
29. Gore JC, Leeman S, Metreweli G, Plessner NJ, Willson K: Dynamic autocorrelation analysis of A-scans in vivo, In: Linzer M (ed), Ultrasonic Tissue Characterization II, Special publication 525, pp. 275–280, NBS, Washington, 1979.
30. Jones JP: Current problems in ultrasonic impediopgraphy, In: Linzer M (ed), Ultrasonic Tissue Characterization II, Special publication 453, pp. 253–258, NBS, Washington, 1976.
31. Robinson DE, Chen F, Wilson LS: Measurement of velocity of propagation from ultrasonic pulse-echo data, Ultrasound Med Biol 8:413–420, 1982.
32. Kuc R, Taylor KJW: Variation of acoustic attenuation slope estimates for in vivo liver, Ultrasound Med Biol 8:403–412, 1982.
33. Lizzi FL, Elbaum ME: Clinical spectrum analysis techniques for tissue characterization, In: Linzer M (ed), Ultrasonic Tissue Characterization II, Special publication 525, NBS, Washington, 1979.

23. APPROACHES TO MYOCARDIAL TISSUE CHARACTERIZATION USING ULTRASOUND ECHO AMPLITUDE INFORMATION

DAVID J. SKORTON, STEVE M. COLLINS AND HEWLETT E. MELTON, JR.

1. INTRODUCTION

Echocardiography has achieved a prominent place as a noninvasive cardiac diagnostic technique, because of its ability to supply the clinician with reliable cardiac morphologic information in a safe, painless, and relatively inexpensive manner [1]. M-mode and two-dimensional echocardiography are extensively used for the evaluation of a wide variety of cardiac abnormalities including valvular, ischemic, congenital and myocardial disorders [2]. The myriad of standard qualitative and quantitative clinical applications of echocardiography are all based on the ultrasonic detection of large, smooth-surfaced (specular) reflectors such as the epicardium, endocardium, walls of the great arteries, and cardiac valves. The clinical echocardiographer observes the position and motion of these specular reflectors and thereby deduces abnormalities of the structure and function of the heart.

In addition to the useful information which can be gained from imaging the specular reflectors of the heart, a growing body of evidence suggests that diagnostically important information is present in the lower amplitude ultrasonic signals returning from, or passing through, myocardial tissue itself. A relatively new area of investigation has grown around the exploration of tissue acoustic properties, an area of endeavor referred to as "ultrasound tissue characterization" [3, 4]. A working definition of ultrasound tissue characterization is the evaluation of some of the structural features of a volume of tissue based upon its acoustic properties. The assumption underlying this approach is that the acoustic properties of tissue are closely related to the structural organization of the tissue and, further, that these acoustic properties may be recognized or measured in a clinically relevant manner. Ultrasound tissue characterization has been intensively studied in other organs such as the breast [5], liver [6], and eye [7]. Investigations of myocardial acoustic properties have been more difficult because of the imaging constraints of thoracic anatomy as well as the complex translational and rotational motion of the heart. Nonetheless, several recent investigations and reports, taken together, supply convincing evidence that myocardial acoustic properties are significantly changed by acute and chronic cardiac disorders [8, 9, 10, 11, 12, 13]; that these changes may be measured or otherwise detected in potentially clinically useful ways [14, 15, 16]; and that ultrasound tissue analysis may supply unique information on myocardial
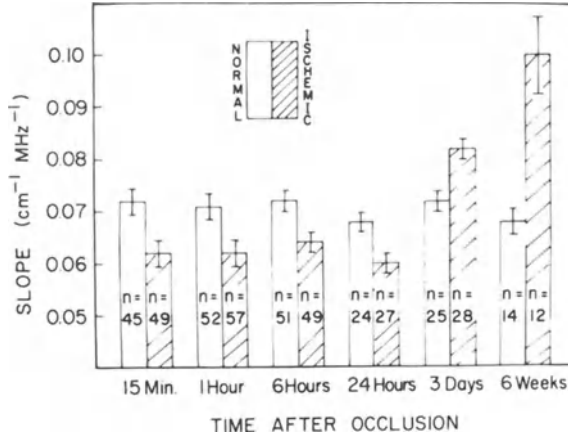
Figure 1. The slope of the attenuation/frequency relationship is shown at various times after experimental coronary occlusion. The attenuation of infarcted myocardium was less than that of normal tissue for the first 24 hours post-occlusion, and thereafter, attenuation was increased. (Reproduced from reference No. 20, with permission of the author and of the American Physiological Society.)

structure which is not available using current echocardiographic techniques.

It is our purpose in this paper to review the basic approaches to measurement or detection of altered myocardial acoustic properties, including the approaches we have studied, and to identify several significant problems in ultrasound tissue analysis – problems which must be confronted and solved in order to utilize myocardial acoustic analysis as a reliable diagnostic method.

2. METHODS OF ULTRASOUND TISSUE CHARACTERIZATION

In another paper in this volume, Chivers has reviewed the important physical and technical considerations underlying ultrasound tissue characterization [17]. Three general categories of approaches have been explored in applying these principles to myocardial analysis: measurement of classic acoustic properties of tissues such as attenuation [10] or backscatter [11]; direct display of regional alterations in acoustic properties using imaging techniques [14, 18]; and the analysis of diagnostic patterns in ultrasonic signals utilizing statistical or other signal or image analytic techniques [15, 16, 19].

The measurement of acoustic properties of tissue is an important approach because it adds to our understanding of the basic mechanisms of ultrasound/tissue interactions. Several acoustic parameters have been studied in normal and abnormal myocardium, including acoustic impedance [8], attenuation [10, 11], and backscatter [11, 12]. In one of the first investigations of cardiac tissue acoustic properties, Namery and Lele measured a lower acoustic impedance in acutely infarcted
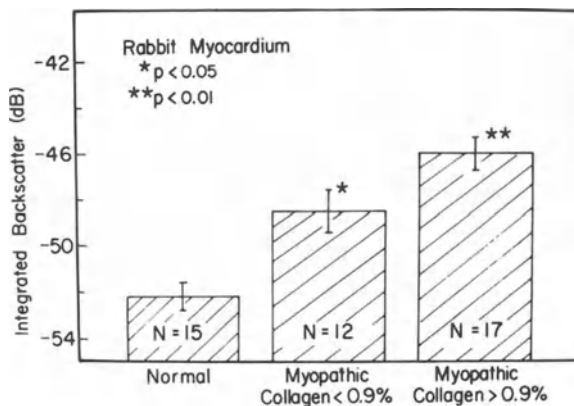
Figure 2. Measurements of integrated backscatter successfully differentiated between normal, myopathic, and fibrotic myocardium in an animal model of doxorubicin cardiotoxicity. (Reproduced from reference No. 13 with permission of the author and publisher.)

myocardium than in normal myocardium [8]. Mimbs and associates confirmed an alteration in myocardial acoustic properties as soon as fifteen minutes after experimental coronary occlusion [20]. These investigators measured a decrease in ultrasound attenuation (slope of the frequency/attenuation relationship) beginning at fifteen minutes postocclusion with a sustained decrease compared to normal myocardium for up to 24 hours (Figure 1). Beginning at three days postocclusion, however, the frequency/attenuation slope was increased compared to normal myocardium.

These early experiments in myocardial ultrasonic tissue characterization had two important implications for further research. First, measurement of the frequency-dependence of attenuation could reliably distinguish normal from acutely infarcted myocardium at a very early stage of injury. Second, the relative change in attenuation from an early decrease to a late increase after myocardial infarction suggested that different mechanisms were responsible for the acoustic alterations in acute compared to subacute myocardial infarction [9]. Although of great theoretical interest, these measurements of attenuation were performed in transmission mode (i.e. with a transmitting crystal on one side of a tissue specimen and a receiving crystal on the opposite side). This technique is not compatible with the constraints of clinical imaging, which require the same crystal to be used as transmitter and receiver. Therefore, a great deal of subsequent investigation has been directed toward the use of reflected ultrasound and the measurement of ultrasound backscatter instead of attenuation [11–13]. Mimbs and coworkers demonstrated an increase in integrated backscatter in acutely infarcted myocardium as soon as one hour after experimental coronary occlusion and this increase persisted for several

weeks after the injury [11, 12]. In subsequent experiments, Mimbs and associates attempted to delineate the mechanism of these alterations in ultrasound attenuation and backscatter in myocardium. These investigators have demonstrated an increase in tissue water (edema) in acute myocardial infarction and have attributed acute alterations in backscatter (and attenuation) to this alteration in water content [12]. In chronic myocardial infarction, with healing and scar formation, the collagen content of the tissue correlated with attenuation and with backscatter [11]. These observations confirmed earlier measurements and predictions by Johnston et al who hypothesized that the relative content of structural protein and water would be important determinants of tissue acoustic characteristics [21]. Mimbs et al have also utilized integrated backscatter measurements to identify myocardium damaged by chronic doxorubicin administration [13], demonstrating an increase in integrated backscatter with increasing duration of doxorubicin administration (Figure 2).

Approaches to myocardial tissue characterization based on the measurement of acoustic parameters will undoubtedly continue to be of importance, especially as methods are developed to deal with the confounding effects of tissue intervening between the transducer and region of interest [22, 23].

Abnormally structured myocardium may occasionally be directly visualized in standard clinical echocardiograms [14, 24]. For example, the bright homogeneous appearance of calcified tissue and the peculiar texture of the ventricular septum in hypertrophic cardiomyopathy [25] are familiar to the clinical echocardiographer. Rasmussen et al have reported a thin dense-appearing ventricular septum in patients with scar due to myocardial infarction [14] (Figure 3). This increased density is due to the increase of integrated backscatter as demonstrated by Mimbs et al [11], and as briefly discussed above. This direct visualization of the acoustically abnormal myocardial regions is unpredictable, however, and is made difficult by signal compression in the echocardiographic system. A very wide amplitude dynamic range (over 80 decibels) is present in a pulsed ultrasound examination [26]. However, most available display monitors can only display 15–20 decibels of this amplitude dynamic range [26]. Thus, the much wider signal dynamic range must be compressed into the available range of the display monitor, sometimes obscuring diagnostic regional differences in amplitude. Furthermore, the nonlinear method of compression generally employed may alter the relative appearances of various echo amplitudes [27]. Color encoding of two-dimensional echocardiograms is one method of attempting to retain contrast resolution and may hold promise for future applications of direct display of abnormal myocardial acoustic properties [18].

Digital computer image analysis techniques may be utilized to characterize the "pattern" of reflector or transmitted ultrasound using statistical or other analytic techniques [15, 16, 19, 28]. Although some of these patterns may be recognizable by the clinician (e.g. the "sparkling" appearance of the septum in hypertrophic cardiomyopathy), other patterns may not be easily appreciated without computer-based analysis. For example, Joynt et al have studied the statistical characteristics of
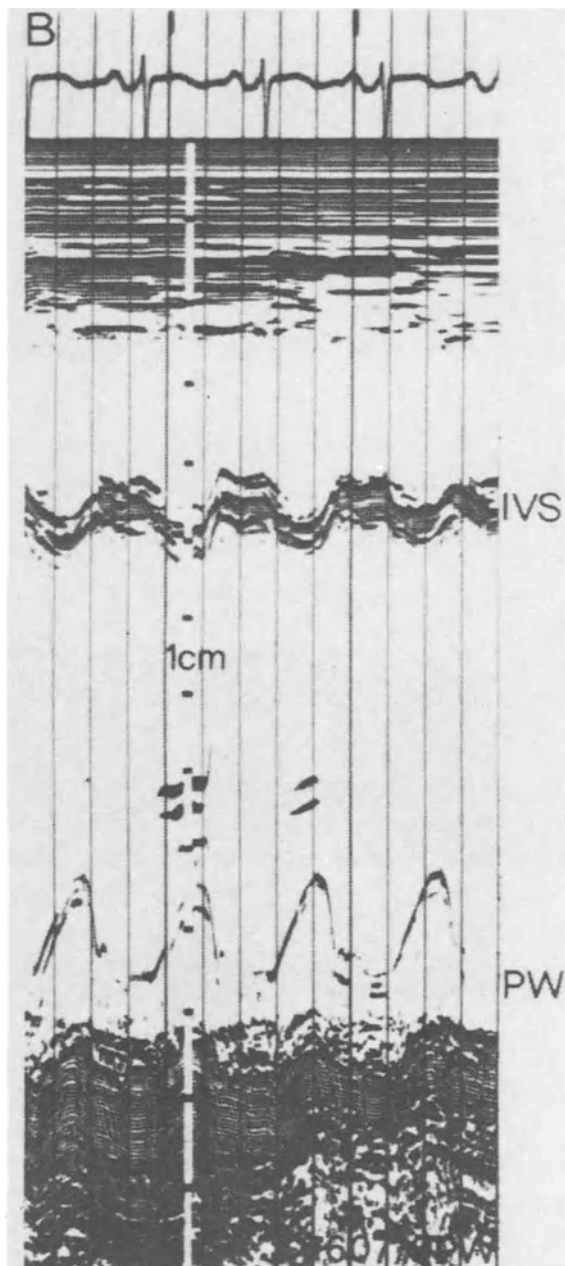
Figure 3. An M-mode echocardiogram at left ventricular level demonstrates bright echoes from the ventricular septum, which was also thin, indicating septal scar. IVS: interventricular septum; PW: posterior wall. (Reproduced from reference No. 14 with permission of the author and the American Heart Association.)
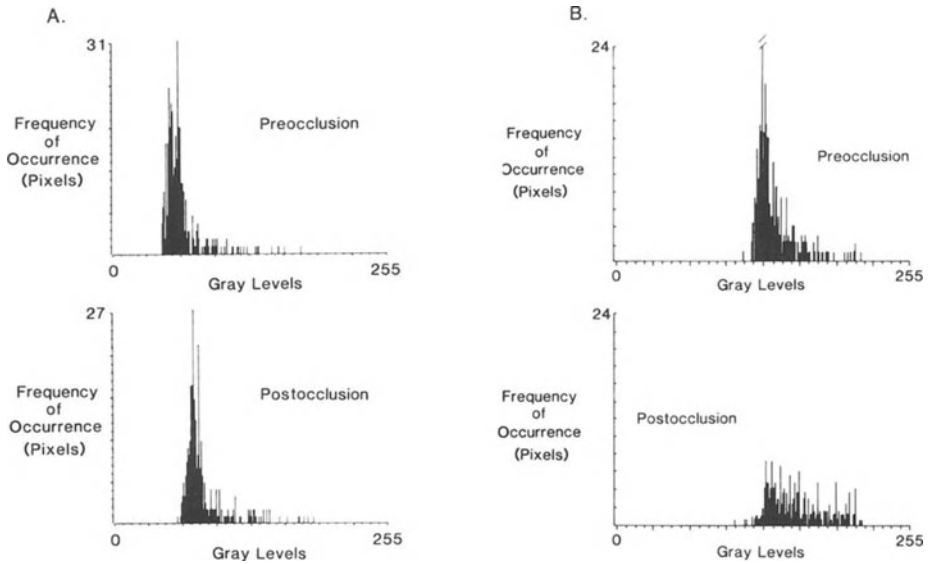
Figure 4. Gray level (echo amplitude) histograms are shown for control (A) and infarcted (B) regions of myocardium before and after experimental coronary occlusion. In the control region, the skewed shape of the gray level distribution did not change after occlusion. In the infarcted region, a relatively larger number of higher gray levels was seen after occlusion, changing the shape of the histogram. (Reproduced from reference No. 16 with permission of the author and the American Heart Association.)

ultrasound radio-frequency signals digitized from a single line-of-sight of a two-dimensional scan [29]. These investigators have demonstrated that the behavior of the frequency spectrum of infarcted myocardium over time differs from that of normal tissue [29], and the probability density function of echo amplitudes may be utilized to differentiate cardiac myxomata from thrombi [15]. Using a somewhat similar approach, Dines and associates have demonstrated statistical characteristics of radio-frequency signals which distinguished infarction and gave clues as to the spacing of myofibrils [19]. It is important to recognize that this type of analysis does not actually measure ultrasonic parameters such as attenuation or backscatter. Instead, first or second order statistical analysis of the ultrasound signal (or image) from a specific region of tissue is used to derive information on the structure of that tissue. Abnormalities are defined based on comparison with normal regions of the same image or by comparison with a previous (normal) examination.

Much of the previous work in ultrasound digital signal analysis has been performed using the radio-frequency ultrasound signal, with the intention of fully exploiting the high frequency content of this signal [30]. Although this approach is attractive and has been used successfully in the past, the rapid sampling rate and large amount of digital data storage necessary to evaluate radio-frequency data currently impose significant practical problems on clinical application of this approach. Further, current commercially available ultrasound instruments do not allow access to the ultrasound signal in its radio-frequency form. Investigations of
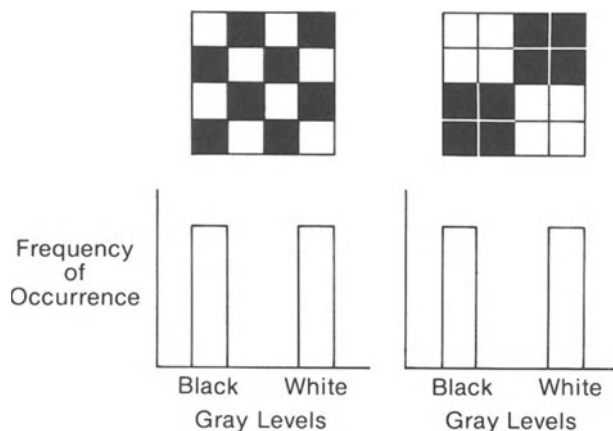
Figure 5. The gray level histogram may not convey information on the spatial pattern of gray levels in a region of interest. Two schematic regions are shown at the top of the figure. Each region is half black and half white; thus, both regions have the same gray level histogram (lower panels). The patterns of black and white (textures) in the two regions are different, but this difference is not apparent in the gray level histograms.

the statistical nature of ultrasound signals have also been performed using the "envelope-detected" or video signal. The motivation for this approach is that successful characterization of tissue structure using ultrasound video data will allow more rapid transfer of the analysis techniques to the clinical setting.

Utilizing two-dimensional echocardiographic image (video) data, we have explored several approaches to ultrasound myocardial analysis [16, 28]. We studied experimental myocardial infarction in a closed-chest dog model, performing two-dimensional echocardiograms before and two days after acute coronary occlusion [16]. Regional average gray level (as an analog of echo amplitude) increased significantly from pre- to postocclusion images in infarcted regions, and did not change significantly in regions which did not sustain infarction. Unfortunately, due to the variability in gray level, this increase in gray level could only be identified by comparison to a control echocardiogram. That is, mean gray level did not vary significantly between infarcted and normal regions within postocclusion images. In an attempt to further evaluate echo amplitude data we studied the distribution of gray levels, that is, the shape of gray level frequency histograms. The shape of the histogram proved to be a reliable discriminator of infarcted myocardium (Figure 4). We successfully utilized the calculation of regional echo amplitude kurtosis to identify regions of infarcted myocardium within postocclusion images and without the need for comparison to a control echocardiogram [16]. Thus, we found that the distribution of gray levels (echo amplitudes) differed significantly between infarcted and normal myocardial regions. This study indicated the feasibility of identifying infarcted myocardium based on 2D echo image data obtained in closed-chest subjects.

The analysis of gray level histograms, while supplying data on the overall content of echo amplitudes in a region of interest, may not convey information on the spatial distribution of gray levels (Figure 5). We hypothesized that the spatial pattern or texture present in regions of 2D echo images would contain information which would aid in identifying abnormal myocardial structure. We tested this hypothesis by studying regional 2D echo image texture in a dog model of acute myocardial contusion [28]. Standard 2D echocardiograms were performed before and immediately after delivery of blunt chest trauma to anesthetized dogs. The regions which sustained contusion exhibited a brighter, "coarser" texture in the 2D images, and this alteration in texture was successfully quantified using a set of classical texture calculations [28]. The results of the calculations suggested that acute myocardial contusion was characterized by brighter myocardium, by increased size of individual echo "spots", and by coalescence of echo reflections producing a coarse texture appearance. Thus, this study demonstrated that quantitative measures of 2D image texture in the model studied could detect injured myocardium.

3. CURRENT PROBLEMS IN ULTRASOUND MYOCARDIAL TISSUE ANALYSIS

One unresolved question concerning ultrasound tissue analysis centers on whether the image data should be analyzed in its radio-frequency form or as a video signal. The relative merits of these approaches are briefly alluded to above, and recent investigation has been directed at comparisons of data collected in both ways [30]. Regardless of the precise data format, however, certain problems of image formation and data generation are inherent in ultrasound imaging, problems which must be taken into account and solved before ultrasound tissue analysis will be clinically useful. We have studied aspects of two of these problems: (a) the need for an accurate, reproducible method of accounting for attenuation of ultrasound by tissue intervening between the transducer and region of interest [23]; and (b) the fact that echo amplitude data appear to vary significantly within the sector field-of-view, as a function of range and azimuth [31].

Currently available echocardiographs compensate for attenuation of the ultrasound signal by tissue solely as a function of range, or distance from the transducer. That is, the scan is partitioned into two or more range intervals, and the image is amplified by varying amounts at each range interval. Unfortunately, within each range interval, the entire azimuthal extent of the scan is amplified to the same degree. The actual amount of signal attenuation encountered varies, however, according to the precise line-of-sight (e.g. a line-of-sight which passes through the center of the left ventricular cavity will be attenuated very little by the blood in the cavity, whereas a line-of-sight which passes through the ventricular septum will encounter much more attenuation). Thus, significant differences in regional attenuation, and therefore in regional average gray level, may occur in scans performed

using currently available methods of gain compensation, differences due mainly to the lack of line-by-line attenuation compensation. In a study of excised, fixed left ventricles in vitro, we performed gain compensation in two ways: using a commercially available time-gain compensation (TGC) system; and using a new method of amplification which applies gain compensation to each line of sight, based on the level of the ultrasound signal encountered [23, 32]. If returning echo amplitudes are relatively low, the signal is assumed to arise from blood in a cavity, and less gain compensation is applied; if the returning amplitudes are relatively high, the signal is assumed to arise from myocardium, and more gain compensation is applied. In our in vitro experiment, we demonstrated significantly less regional variability in average gray level when using the new method of gain compensation (rational gain compensation, RGC) than when using the standard, TGC [32]. Thus, regional differences arising from actual alterations in tissue structure (e.g. scar) would be less likely to be masked or mimicked by artifactual differences in gray level which are due solely to the method of gain compensation.

Cohen et al have recently reported another, different method of accounting for attenuation by the chest wall in studies designed to measure regional integrated backscatter [22]. An empirical correction factor was developed, based upon measurements of excised chest wall specimens. This correction factor was then used to approximately correct integrated backscatter measurements for the effects of intervening chest wall tissue. The corrected measurements agreed closely with those obtained directly from the epicardial surface, demonstrating that this method of gain compensation (or correction) is also a useful approach [22].

Another important problem which must be addressed in studies of tissue analysis based on pulse echo methods is the regional variability of echo amplitude information within the ultrasound field of view. Flax et al have developed a computer analysis of B-scan image formation, and have predicted that texture in a B-scan will vary as a function of range and azimuth within the scan [33]. The causes of this variability are complex and include changes in system resolution, transducer geometry, and the effect of the signal detection and display processes. In order to study the relevance of these factors to clinical echocardiographic images, we performed standard, 2D echos on a commercially available, graphite-in-gel, tissue equivalent phantom. The distribution of the scatterers in this phantom is uniform. Therefore, we would expect the displayed texture in a 2D echo image to also be uniform if the texture pattern were due solely to the target characteristics. We measured significant differences in several quantitative texture measures, however, as a function of range and azimuth in the scans [31]. This high degree of variability supports the previous model study by Flax et al [33] and is further evidence that the displayed texture in a 2D echo image is the result of several factors related to the imaging system. Therefore, regional alterations in image texture may not be equated with actual changes in tissue structure, until methods are found of correcting for, or circumventing these significant regional differences in echo amplitude information.

4. FUTURE OF ULTRASOUND TISSUE ANALYSIS

Several problems must be solved before ultrasound tissue analysis can take its place as a clinical technique. In addition to the problems we have discussed in this article, a great need exists for further studies of the mechanisms of tissue scattering and attenuation. Such studies will allow more rational, deliberate approaches to ultrasound tissue analysis and will also improve our knowledge of basic ultrasound/tissue interactions.

Thus, ultrasound tissue analysis should be considered currently an investigational technique. However, the promising studies reviewed here, and a great deal of additional current investigation suggests that in the near future, ultrasound tissue characterization will be added to the growing diagnostic arsenal of the clinical cardiologist, and will extend the utility of echocardiography in cardiac diagnosis.

REFERENCES

1. Feigenbaum H: Echocardiography. 3rd ed. Lea and Febiger, Philadelphia, 1981.
2. Kleid JJ, Arvan SB: Echocardiography: Interpretation and Diagnosis. Appleton-Century-Crofts, New York, 1978.
3. Chivers RC: Tissue characterization. Ultrasound in Med & Biol 7:1–20, 1981.
4. Linzer M (ed): Ultrasonic Tissue Characterization II, National Bureau of Standards, Spec Publ 525 (U.S. Government Printing Office, Washington, D.C.), 1979.
5. Kobayashi T: Review: Ultrasonic diagnosis of breat cancer. Ultrasound in Med & Biol 1:383–391, 1975.
6. Lerski RA, Barnett E, Morley P, Mills PR, Watkinson G, MacSween RNM: Computer analysis of ultrasonic signals in diffuse liver disease. Ultrasound in Med & Biol 5:341–350, 1979.
7. Lizzi FL, Elbaum ME: Clinical spectrum analysis techniques for tissue characterization. In: Linzer M (ed), Ultrasonic Tissue Characterization II, National Bureau of Standards, Spec Publ 525 (U.S. Government Printing Office, Washington, D.C.) 111–119, 1979.
8. Namery J, Lele PP: Ultrasonic detection of myocardial infarction in dog. Proceedings IEEE Ultrasonics Symposium 1972; 72CH0708-8SU:491–494.
9. Miller JG, Yuhas DE, Mimbs JW, Dierker SB, Busse LJ, Laterra JJ, Weiss AN, Sobel BE: Ultrasonic tissue characterization: correlation between biochemical and ultrasonic indices of myocardial injury. Proceedings IEEE Ultrasonics Symposium 1972; 76CH1120-55U:33–43.
10. Mimbs JW, Yuhas DE, Miller JG, Weiss AN, Sobel BE: Detection of myocardial infarction based on altered attenuation of ultrasound. Circ Res 41:192–198, 1977.
11. Mimbs JW, O'Donnell M, Bauwens D, Miller JG, Sobel BE: The dependence of ultrasonic attenuation and backscatter on collagen content in dog and rabbit hearts. Circ Res 47:49–58, 1980.
12. Mimbs JW, Bauwens D, Cohen RD, O'Donnell M, Miller JG, Sobel BE: Effects of myocardial ischemia on quantitative ultrasonic backscatter and identification of responsible determinants. Circ Res 49:89–96, 1981.
13. Mimbs JW, O'Donnell M, Miller JG, Sobel BE: Detection of cardiomyopathic changes induced by doxorubicin based on quantitative analysis of ultrasonic backscatter. Am J Cardiol 47:1056–1060, 1981.
14. Rasmussen S, Corya BC, Feigenbaum H, Knoebel SB: Detection of myocardial scar tissue by M-mode echocardiography. Circulation 57:230–237, 1978.
15. Green SE, Joynt LF, Fitzgerald PJ, Rubenson DS, Popp RL: In vivo ultrasonic tissue characteri-

zation of human intracardiac masses (abstr). Circulation 64:IV–257, 1981.

16. Skorton DJ, Melton HE Jr, Pandian NG, Nichols J, Koyanagi NS, Marcus ML, Collins SM, Kerber RE: Detection of acute myocardial infarction in closed-chest dogs by analysis of regional two-dimensional echocardiographic gray-level distributions. Circ Res (In press), Jan. 1983.

17. Chivers RC: Tissue quantification by ultrasound – technical aspects. In: Proceedings of the International Symposium on Advances in Non-Invasive Cardiology (In press), Aachen, Western Germany, Sept. 16–18, 1982.

18. Logan-Sinclair R, Wong CM, Gibson DG: Clinical application of amplitude processing of echo-cardiographic images. Br Heart J 45:621–627, 1981.

19. Dines KA, Weyman AE, Franklin T Jr: Quantization of changes in myocardial fiber bundle spacing with acute infarction, using pulse-echo ultrasound signals (abstr). Circulation 59:II–17, 1979.

20. Mimbs JW, O'Donnell M, Miller JG, Sobel BE: Changes in ultrasonic attenuation indicative of early myocardial ischemic injury. Am J Physiol 236:H340–H344, 1979.

21. Johnston RL, Goss SA, Maynard V, Brady JK, Frizzell LA, O'Brien WD Jr, Dunn F: Elements of tissue characterization I. Ultrasonic propagation properties. In: Linzer M (ed), Ultrasonic tissue Characterization II, National Bureau of Standards, Spec Publ 525 (U.S. Government Printing Office, Washington, D.C.), 1979.

22. Cohen RD, Mottley JG, Miller JG, Kurnik PB, Sobel BE: Detection of ischemic myocardium in vivo through the chest wall by quantitative ultrasonic tissue characterization. Am J Cardiol 50:838–843, 1982.

23. Melton HE Jr, Skorton DJ: Rational gain compensation for attenuation in ultrasonic cardiac imaging, 1981 IEEE Ultrasonics Symposium 81CH1689–9:607–611.

24. vonRamm OT, Smith SW: Prospects and limitations of diagnostic ultrasound. Proceedings of the Society of Photo-optical Instrumentation Engineers (SPIE) 206:6–18, 1979.

25. Martin RP, Rakowski H, French J, Popp RL: Idiopathic hypertrophic subaortic stenosis viewed by wide-angle, phased-array echocardiography. Circulation 59:1206–1917, 1979.

26. White DN: Ultrasound in medical diagnosis, pp. 167–174. Ultramedison, Kingston, Ontario, 1976.

27. Geiser EA, Skorton DJ, Conetta DA: Quantification of left ventricular function from 2-dimensional echocardiography. Am Heart J 102:905–910, 1982.

28. Skorton DJ, Collins S, Nichols J, Pandian NG, Kerber RE: Quantitative texture analysis of two-dimensional echocardiograms: application to the diagnosis of acute myocardial contusion (abstr). Am J Cardiol 49:931, 1982.

29. Joynt L, Boyle D, Rakowski H, Popp R, Beaver W: Identification of tissue parameters by digital processing of real-time ultrasonic clinical cardiac data. In: Linzer M (ed), Ultrasonic Tissue Characterization II, National Bureau of Standards, Spec Publ 525 (U.S. Government Printing Office, Washington, D.C.) 267–273, 1979.

30. Lerski RA, Morley P, Barnett E, Mills PR, Watkinson G, MacSween RNM: Ultrasonic characterization of diffuse liver disease – the relative importance of frequency content in the A-scan signal. Ultrasound in Med & Biol 8:155–160, 1982.

31. Skorton DJ, Collins SM, Melton HE Jr, Woskoff SD: Texture in two-dimensional echocardiograms: regional variability (abstr). J Am College Cardiol (In press).

32. Melton HE Jr, Skorton DJ: Rational gain compensation for attenuation: a step toward quantitative two-dimensional echocardiography (abstr). Am J Cardiol 49:931, 1982.

33. Flax SW, Glover GH, Pelc NJ: Textural variations in B-mode ultrasonography: a stochastic model. Ultrasonic Imaging 3:235–257, 1981.

24. DIGITAL ANALYSIS OF ECHO-SIGNALS
FOR TISSUE CHARACTERIZATION

P. Jensch, J. Meyer, P. Schweizer, R. Erbel, W. Kubalski,
W. Krebs, W. Ameling and S. Effert

1. INTRODUCTION

Ultrasonic cardiac tissue characterization on the basis of signal-speed and signal-attenuation measurements is covered with problems [1]. It has been evaluated, however, that the frequency dependence of the attenuation coefficient is different in normal and infarcted myocardium [1]. Joynt et al have shown that the histogram of echo amplitude distribution taken from A-scans is shifted and broadened in da-maged myocardium [3]. These findings are obtained by applying Fourier transfor-mation, spectral analysis and other methods well known in the field of system theory.

The simplest class of commonly used measures is segment statistics such as mean, and variance. Such measures are easily computed and have been used effectively in the analysis of images where structures are less important than discrimination. More sophisticated methods are those which analyse structures by autocorrelation methods with selected templates.

Some effects of system theoretical methods can be visualized by using a second and third dimension. This opens the door for the application of image processing approaches. Our first results are derived from histogram evaluations. This ap-proach plays a fundamental role in establishing and classifying objects and regions. In the context of tissue characterization on the basis of B-mode image analysis the following problems are of concern:

- given a segment of a sector scan image
  to which of a finite number of classes does the segment belong?
- given a segment of a sector scan image
  how can it be described?
- given a whole sector scan image
  how can the boundaries between different tissue regions be established?

These problems cannot be solved by analysing single sector scan images. Because of the nature of the ultrasonic signal passing the tissue there are a lot of disturbances which are different from patient to patient. A satisfying answer can only be found after successful evaluation of a sufficiently large database. Therefore it is imperative to collect in vitro and in vivo relevant data.
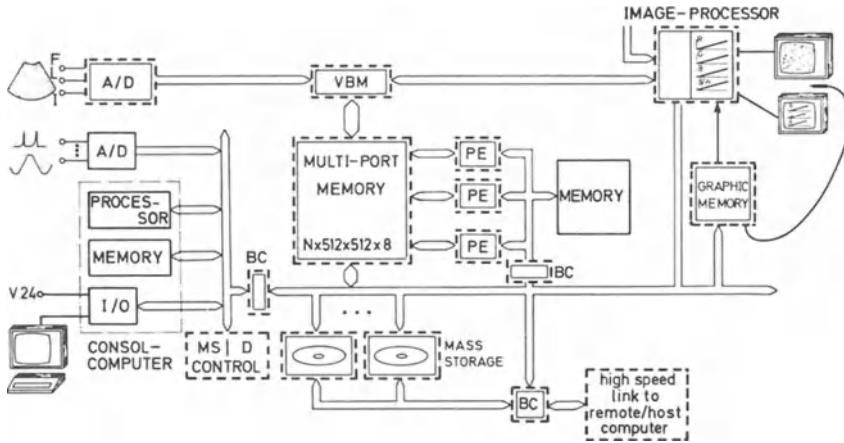
Figure 1. Image Sequence Processing System. (VBM = video bus module, BC = bus connection, MS/D control = mass storage/display control, PE = processing element) – description in detail within the text.

2. DATA REGISTRATION

For studies of ultrasound images we have developed an Image Sequence Processing System (see also [4]). The system (Figure 1) is primarily used for image enhancement and feature extraction. To allow other applications especially tissue characterization, the system permits the following task decomposition:

registration
– real-time data acquisition of ultrasound signals (also scenes of B-mode images)
– transient recording

processing
– image enhancement by real-time filtering
– fast off-line data processing.

The system has several data input channels as shown in Figure 1. A real-time output of a sector scanner (ultrasound signal itself or the equivalent video signal) may be connected to the analog-digital-converter (A/D). Along with each pulse transmitted by the ultrasonic scanner a scan start signal (L) is generated which initiates the sampling of the analog signal (I) and the buffering of the digitized values in the multi-port memory via the video bus module (VBM). For synchronization purposes a frame start signal (F) may also be used. Data are then transmitted from the memory to the mass storage devices. The whole system is controlled by a console computer (microprocessor system) which is capable of sampling ECG and pressure or of receiving digital data via a V.24 link. This link is the slow standard data exchange channel for some ultrasonic scanner.
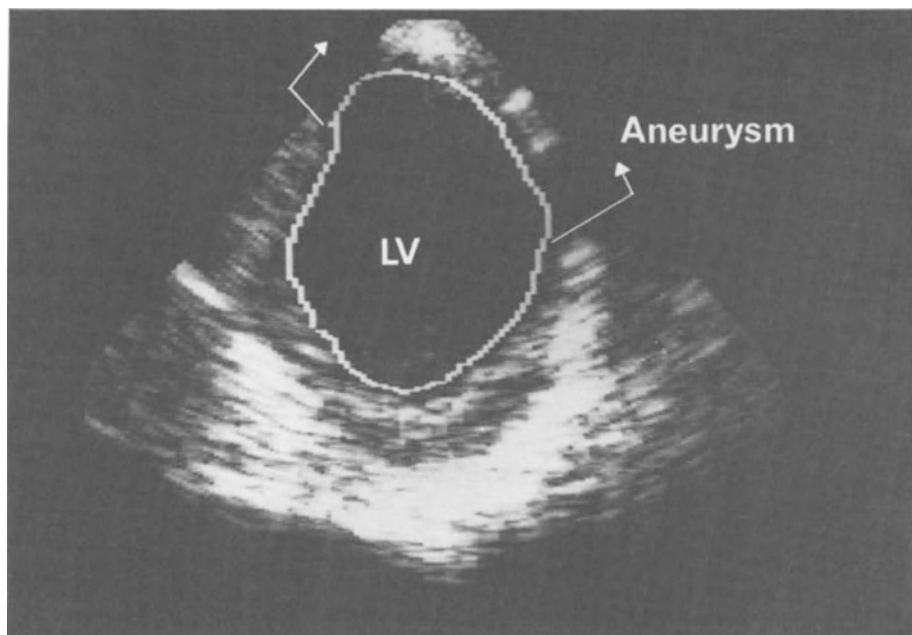
Figure 2a. Two-dimensional parasternal short axis cross section: left ventricular (LV) aneurysm of the anterior and lateral wall (arrows), encircled area: endocardial border.
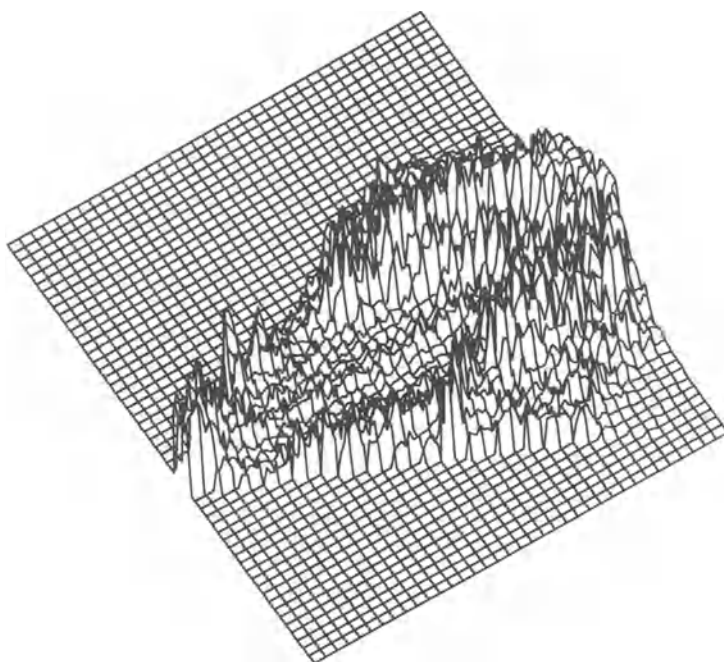
Figure 2b. Echo intensity plot of the two-dimensional short axis view of Figure 2a. The region of the aneurysm shows echo intensity patterns being different from those of the normal myocardial regions.
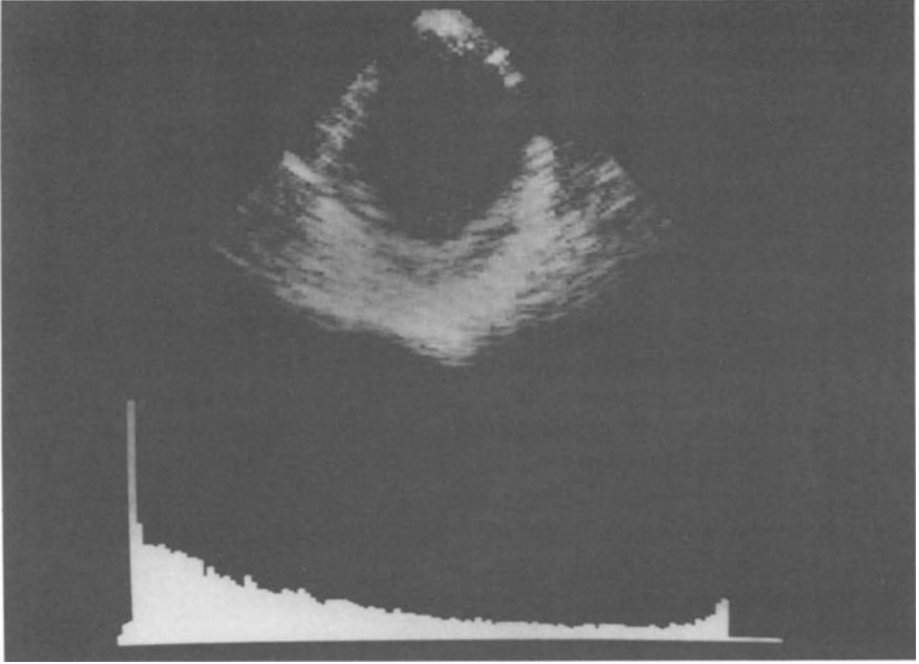
Figure 2c
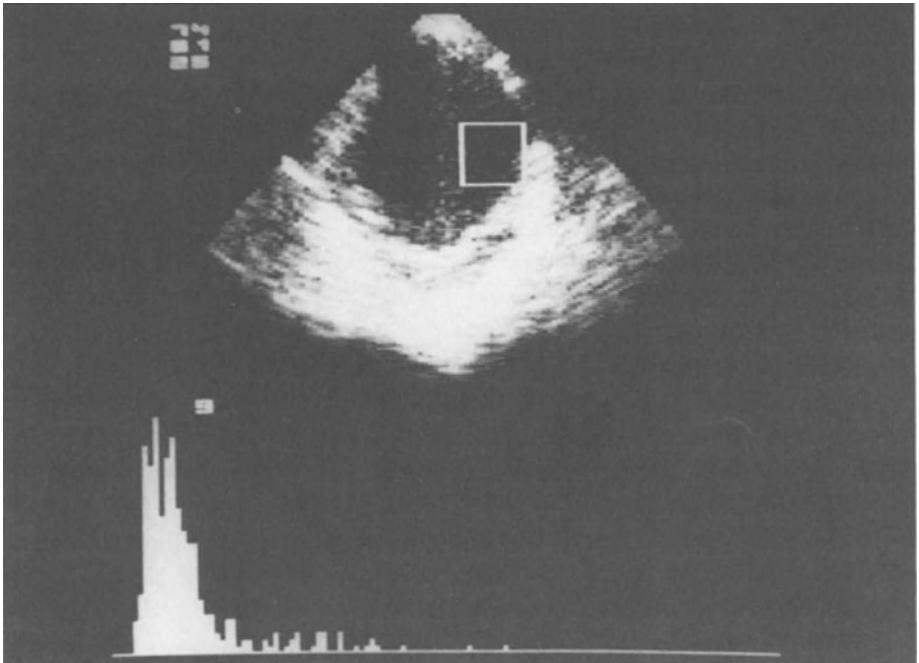
Figure 2d
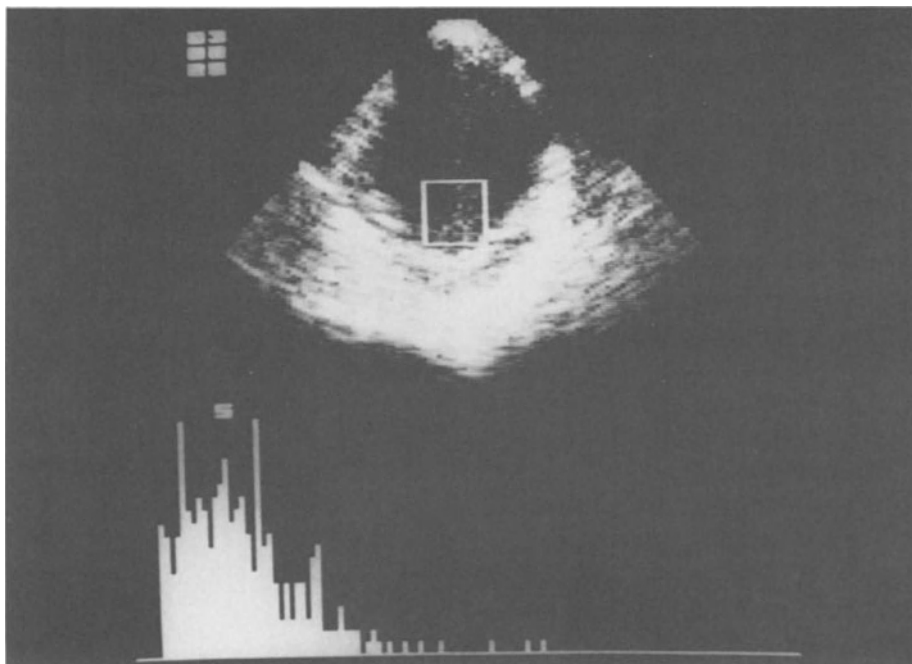
Figure 2e

Figure 2c–e. Echo histogram patterns of the two-dimensional short axis view of Figure 2a. The Figure 2c shows the histogram distribution of the whole cross section. The grey-level distribution of Figure 2d is quite normal, being in contrast to the grey-level distribution depicted in Figure 2b. Figure 2e depicts the histogram of a small myocardial window, selected at random. The distribution of grey-levels is also quite normal.

The system is prepared for transient recording at a sample rate of up to 20 MHz for a standard system configuration and a higher sample rate after extending the A/D converter. All sampling operations may be synchronized by the ECG which is evaluated by the console computer or the ultrasonic scanner. Data processing may be performed by:

– the console computer (speed is moderate)
  and/or
  the image-processor (a special hardware device for real-time processing)

For sophisticated processing a cluster of processing elements (PE) with a separate memory is foreseen.

Visualization is realized by the image processor which comprises programmable look-up-tables and an arithmetic unit. All operations are performed at video speed. Operations are:
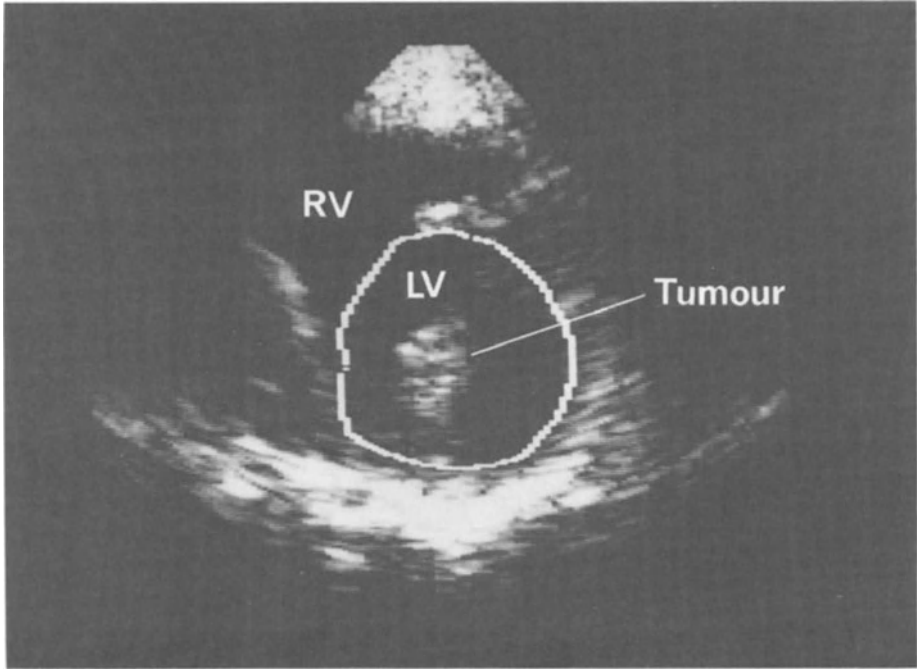
Figure 3a. Two-dimensional parasternal short axis view; registration of the prolapsing left atrial tumour within the left ventricular cavity (encircled area), RV = right ventricle, LV = left ventricle.
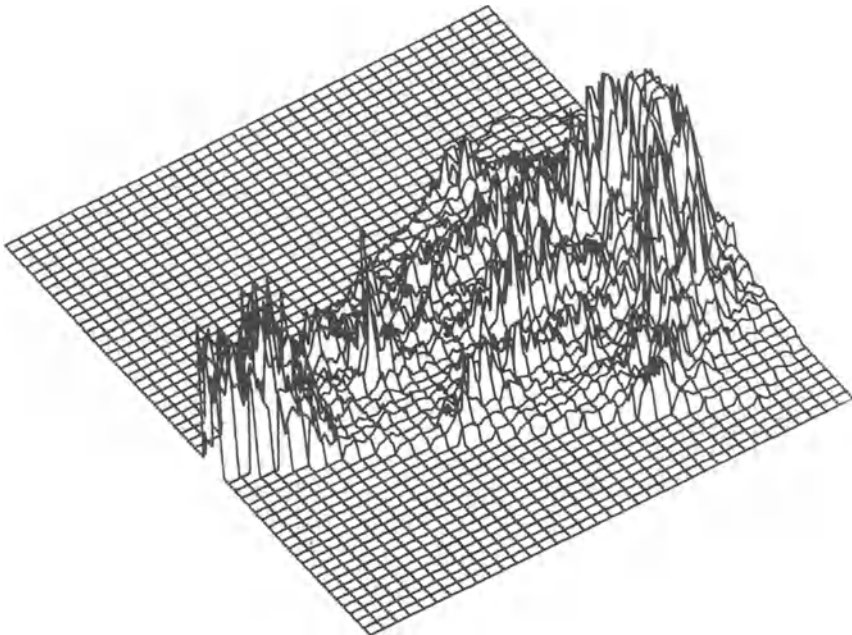
Figure 3b. Echo intensity plot of the two-dimensional parasternal short axis view of Figure 3a. The tumour region shows a distribution of echo intensities being different from that of the myocardium.
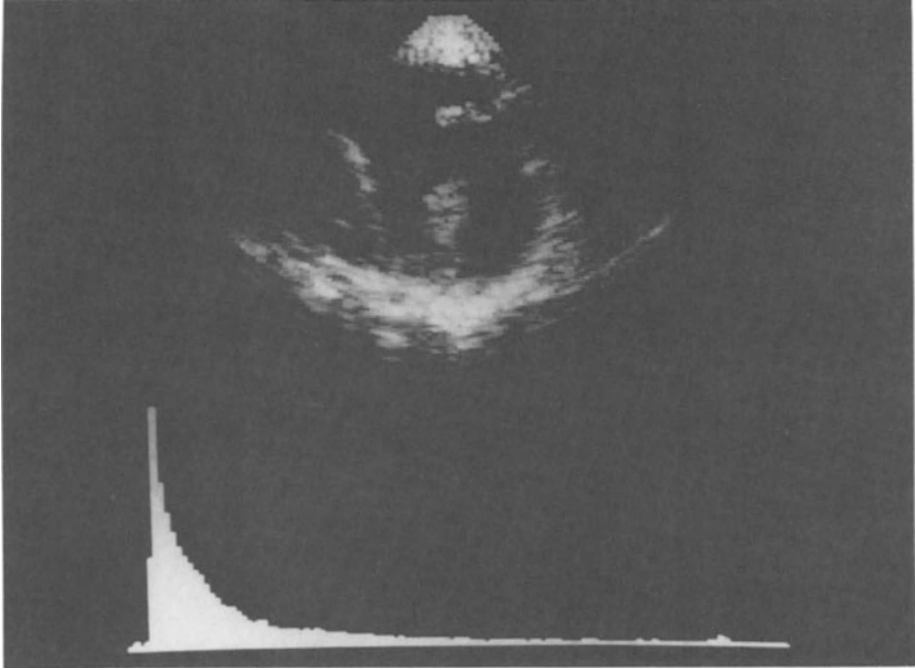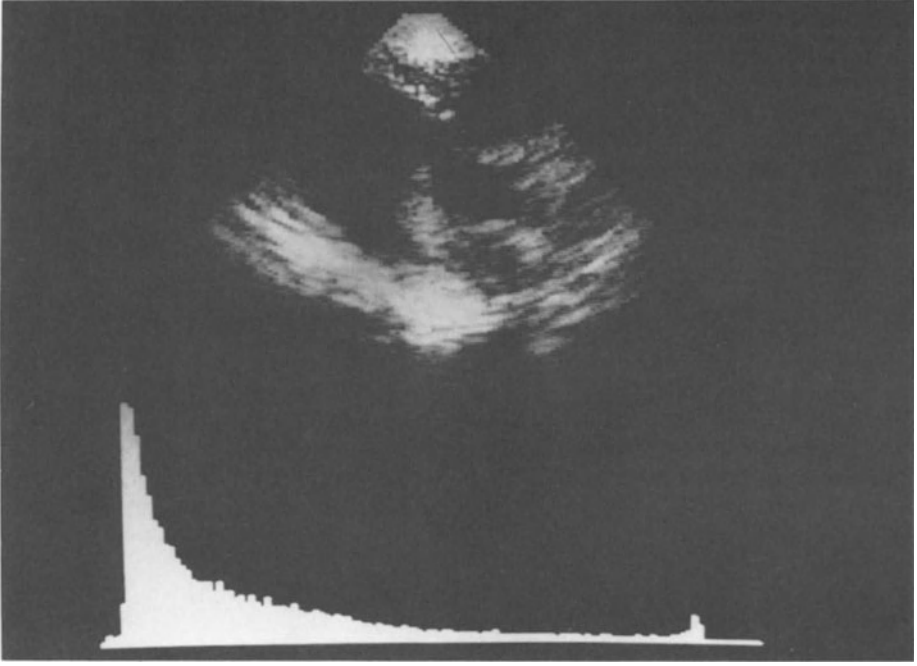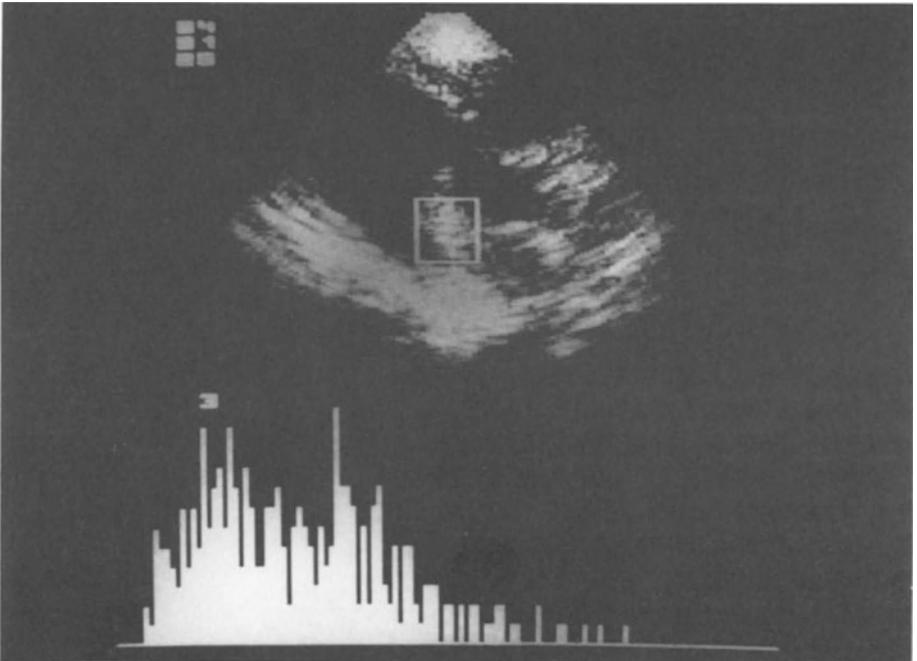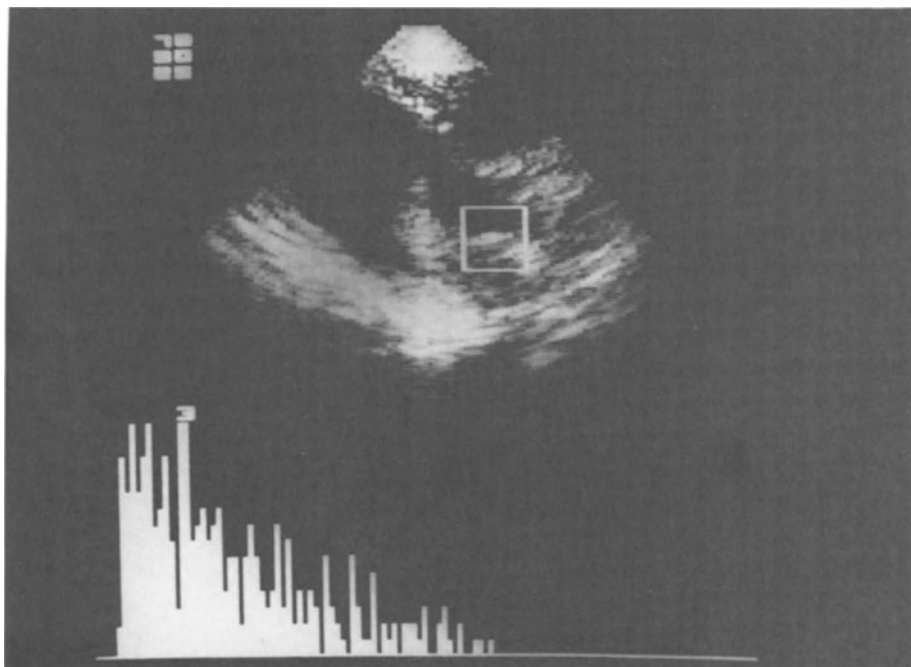
Figure 3c
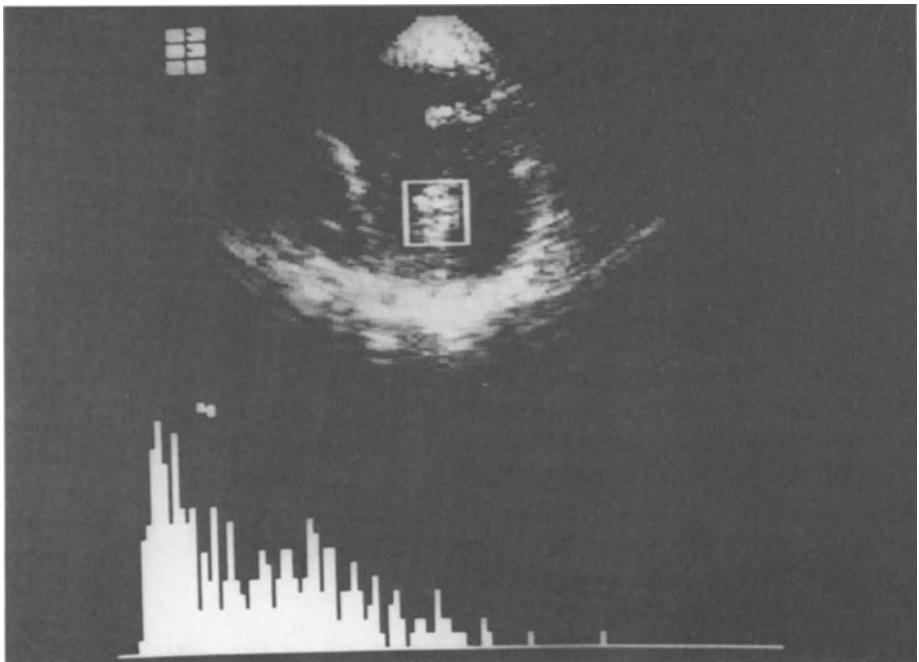
Figure 3d
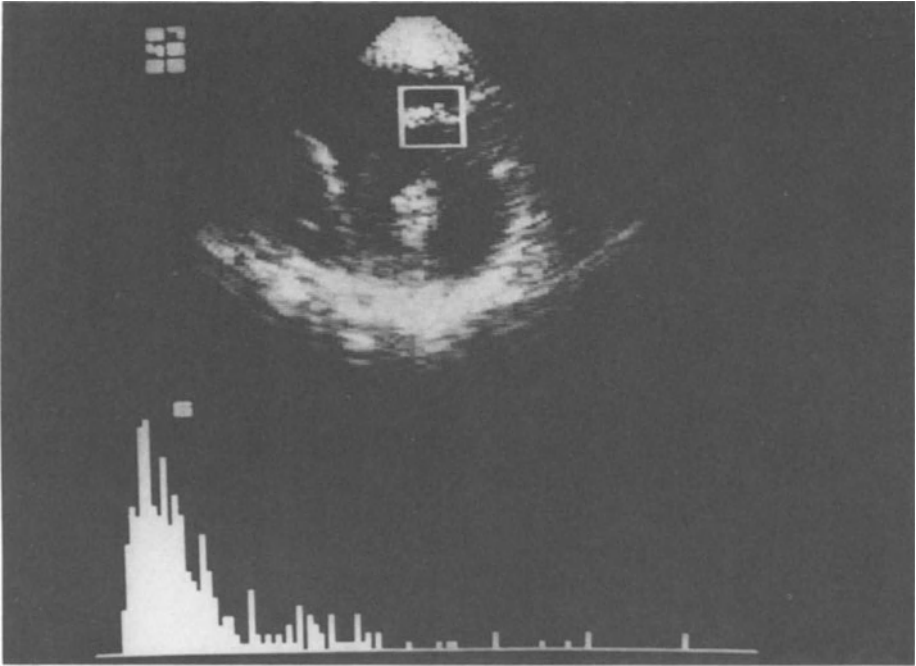
Figure 3e

Figure 3c–e. Echo histogram distributions of the two-dimensional short axis view. Figure 3c shows the histogram of the whole cross section. The distribution of the   of Fig 3d belongs to the rectangular window and shows abnormal echo characteristics. Figure 3e shows the histogram of a randomly selected region of the same window size as in Figure 3d. The grey-level distribution is quite normal.

○ normal addition,
○ normal subtraction,
○ weighted addition, and
○ weighted subtraction
    used instead of multiplication and division.

Operands of these operations may be part of pictures or even whole images passing the processing unit as data streams.

The graphic memory supports an additional bitplane which can be used for interactive image segmentation (contouring) with a lightpen or joystick.

Analysis with our Image Processing System is completely digital, i.e. the well known problems in analog signal processing are eliminated. But in digital processing there still remains the problem of noise caused by the nature of the ultrasonic signal. Noise filtering can be accomplished by smoothing algorithms. Postprocessing of numerical results must be performed with care because the image one ultimately sees is the visualized equivalent of the electrical signals from the trans-
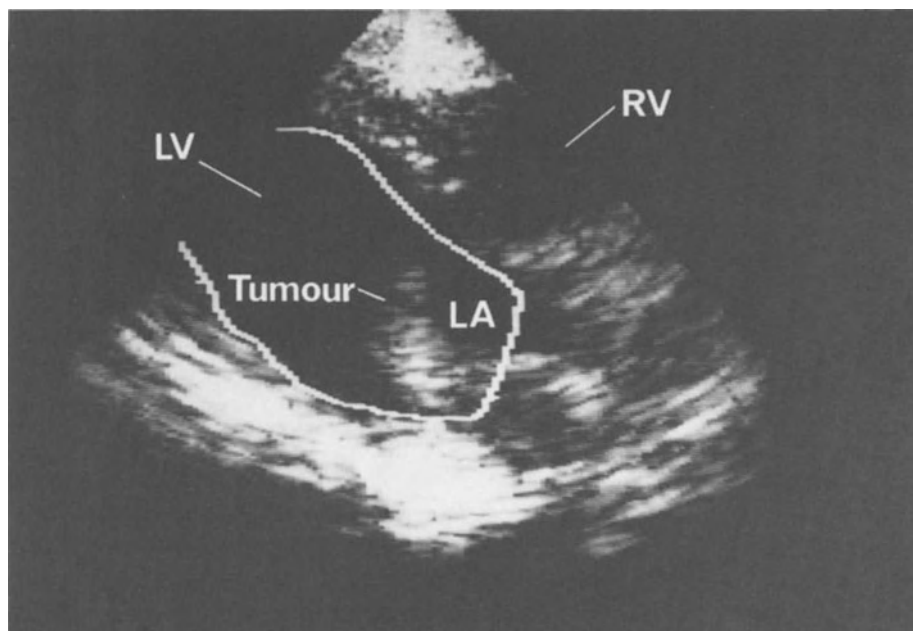
Figure 4a. Two-dimensional parasternal long axis cross section: demonstration of a large left atrial (LA) tumour (myxoma) prolapsing into the left ventricular cavity (LV). Within the encircled area left ventricular cavity and parts of the tumours. RV = right ventricle.
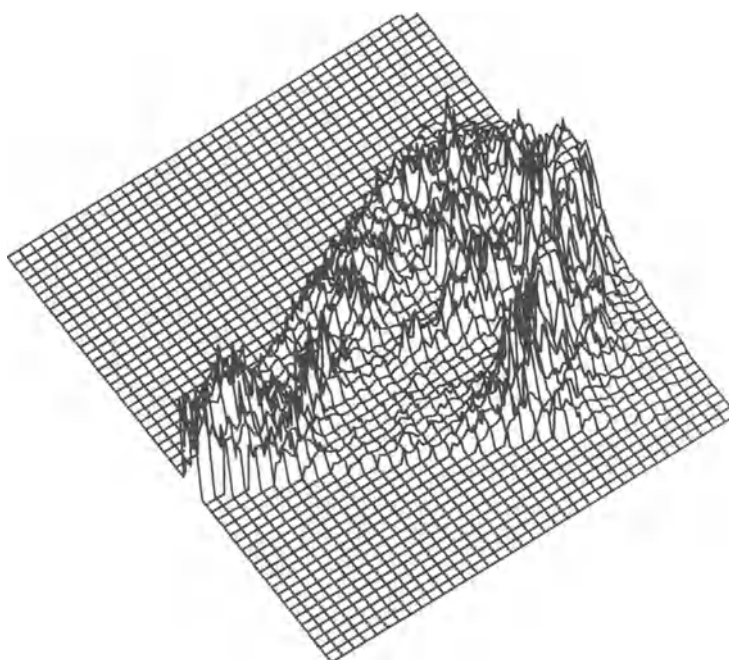
Figure 4b. Echo intensity plot of the two-dimensional long axis cross section of Figure 4a. The tumour region shows a distribution of echo intensities being different from that of the myocardium.

Figure 4c

Figure 4d

Figure 4e

Figures 4c–e. Echo histogram patterns of the two-dimensional long axis view of Figure 4a. Figure 4c is the histogram of the whole cross section. Figure 4d is the histogram distribution of the shown window, being significantly different from normal. Figure 4e shows the histogram pattern of an randomly selected region with a normal distribution.

ducer. By homomorphic filtering one can extract the effect of the transducer. What remains after that is a description of the material in the focal zone, i.e. the region of interest.

3. APPLICATION

While studying echocardiographic images we got the impression that within the images there might be some information which might correlate with tissue conditions. We observed different patterns in reflected echoes. The echocardiogram of Figure 2a is a short axis view of the left ventricle and in the upper part of this image there is an aneurysm. Under normal conditions one would expect echoes in this region. One gets an overview about the quality of the signals and structure information by viewing these grey leveled image in a 3-dimensional space – like a mountain view (Figure 2b). it is easily realized that the pictorial impression of the aneurysmic region is quite different from the normal tissue nearby.

Another example is given in Figures 3 and 4. The outer left ventricular boundaries are normal but within the cavity there are abnormal echoes caused by a prolapsing left artrial tumour. Figures 3b and 4b show the 3-dimensional representation.

Figures 2b–e, 3b–e and 4b–e show grey-level histograms of the original figures. We observed that histograms according to Figures 3d and 4d are typical and clearly different from histograms of other regions.

It can be seen from most of the histograms that the relevant content of information is related to signals of low amplitudes. This condition may be considered when defining the colour-look-up-tables in order to obtain enhanced pictures (as demonstrated in the oral presentation).

The currently available histogram software employs two methods to calculate its transformation specifications:

(1) a region of interest is interactively definable for transformation in the large and
(2) for motion analysis the region of interest may be frozen and the transformation parameters may be changed in certain time intervals.

To verify these findings we have set up a screening program to collect relevant ultrasonic data for in vitro and in vivo tissue characterization. With this database we try to verify some results which are mentioned in the literature by some researchers and obtained by the analysis of signal speed and signal attenuation as well as data scattering. Independently of this comparison we register patterns of one- and two-dimensional histograms. Our aim will be to decribe histogram patterns which correspond to tissue conditions. As can be anticipated by the 3-dimensional representation, this may go on with consideration of the context, i.e. the structure type of grey level intensities or with consideration of anatomy information.

We think that these selected examples show that it is reasonable to continue with our studies in finding correlations between echo-patterns and tissue types.

Since the information obtained for this purpose is of such a critical character a greater understanding of the interaction between ultrasound and tissue is necessary. Typical sector B-scan pictures contain extra information, decribed as anomalies. To locate artefacts motion analysis may give some additional information. This problem again is another motivation for an appropriate database.

4. SUMMARY

We are in the process of exploring a pattern recognition approach to tissue characterization. We have built an experimental system and used it to several B-scans. In the cases in which we were able to compare our results with the medical diagnostics we found that tissue regions can be segmented by a histogram method. Because of our encouraging initial experiments we have extended our Image Sequence Process-

ing System to establish a database. We plan to perform further evaluations to obtain correlation figures between automatically segmented regions of B-scans and tissue types.

REFERENCES

1. Chivers RC: Tissue characterization. Ultrasound in Med Biol 7:1–20, 1981.
2. Wells PNT: Present status of tissue identification. In: H. Rijsterborgh, ed: Echocardiology 455–460, 1981.
3. Joynt L, Martin R, Macovski A: Techniques for in vivo tissue characterization. Acoustical Imaging 8:527–538, 1980.
4. Ameling W: Computer structures for digital imaging (in this volume).

25. DIGITAL TWO-DIMENSIONAL ECHOCARDIOGRAPHY: LINE-MODE DATA ACQUISITION, IMAGE PROCESSING, AND APPROACHES TO QUANTITATION

ANDREW J. BUDA, EDWARD J. DELP, JANICE M. JENKINS, DAVID N. SMITH, CHARLES R. MEYER, FRED L. BOOKSTEIN AND BERTRAM PITT

Two-dimensional echocardiography (2D echo) is a powerful noninvasive technique for the diagnosis of cardiac disease. This technique is particularly well suited to left ventricular functional analysis, in view of the many unique tomographic views that are available for study. However, the assessment of left ventricular function by 2D echo remains largely qualitative because of intrinsic limitations of the ultrasound data, poor border definition in the stop frame video image, and the tedium of manual tracing of appropriate images. Despite these limitations, operator defined 2D echo video images of tomographic left ventricular sections have yielded important quantitative information concerning left ventricular volume [1, 2], mass [3], and function [4, 5] with acceptable error. Further developments in computer processing of the 2D echo images will improve the assessment of these parameters.

Automatic computer processing of 2D echo images would avoid the excessive time, labor, and subjectivity of manual tracing and would ultimately improve the reliability and validity of quantitative measures. Various published techniques [6–10] for digitizing single frames of 2D echo information are unsatisfactory because of the lengthy time required for digitizing a simple frame of information, which eliminates any real-time capability, and the significant deterioration of the image as it is transferred through several optical systems into the computer memory.

Garcia et al [11] described an interface to a standard medical imaging computer from the video-output of the 2D echo unit or its video tape recorder. After space-time smoothing, beat to beat and frame by frame, they were able to automatically detect endocardial interfaces by standard threshold and second derivative methods. Skorton et al [6] digitized ultrasound data by an optical densitometer then submitted it to multiple image averaging and grey level thresholding. Measures of wall thickness and left ventricular internal dimensions from the computer processed 2D echo images correlated well with the same measurements from M-mode; correlations using the unprocessed 2D echo images were much worse.

This report summarizes our recent work in computer acquisition and processing of 2D echo images for the purpose of quantifying left ventricular global and regional function. Our efforts initially involved acquisition and processing of 2D echo video data, [12] but, more recently, we have developed a method of direct line mode data acquisition for 2D echo [13] which we presently employ. Using the
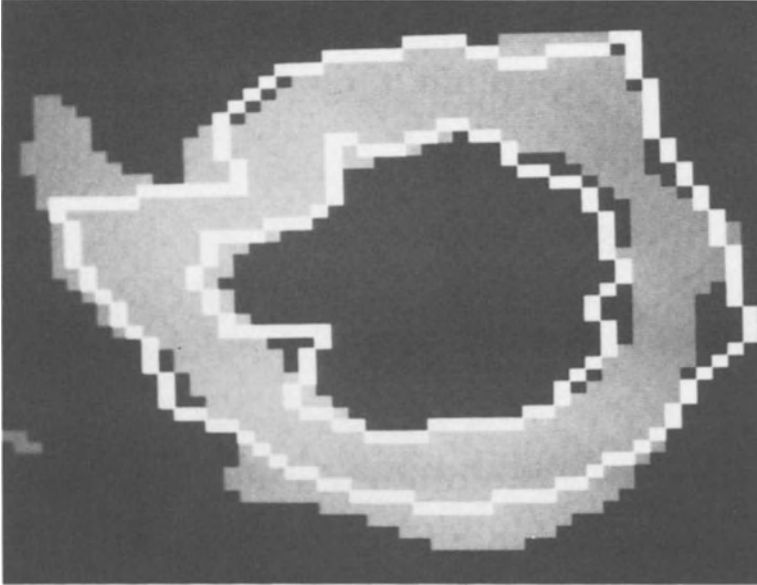
Figure 1. A parasternal left ventricular short-axis video-output acquired 2D echo image following processing with superimposition of endocardial and epicardial edges.

directly acquired data, we have used a number of edge detection algorithms to determine most anatomically appropriate borders. In parallel with this, we have developed a program for left ventricular functional analysis which we presently employ for our clinical and research studies.

DIGITIZATION AND PROCESSING OF 2D ECHO VIDEO DATA

Our initial attempts at computer processing of 2D echo images were performed using a medical imaging system coupled to the video output of our 2D echo unit [12]. The imaging system (A², Medical Data Systems, Ann Arbor, Michigan) consisted of a Nova III Central Processor Unit, 48K 16-bit word main frame memory, a 5 megabyte magnetic disk, a video display with 512 × 512 pixel resolution and 256 gray level representation. The parasternal left ventricular short axis at the midpapillary muscle level was digitized into a 64 × 64 array at 30 frames per second and stored on magnetic tape for further processing. A total of 20 cardiac cycles were collected, ECG gated on the R wave.

   These digitized data were transferred via magnetic tape to the University of Michigan Computer and Image Processing Research Network (CIPRNET). This facility consists of a Dec Vax II/780 with four megabytes of main memory, two 28 megabyte disks, two 300 megabyte disks, a Ramtek 9300 image display system, and
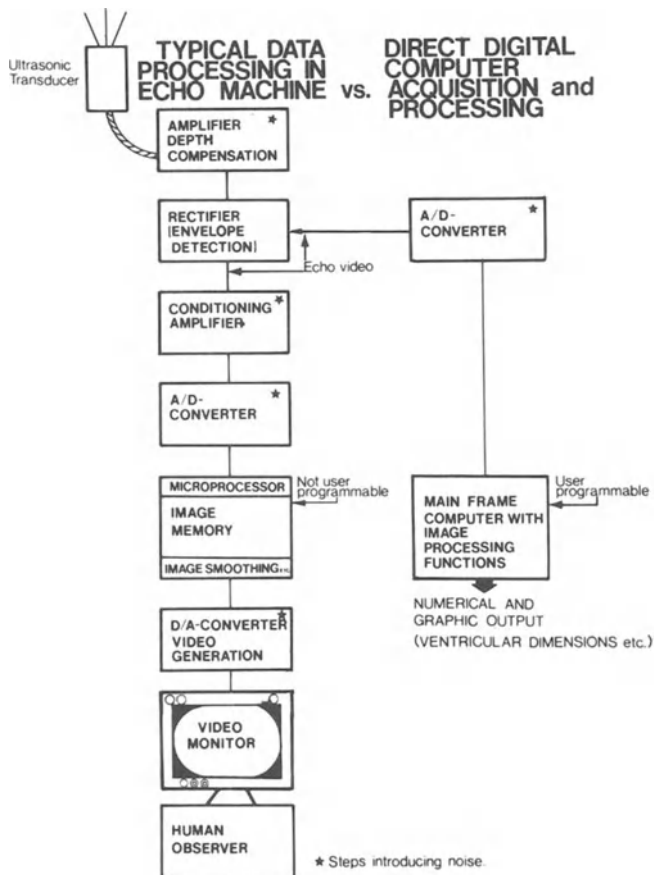
Figure 2. A block diagram outlining the processing steps in a commercial sector scanner and our method of direct digitization of the envelope detected signal. Note that several steps of noise introduction are avoided by the direct digitization.

a DeAnza IP 600 image processor. The system operates under the UNIX operating system. All programs for echo image analysis were written in the language C.

Our processing began with the spatial averaging of time-aligned frames to produce a composite cardiac cycle of 29 images. Spatial smoothing further eliminated noise. An axially applied gradient method using 12 radial chords spaced 30 degrees apart and originating at the center of the ventricular cavity was used to identify endocardial and epicardial boundaries. This approach produced short axis left ventricular images that were anatomically appropriate (Figure 1).

Our initial experience with digitization of video 2D echo data suggested to us that further improvements in real-time data acquisition at the source would be required for improved results.
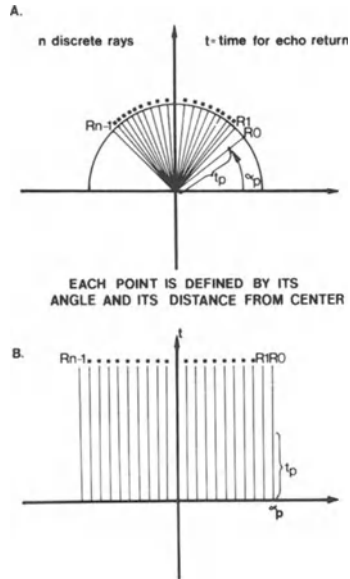
Figure 3. Schematic illustration of the mapping of the sector B-mode fan format (A) into a rectangular matrix (B).

REAL TIME LINE MODE DATA ACQUISITION

In their review, Wells and Woodcock [14] distinguished between two approaches to echo signal digitization. They termed methods which digitized the usual visual output of the echo unit "digitization of analog recordings" and termed methods in which the RF-signal or the envelope detected signal was directly fed to an A/D converter "direct digitization". The term "line-mode data" has been applied to data digitized along the ultrasonic line of sight with positional information [15].

To further improve the data at its source, we implemented direct line mode digitization of our 2D echo data (Figure 2). The computer system used consisted of a Nova 4 Central Processor Unit, 96K 16-bit word main frame memory, a 92.5 megabyte magnetic disk, a video display with 512 × 512 pixel resolution and 256 gray level display. We modified our computer's video A/D-converter for horizontal and vertical synchronization by external digital signals. The analog section was rebuilt to adapt to the post-TGC envelope detected RF signal from the echo machine. The pixel clock which determines the sampling rate along a line was set to 2 MHz.

From the digital-beam steering logic in the phased array echo machine, two synchronization signals are derived: one for the firing of the center transducer element and one at the beginning of the first fan beam. The envelope detected signal is amplified and transmitted directly to the A/D converter through a coaxial cable. Synchronization signals are sent through line drivers and coaxial cable to the
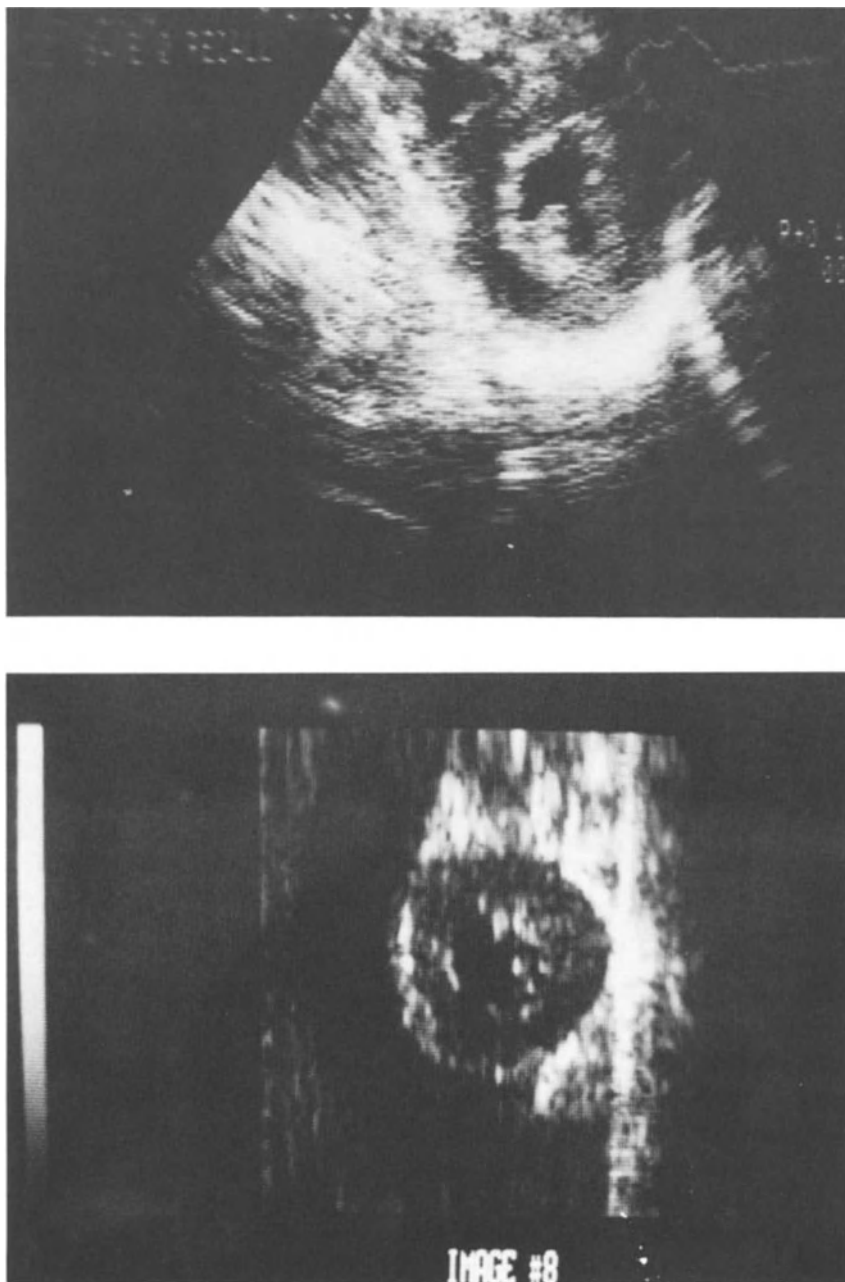
Figure 4. (Top) a parasternal left ventricular end-systolic 2D echo image taken directly from the video display. (Bottom) the same image acquired using directly line mode digitization. There is some distortion of the hape of the left ventricle because of the rectangular matrix format but endocardial and epicardial definition is improved.
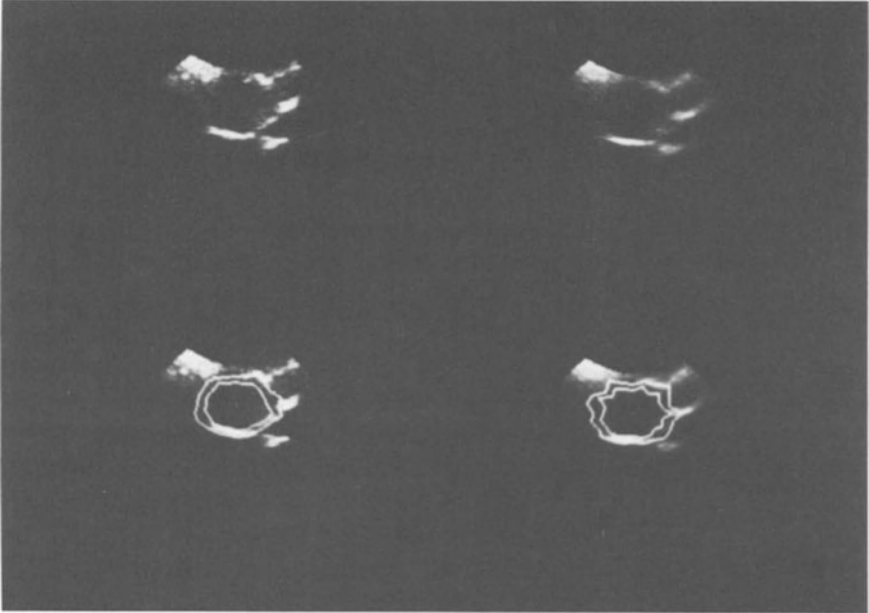
Figure 5. Effect of preprocessing using spatial and temporal smoothing on line mode data interpolated to sector format. Upper left: original image; lower left: original image with edges overlayed; upper right: image after spatial and temporal smoothing; lower right: smoothed image with edges overlayed. Note the distortions in the endocardial and epicardial borders produced by the smoothing process.

synchronization input of the A/D converter. The process is controlled by an assembly language program with the same features as the TV-image digitization control programs, except that the image size is flexible to 128×256 pixels. R wave triggering is used to synchronize the digitization.

The B-mode signal fan rays are thus mapped into a rectangular matrix (Figure 3). Since 128 fan lines are produced by the echo machine and all of them are digitized, there is no data loss within a single fan frame (Figure 4). However, the digital transfer rate of the whole frame to magnetic disk is too slow to begin acquisition of the next fan frame. Thus only every other fan frame is digitized. The row index of a matrix element is the ray number in which a specific resolution element was sampled; the column index is the time of sampling measured from the center element transmit pulse. Only straight lines through the center of the source data coordinate system map into straight lines in the rectangular data matrix. An M-mode reconstruction from the columns of the rectangular matrix represents M-mode lines along the fan lines; an M-mode reconstruction along any other line is possible using the mapping function. Frame to frame and cycle to cycle averaging techniques for noise reduction are implemented easily in the software of this system using the programming language.

University of Michigan
Regional Echo Report   File: D2BASE
Global Ejection Fraction = 59.54%

Diastole   Systole

Area Ejection Fraction   Wall Thickness Change
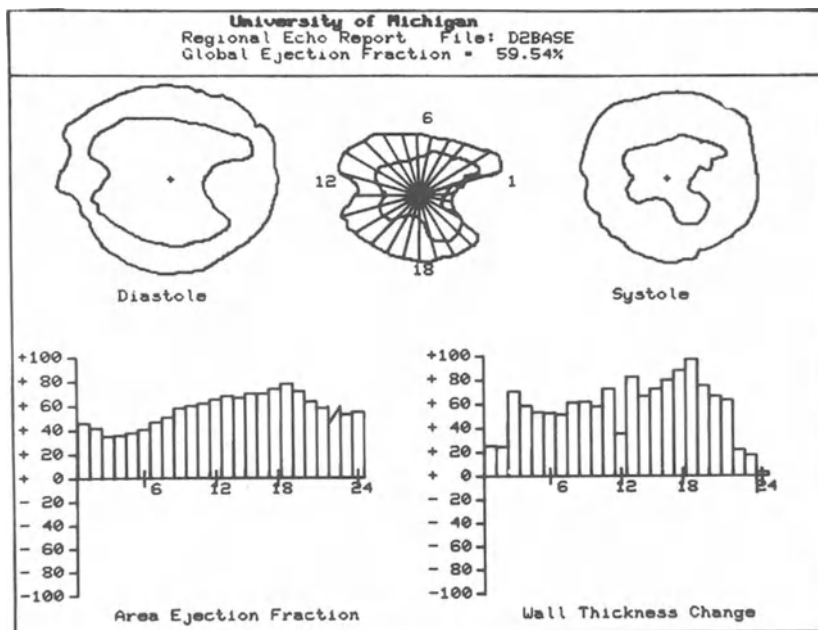
Figure 6. Regional analysis program used for quantitative 2D echo studies. See text for details.

DIGITAL PROCESSING OF LINE-MODE DATA

The digitized line-mode data was processed using our previously described algorithms [12]. For this data, cycle-averaging and spatial smoothing may not be necessary. In fact, the edges found for each image in a cycle have fewer artifacts and tend to preserve edge connectivity throughout the cycle (Figure 5).

We are extending these results by treating the edge detection problem using dynamic scene analysis. We plan to use boundary locations in one frame to aid in finding edges in previous and subsequent frames. We have just begun to apply time-varying edge detectors to our 2D echo data and our preliminary results appear promising.

After further processing, we will examine various shape descriptors for use as indices of cardiac status. The development of new shape descriptors based on local radius of curvature should provide further information regarding left ventricular function.

QUANTITATIVE ANALYSIS OF THE LEFT VENTRICULAR IMAGE

In parallel with our efforts at 2D echo direct line mode digital acquisition, image

processing and edge detection, we have developed a program to analyze regional left ventricular function. This analysis may be applied to any left ventricular short-axis projection and the derived data in combination with long-axis data may be used to estimate global left ventricular function and mass using well described algorithms, such as Simpson's rule.

In this analysis, the endocardial and epicardial borders of the left ventricle at end-diastole and end-systole are manually entered into the computer using a Tektronix digitizing tablet. A menu displayed on the image device guides and prompts the operator for data input. The data input consists of epicardial and endocardial borders, external alignment points for the systolic and diastolic images and five centimeter magnification calibration points. once all the data have been entered, the program calculates the center of mass of the diastolic endocardial border, the rotation angle and translation coordinates for alignment of the systolic borders over the diastolic borders. These aligned borders are then stored in a protected disk file for archival and research use. All calculations are performed using the center of mass of the end-diastolic endocardial border as the reference point. The continuous borders are divided into 24 segments, each of 15 degrees, for calculation of regional ejection fraction, regional wall area, and regional wall thickness (Figure 6). There is a graphical display of proportional change, diastole to systole, along with the segmented systolic and diastolic borders.

We have used this approach to regional left ventricular analysis in a chronic canine model of acute coronary occlusion and reperfusion to investigate myocardial functional response to reperfusion in specific segments according to pathologic data. Our approach should be useful in the quantitative evaluation of acute ischemic syndromes in animal models and in man.

DISCUSSION

The interpretation of left ventricular function by 2D echo has largely remained a descriptive technique requiring expert observers. Quantitative analysis has involved manual delineation of endocardial and epicardial boundaries of end-diastolic and end-systolic frames by trained operators. Other frames of the cardiac cycle are generally not analyzed because of the time and labor involved.

The ability to further automatically process these 2D echo images should improve our ability to quantitate 2D echo data, provide a more objective approach to interpretation, and improve inter-observer variability. The major limiting factor to the development of computer processing of 2D echo has been the long acquisition times required to digitize a single frame of data. Digital interfaces specific to ultrasound make it possible to acquire digital 2D echo data in real-time. Owing to the inherent complex interaction of ultrasound in tissues and the several steps of processing that occur within the commercial 2D echo unit, this digitized data is unfortunately noisy.

In our initial approach to acquisition of 2D echo data, the video output of the unit [12] was digitized. This method has several flaws. First, the resampling process required to form a video image from the line mode data tends to produce under-sampling of data in the near field and oversampling in the far field. Second, the ultrasound frame generation does not necessarily match the video frame rate. Third, the scan converter within the echo unit maps the information into a range of gray values with a dynamic range matched to the human visual system; however, the usable dynamic range of the data is significantly greater. Fourth, the averaging technique for speckle reduction is usually not under user control. Fifth, the video image data depends on the processing performed by the echo technician who varies the control settings on the echo unit to achieve an image which looks "best" to the human observer; however, this image may not necessarily be optimal for computer processing.

For these reasons, we presently approach the digital acquisition of 2D echo data through direct line mode digitization [13]. With this approach, RF envelope detected data are digitized before data transfer to the digital scan converter. This avoids the introduction of noise at several levels of data conversion and provides improved signal to noise ratios.

Robinson and Williams [15] indicated that this method is superior to other methods of digitization for 2D echo processing. In addition, this line mode digitization method has several advantages compared to conventional video image digitization. (1) The ultrasound frame generation rate is equal to the A/D frame conversion rate; this condition is not necessarily fulfilled by video image digitization. (2) The envelope detected signal is independent of all control settings on the echo unit except for gain control. (3) The dynamic range of the 8-bit line mode data significantly exceeds that of the typical 4- to 6-bit output of the digital scan converter used for video data acquisition. For these reasons, we believe that line mode data digitization is presently the preferred method of ultrasound data acquisition for computer processing.

Image processing and algorithm development have been undertaken at our CIPRNET facilities. After applying Laplacian, Sobel, trapezoidal and high pass filtering edge detection routines, our previously described approach of axial gradient edge detection appears to be the simplest and most accurate detector for providing anatomically appropriate endocardial and epicardial definition. With the line mode digitization, temporal and/or spatial smoothing may produce artifacts in our automatically derived edges. These smoothing techniques may be better suited to 2D echo video data for which they provide some improvement in signal to noise ratios.

Further algorithm development, testing, and validation are required before clinical applications of these techniques can be attempted. Although our axial gradient technique is useful, we believe that edge detection would be improved by using a time-varying image analysis approach in which edge redundancy in frame by frame analysis would be used to provide further improvement in edge tracking. This form

of dynamic scene analysis has been used in other imaging problems with success [16, 17].

Assuming that appropriate edges can be found and validated, a quantitative approach to global and regional analysis would then be necessary. Several attempts at left ventricular function quantitation have been attempted with manually defined edges with variable success [1–5]. Although good correlations with gold standard measurements have been achieved, there remains 10% to 20% variability in the measurement of left ventricular volumes and mass. This variability derives from tomographic trajectory, poor endocardial definition, observer error and, of course, additional variability of the gold standard method. For instance, in contrast left ventriculography, the contrast material produces volume loading and a negative inotropic effect [18] contributing to discrepancies with other imaging techniques. Automatic methods of edge detection and quantitation for 2D echo should reduce inter-observer variability but will not influence these other factors, which require different solutions. A major impact of automatic quantitated processing will be the time saved in analysis and the ability to measure dynamic information contained within the entire cardiac cycle.

The quantitative analysis of regional function which we have developed is similar to approaches previously described [5, 11]. However, controversy continues regarding the use of coordinate systems and correction of three dimensional movement [19]. This problem is best illustrated by the variability of regional analysis depending on whether a fixed or floating center of mass is used. Although axial coordinates have been traditionally used with most cardiac imaging modalities, the unique tomographic information provided by 2D echo permits an approach to shape descriptors using Fourier shape analysis or mean tensor analysis [20]. These forms of analysis may circumvent the problem introduced with a coordinate, axial approach to quantitative regional left ventricular function.

We anticipate further improvements in digital data acquisition, image processing, development of edge detection algorithms, and methods of quantitation of 2D echo images. These improvements should then provide a basis for meaningful three dimensional reconstruction of 2D echo images.

REFERENCES

1. Wyatt HL, Heng MK, Meerbaum S, Hestenes JD, Dula E, Corday E: Cross-sectional echocardiography. II. Analysis of mathematical models for quantifying volume of the formalin-fixed left ventricle. Circulation 61:119–1125, 1980.
2. Schiller NB, Acqnatella H, Ports TA, Drew D, Goerke J, Ringertz H, Silverman NH, Brundate B, Botvinick EH, Boswell R, Carlsson E, Parmley WW: Left ventricular volume from a paired biplane two-dimensional echocardiography. Circulation 60:547–555, 1979.
3. Wyatt HL, Heng MK, Meerbaum S, Hestenes JD, Cobo JM, Davison RM, Corday E: Cross-sectional echocardiography. I. Analysis of mathematic models for quantifying mass of the left ventricle in dogs. Circulation 60:1104–1113, 1979.

4. Folland ED, Parisi AF, Moynihan PF, Jones RJ, Feldman CL, Tow DE: Assessment of left ventricular ejection fraction and volumes by real-time two-dimensional echocardiography. A comparison of cineangiographic and radionuclide technique. Circulation 60:760–766, 1979.
5. Parisi AF, Moynihan PF, Folland ED, Feldman CL: Quantitative detection of regional left ventricular contraction abnormalities by two-dimensional echocardiography. II. Accuracy in coronary artery disease. Circulation 63:761–767, 1981.
6. Skorton DJ, McNary CA, Child JS, Shah PM: Computerized image processing in cross-sectional echocardiography. Am J Cardiol 45:403–486, 1980.
7. Matsumoto M, Matsuo H, Kitabatake A, Inoue M, Hamanaka Y, Tamura S, Tanaka K, Hiroshi A: Three-dimensional echocardiograms and two-dimensional echocardiographic images at desired planes by a computerized system. Ultrasound Med Biol 3:163, 1977.
8. Matsumoto M, Matsuo H, Kitabatake A, Inoue M, Hamanaka Y, Tamura S, Tanaka K, Hiroshi A: Three-dimensional echocardiograms and two-dimensional echocardiographic images at desired planes by a computerized system. Ultrasound Med Biol 3:163, 1977.
9. Garrison JB, Weis JL, Manghan WL, Tuck ON, Guier WN, Fortuin NJ: Quantifying regional wall motion and thickening in two-dimensional echocardiography with a computer-aided contouring system. In: Computers in Cardiology. Long Beach, September, 1977, pp. 25–35, IEES Computer Society.
10. Skolnick ML: A new approach to ultrasound image recording using a video disk recorder. Radiology 133:530, 1979.
11. Garcia E, Gueret P, Bennett M, Corday E, Zwehl W, Meerbaum S, Corday S, Swan JHC, Berman D: Real time computerization of two-dimensional echocardiography. Am Heart J 101:763–792, 1981.
12. Jenkins JM, Qian G, Besozzi M, Delp EJ, Buda AJ: Computer processing of echocardiographic images for automated edge detection of left ventricular boundaries. Computers in Cardiology, 1981, pp. 391–394.
13. Splittgerber FH, Bach CG, Smith DN, Buda AJ, Pitt B: Digital line mode data acquisition for a phased array cardiac ultrasound scanner. Ultrasonic Imaging 4:198–199, 1982 (abstr).
14. Wells PNT, Woodcock JP: Computers in ultrasonic diagnostics. Forest Grove, Oregon, Research Studies Press, 1977.
15. robinson DE, Williams BG: Computer acquisition and processing of ultrasonic data In: Kazner E et al (ed), Ultrasonics in Medicine Excerpta Medica, pp. 96–102, 1975.
16. Martin WN, Aggarwal JK: Survey: Dynamic Scene Analysis. Computer Graphics and Image Processing 14:12–18, 1981.
17. Yachida M, Ikeda M, Tsuji S: A plan-guided analysis of cineangiograms for measurement of dynamic behavior of heart wall. IEEE Trans on Pattern Analysis and Machine Intelligence, IEEE. PAMI-2, No. 6, Nov. 1980, pp. 537–543.
18. Vine DL, Hegg TD, Dodge HT, Steward DK, Frimer M: Immediate effect of contrast medium injection of left ventricular volumes and ejection fraction. Circulation 56:379, 1977.
19. Clayton PD, Jeppson GM, Klausner SC: Should a fixed external reference system be used to analyze left ventricular wall motion? Circulation 65:1518–1521, 1982.
20. Bookstein FL; The measurement of biological shape and shape change. Lecture notes in biomathematics, V. 24. Spring-Verlag, 1978.

26. ANALYSIS OF MYOCARDIAL STRUCTURE
BY COMPUTED TOMOGRAPHY

K. LACKNER, O. KÖSTER AND P. THURN

Computed tomography of the heart represents an expansion of the non invasive roentgenological diagnosis of cardiac lesions

1. by the representation of the heart in a horizontal sectional image, free from overlapping effects, with the resulting additional anatomical information;
2. by the visualization of all chambers of the heart in a single examination;
3. by the direct demonstration of the ventricular septum and ventricular myocardium;
4. using ECG-gated cardio-CT, by the non invasive assessment of ventricular wall motion;
5. by the non invasive demonstration of coronary bypass perfusion.

By intravenous injection of approximately 250 ml 65% contrast medium, intermittently throughout the duration of the examination a difference in density between the cavities of the heart and the myocardium adequate for CT-imaging is achieved. Ungated cardio-CT is handicapped by more or less distinct motion artefacts. Nevertheless, good imaging results are possible with respect to the morphological point of view. ECG-gated cardio-CT enables the image reconstruction of the heart in diastole and systole or any position in between with a time resolution of approximately 0.1 s and allows functional assessments. The normal anatomy of the heart in ungated and ECG-gated cardio-CT is demonstrated in Figure 1. The analysis of myocardial structure in cardio-CT is based on:

1. measurement of the wall thickness;
2. measurement of the tissue density;
3. assessment of size, shape and wall motion of the cavities.

The increased wall thickness of the left ventricle in the course of pressure overload is well demonstrated in the ungated CT-image (Figure 2). ECG-gated cardio-CT in addition demonstrates the systolic thickening of the intact myocardium, the wall motion and the residual blood volume [2, 7, 10, 12, 14, 15, 18].

Quantitative assessment of the myocardial thickness is possible by means of cardio-CT. Points of measurement are the interventricular septum and the lateral
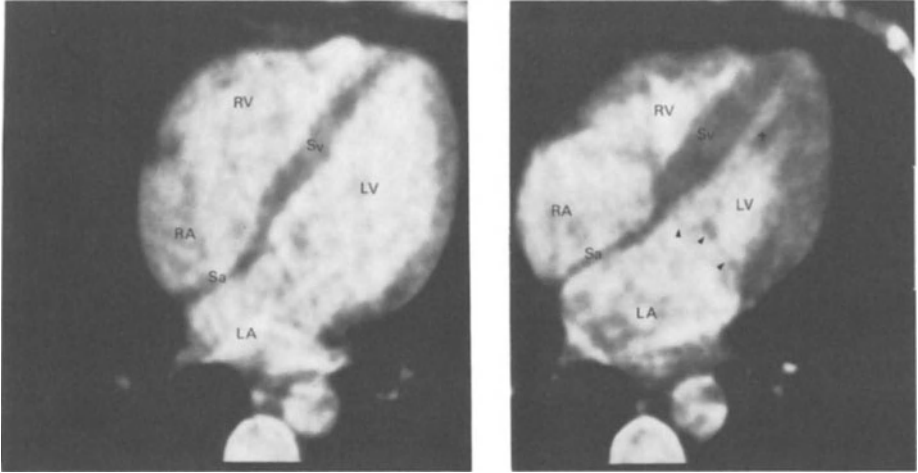
Figure 1. Normal anatomy (ECG-gated scan); (left) diastole, (right) systole. RA = right atrium, RV = right ventricle, Sv = interventricular septum, LV = left ventricle, @ = mitral valve closed in systole, LA = left atrium, Sa = interatrial septum, + = anterior papillary muscle.

wall of the left ventricle. The results in normal conditions and pressure overload of the left ventricle are compared in Table 1.

Increased myocardial thickness occurs also in restrictive cardiomyopathy and idiopathic hypertrophic subaortic stenosis. In IHSS, cardio-CT demonstrates the circumscribed thickening of the ventricular septum (Figure 3). The ratio of the diameter of the myocardium in the area of the hypertrophic ventricular septum and
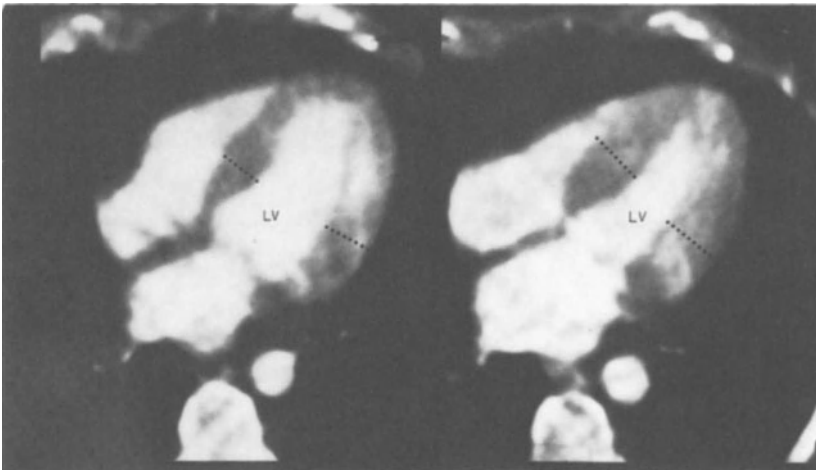
Figure 2. Aortic valve stenosis (ECG-gated scan); (left) diastole, (right) systole. Concentric hypertrophy of the left ventricle (....). Normal contraction.
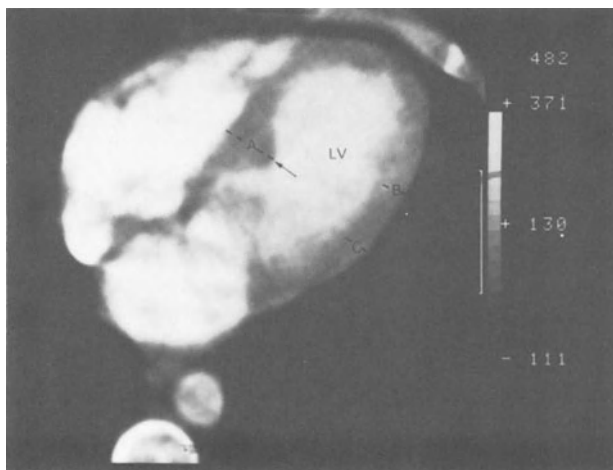
Figure 3. Idiopathic hypertrophic subaortic stenosis (↑). A $\frac{(B + C)}{2}$ ratio of myocardial thickness enlarged in case of IHSS.

left ventricular lateral wall is increased and shows in cardio-CT similar results as the ratio between ventricular septum and posterior wall in echocardiography (Table 2).

Myocardial scars in patients with coronary heart disease appear in cardio-CT as wall segments with decreased wall thickness and circumscribed ventricular dilatation (Figure 4). ECG-gated cardio-CT shows the abnormal contraction of ischemic wall lesions and allows quantitative assessments of systolic shortening of ventricular axes and the calculation of the ejection fraction. The correlation coefficient comparing the ejection fraction calculated by ECG-gated cardio-CT and laevocardiography was $r = 0.72$. In addition the systolic thickening of the normal myocardium and decreased systolic thickening of the ischemic myocardium can be demonstrated by CT.

Table 1. Myocardial thickness of the left ventricle (mm)

		Ungated	Diastolic	Systolic
	x	11	9.5	13.5
	x–	11.1	9.8	14
Normal	Sx	1.8	1.7	2.5
	n	118	114	114
	x̂	16	13.5	20.5
Pressure	x–	16.6	14.3	20.3
Overload	Sx	3.5	2.5	2.9
Left ventricle	n	45	26	26
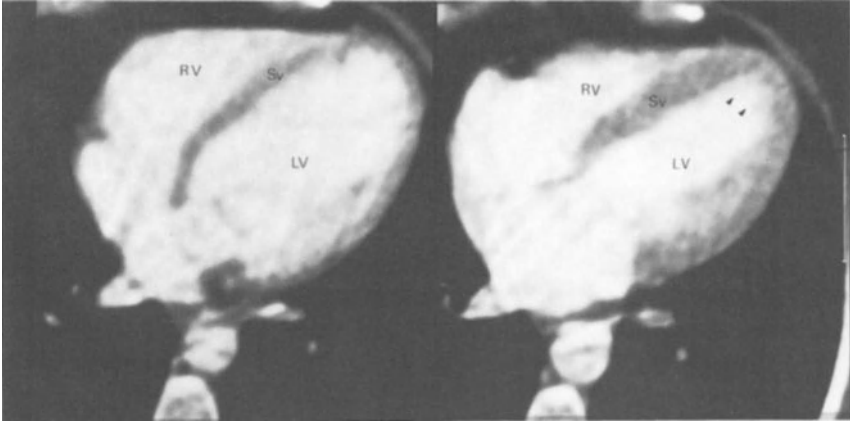
Figure 4a. Hypokinesia of the anterior wall of the left ventricle (↑).
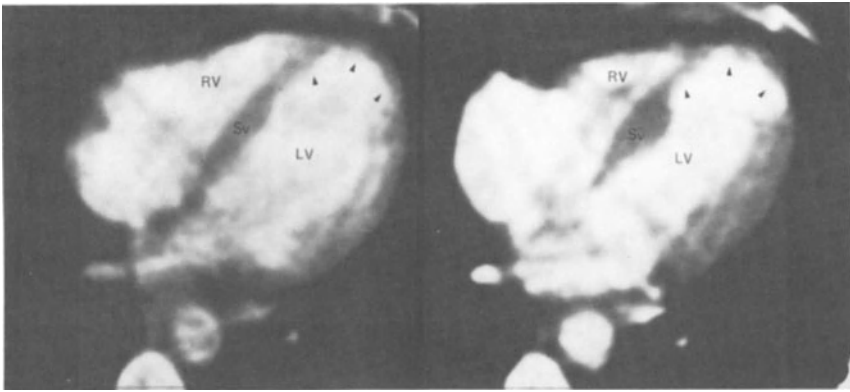
Figure 4b. Akinesia of the anterior wall of the left ventricle (↑). Myocardial attenuation of the infarcted wall area.
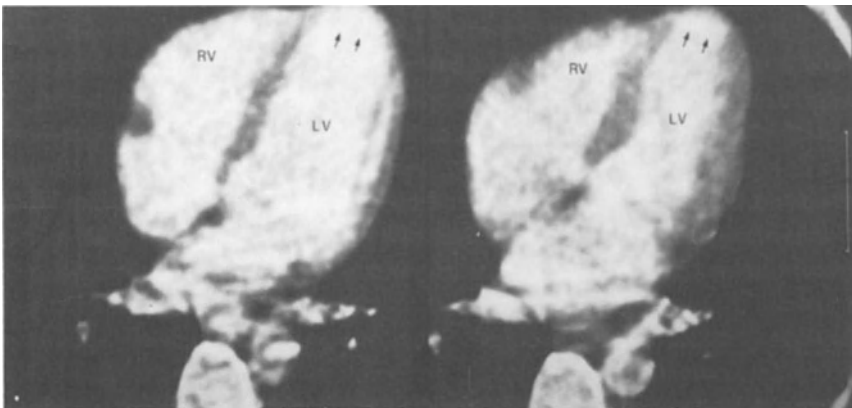
Figure 4c. Aneurysm (@) of the anterior wall of the left ventricle and ventricular septum. Myocardial attenuation of the infarcted wall area.
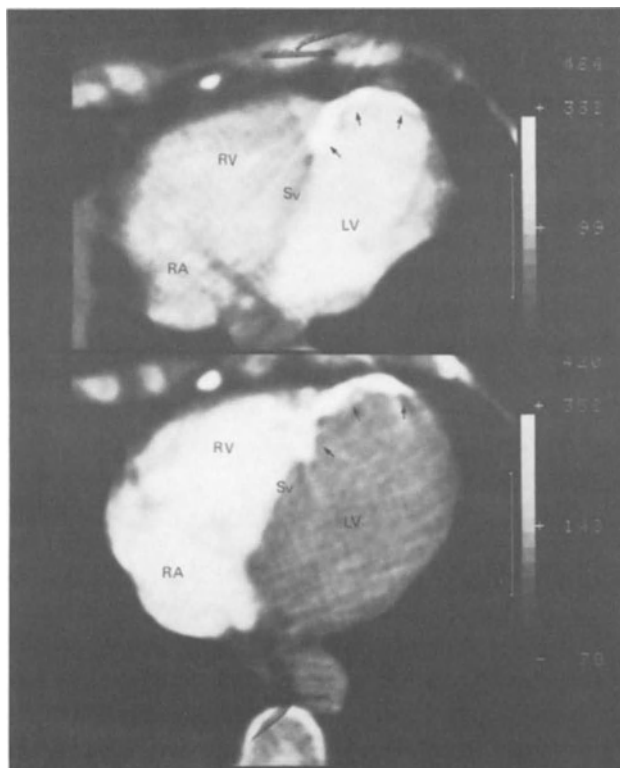
Figure 5. Myocardial calification (↑) of the anterior wall of the left ventricle following myocardial infarct.

Changes of cardiac tissue density in cardio-CT appear in the presence of cardiac calcifications, tumors, thrombi and acute ischemic lesion of the myocardium; in addition tissue density measurements are of diagnostic value in the assessment of coronary bypass perfusion [3, 4, 8] and in pericardial effusions.

The exact localisation and differential diagnosis of cardiac calcifications is improved by the visualization in the horizontal slice plane of the CT-image. Paracardial, pericardial, myocardial or intracavitary calcifications are easier and more accurately separated using CT (Figure 5). Intracavity thrombi are of lower tissue

Table 2. Ratio of myocardial thickness ventricular septum / lateral wall in CT

Normal	x̃	1.1
IHSS	x̄	1.7

←

Figures 4a–c. ECG-gated scans in patients with coronary heart disease; (left) diastole, (right) systole.
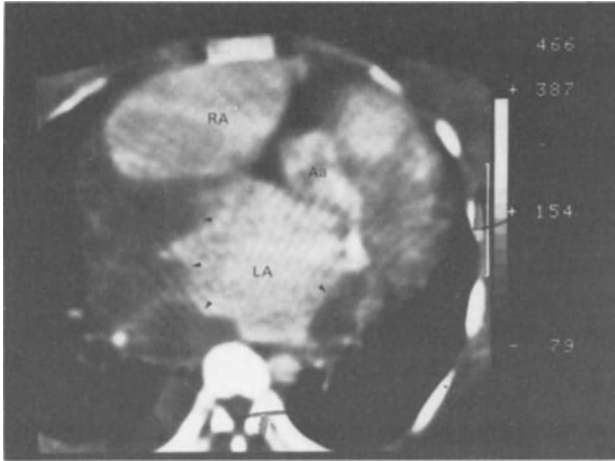
Figure 6a. Mitral valve stenosis. Parietal thrombi (@) in the enlarged left atrium (LA). RA = right atrium, Aa = ascending aorta.
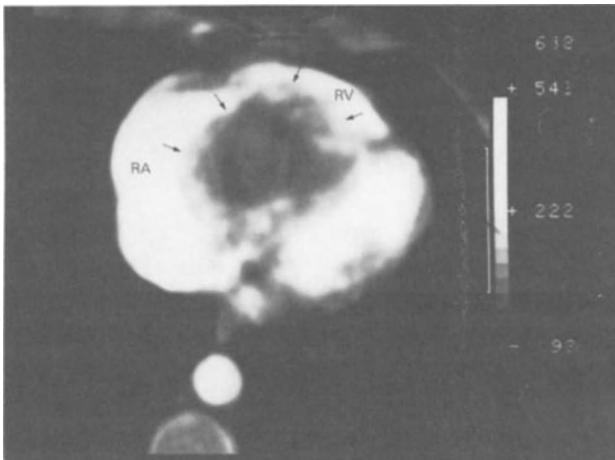
Figure 6b. Myxoma (↑) of the right ventricle (RV). Right atrium (RA) enlarged.

density than the myocardium or most of the other cardiac tumors [5, 6, 13]. Besides the patient's history, clinical findings and the localisation tissue density measurements done by cardio-CT provide additional diagnostic criteria for the differentiation of thrombi and tumors. The tissue density of thrombi was found to be below 60 HU in general, and the tissue density of myxomas was between 50 and 100 HU in the post contrast scans. In the very few cardiac sarcomas we observed, the tissue density was more or less inhomogenous and of higher level than in myxomas between 100 and 200 HU (Figure 6).

The changes of tissue density in acute ischemic lesions of the myocardium were
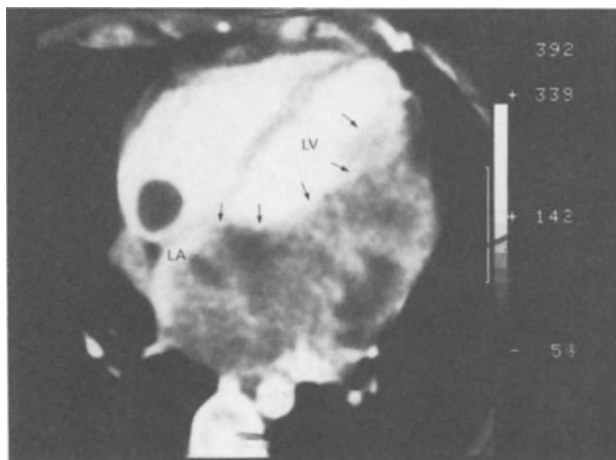
Figure 6c. Mesothelioma with sarcomatous parts infiltrating the left ventricular wall (↑) and nearly obstructing the left atrium (LA). LV = left ventricle.

until now of interest primarily for experimental studies. Several authors using canines showed the ischemic area following coronary artery occlusion as hypodens area, as the contrast perfusion of the ischemic myocardium is decreased [1, 9, 11, 16, 17]. Tissue density measurements of the normal and ischemic myocardium allow quantitative assessments of the myocardial perfusion. After bolus injection of contrast medium a quick increase in density within the normal perfused myocardium occurs. The time/density curve is characteristic and similar to the one which can be measured in the aorta. The post contrast injection increase in density of the ischemic myocardium is much slower and of lower degree. This experimental model can be used to visualize the effect of different drugs on myocardial perfusion, especially of the ischemic area. (Figure 7). In combination with the ECG-gated cardio-CT, also positive inotropic effects can be demonstrated.

CONCLUSION

In conclusion, cardio-CT allows a wide range analysis of cardiac structures. In part, indications and diagnostic findings are similar to echocardiography, for example in coronary heart disease, cardiomyopathy, assessment of wall thickness, cardiac tumors or pericardial effusions and tumors. As the time resolution of cardio-CT is less as compared to echocardiography, scintigraphy and DVI, functional assessments using ECG-gated cardio-CT are not as precise. Cardio-CT is superior in the demonstration of thrombi, calcifications, assessment of bypass perfusion, the differentiation of cardiac or pericardial tumors, the assessment of cardiac rotation, the demonstration of the ventricular apex and by the possibility of tissue density

256
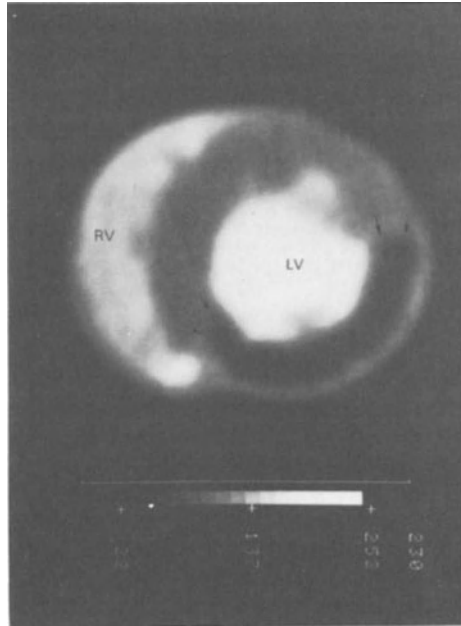
Figure 7a. Experimental myocardial infarct (dog) following ligation of the circumflex artery. Subendocardial ischemia (←) of the posterior wall of the left ventricle appears hypodens (dark) in the CT-image.
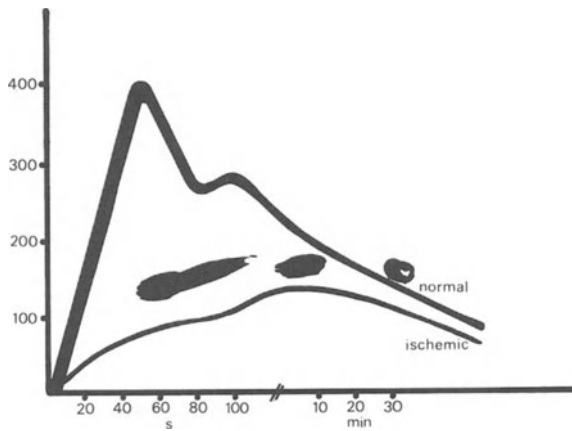
Figure 7b. Time/density curve of the ischemic and normal myocardium after bolus injection of 60 ccm 75% contrast material intravenously. The density increase of the ischemic myocardium is much slower and of lower degree as measured in the normal myocardium.

measurements. Contraindications are contrast medium allergy, cardiac failure with pulmonary edema, renal failure, acute myocardial infarct. The rate of technical insufficent examinations is approximately 5%. The value of echocardiography as a non invasive screening method is not influenced by cardio-CT. It should be used if its potential additional diagnostic criteria might be of help, if echocardiography is not conclusive or technically impossible and for the confirmation of diagnoses at the non invasive level.

REFERENCES

1. Adams DF, Hessel SJ, Judy PF, Stein JA, Abrams HL: Computed tomography of the normal and infarcted myocardium Am J Roentgenology 126:786–791, 1976.
2. Berninger WH, Redington RW, Doherty P, Lipton MJ, Carlsson E: Gated cardiac scanning: canine studies. J Comput Assist Tomogr 3:155–163, 1979.
3. Brundage BH, Lipton MJ, Herfkens RJ, Berninger WH, Redington RW, Chatterjee K, Carlsson E: Detection of patent coronary bypass grafts by computed tomography. Circulation 61:826–831, 1980.
4. Carlsson E, Lipton MJ, Skiöldebrand CG, Berninger WH, Redington RW: Erfahrungen mit der Computertomographie bei der in vivo Herzdiagnostik. Radiologe 20:44–49, 1980.
5. Felix R, Lackner K, Simon H, Grube E, Thurn P: Das Herz im "schnellen" Computertomogramm. "Computer-Kardio-Tomographie" (CKT). Fortschr Röntgenstr 129:401–409, 1978.
6. Godwin JD, Herfkens RJ, Skiöldebrand CG, Brundage BC, Schiller NB, Lipton: Detection of interventricular thrombi by computed tomography. Radiology 138:717–721, 1981.
7. Guthaner DF, Wexler L, Harell G: CT demonstration of cardiac structures. Am J Roentgenology 133:75–81, 1979.
8. Guthaner DF, Brody WR, Ricci M, Oyer PE, Wexler L: The use of computed tomography in the diagnosis of coronary artery bypass graft patency. Cardiovasc Intervent Radiol 3:3–8, 1980.
9. Hessel SJ, Adams DF, Judy PF, Fishbein MC, Abrams HL: Detection of myocardial ischemia in vitro by computed tomography. Radiology 127:413–418, 1978.
10. Heuser L, Tauchert M, Niehues B, Friedmann G, Behrenbeck DW: Die axiale Computertomographie (CT) in der Diagnostik der Erkrankungen des Herzens und der Aorta Dtsch med Wschr 104:243–248, 1979.
11. Higgins CB, Siemers PT, Schmidt W, Newell JD: Evaluation of myocardial ischemic damage of various ages by computerized transmission tomography. Circulation 60:284–291, 1979.
12. Janson R, Lackner K, Grube E, Brecht G, Thurn P: Computer-Kardio-Tomographie der idiopathischen hypertrophischen subvalvulären Aortenstenose (IHSS) – ein neuartiger Beitrag zur nicht-invasiven Diagnostik. Fortschr Röntgenstr 130:536–542, 1979.
13. Lackner K, Heuser L, Friedmann G, Thurn: Computerkardiotomographie bei Tumoren des linken Vorhofs Forschr Röntgenstr 129:735–739, 1978.
14. Lackner K, Simon H, Thurn P: Kardio-Computertomographie – neue Möglichkeiten in der radiologischen nicht invasiven Herzdiagnostik. Z Kardiol 58:667–675, 1979.
15. Lackner K, Thurn P: Computed tomography of the heart: ECG-gated and continous scans. Radiology 140:413–420, 1981.
16. Lipton MJ, Brundage BH, Doherty PW, Herfkens R, Berninger WH, Redington RW, Chatterjee K, Carlsson E: Contrast medium-enhanced computed tomography for evaluating ischemic heart disease. Cardiovasc Medicine 4:1219–1229, 1979.
17. Newell JD, Higgins CB, Abraham JL, Kelley MJ, Schmidt WS, Haigler F: Computerized tomographic appearance of evolving myocardial infarctions. Invest Radiol 15:207–214, 1980.

18. Ter-Pogossian MM, Weiss ES, Coleman RE, Sobel BE: Computed tomography of the heart. Am J Roentgenology 127:79–90, 1976.

27. ANALYSIS OF CORONARY BYPASS GRAFT PATENCY BY COMPUTED TOMOGRAPHY

W.G. DANIEL, W. DÖHRING, P.R. LICHTLEN AND H.-ST. STENDER

Accurate determination of aortocoronary bypass graft patency is still dependent on angiography, an invasive procedure. A non-invasive method, easily performed, repeatable and without special risks, visualizing the anatomy and providing direct information on graft patency would be very useful in the postoperative control of patients after bypass graft surgery. In this aspect, computed tomography (CT) has been reported to represent an ideal tool [1–12]. However, merits and limits of this method need to be defined, since in the studies published so far, the number of investigated grafts are often small and angiographic controls of the results are not always available. Therefore, in a consecutive series of patients who underwent postoperative coronary angiography due to persistent or recurrent angina pectoris, CT scanning was also performed for assessment of bypass graft patency in close temporal relation to angiography.

MATERIALS AND METHODS

Sixty-seven consecutive patients (65 males and 2 females), age 40–67 years, with a total of 125 grafts (1–4 grafts per patient; average 1.87 grafts) were entered into the study. All patients underwent angiography for assessment of graft patency due to recurrent postoperative chest pain.

Twenty-seven patients with 54 grafts were studied by CT 1 to 126 days before angiography (average 35 days); in 40 patients with 71 grafts, CT followed angiography 1 to 41 days (average 7 days).

CT examinations were performed during suspended inspiration using a "Somatom" total body scanner (Siemens AG, West Germany) without additional equipment for dynamic scanning or gating of the cardiac cycle. Scan duration for one section (x-ray beam rotation of 360°) amounted to 5 sec, the thickness of the tomographic section obtained being 8 mm; scans could be repeated after an interval of 6 sec.

A metal clip attached to the proximal anastomosis of each graft during operation, served as a marker of the search of the ideal scan level, just below the proximal anastomosis, yet still above the origin of the coronary arteries. In addition, polaroid photographs taken intraoperatively, showing the exact position of the graft, were
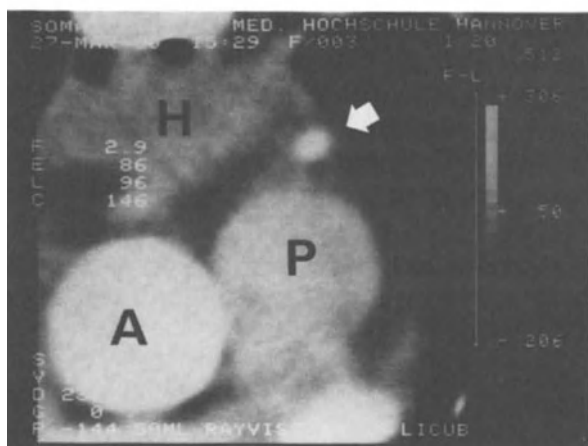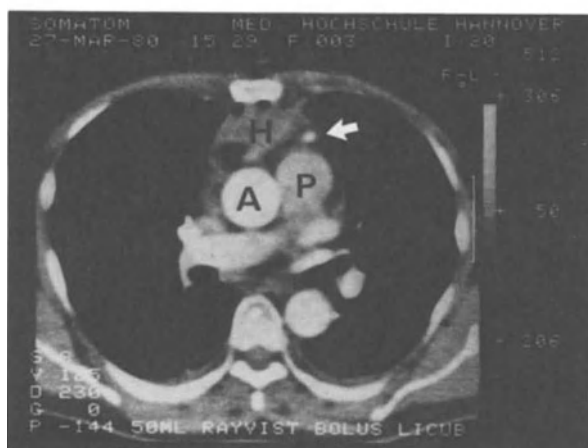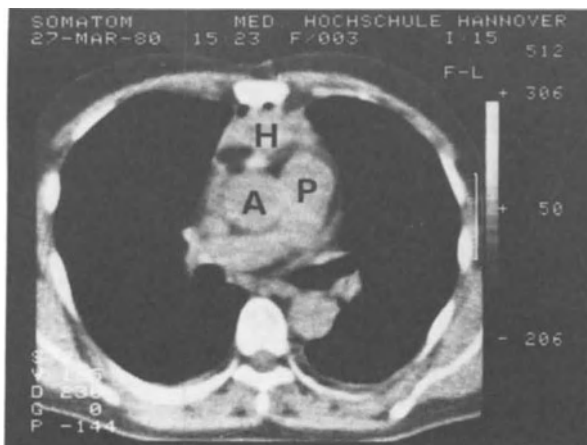
Table 1. Angiographic results of the studied bypass grafts

Angiography	Patent	Occluded	No.
LAD	45	15 (25%)	60
RCA	19	6 (24%)	25
Obtuse marg.	20	11 (36%)	31
Diagonal	5	1 (17%)	6
Int. mammary	3		3
Total	92	33 (26%)	125

LAD = left anterior descending coronary artery; RCA = right coronary artery; Obtuse marg. = obtuse marginal branch of the circumflex artery; Diagonal = diagonal branch of the LAD; Int. mammary = internal mammary artery graft. For details see text.

available for most of the patients.

CT scans were obtained before and after one to three bolus injections of 50 ml Megluminioglicinate (Rayvist® 300) into an anticubital vein. At the average, 1.98 ± 0.65 contrast injections per patient were made. Scanning started usually 5 to 8 sec after the end of the bolus injection and 2 to 3 scans followed each injection. Evaluation of graft patency was based on the typical contrast enhancement of the graft structure associated with an increase of the attenuation values, and patency was judged qualitatively by two independent observers, at least one having no knowledge of the angiographic results.

RESULTS

Angiography

Angiography revealed that 92 of 125 grafts were patent (patency rate 73.6%) and 33 were occluded. The details of the angiographic findings are summarized in Table 1. Whereas 79 grafts appeared unobstructed both with regard to the proximal and distal anastomoses as well as the veins themselves, 13 grafts showed a stenosis of 75% or higher: 5 grafts to an obtuse marginal branch (OMB) of the circumflex coronary artery (LCX), 4 to the left anterior descending coronary artery (LAD), 3 to the right coronary artery (RCA) and 1 to a diagonal branch (DB) of the LAD. In 9 cases the stenosis was localized in the proximal half, in 4 cases in the distal half of the bypass vein or in the region of the corresponding anastomosis.

←

Figure 1. CT scan of a single LAD bypass graft (arrows) before (a) and after (b, c) contrast material administration, with enlargement of the area of interest (c). The patient was studied in the early postoperative period; a retrosternal hematoma (H) can still be seen. A = ascending aorta; P = pulmonary artery.
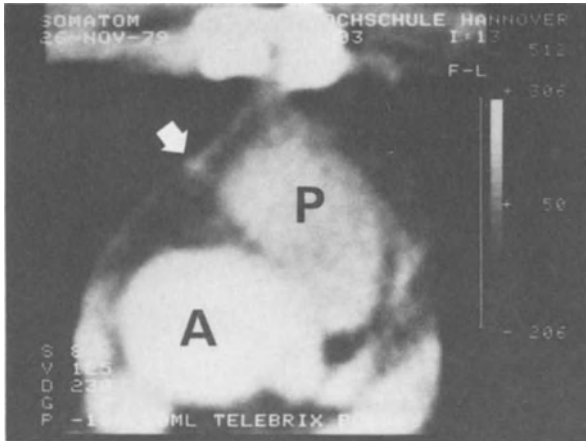
Figure 2. CT scan of a single RCA graft (arrow) after contrast material administration (enlargement of the area of interest). A = ascending aorta; P = pulmonary artery.

Computed tomography

Eighty-four of the 92 angiographically patent grafts were also visualized by CT (Table 2): 44 of 45 patent grafts to the LAD (97.7%), 16 of 19 patent grafts to the RCA (84.2%), 17 of 20 patent grafts to an OMB of the LCX (85%), 4 of 5 patent grafts to a DB (80%), and all 3 internal mammary artery grafts. Typical CT examples are shown in Figures 1–3. Sensitivity for CT scan detection of graft

Table 2. Visualization of bypass grafts by CT in comparison to angiography

Grafted vessel	Angiographically patent grafts		Angiographically occluded grafts		All grafts	No.
	CT +	CT −	CT +	CT −	CT correct	
LAD	44	1	1	14	58 (96.7%)	60
RCA	16	3	1	5	21 (84.0%)	25
Obtuse marg. branch	17	3	2	9	26 (83.9%)	31
Diagonal branch	4	1	–	1	5 (83.3%)	6
Int. mammary	3	–	–	–	3 (100.0%)	3
Total	84	8	4	29	113 (90.4%)	125

CT + ( ) = grafts patent (occluded) by computed tomography; LAD = left anterior descending coronary artery; RCA = right coronary artery; Obtuse marg. branch = obtuse marginal branch of the circumflex coronary artery; Diagonal branch = diagonal branch of the LAD; Int. mammary = internal mammary artery graft. For details see text.

Figure 3. CT scan of bypass grafts to the LAD (curved arrow), RD (white long arrow) and OMB (black arrow); the latter is positioned behind the aorta running parallel to the scan level. Scan was taken following contrast material administration. A = adcending aorta; P = pulmonary artery.
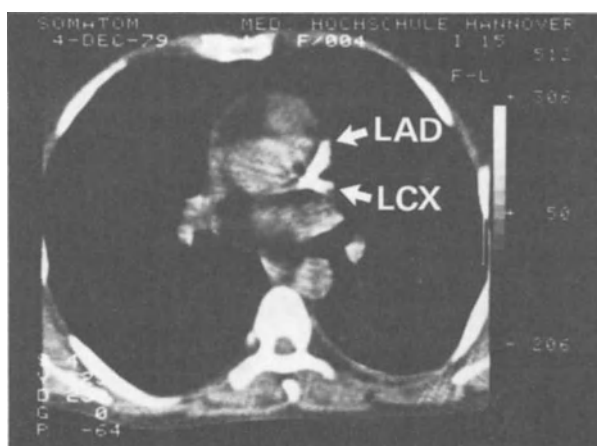
Figure 4. CT scan of a verely calcified left coronary artery without contrast material administration. The left main stem and proximal parts of the LAD and LCX are clearly visualized.

patency (S = (graft patent by CT and angiography/graft patent by angiography alone) $\cdot$ 100) amounted to 91.3%.

Of the 33 grafts occluded at angiography, 29 (87.9%) were considered to be occluded also on CT (Table 2): 14 of 15 occluded grafts to the LAD (93.3%), 5 of 6 occluded grafts to the RCA (83.3%), 9 of 11 occluded grafts to an OMB of the LCX (81.8%) and 1 graft to a DB of the LAD. Hence, 4 grafts found occluded at angiography were considered to be patent by CT. In these 4 false-positive cases, the CT study was performed 9 to 32 days before angiography. Thus, it cannot be ruled
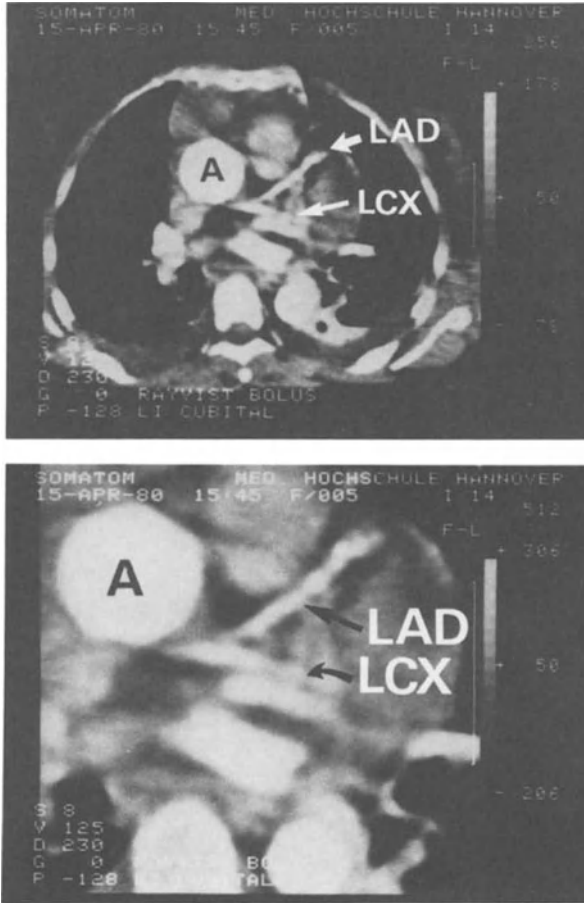
Figure 5. CT scan of left coronary artery following contrast material administration (a, b), with enlargement of the area of interest (b). LAD and LCX can clearly be visualized. A = ascending aorta.

out that some of the 4 grafts became occluded during the time between CT and angiography, especially since all 4 patients were studied because of recent onset of chest pain.

Accordingly, the study revealed a specificity (SP = (grafts occluded by CT and angiography/grafts occluded by angiography) · 100) of CT for assessment of bypass graft patency of 87.9% and an accuracy (ACC = (patent and occluded grafts diagnozed correctly by CT/all studied grafts) · 100) of 90.4%.

In 13 grafts, angiography demonstrated one or more significant stenoses either of the graft itself or of one of the anastomoses. Eleven (84.6%) of these partially obstructed bypass grafts were considered to be patent by CT.

Interobserver disagreement existed with regard to the evaluation of 4 grafts (3.2%): 2 angiographically patent grafts (1 to a DB and 1 to an OMB) and 2 occluded grafts (1 to the LAD and 1 to an OMB). Fifteen months after the last

patient of this study was investigated by CT all scans were reevaluated by one of the two observers. Reevaluation differed from the initial scan interpretation in only two cases (2 grafts to an OMB of the LCX) amounting to an intraobserver-variability of 1.6%.

Finally, it should be mentioned that native coronary arteries could also be visualized by CT without contrast enhancement, when they were calcified (Figure 4) or following injection of contrast material when a corresponding scan level was chosen (Figure 5).

CONCLUSIONS

1. Non-dynamic computed tomography permits the correct identification of patent aorto-coronary bypass grafts in a high percentage of cases.
2. This is in particular true for the clinically most important grafts to the LAD.
3. False-positive results are rare.
4. Thus, in postoperatively asymptomatic or, at least, markedly improved patients, CT scans demonstrating one or more patent grafts may be sufficient for the anatomical documentation of the success of bypass graft surgery.
5. However, current CT scanning does not provide definite information on partial graft obstruction or graft function, and therefore, in clinically symptomatic patients, this method is still not informative enough to replace coronary angiography.

REFERENCES

1. Vasile N, Usdin JP, Belloir C, Ferrane J, Galley JJ, Vernant P: Perméabilité des pontages aorto-coronaires explorés par tomodensitométrie. Arch Mal Coeur 11:1346, 1979.
2. Brundage BH, Lipton MJ, Herfkens RJ, Berninger WH, Redington RW, Chatterjee K, Carlsson E: Detection of patent coronary bypass grafts by computed tomography. A preliminary report. Circulation 61:826, 1980.
3. Daniel WG, Döhring W, Lichtlen PR, Stender H-St: Non-invasive assessment of aortocoronary bypass graft patency by computed tomography. Lancet I:1023, 1980.
4. Daniel W, Döhring W, Elgeti H, Lichtlen PR, Stender H-St, Borst HG: Darstellung von aortocoronaren Venengrafts mit Hilfe der nichtdynamischen Computertomographie. Schweiz Med Wschr 110:1654, 1980.
5. Guthaner DF, Brody WR, Ricci M, Oyer PE, Wexler L: The use of computed tomography in the diagnosis of coronary artery bypass graft patency. Cardiovasc Intervent Radiol 3:3, 1980.
6. Hauser H, Perrenoud JJ, BoppP, Rutishauser W, Hahn Ch: La tomoradiométrie transverse dans le contrôle de la perméabilitédes ponts aorto-coronariens: valeur et intérêt par rapport à la coronarographie. Schweiz Med Wschr 110:1651, 1980.
7. Moncada R, Salinas M, Churchill R, Love L, Reynes C, Demos TC, Hale D, Schreiber R: Patency of saphenous aortocoronary-bypass grafts demonstrated by computed tomography. N Engl J Med 303:503, 1980.
8. Daniel W, Döhring W, Ziemer G, Flohr E, Lichtlen PR, Stender H-St: Computertomographischer Nachweis der Patency von aortocoronaren Venengrafts. (abstr). Z Kardiol 70:303, 1981.

9. Kahl FR, Wolfman NT, Watts LE: Evaluation of aortocoronary bypass graft status by computed tomography. Am J Cardiol 48:304, 1981.

10. McKay ChR, Brundage BH, Herfkens RJ, Lipton MJ, Turley K, Ullyot DJ, Ebert PA: The clinical usefulness and feasibility of determining coronary artery bypass graft patency by contrast enhanced computed tomography during the early postoperative period. (abstr) Am J Cardiol 47:495, 1981.

11. Mühlberger V, z Nedden D, Knapp E, Unger F, Scharfetter H, Braunsteiner H: Computertomographische Darstellung aortocoronarer Venengrafts. Vergleich mit der selektiven Koronarographie. Z Kardiol 70:377, 1981.

12. Ullyot DJ, Turley K, McKay ChR, Brundage BH, Lipton MJ, Ebert PA: Assessment of saphenous vein graft patency by contrast-enhanced computed tomography. J Thorac Cardiovasc Surg 83:512, 1982.

SUBJECT INDEX